NUCLEIC BASE-DIRECTED ADSORPTION OF COLLOIDS AND POLYELECTROLYTES

by

Marianne S. Terrot

B.A., Chemistry
Wellesley College, 2001

SUBMITTED TO THE CHEMICAL ENGINEERING DEPARTMENT IN PARTIAL FULFILLMENT OF THE REQUIREMENTS FOR THE DEGREE OF

DOCTOR OF PHILOSOPHY
AT THE
MASSACHUSETTS INSTITUTE OF TECHNOLOGY

JANUARY 2007

Signature of Author:_____

Certified by:_____
Paula T. Hammond
Professor of Chemical Engineering
Thesis Supervisor

Accepted by:_____
William M. Deen
Professor of Chemical Engineering
Chairman, Committee for Graduate Students

Nucleic Base-Directed Adsorption of Colloids and Polyelectrolytes

by

Marianne S. Terrot

Submitted to the Chemical Engineering Department in Partial Fulfillment of the Requirements for the Degree of Doctor of Philosophy in Chemical Engineering

ABSTRACT

The primary objective of this work has been the advancement of selective adsorption techniques by use of new interactions and development of new approaches to the directed assembly of colloidal species. The ability to control the assembly from solution of complex and composite surface arrays by chemical patterning of surfaces is of great interest for the creation of nano- and micro-scale features without the costs and constraints of traditional lithography. Previous work in this group having demonstrated the patterning of polyelectrolyte multilayers by assembly on chemically-patterned surfaces, this thesis features a variation of selective adsorption in which polyelectrolytes of known substrate selectivity control the adsorption of the colloids onto which they are layered.

The first section of this thesis will describe the evolution of this technique in response to certain limitations inherent to the patterning of multilayered films. Perfluorinated surfaces, proposed as potential adsorption resists, were found to display only partial or relative selectivity to common polyelectrolytes in the context of layer-by-layer assembly, an observation consistent with trends predicted by free-energy modeling. However, when these same polymers were layered on colloids, absolute selectivity could be more easily achieved. Polyamine-directed colloidal assembly was studied first, demonstrating that layer-by-layer selectivity observations still held in this new approach and illustrating some unique advantages with regards to multicomponent assembly.

To expand the reach of selective adsorption, specific recognition via multiple hydrogen bonding was explored as a guiding interaction. Nucleic base pairing, the MHB system at the heart of molecular biology, proved highly effective for selectivity. In particular, the mutual indifference of non-complementary groups makes MHB ideally suited to side-by-side deposition of different species. Natural RNA homopolymers were used at first for surface and colloidal modification, but proved too fragile and costly for extensive use. Instead, novel biomimetic polymers combining nucleic base side chains and stable backbone charge were synthesized, along with nucleic base-terminated triethoxysilanes for facile microcontact printing of nucleic base patterns. These new materials successfully replaced RNA as directors of selective assembly while improving reproducibility; in particular, their stability allowed exploration of new approaches to asymmetric functionalization. Multilayered films of these polymers were also studied and found to exhibit interesting responses to changes in chemical environment.

In the last section of this thesis, the synthesis and characterization of the nucleic base-grafted polyelectrolytes and triethoxysilanes will be reported.

Thesis Supervisor: Paula T. Hammond, Bayer Chair Professor of Chemical Engineering

TABLE OF CONTENTS

LIST OF FIGURES

CHAPTER 2

CHAPTER 3

CHAPTER 4

CHAPTER 5

CHAPTER 6

LIST OF TABLES

ACKNOWLEDGEMENTS

First and foremost, I wish to thank my advisor, Paula Hammond, for her guidance and support over the last five years. It was the breadth of her expertise and interests that allowed me to explore the many different facets of this project. I am also indebted to the members of my thesis committee Prof. Bob Cohen, Prof. Klavs Jensen, and Prof. Christine Ortiz for their helpful comments and advice; their fresh perspectives more than once provided ways around vexing impasses.

Along the way, I benefited from the help of many wonderful collaborators. Prof. Alice Gast and Bethany Lyles initiated the magnetic tether patterning project, which in conjunction with the work of Xueping Jiang inspired the use of polyelectrolyte functionalization to direct colloidal adsorption. Prof. Anne Mayes and Chris Barrett were of great help in adapting their free-energy adsorption model. I was also assisted by two excellent undergraduate researchers, Josephine Elia of MIT and Celina Dozier of Florida AMU, to whom I wish great success in her own graduate career.

This work was made possible by financial and material support from the Center for Materials Science and Engineering, funded under the MRSEC program of the National Science Foundation, the Office of Naval Research, and the Dupont-MIT Alliance.

I would like to thank past and present Hammond group members for making our lab a friendly and supportive community. Avni Argun, Nathan Ashcraft, Mike Berg, Daniel Bonner, Shujun Chen, Helen Chuang, Dean DeLongchamp, Tarek Farhat, Amanda Engler, Shoshana Gourdin, Jijun Huang, LaShanda James-Korley, Xueping Jiang, Mark Johnson, Heejae Kim, Yong Hoon Kim, Youn Sang Kim, Kevin Krogman, Ilsoon Lee, Seung Woo Lee, Geoff Lowman, Jodie Lutkenhaus, Mara Lee MacDonald, LaRuth McAfee, Don McGaffigan, Andy Miller, Linda Mousseau, Phuong Nguyen, Juhyun Park, Greg Pollock, Zhiyong Poon, Mohit Rawat, Cathy Santini, Dan Schmidt, Jinhwa Seo, Anita Shukla, Renee Smith, Kris Stokes, Lu Tian, Hiroaki Tokuhisa, Kris van Hege, Eric Verploegen, Ryan Waltetzko, Kris Wood, Jung-Sheng Wu, Piljin Yoo, Bruce Yu, Michael Yurchenko, Nicole Zacharia, and Haipeng Zheng – one perk of being Graduation Mug Maker is having ready access to the complete lab membership archives so no one gets left out accidentally.

My classmates Juhyun and Kris and my CC cofounders Nicole and Jodie were there for me every step of the way, always willing to lend an ear or a bottle of LPEI. The last paragraph notwithstanding, I do know a few people outside of macro@mit.edu. To Camille, Emily, and Susie – friends like you are rare and treasured. To Seth, Pentacrack and associates, and the Ranters – life is better when it's funny. And to Jason – the best part about graduating is coming home to you.

And finally, I thank my parents for, well, everything.

CHAPTER 1 – INTRODUCTION

1.1 Introductory Remarks

Controlling and understanding macromolecular adsorption at surfaces is critical to the construction of microscale and nanoscale features, especially in applications ill-suited to traditional lithographic methods. Patterns of contrasting chemical functionality are of particular interest for guided self-assembly, especially if these patterns can be made and used with few logistical constraints. This thesis aims to explore new ways of creating such adsorption-directing surfaces and to identify materials and strategies best suited to the endeavor. In essence, we seek to design simple routes to complex structures, expanding on previous achievements in the field and applying them to a greater range of substrates and adsorbates.

In this introduction, a broad overview to topics relevant to this thesis will be given, providing background for the more detailed reviews of past and present work at the start of each chapter. The nature and solution assembly of polymeric thin films will be discussed first, followed by approaches to the creation of three-dimensional features within such films and the chemical patterning of surfaces.

1.2 Background

Thin films having lateral heterogeneity are of great interest for use as optical waveguides, electrochromic devices, power storage devices, biomaterial coatings, and as platforms for nano-scale electronics, proteomic arrays, and sensors based on molecular recognition. While there exist many approaches to the creation of micron-scale surface features, non-lithographic techniques based on polymer adsorption from solution are of particular interest due to their low cost and applicability to a broad range of materials and conditions. The adsorption of polymers and in particular polyelectrolytes will be reviewed first, followed by the layer-by-layer approach to thin film assembly. Micropatterning techniques will then be discussed, as will previous results regarding the ability of chemical surface patterns to determine polyelectrolyte adsorption.

Experimentally, thin polymer films adsorbed on planar surfaces can be characterized in many ways. Thickness can be evaluated by ellipsometry, a non-destructive method, as well as by the use of profilometry or atomic force microscopy (AFM) to image trenches. Recently, quartz crystal microbalances have been used for continuous tracking of adsorbed mass during assembly, and ellipsometry can also be performed live and in situ. After assembly, films can be characterized topographically and chemically by use of AFM, chemical force microscopy, infrared spectroscopy, X-ray photoelectron spectroscopy; techniques like neutron scattering and wide and small-angle X-ray scattering also allow full-depth study of composition and structure.

However, despite a great array of experimental characterization techniques, the specific mechanisms of polymer and polyelectrolyte adsorption remain only partially elucidated due to the complex combinations of environmental forces and intra-chain interactions involved. Modeling the adsorption of ideal-coil polymers on planar surfaces has been the subject of extensive study, lately extended to more complex polymers (polyelectrolytes, random and block copolymers, globular biopolymers) and more complex surfaces (charged surfaces, surfaces with random physical or chemical heterogeneity). Such approaches will be briefly described here; much greater detail and analysis can be found in reviews from Fleer and Lyklema and from Sergeeva and Lipatov.*[1, 2]*

1.2.1 Polyelectrolyte Adsorption from Solution

In order to describe polyelectrolyte adsorption, theories of polymer adsorption were expanded with an electrostatic term. One of the first attempts to model polyelectrolyte adsorption was made by Hesselink, who was able to semi-quantitatively explain several experimental phenomena, although his approximation for the segmental distribution was still rough.*[3]* Later, Van der Schee and Lyklema built a model describing the solution phase as a lattice in which each site can be occupied by either a single polymer segment or a single solvent molecule, as in Flory-Huggins theory, establishing equations to describe adsorbed segment distributions for both strongly- and weakly-charged polyelectrolytes.*[4]* This model can be adapted to polymers with segments larger in size than the solvent molecules, but not to heteropolymers. More refined models have since been constructed to account for complex surfaces and polymers. Monte Carlo simulations were used by Muthukumar to define theoretical adsorption criteria based on surface and polymer backbone charge density, Kuhn segment length, Debye length, and Bjerrum length, giving limiting laws indicating which polyelectrolytes will adsorb onto which surfaces.*[5]* A Balazs model for adsorption on chemically heterogeneous surfaces provides a framework for describing charged polymer adsorption on surfaces combining oppositely-charged and neutral sites, and Gupta found that experimental data for the adsorption of a polyanion on such a surface was consistent with these theoretical predictions.*[6-9]*

Models described thus far have focused on the adsorption of a single polymeric layer, not the multilayered polymeric assemblies to be studied in this thesis; modeling these more complex systems requires also taking into account polymer-polymer interactions and the nature of the new surface constituted by the most recently adsorbed layer. Several theoretical models for multilayered film assembly have been developed, including a free-energy approach from Mayes and coworkers applicable to strong and weak polyelectrolytes and another from Joanny in which interpenetration is captured*[10-13]*. While such models cannot yet quantitatively predict film thickness and morphology, they do capture experimentally-observed qualitative trends.

1.2.2 Layer-by-Layer Assembly

Layer-by-layer (LBL) assembly is a simple but powerful approach to the construction of thin films with highly specific properties. The technique utilizes the interaction forces existing between two polymers or other macromolecular species to direct their alternating adsorption, building up a multilayered film. The earliest work in the LbL field, involving the creation of colloid multilayers by sequential adsorption, was done by Iler in the 1960s*[14]*, and the technique was "rediscovered" and applied to polyelectrolyte multilayers by Decher and colleagues in the early 1990s*[15, 16]*. Much of the work done to date has centered on electrostatic multilayer assembly, in which Coulombic forces direct the sequential adsorption of oppositely charged species; however, in many cases other interaction forces also influence adsorption behavior, including hydrophobicity and hydrogen bonding*[17-20]*. The sheer volume of research reported since 1991 involving LbL techniques is testament to the power and versatility of this approach; comprehensive summaries of current progress in the field can be found in recent review articles by Hammond, Decher, and Laschewsky*[21-23]*.

Polyelectrolytes are of particular interest as LbL assembly materials as they form stable films whose properties can be finely tuned by control of deposition conditions. These polyelectrolyte multilayers (PEMs) are typically formed by alternately immersing a substrate in dilute polycationic and polyanionic solutions, with ample rinsing between adsorption steps. The thickness added by each bilayer cycle can range from 1-20 nm, and total film thickness usually increases linearly with the number of bilayers added, although there have been recent reports of films displaying extended exponential growth regimes.*[24]* Exponential growth regimes are thought to occur when the structure of the LbL film and its constituent polyelectrolytes allow for the inward and outward diffusion through the film of free polyelectrolyte chains which then complex or exchange with previously adsorbed chains, increasing the total adsorbed mass throughout the film rather than merely near the solution interface.*[25-27]* Theoretical description of LbL assembly mechanisms has an added layer of complexity due to the fact that the substrate is constantly changing, with each adsorbed layer creating a new surface. Unlike the smooth, solid silicon substrates generally considered in modeling, the outermost surface of a LbL film during assembly is irregular and penetrable. Free chain ends and loops extend above the film surface, while solvent swelling and loose chain entanglement allow newly-adsorbing chains to infiltrate

underlying layers. The resulting highly-interpenetrated film structure is exquisitely sensitive to variations in solvent conditions and polymer structure.

Essential to the understanding of polyelectrolyte multilayer adsorption is the concept of charge overcompensation and reversal: continued PEM assembly requires that surface charge be fully reversed by each adsorption step, implying that each newly adsorbed polyelectrolyte layer must not just match, but overcompensate for, the charge of the previous layer.*[18]* Polymer backbone flexibility, degree of ionization, and solvent electrostatic shielding, along with the availability of attractive surface sites, all influence the conformation in which chains approach and then adsorb on the surface, determining the charge density of the new surface. While adsorption occurs in discrete steps and surface properties such as contact angle and surface potential often oscillate between two fixed values,*[28, 29]* PEM films are not themselves discretely layered; extensive interpenetration of layers occurs, as evidenced by the lack of Bragg peaks in X-ray reflectivity studies.*[30]* The interpenetration of multilayer films means that charge-reversal cannot be thought of only in terms of surface charge density, but must also take into account the availability of free charges throughout the film.*[31]* PEMs generally display excellent solvent resistance, even at high ionic strength or at extreme pH, and their properties usually are stable over time.*[32-35]* While films assembled from weak polyelectrolytes may be destabilized by pH conditions minimizing their degree of ionization, this can be prevented by post-assembly covalent crosslinking of the layers, and can even be exploited to create films with programmed degradability.*[36-38]*

While electrostatic attraction is the original and principal driving force for LbL assembly, other forces can contribute to or wholly direct film formation, chief among them hydrogen bonding. Multilayered films can be assembled by alternating adsorption of a neutral polymer containing hydrogen bond donor groups and a second neutral polymer containing hydrogen bond acceptor groups,*[17]* and these films often display interesting stability properties allowing their controlled erosion at pH conditions which ionize the hydrogen bonding groups.*[39, 40]* Films assembled entirely via hydrogen bonding can display superior ionic conductivity compared to electrostatically-assembled films, as well as improved stability towards extreme ionic strength conditions.*[41]* Hydrophobic interactions also play an important and sometimes necessary role in LbL assembly; in thermodynamic modeling, hydrophobic contributions to the entropy associated with LbL adsorption have been found to be of comparable magnitude to contributions from ion-

ion and ion-dipole interactions.*[42]* A more detailed description of intermolecular interactions will be given in Chapter 2. When considering films constructed exclusively from neutral species, the concept of charge over-compensation still applies in the broader sense of surface functionality reversal.

pH effects have been extensively studied by Rubner and Shiratori, who found that careful control of the linear charge density during assembly of weak polyelectrolytes allowed for dramatic variations not only in film thickness, but also in the degree of interpenetration and relative amounts of the constituent polyelectrolytes.*[43, 44]* Variations in linear charge density can also be used to modulate the balance between hydrogen bonding and electrostatic interactions of weak polyelectrolytes and thus the film architecture and mechanical properties.*[45]* Ionic concentration is also known to have a strong influence on LbL assembly via its screening of polyelectrolyte-surface and polyelectrolyte-polyelectrolyte electrostatic interactions. When the latter dominate, increased ionic strength leads to increased adsorption by allowing polyelectrolytes in solution to adopt a more coiled conformation and deposit in thicker layers; this is referred to as screening-enhanced adsorption.*[46, 47]* However, when electrostatic attraction between the surface and polyelectrolyte is key to adsorption, increased ionic strength reduces adsorption by screening its driving force.*[48]* Even in the case of screening-enhancement, there is usually some optimal ionic strength above which the charges on both the polycation and polyanion become so shielded as to reduce their attractive interactions, limiting and eventually halting film assembly.

LbL film permeability has been of great interest, especially to those hoping to develop high-performance solid polymer electrolytes. Compared to traditional liquid electrolytes, solid polymer polyelectrolytes offer improved mechanical properties while also simplifying processing, but high ionic conductivity is required if these films are to be commercially relevant.*[49]* Bruening and coworkers studied the effect of film thickness, assembly pH, and solution pH on the ion permeability of multilayered films and found that pH has a strong influence via its effect on the swelling of films.*[50]* To develop LbL systems suitable for use as solid polymer electrolytes, Hammond and DeLongchamp focused on increasing mobile ion concentrations and reducing crosslink density, which in this context refers to chain entanglement rather than covalent bonding. Notably, films assembled via hydrogen bonding rather than

electrostatic interactions exhibited improved ionic conductivity, as did electrostatically-assembled films plasticized by the addition of oligomeric ethylene glycol.*[41, 51]*

The relevance of layer-by-layer assembly is not limited to linear polymers; to the contrary, a great variety of non-linear species can be incorporated into multilayered assemblies via alternating adsorption. Films have been built containing dendrimers, charged biopolymers such as DNA, micellar compounds, Buckminster fullerenes (C_{60}), organic and inorganic nanospheres, clay platelets, enzymes and other linear or globular proteins.*[52-67]*

Heterogeneous LbL assemblies can be made even more versatile by the inclusion of degradable polymers, allowing for controlled film erosion and release of incorporated species. For example, hydrolytically degradable polyamines have been used by the Hammond and Lynn groups to release heparin and transcriptionally active plasmid DNA under physiological conditions, whereas earlier reports of release via film degradation had relied on changes in ionic strength or pH not compatible with *in vivo* applications.*[38, 40, 68-72]* Alternating assembly need also not be limited to two components; trilayered and tetralayered adsorption cycles as well as vertical composites of multiple LbL systems have all been explored and are of particular interest for drug release applications.*[70, 73]*

1.2.3 Creation of Two- and Three-Dimensional Features

Microfabrication is at the heart of the ever-increasing array of technologies becoming ubiquitous to modern life; few are the tools and conveniences now taken for granted in the developed world which do not in some way rely on microelectronic technology. In addition to the integrated circuits, data storage devices, and display units essential to computers and consumer electronic products, microfabricated features are essential to a wealth of new scientific instruments such as microfluidic reactors and microanalytical systems, combinatorial arrays for genomics and proteomics, and micro-optical devices.*[74, 75]* Photolithography, in which a mask is used to selectively expose photosensitive materials which then serve as sacrificial masks for further processing of the underlying substrate (very often, chemical etching), is by far the best-established and most industrially-utilized of the microfabrication approaches, but there are many applications for which it is either impractical or entirely unsuitable. Photolithography requires

specialized equipment and strictly-controlled environments, is limited to the creation of two-dimensional features, offers little control of surface functionality, and is of difficult use in patterning non-planar substrates; while traditional photolithography has been ideally suited to integrated circuit production, more versatile and adaptable techniques are desired for many of today's microfabrication challenges.

In the last decade, a large class of non-photolithographic microfabrication approaches generally known as *soft lithography* have been the subject of intense research interest. The chief defining characteristic of soft lithography is its use of flexible elastomeric stamps, molds, or masks rather than the rigid photomasks employed in photolithography. Two of the techniques most relevant to this thesis, microcontact patterning and micromolding, will be presented here, but several extensive reviews of the field can be consulted for greater detail as well as discussion of other soft lithographic methods.*[74-76]* Microcontact printing (μCP) and micro-molding both begin with creation of a patterned elastomeric block, usually by casting a cross-linkable polymer over a master with relief structure, itself most often prepared by photolithography, micromachining, or e-beam irradiation. Depending on the choice of elastomer and master fabrication route, features as small as 30 nm can be created over cm-scale areas and masters can be used 100+ times without degradation. Poly(dimethylsiloxane) silicone rubbers are the most commonly-used block materials, offering good chemical, thermal, and solvent stability, resistance to irreversible ink adhesion, and durability. However, PDMS is not suitable for the smallest features (<150 nm) and its softness limits the height:width ratios than can be used without distortion of the pattern by sagging (when height << width) or pairing (when height >> width). Height:width ratios between 0.2 and 2 generally yield the most faithful pattern transfers.*[77]*

Micromolding approaches are used to create three-dimensional surface features of specific size, shape, and composition. In replica molding (REM), the simplest of the micromolding approaches, a curable material is cast over the patterned elastomer block, allowed to harden, and lifted off, yielding in one step a reversed copy of the mold pattern (and thus an exact copy of the original master used to prepare the elastomer block). REM can accurately and inexpensively reproduce features much smaller than the 100 nm limitation of photolithography and is of great use when mass production of a given relief pattern is desired, such as in the manufacture of compact disks.*[78]* In microtransfer molding (μTM), excess curable material is

removed from the surface of the mold such that only the embossed regions are filled, after which the mold is placed flush against a substrate. Assuming materials have been chosen carefully, the mold can be peeled away after curing, leaving a patterned microstructure on the substrate. Serial μTM steps can be combined to create complex three-dimensional features via layer-by-layer addition.*[79]* Micromolding in capillaries (MIMIC) is a variant of μTM in which the mold is first placed flush against a substrate, and the curable material is then flowed into the channels by capillary action; MIMIC is restricted to the creation of interconnected features but can be used to create features of multiple thicknesses, fabricating three-dimensional features in a single step.*[80]*

The micromolding techniques allow creation of physical features; to create chemical patterns as well as physical, such as regions of contrasting surface functionality on a planar or non-planar substrate, microcontact printing is preferred. The basic principle of μCP is simple: the relief pattern of the elastomeric block is used to transfer a given chemical species only to those regions of a substrate in contact with the raised features of the patterned block, just as in the use of macro-scale stamps and ink pads, or movable-type printing presses. A seemingly-endless variety of materials can be used as inks, including pure or mixed and small or polymeric organic species. Alkanethiols and alkoxysilanes are particularly useful inks since they form a chemical bond with the substrate, improving pattern stability, rather than merely physisorbing on the surface.

Self-assembled monolayers are ordered surface assemblies of active surfactant molecules which can be assembled by immersion of the substrate in a dilute solution of the surfactant. At the heart of this phenomenon is a spontaneous chemical reaction between substrate surface groups and active surfactant moieties. Among the many classes of molecules capable of surface self-assembly, organosilicon compounds, which assemble on hydroxylated surfaces and can be built on a wide range of inorganic substrates, and organosulfur compounds, which assemble on transition metal surfaces, will be of particular relevance to this thesis as they can be used to simply and stably impart almost any kind of chemical functionality to a surface. SAM surfaces can be tailored not only via selection of their terminal groups, but also by control of the length and intermolecular interaction potential of the linking chains, which determine packing density and terminal group orientation.*[81]*

The rapid and self-limiting nature of alkanethiol and alkoxysilane monolayer assembly makes it readily applicable to a number of surface patterning techniques. Most simply, alkanethioles and alkoxysilanes can be used as inks for "writing" chemical patterns with a micro- or nano-scale stylus, such as in dip-pen nanolithography (DPN).*[82]* This approach is useful when intricate, non-repeating patterns of narrow lines are desired; when broader features are desired, or when one wants to repeat a pattern motif over a large area, micro-contact printing (μCP) of a SAM is preferable.

Both alkoxysilanes and alkanethiols can be stamped but the former are less commonly used as they tend to be less stable under ordinary benchtop conditions, auto-crosslinking in moist environments; alkoxysilanes also tend to require longer stamp contact times to form high-quality SAMs than alkanethiols, which can lead to pattern edge spreading. Silicon substrates must be aggressively cleaned and hydroxylated immediately prior to alkoxysilane SAM formation, whereas the relative inertness of gold makes those surfaces more resistant to atmospheric contamination or oxide formation.*[83, 84]*

Patterned SAMs have been applied to the creation of three-dimensional microstructures in many ways, including by protecting certain regions from chemical etching, by initiating covalent grafting in certain regions, and by creating surfaces whose contrasting chemical functionalities determine which species can adsorb.*[85]* This last application of μCP to the creation of adsorption-directing surface templates will be discussed in detail in Chapter 2.

Polymer-on-polymer stamping, or POPS, is an alternative form of soft lithography offering much greater freedom in choice of materials. Crooks and coworkers were the first to report μCP of a polymer (PAA) onto a polymeric substrate (polyethylene), but their protocol requires extensive pre-treatment of the surface and post-treatment of the transferred polymer layer.*[86]* Hammond and coworkers have since developed more efficient POPS techniques requiring far fewer pre- and post-stamping treatments, allowing the addition of patterned polymeric features on top of LbL films or substrates not amenable to aggressive pretreatments. *[87-89]* In some cases, POPS is preferable even though SAM creation is possible – for instance, stamping polymers onto glass requires far simpler and milder substrate pre-treatment than would the creation of a silane SAM. While thiol and silane SAMs remain the system of choice when solvent stability and patterned region homogeneity are critical, such as fundamental studies of

selectivity, POPS protocols are of greater industrial relevance, keeping patterned LbL assembly as inexpensive and simple as continuous LbL assembly.

POPS has recently been extended to the transfer of LbL films rather than single polymer layers. Via fine control of ink-stamp interaction forces, Hammond and Park were able to construct multilayered thin films, including polyelectrolyte-nanoparticle composites, on elastomeric stamps and then transfer the entire film to a planar substrate by stamping.*[90-92]* The multilayer transfer printing (MTP) technique makes it possible to create three-dimensional surface features without need for selective adsorption or for post-assembly patterned etching, another approach that has been explored.*[93]*

1.3 Aims and Approaches

The primary objective of this work will be the advancement of surface-directed adsorption capabilities. By identifying and studying chemical functionalities capable of highly specific and tunable interactions, we hope to increase our ability to direct adsorption on chemically-patterned surfaces. We also seek new applications of selective adsorption, such as the control of object-object interactions in solution and the incorporation of functional materials into selectively-adsorbing systems.

In the second chapter, the potential role of perfluorinated materials in selective adsorption will be studied. To provide a context for some experimentally-observed counter-intuitive behaviors, a brief theoretical discussion of the nature of polyelectrolyte surface preferences will also be presented. In the next chapter, insights gained from the study of surface-patterned polyelectrolyte multilayer assembly will be adapted to the templated assembly of colloidal arrays. In the fourth chapter, the potential of multiple hydrogen bonding to direct multi-component selective adsorption via specific recognition will be explored using both natural and synthetic polymers having complementary hydrogen bonding motifs. The inclusion of such materials in multilayered films and its effect on film morphology will be studied in the fifth chapter. In support of this work, several new materials were synthesized; their design and characterization are the subject of the sixth chapter. In all of these explorations, special attention will be given to the robustness and adaptability of the methods used so as to ensure their usefulness to future applications.

WORKS CITED

[1] G. Fleer, J. Lyklema, in *Adsorption from Solution at the Solid/Liquid Interface*, (Eds: G. Parfitt, C. Rochester), Academic, New York **1983**.
[2] Y. Lipatov, L. Sergeeva, *Adsorption of Polymers*, Wiley, New York **1974**.
[3] F. Hesselink, in *Adsorption from Solution at the Solid/Liquid Interface*, (Eds: G. Parfitt, C. Rochester), Academic Press, London **1983**.
[4] H. Van der Schee, J. Lyklema, *J. Phys. Chem.* **1984**, *88*, 6661.
[5] M. Muthukumar, C. Kong, *J. Chem. Phys.* **1998**, *109*, 1522.
[6] A. Balazs, K. Huang, P. McElwain, J. Brady, *Macromolecules* **1991**, *24*, 714.
[7] A. Balazs, M. Gempe, Z. Zhou, *Macromolecules* **1991**, *24*, 4918.
[8] V. Gupta, Y.-W. Huang, K.-Y. Chun, *Langmuir* **2003**, *19*, 2175.
[9] V. Gupta, Y.-W. Huang, K.-Y. Chun, *J. Chem. Phys.* **2003**, *118*, 3252.
[10] J.-F. Joanny, *Eur. Phys. J. B* **1999**, *9*, 117.
[11] J.-F. Joanny, R. Netz, *Macromolecules* **1999**, *32*, 9013.
[12] S. Y. Park, C. J. Barrett, M. F. Rubner, A. M. Mayes, *Macromolecules* **2001**, *34*, 3384.
[13] S. Y. Park, M. F. Rubner, A. M. Mayes, *Langmuir* **2002**, *18*, 9600.
[14] R. K. Iler, *J. Colloid Interface Sci.* **1966**, *21*, 569.
[15] G. Decher, J.-D. Hong, *Berichte der Bunsen-Gesellschaft* **1991**, *95*, 1430.
[16] G. Decher, J.-D. Hong, *Makromolekulare Chemie, Macromolecular Symposia* **1991**, *46*, 321.
[17] M. Rubner, W. Stockton, *Macromolecules* **1997**, *30*, 2717.
[18] J. Schlenoff, S. Dubas, *Macromolecules* **2001**, *34*, 592.
[19] N. Kotov, *Nanostructured Materials* **1999**, *12*, 789.
[20] A. Delcorte, P. Bertrand, E. Wischerfhoff, A. Laschewsky, *Langmuir* **1997**, *13*, 5125.
[21] A. Laschewsky, X. Arys, A. Jonas, R. Legras, in *Supramolecular Polymers*, (Ed: A. Ciferri), Marcel Dekker, New York **2000**, 505.
[22] G. Decher, *Science* **1997**, *277*, 1232.
[23] K. M. Chen, X. P. Jiang, L. C. Kimerling, P. T. Hammond, *Langmuir* **2000**, *16*, 7825.
[24] D. DeLongchamp, M. Kastantin, P. Hammond, *Chem. Mater.* **2003**, *15*, 1575.
[25] P. Lavalle, C. Gergely, F. J. G. Cuisinier, G. Decher, P. Schaaf, J. C. Voegel, C. Picart, *Macromolecules* **2002**, *35*, 4458.
[26] P. Lavalle, C. Picart, J. Mutterer, C. Gergely, H. Reiss, J. C. Voegel, B. Senger, P. Schaaf, *J. Phys. Chem. B* **2004**, *108*, 635.
[27] N. Zacharia, D. DeLongchamp, M. Modestino, P. T. Hammond, *Macromolecules* **Submitted**.
[28] M. Rubner, D. Yoo, S. Shiratori, *Macromolecules* **1998**, *31*, 4309.
[29] H. Mohwald, E. Donath, F. Caruso, *J. Phys. Chem. B* **1998**, *102*, 2011.
[30] Y. Lvov, G. Decher, H. Mohwald, *Langmuir* **1993**, *9*, 481.
[31] S. T. Dubas, J. B. Schlenoff, *Macromolecules* **1999**, *32*, 8153.
[32] G. Decher, G. Sukhorukov, J. Schmitt, *Ber. Bunsenges. Phys. Chem.* **1996**, *100*, 948.
[33] J. Schlenoff, M. Li, *Ber. Bunsenges. Phys. Chem.* **1996**, *100*, 943.
[34] F. Caruso, C. Schuler, D. Kurth, *Chem. Mater.* **1999**, *11*, 3394.
[35] N. Kotov, I. Dekany, J. Fendler, *Advanced Materials* **1996**, *8*, 637.
[36] A. Laschewsky, E. Wischerfhoff, P. Bertrand, A. Delcorte, *Macromol. Chem. Phys.* **1997**, *198*, 3239.

[37] G. Mao, Y.-H. Tsao, M. Tirrell, H. Davis, V. Hessel, H. Ringsdorf, *Langmuir* **1995**, *11*, 942.
[38] S. T. Dubas, J. B. Schlenoff, *Macromolecules* **2001**, *34*, 3736.
[39] S. A. Sukhishvili, S. Granick, *Journal of the American Chemical Society* **2000**, *122*, 9550.
[40] S. A. Sukhishvili, S. Granick, *Macromolecules* **2002**, *35*, 301.
[41] D. M. DeLongchamp, P. T. Hammond, *Langmuir* **2004**, *20*, 5403.
[42] N. Kotov, *Nanostructured Materials* **1999**, *12*, 789.
[43] S. S. Shiratori, M. F. Rubner, *Macromolecules* **2000**, *33*, 4213.
[44] M. F. Rubner, D. Yoo, S. S. Shiratori, *Macromolecules* **1998**, *31*, 4309.
[45] J. L. Lutkenhaus, K. D. Hrabak, K. McEnnis, P. T. Hammond, *Journal of the American Chemical Society* **2005**, *127*, 17228.
[46] B. C. Bonekamp, H. Van der Schee, J. Lyklema, *J. Croat Chem. Acta* **1983**, *56*.
[47] M. A. Cohen Stuart, H. Tamai, *Langmuir* **1988**, *4*, 1184.
[48] G. Durand, F. Lafuma, R. Audebert, *Prog. Colloid Polym. Sci.* **1988**, *76*.
[49] D. M. DeLongchamp, P. T. Hammond, *Chemistry of Materials* **2003**, *15*, 1165.
[50] J. J. Harris, M. L. Bruening, *Langmuir* **2000**, *16*, 2006.
[51] G. M. Lowman, H. Tokuhisa, J. L. Lutkenhaus, P. T. Hammond, *Langmuir* **2004**, *20*, 9791.
[52] G. Sukhorukov, H. Mohwald, G. Decher, Y. Lvov, *Thin Solid Films* **1996**, *284-285*, 220.
[53] G. Decher, *Nachr. Chem. Tech. Lab.* **1993**, *41*, 793.
[54] Y. Lvov, G. Decher, G. Sukhorukov, *Macromolecules* **1993**, *26*, 5396.
[55] J. Schmitt, *Advanced Materials* **1997**, *9*, 61.
[56] S. W. Keller, H.-N. Kim, T. E. Mallouk, *Journal of the American Chemical Society* **1994**, *116*, 8817.
[57] Y. Lvov, K. Ariga, I. Ichinose, T. Kunitake, *Journal of the American Chemical Society* **1995**, *117*, 6117.
[58] E. R. Kleinfeld, G. S. Ferguson, *Science* **1994**, *265*, 370.
[59] Y. Lvov, K. Ariga, I. Ichinose, T. Kunitake, *Langmuir* **1996**, *12*, 3038.
[60] D. L. Feldheim, K. C. Grabar, M. J. Natan, T. E. Mallouk, *Journal of the American Chemical Society* **1996**, *118*, 7640.
[61] N. Kotov, I. Dékány, J. H. Fendler, *J. Phys. Chem.* **1995**, *99*, 13065.
[62] N. Kotov, I. Dékány, J. H. Fendler, *Advanced Materials* **1996**, *8*, 637.
[63] Y. Lvov, K. Ariga, T. Kunitake, *Chem. Lett.* **1994**, *1994*, 2323.
[64] W. Jin, X. Shi, F. Caruso, *Journal of the American Chemical Society* **2001**, *123*, 8121.
[65] V. V. Tsukruk, F. Rinderspacher, V. N. Bliznyuk, *Langmuir* **1997**, *13*, 2171.
[66] K. U. Fulda, A. Kampes, L. Krasemann, B. Tieke, *Thin Solid Films* **1998**, *329*, 752.
[67] J. A. He, R. Valluzi, K. Yang, *Chem. Mater.* **1999**, *11*, 3268.
[68] J. Zhang, L. S. Chua, D. M. Lynn, *Langmuir* **2004**, *20*, 8015.
[69] E. Vazquez, D. M. Dewitt, P. T. Hammond, D. M. Lynn, *Journal of the American Chemical Society* **2002**, *124*, 13992.
[70] K. C. Wood, H. F. Chuang, R. D. Batten, D. M. Lynn, P. T. Hammond, *Proceedings of the National Academy of Sciences* **2006**, *103*, 10207.
[71] C. Schuler, F. Caruso, *Biomacromolecules* **2001**, *2*, 921.
[72] J. Cho, F. Caruso, *Macromolecules* **2003**, *36*, 2845.
[73] S. Joly, R. Kane, L. Radzilowski, *Langmuir* **2000**, *16*, 1354.

[74] Y. N. Xia, G. M. Whitesides, *Annual Review of Materials Science* **1998**, *28*, 153.
[75] M. Geissler, Y. N. Xia, *Advanced Materials* **2004**, *16*, 1249.
[76] J. A. Rogers, R. G. Nuzzo, *Materials Today* **2005**, *8*, 50.
[77] E. Delamarche, H. Schmid, H. A. Biebuyck, B. Michel, *Advanced Materials* **1997**, *9*, 741.
[78] H. Haverkorn von Rijsewijk, P. E. J. Legierse, G. E. Thomas, *Philips Tech. Rev.* **1982**, *40*, 2658.
[79] X. M. Zhao, Y. N. Xia, G. M. Whitesides, *Advanced Materials* **1996**, *8*, 837.
[80] Y. N. Xia, E. Kim, G. M. Whitesides, *Chem. Mater.* **1996**, *8*, 1558.
[81] A. Ulman, *Chemical Reviews* **1996**, *96*, 1533.
[82] D. S. Ginger, H. Zhang, C. A. Mirkin, *Angewandte Chemie-International Edition* **2004**, *43*, 30.
[83] C. D. Bain, E. B. Troughton, Y. T. Tao, J. Evall, G. M. Whitesides, R. G. Nuzzo, *Journal of the American Chemical Society* **1989**, *111*, 321.
[84] N. L. Jeon, K. Finnie, K. Branshaw, R. G. Nuzzo, *Langmuir* **1997**, *13*, 3382.
[85] J. L. Wilbur, A. Kumar, K. Enoch, G. M. Whitesides, *Advanced Materials* **1994**, *6*, 600.
[86] P. Ghosh, R. M. Crooks, *Journal of the American Chemical Society* **1999**, *121*, 8395.
[87] X. P. Jiang, P. T. Hammond, *Langmuir* **2000**, *16*, 8501.
[88] X. P. Jiang, H. P. Zheng, S. Gourdin, P. T. Hammond, *Langmuir* **2002**, *18*, 2607.
[89] J. Park, Y. S. Kim, P. T. Hammond, *Nano Letters* **2005**, *5*, 1347.
[90] J. Park, L. D. Fouche, P. T. Hammond, *Advanced Materials* **2005**, *17*, 2575.
[91] J. Park, P. T. Hammond, *Advanced Materials* **2004**, *16*, 520.
[92] J. Park, P. T. Hammond, *Macromolecules* **2005**, *38*, 10542.
[93] J. S. Mohammed, M. A. DeCoster, M. J. McShane, *Langmuir* **2006**, *22*, 2738.

CHAPTER 2 – ELECTROSTATIC MULTILAYER ASSEMBLY

2.1 Introduction

Since non-covalent polymer-surface and polymer-polymer interactions will be of central importance to this chapter, a brief review of the possible forces involved and their comparative strength will be given before discussing the specific motivation, aims, and founding results for the work reported in Chapter 2.

2.1.1 Intermolecular Interactions

Intermolecular interactions are conventionally classified into three types - electrostatics, hydrogen bonding, and van der Waals forces – and all relate to the influence of nuclei on electron density distributions over molecules, as well as the susceptibility of those electrons to external fields. Electrostatics, also known as Coulombic interactions, exist between ions and permanent dipoles; of these, ion-ion interactions are the strongest (~200 kJ/mol, compared to 350 kJ/mol for a carbon-carbon covalent bond), as well as those able to act at the longest range, scaling inversely with distance. Permanent dipoles interact much more weakly, with typical energies of ~1 kJ/mol among themselves and ~15 kJ/mol with ions, and dissipate more rapidly with distance, scaling with $1/r^2$ (ion-dipole) or $1/r^3$ (dipole-dipole). Coulombic interactions can be attractive or repulsive and they can be modulated, in the case of macromolecules and surfaces, via ionic strength, with high concentrations of small ions effectively shielding charges carried by polymers or surfaces.*[1]*

Hydrogen bonding is an attractive interaction of the form A-H···B, where A and B are both highly electronegative elements and B possesses a lone pair of electrons; A is known as the

hydrogen bond donor and B as the acceptor. Nitrogen, oxygen, and fluorine are the most effective participants (both as A or B) in hydrogen bonding, although anionic species may also participate as acceptors. Hydrogen bonding, whose energy is generally ~20 kJ/mol, can be described in purely electrostatic terms as the attractive interaction between the partial positive charge on the proton and the partial negative charge of the acceptor, or in terms of molecular orbital theory as the formation of three delocalized molecular orbitals to which A, B, and H all contribute one atomic orbital. As the interaction depends on orbital overlap, it is nearly a contact interaction, appearing when A-H touches B and disappearing as soon as they are separated. Hydrogen bonding between macromolecules and surfaces can be disrupted by the addition of chaotropic agents, small molecules with high hydrogen bonding potential and mobility which effectively screen polymer-surface and polymer-polymer interactions analogously to ionic shielding of electrostatics.*[2]*

The name "van der Waals (vdW) forces" refers to a class of interactions related to dipole and induced-dipole interactions at an atomic level. There are three major types of vdW forces: Keesom interactions, which occur between two permanent dipoles, Debye interactions, which occur between an induced dipole and a permanent dipole, and London interactions, which occur between two induced dipoles. London interactions, often referred to as the dispersion force, derive from the spontaneous formation of transient dipoles due to fluctuations in a molecule's electron density. These dipoles then induce polarization of neighboring molecules, leading to dipolar attraction forces. London forces are of particular importance to adsorption phenomena and thin film stability as they are omnipresent, occurring even between neutral compounds, and act at a relatively long range (0.2 – 10 nm) compared to other atomic and molecular-level forces. Carbon atoms within aliphatic chains can display London binding energies on the order of 2.5 kJ/mol. All of the vdW forces scale with r^{-6} and are attractive, with the exception of interactions between dissimilar particles in a medium whose Hamaker constant (a measure of vdW interaction potential) is between those of the particles.*[2, 3]*

While non-covalent interactions are individually much weaker than covalent bonds, when macromolecules with many weak interaction groups are considered, the cumulative interaction energy can be very large and on the order of covalent bonding.

The central theme of this chapter will be the use of non-covalent interactions to direct bottom-up assembly of microstructures and especially the ability of chemically-patterned surfaces, described in Chapter 1, to direct regioselective adsorption of macromolecular species. Patterned deposition of single polymeric layers, inorganic species, and polyelectrolyte multilayer assemblies will be reviewed before discussion of the specific objectives and strategies for the work to be reported in Chapter 2.

2.1.2 Surface-Directed Patterned Assembly

Selective dewetting of substrates with patterns of hydrophobic and hydrophilic regions was one of the first examples of surface-directed assembly of three-dimensional features. Liquid polyurethane prepolymer applied on a surface patterned with methyl- and carboxylic acid-terminated SAMs will selectively dewet the hydrophobic methyl surface; UV can then be used to crosslink in place a robust polyurethane coating constrained to the hydrophilic regions of the pattern.*[4]* Dewetting approaches have also been used to form patterned crystalline structures by evaporation of electrolyte solutions over hydrophilic/hydrophobic surfaces.*[5]* The ability of certain chemical functionalities to promote or prevent nucleation allows patterned SAMs to direct chemical vapor deposition (CVD) such as the deposition of $LiNbO_3$ exclusively over the polar regions of a polar/hydrophobic pattern; hydrophobic methyl-terminated SAMs have also been used to prevent CVD copper deposition.*[6]*

LbL assembly, a simple but elegant approach to the creation of polymer composite films (see Chapter 1), can be made yet more powerful if it can be patterned during assembly rather than through post-treatments such as shadow-masked etching. Hammond and Whitesides first demonstrated that chemically patterned surfaces (in the original case, a carboxylic acid/oligo(ethylene glycol) thiolate SAM) can direct the adsorption of certain polyelectrolyte multilayered films.*[7]* Similarly, Rubner and coworkers showed that fluoropolymer substrates selectively defluorinated via shadow-masked plasma treatment prevented deposition of

poly(aniline)/poly(styrene sulfonate) (PANI/SPS) and poly(pyrrole)/SPS (PPY/SPS) multilayers outside of the defluorinated regions.*[8]*

Ionic content, already known to have a strong influence on LbL adsorption via its modulation of intra-polymeric electrostatic repulsion, was also found to affect selectivity. As ionic strength increases, the thickness of the layers adsorbed on the attractive surface usually increases, effectively increasing selectivity. However, as ionic shielding of the polyelectrolyte and surface charges increases, the electrostatic driving force for adsorption decreases, and past some critical salt concentration (around 1 M for NaCl) no adsorption occurs at all.*[9]* Ion type as well as concentration has an effect, with the smallest halogenate ion investigated, chloride, contributing to higher selectivity than the larger bromide and iodide ions. These experimental results are consistent with van de Steeg's earlier theoretical modeling of the effects of ionic strength and ion type on the adsorption of single polyelectrolyte layers.*[10, 11]*

Clark and Hammond also found that while the molecular weight of polyelectrolytes has limited effect on the thickness of LbL films formed, it does have a significant influence on the regioselectivity of adsorption, with shorter chains providing the best feature resolution while extremely large chains can allow chains to bridge the resist surface. Adding an ultrasonication step to the LbL assembly cycle further improves selectivity by removing loosely-bound material.*[12]*

Strikingly, seemingly-similar polyelectrolytes can exhibit distinctly different and even opposite selectivity behavior. Under certain pH conditions, the primary polyamine poly(allyl amine hydrochloride) prefers to adsorb on the hydrophobic EG region rather than COOH (partially charged at this pH), while linear poly(ethylene imine), a more hydrophilic secondary amine, displays the more common preference for the charged surface and resistance to EG.*[13]* These surprising results were confirmed by chemical force microscopy studies of the interaction strength between each polyamine and each surface at a range of pH conditions.*[14]* It is thought that the highly hydrated LPEI backbone is sterically hindered from adsorbing on the equally highly-hydrated oligo-ethylene oxide, while hydrogen bonding and hydrophobic interactions encourage complexation of PAH with the EG surface but only over a very specific pH range.

The nature of oligo(ethylene glycol)'s and poly(ethylene glycol)'s adsorption resistance has been the subject of much study, especially as relates to protein adhesion control. Solvation of OEG appears to be critical, with dehydrated OEG surfaces offering no protein resistance.*[15]*

Jeon and coworkers evaluated the different interactions possible between PEG and found that the principal competing forces are a steric repulsion, due to solvation and conformational entropy of PEG chains, and an attractive hydrophobic interaction, with van der Waals forces contributing little.*[16, 17]* Via ab initio Hartree-Fock methods, Kreuzer and Grunze modeled the interactions of water with OEG-terminated SAMs when OEG segments were in their helical versus planar forms, concluding that the helical conformation binds water much more strongly than the planar, leading to greater resistance. Their theoretical results also support the experimental observation that less dense, more disordered OEG surfaces also display greater adsorption resistance due to hydration and entropic effects.*[18, 19]*

By sequential layer-by-layer assembly of polyelectrolyte pairs with opposite selectivity, lateral heterostructures can be created on patterned surfaces. Exploiting PAH's preference for adsorption on an EG surface, Hammond and coworkers were able to build PDAC- and PAH-directed multilayered films, each containing a different fluorescent marker, side-by-side on a patterned surface without need for etching or dissolution steps, as is usually required for this kind of heterostructure construction. However, it is often necessary to cap the first LbL system with some kind of adsorption-resistant functionality to avoid overlayering it with the second LbL system, a limitation we hope to address in this work.*[20, 21]* Polymeric substrates patterned by POPS have proven equally capable of directing LbL adsorption, allowing for many more applications in realms where SAM formation on surfaces is impossible or impractical. In particular, a block co-polymer combining a charged segment with a poly(ethylene oxide) segment has been stamped atop a LbL film and found to exhibit the same resistance to the adsorption of most polyelectrolytes as the oligo-ethylene glycol-terminated EG SAM.*[22, 23]*

Chemically-patterned surfaces have also been used to template the adsorption of non-linear macromolecules and colloidal species, a topic that will be discussed in detail in Chapter 3.

2.1.3 Interactions of perfluorinated species and surfaces

The aim of the work presented in this chapter is the expansion of selective adsorption capabilities by the identification and characterization of new controlling interactions. Perfluorinated materials and surfaces are of considerable interest for selective adsorption applications due to their extremely low wettability and surface energy, and thiols terminated by partially or fully perfluorinated alkyl chains provide an efficient route to the creation of well-ordered SAMs presenting a fluorinated surface. Given the larger van der Waals radius of fluorine compared to hydrogen, these SAMs typically display packing densities 10-25% lower than those of comparable alkylthiol SAMs.*[24]* However, unlike alkyl thiols, perfluorinated thiol SAMs conserve their regular molecular orientation and order on gold even when sparse or prepared from a mixture of perfluoroalkylthiols of different lengths.*[25]* The exact molecular orientation of perfluorinated SAMs, which affects their ionic permeability and wettability, is chiefly determined by the length of the perfluorinated segment of the thiol.*[26]*

While CF_3-terminated and perfluorinated ($HS-(CH_2)_n-CF_3$ and $HS-(CH_2)_n-(CF_2)_m-CF_3$) SAMs exhibit significantly lower surface energy than comparable methyl-terminated SAMs and are generally less wettable by both polar and apolar liquids, SAMs prepared from alkylthiols terminated by a single perfluorinated group are actually more easily wet by water and other polar species like glycerol than the equivalent methyl-terminated surfaces. This surprising behavior is thought to stem from the existence of CF_3-CH_2 dipoles at the surface; C-F···H-O hydrogen bonding has also been proposed to contribute to the improved wettability of CF_3-terminated SAMs by polar liquids, but the fact that perfluorinated SAMs show no such wettability makes it unlikely that hydrogen bonding has more than a minor role.*[24]*

The above-described characteristics of perfluorinated thiols have led to their consideration for use in surface-directed adsorption and this thesis will include study of the adsorption of LbL films on continuous and patterned perfluorinated SAMs. The Whitesides group has previously examined the adsorption of micron-scale charged gold disks and report that CF_3-terminated surfaces resist deposition of both positively and negatively charged disks, suggesting they might be effective in preventing polyelectrolyte deposition as well.*[27]*

However, other groups have characterized such surfaces via chemical force microscopy and surface potential measurements and found them to be negatively charged. Evans and Ulman propose that the negative surface potential of perfluorinated surfaces is due to the strong electronegativity of fluorine atoms, but Lee and coworkers suggest that the high solubility of gases in fluorocarbon species could also be involved, with dissolved CO_2 ionizing at the perfluorinated interface. This theory is of considerable interest, as it would apply to perfluorinated thiols as well as merely CF_3-terminated alkyl thiols.*[28, 29]* In the consideration of perfluorinated materials for adsorption resists, it should be noted that fluorocarbons are not universally inert; to the contrary, halogen bonding with electron-donating groups such as amine and pyrididyl nitrogen atoms can actually be used to direct non-covalent self-assembly.*[30]*

In this chapter, several approaches to directed assembly via non-specific electrostatic and hydrophobic interactions will be considered. Adsorption at perfluorinated surfaces will be examined first, followed by use of a thermodynamic model for polyelectrolyte adsorption to explore possible theoretical rationales for observed selectivity trends.

2.2 Perfluorinated Surfaces and Polyelectrolytes

2.2.1 Materials and Methods

2.2.1.1. Template Preparation

Chemically-patterned templates were created by micro-contact printing (μcp) of alkanethiols on gold substrates. Test-grade silicon wafers with orientation <1-0-0> were obtained from Silicon Quest International and coated with a 1000 Å layer of gold over a 100 Å adhesion layer of chromium using a thermal evaporator. 16-mercaptohexadecanoic acid (15-COOH), 12-mercaptododecanoic acid (11-COOH), 16-mercaptohexadecane ($CH_3$15), and 12-mercaptododecane ($CH_3$11) were purchased from Sigma-Aldrich. 1H,1H,2H,2H-Perfluorooctanethiol (7-CF_3) and 1H,1H,2H,2H-perfluorohexanethiol (5-CF_3) were obtained from Oakwood Products. 11-mercaptoundecyltriethylene glycol (EG) was synthesized in our lab according to published procedures.*[31]* All thiols were used as delivered, without further purification.

Chromium photo masks (Advanced Reproductions) and corresponding silicon masters (Microsystems Technology Laboratory, MIT) were prepared as templates for poly(dimethylsiloxane) (PDMS, Sylgard 184, Dow-Corning) stamps. Several different stamp patterns were used, including stripes of varying width and distance from each other, and circles or squares printed with both positive (ink transferred to isolated circular or square regions) and negative (ink transferred to continuous background around empty circular or square regions) stamps. Stripe patterns were generally of 1-20 μm size, while circle and square stamps were of 50-150 μm size. Prior to use, PDMS stamps were washed with soap and water, rinsed with MilliQ water and dried under nitrogen flow before being inked with concentrated (10 mM or saturated) solutions of the desired thiol in hexadecane. Nitrogen flow was used to fully evaporate the carrier solvent before bringing the stamp surface into contact with a freshly prepared gold-coated substrate. After 1 min, the stamp was removed and the surface was rinsed with ethanol and dried under nitrogen flow before being immersed for 5-60 min in a second thiol solution,

generally prepared at 2 mM concentration in ethanol. The resulting patterned surfaces were again rinsed with ethanol, dried under nitrogen flow, and stored under vacuum until use. To prepare homogeneous (non-patterned) surfaces, only the latter immersion step was used.

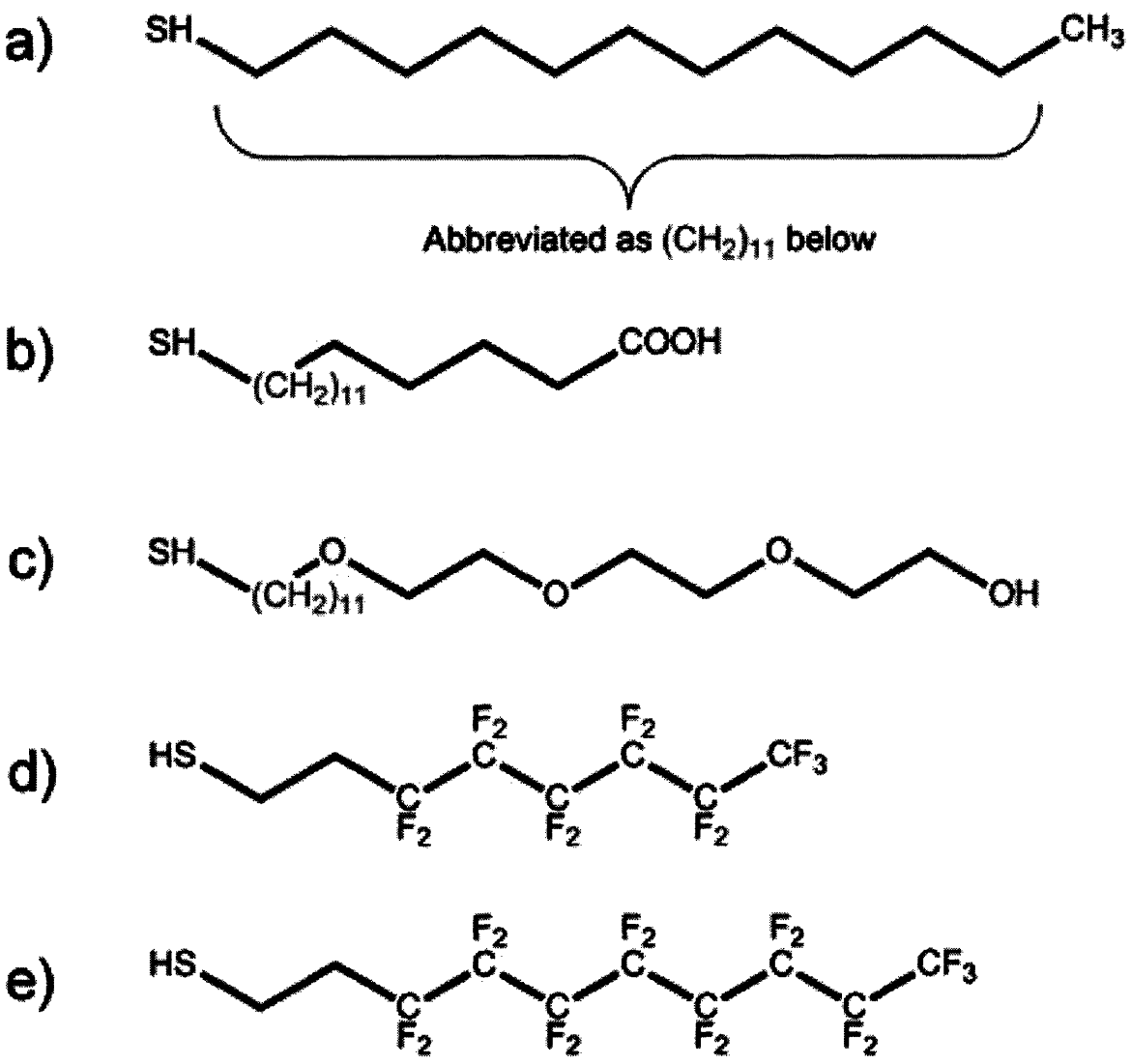

Figure 2.2.1.1. Chemical structure of thiols used in this chapter: 11-mercaptododecane (**a**), 15-mercaptohexadecanoic acid (**b**), 11-mercaptoundecyltriethylene glycol (**c**), 1H,1H,2H,2H-perfluorooctanethiol (**d**), and 1H,1H,2H,2H-perfluorohexanethiol (**e**).

2.2.1.2. Polyelectrolyte Multilayer Assembly

Polyelectrolyte multilayers were assembled on chemically-patterned substrates via the layer-by-layer technique. Sulfonated poly(styrene) (SPS, 70,000 g/mol) and poly(diallydimethylammonium chloride) (PDAC, 100,000-200,000 g/mol) were obtained from Sigma-Aldrich. Linear poly(ethyleneimine) (LPEI, 35,000 g/mol) was purchased from Polysciences. Aqueous polyelectrolyte solutions were prepared in MilliQ-filtered water (18 MΩ*cm resistivity) at concentrations of 20 mM for PDAC and LPEI and 10 mM for SPS. All polyelectrolyte concentrations are calculated on a repeat-unit basis. Poly(tetrafluoroethylene-*co*-perfluoro-3,6-dioxa-4-methyl-7-octenesulfonic acid) (Nafion®) was obtained from Fluka as the Nafion® 117 formulation, a 5 wt% solution of the polymer in an unspecified mixture of light alcohols. Nafion® 117 has a repeat unit molecular weight of 1100 g/mol per sulfonic acid group; the polymer molecular weight is unknown. The as-received solution was diluted with MilliQ water for a final Nafion® concentration of 2 mM and a final alcohol concentration of 4.4%. Polyelectrolyte solutions were adjusted to the desired pH by addition of dilute HCl or NaOH. In some cases, sodium chloride (NaCl, from Sigma-Aldrich) was added at a concentration of 0.1 M to increase ionic strength.

A modified Carl Zeiss DS50 programmable slide stainer equipped with an ultrasonication bath (Advanced Sonic Processing) was used to automate bilayer addition. For each bilayer cycle, the substrate was dipped into each polyelectrolyte solution for 15-20 min with two 1.5 min water immersions to rinse between polycation and polyanion addition; between bilayer cycles the substrate was sonicated for 3 min to remove any loosely-bound material. Rinse baths were adjusted to the same pH as the polyelectrolyte solutions being used. After assembly, films were rinsed with MilliQ water, dried under nitrogen flow, and stored under vacuum until characterization.

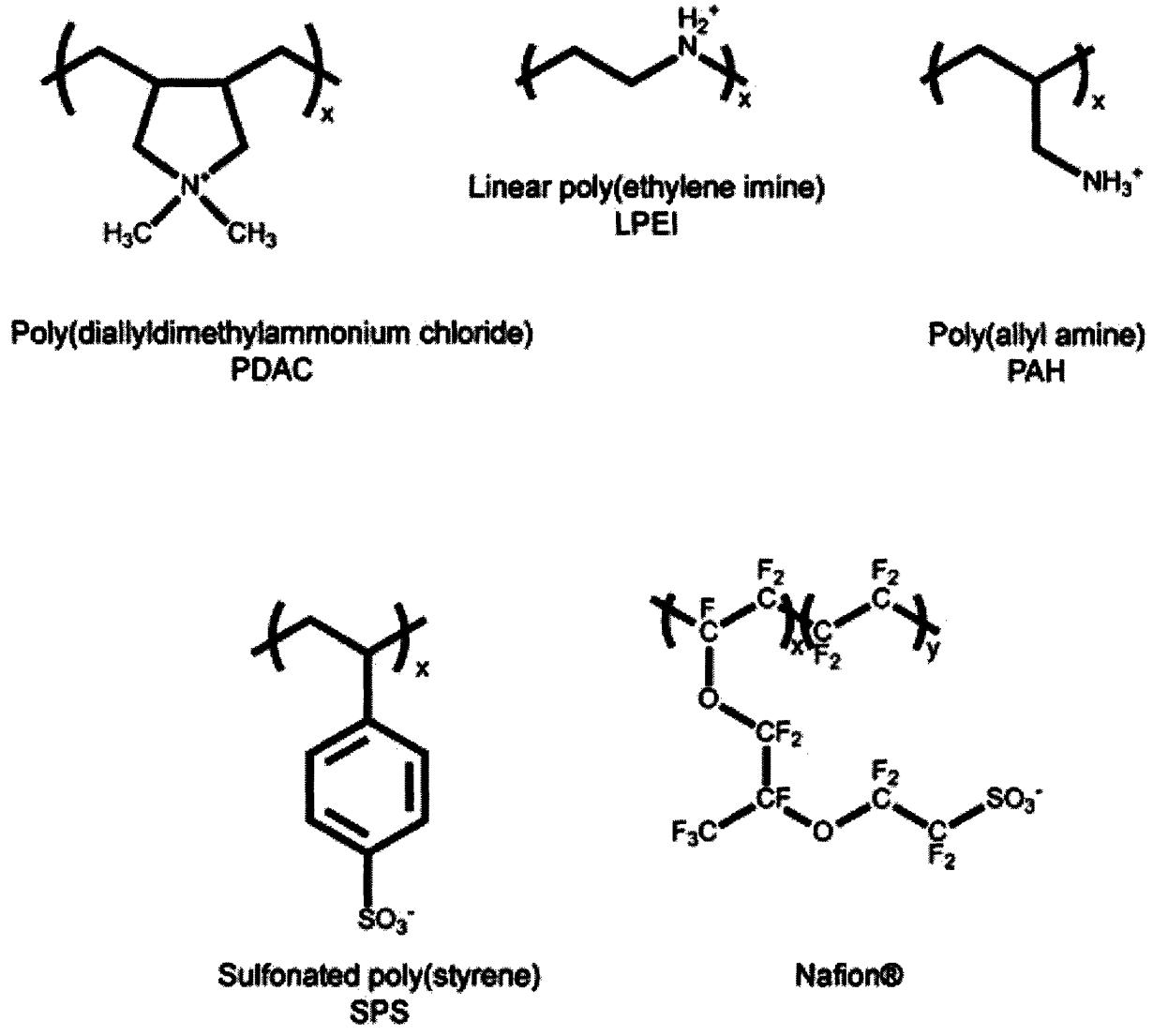

Figure 2.2.1.2. Chemical structures of the polyelectrolytes used in this chapter.

2.2.1.3. Characterization

Polyelectrolyte multilayer films assembled on chemically-patterned substrates were studied to evaluate the amount adsorbed on each type of surface. Ellipsometry (LSE Stokes Ellipsometer from Gaertner Scientific) was used to determine the thickness of films built on homogeneous (non-patterned) substrates; very thick films were also studied by profilometry (P10 Surface Profiler from KLA-Tencor). Films assembled on patterned substrates were observed first by optical microscopy (Zeiss Axioplan) and then by atomic force microscopy (Dimension 3000 SPM from Veeco Instruments). Prior to film assembly, thiol-functionalized gold substrates were also characterized by ellipsometry, goniometry, and XPS (Kratos AXIS).

2.2.2 LbL Assembly on Homogeneous SAMs

2.2.2.1. SAM Characterization

Continuous (non-patterned) self-assembled monolayers of 5-CF_3, 7-CF_3, 11-COOH, EG, and 11-CH_3 were built on silicon wafers coated with 1000 Å of gold over a 100 Å adhesion layer of titanium or chromium. For creation of continuous layers, substrates were immersed in 2 mM solutions of thiols in absolute ethanol; dipping times varied from 30 minutes (for COOH) to 24 hours (for the perfluorinated thiols). Published data regarding perfluorinated thiols consistently reports that formation of a dense, ordered SAM is slow; however, the reported necessary times are inconsistent and vary from 24 to 96 hours*[24, 28, 32, 33]*. Given the molecular structures of 5-CF_3 and 7-CF_3 and the tilt normally found in well-packed perfluorothiol monolayers, their SAMs are expected to have thicknesses around 10 Å, close to the lower limit for detection by standard single-wavelength ellipsometry. Perfluorinated SAMs allowed less than 12 hours to assemble gave inconsistent results and sometimes could not be detected by ellipsometry at all, whereas substrates immersed for 24 vs. 120 hours could not be distinguished by ellipsometry nor in their use as adsorption templates, so 24 hours was judged sufficient for our purposes. In addition to ellipsometry, SAM formation was also confirmed by XPS, which found a nearly 2:1 ratio of fluorine to carbon atoms on a gold substrate immersed for 24 hours in 7-CF_3, consistent with the 17:10 ratio of F:C in 7-CF_3 ($C_{10}H_5F_{17}S$), especially given the particular sensitivity of XPS towards fluorine detection. The thicknesses measured by ellipsometry for 5-CF_3, 7-CF_3, 11-COOH, EG, and 11-CH_3 SAMs assembled for 24 hours on freshly-prepared and freshly-cleaned gold substrates are reported in Table 2.3.1.

5-CF_3	**7-CF_3**	**11-COOH**	**EG**	**11-CH_3**
10.0 Å +/- 1.5	11.0 Å +/- 1.0	12.0 Å +/- 1.0	16.5 Å +/- 0.25	11.0 Å +/- 0.5

Table 2.2.2.1. Ellipsometric thickness of alkanethiolate SAMs used in this chapter. Thiols were assembled from 2 mM ethanol solutions overnight; thickness data were averaged over ten points.

2.2.2.2. LbL Assembly

Ten bilayers of the strong polycation PDAC and the strong polyanion SPS were built on unpatterned substrates of varying surface functionality by use of an automated dipping machine. In some cases, 0.1 M sodium chloride was added to reduce intra-chain electrostatic repulsion via ionic shielding; the chosen salt concentration was that previously reported to yield the thickest PDAC/SPS multilayers*[9, 10]*. Thicknesses determined for $(PDAC/SPS)_{10}$ films on the various substrates are reported in Figure 2.2.2.2.1; these thicknesses were calculated by subtracting the appropriate SAM height from the average of ten ellipsometric measurements on different regions of the sample.

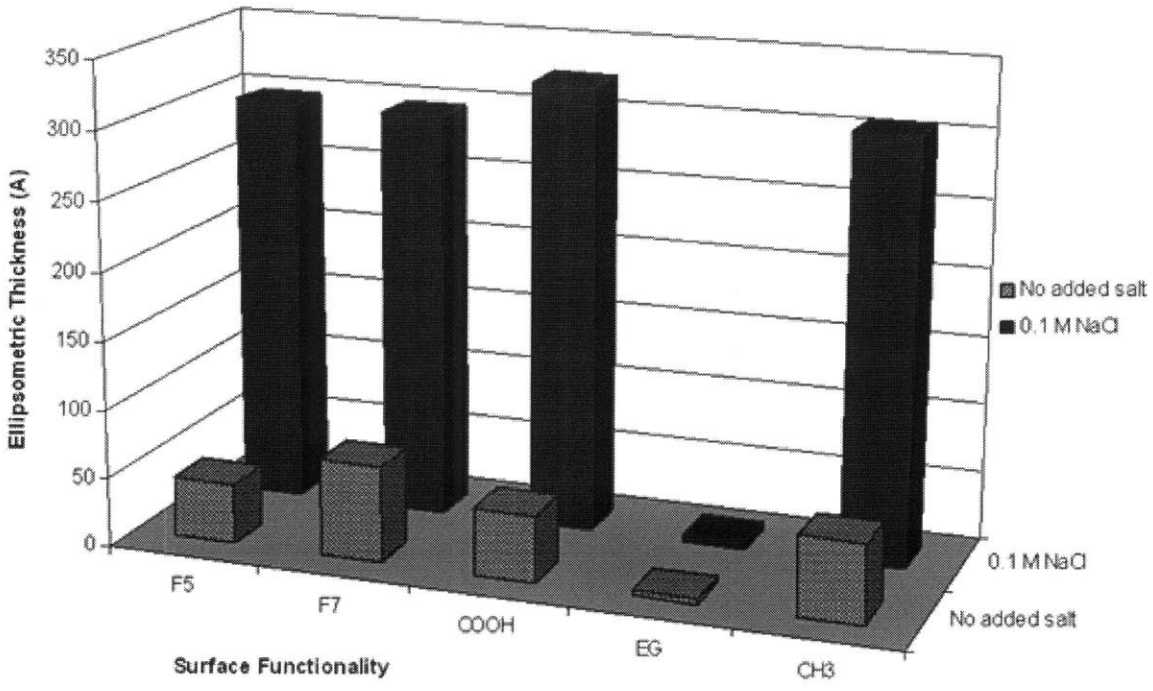

Figure 2.2.2.2.1. Ellipsometric thickness of $(PDAC/SPS)_{10}$ films auto-dipped onto alkanethiolate SAMs in the absence and presence of salt-induced electrostatic shielding.

Contrary to expectations, the perfluorinated SAMs did not prove adsorption-resistant and instead allowed for film growth nearly as thick as on carboxylic acid- and methyl-terminated SAMs. Atomic force microscopy was used to study the nature of the LbL films assembled on

perfluorinated SAMs; in Figure 2.2.2.2.2, films assembled in the presence and absence of added electrostatic shielding are shown.

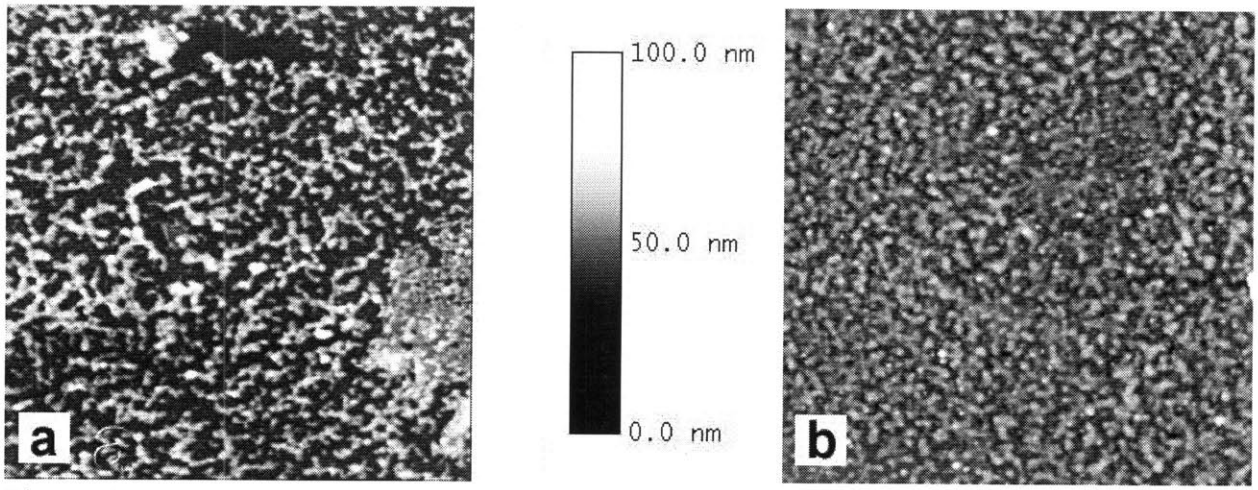

Figure 2.2.2.2.2. 5 μm x 5 μm atomic force microscope scans of $(PDAC/SPS)_{10}$ films built on continuous perfluorinated SAMs in the absence (**a**) and presence (**b**) of salt-induced electrostatic shielding.

AFM imaging revealed that films built on perfluorinated SAMs had a rough, mottled morphology. Our ellipsometry data were collected using an instrument with a 1 mm-wide laser beam, meaning that calculated thicknesses are actually the average thickness within an area roughly $8x10^6$ μm^2. However, from AFM it is clear that the polyelectrolytes deposited in spidery clusters on the order of 100 nm wide in the absence of electrostatic shielding and that surrounding regions saw no adsorption at all (Figure 2.2.2.2.2.a). Comparing the ellipsometric thickness with the feature heights observed by AFM (both measurements were performed on dry films), we see that the patches of adsorbed film are actually up to 900 Å high and that it is the surrounding bare regions that lower the ellipsometric thickness to less than 100 Å. Such films had an average surface roughness of 9.8 nm. When 0.1 M NaCl was added to increase electrostatic shielding (Figure 2.2.2.2.2.b), surface coverage and smoothness improved greatly – the average feature height seen by AFM, 300 Å, is a good match for the ellipsometric data, and the roughness decreased to 6.0 nm.

To see whether perfluorinated polyelectrolytes had any specific interactions with perfluorinated SAMs not exhibited by other polyelectrolytes or on other surface functionalities, LbL films were built using Nafion® paired with a variety of polyamines. Nafion® is a random copolymer of poly(tetrafluoroethylene) (PTFE) and poly(tetrafluoroethylene-*co*-perfluoro-3,6-

dioxa-4-methyl-7-octenesulfonic acid) often used to make membranes and ion-conductive layers. A polyanion, Nafion® was paired with polycations containing primary (PAH), secondary (LPEI), or quaternary (PDAC) amine groups. Assembly was studied in the presence and absence of added electrostatic shielding, with 0.025 M NaCl being the salt concentration identified by others as leading to the best Nafion®-containing LbL films*[34]*. Ellipsometric thicknesses of these films are reported in Figure 2.2.2.2.3 below.

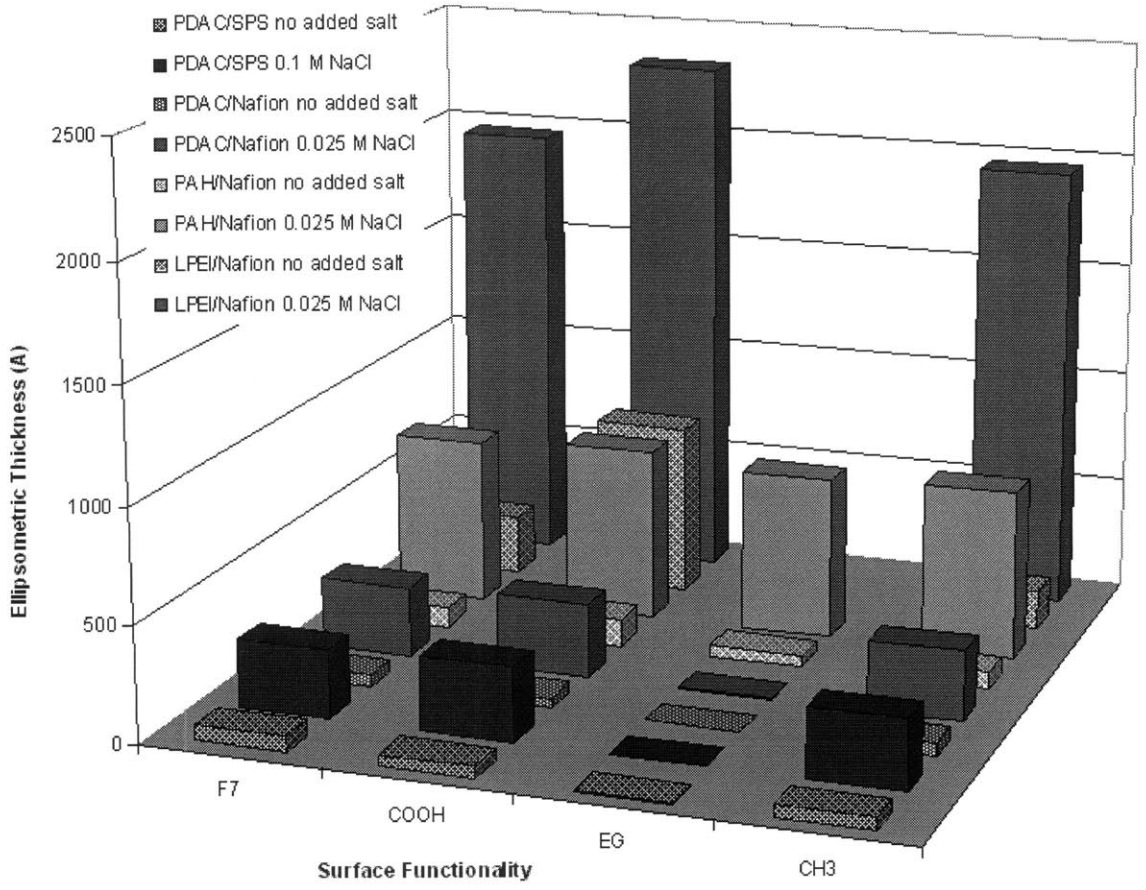

Figure 2.2.2.2.3. Ellipsometric thickness of 10-bilayer Nafion® -containing films and (PDAC/SPS) reference films auto-dipped onto homogeneous alkanethiolate SAMs in the absence and presence of salt-induced electrostatic shielding.

It would appear that the inclusion of Nafion® had little effect and that only the choice of polycation influenced adsorbed layer thickness. Films built using PDAC, LPEI, or PAH as the polycation had very different thicknesses, and, in some cases, preferences for certain surfaces, while (PDAC/Nafion®) and (PDAC/SPS) films assembled nearly identically. In all cases,

increasing electrostatic shielding led to much thicker adsorption, as reported previously and expected, given the loopier adsorption made possible by a reduction in intrachain repulsion*[9, 10, 34]*. The successful assembly on CF_3 of all multilayer systems considered is consistent with the slightly negative surface charge of perfluorinated SAMs reported by some investigators rather than others' descriptions of these surfaces as neutral and adsorption-resistant*[27, 28]*. Based on these results alone, perfluorinated thiols would not seem ideal for the creation of adsorption-controlling patterned surfaces. However, surprising observations were made when these same multilayer systems were assembled on substrates patterned by micro-contact printing of CF_3 and other SAMs.

2.2.3 LbL Assembly on Patterned SAMs

Micron-scale patterns of chemical functionality were created on gold substrates via micro-contact printing (μCP) of alkanethiols; after patterning, ten bilayers of a range of polycation/polyanion pairs were built on these substrates by use of an automated dipping machine. Films were built in both the presence and absence of salt-induced electrostatic shielding, using the same conditions as described for assembly on continuous substrates in 2.2.2. The resulting surfaces were characterized by optical and atomic force microscopy, with AFM normally providing the greatest information. Profilometry was also performed, but most films were found to be too thin for accurate profilometry.

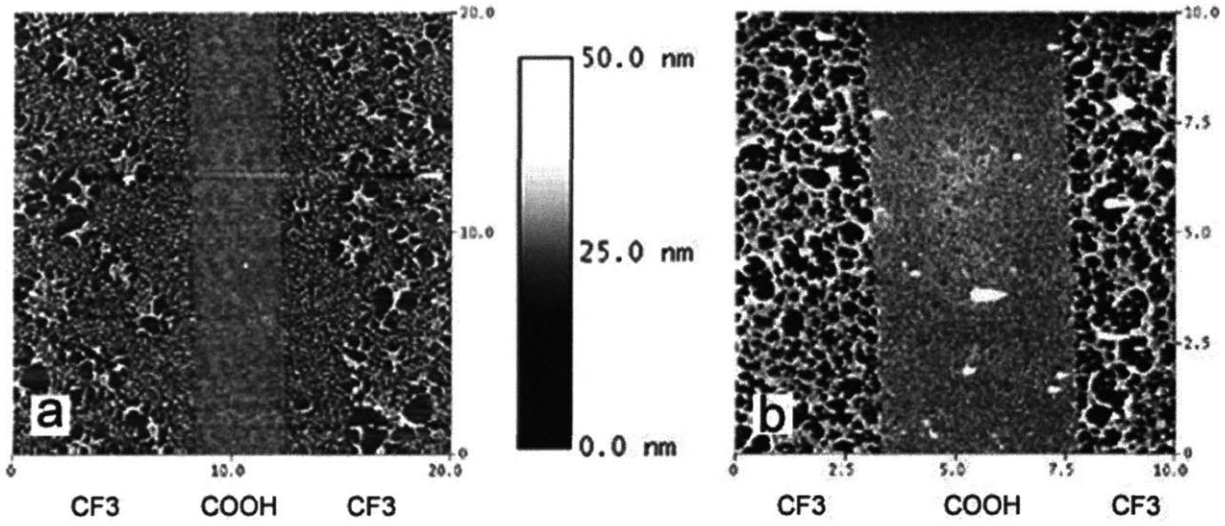

Figure 2.2.3.1. 20 μm x 20 μm (**a**) and 10 μm x 10 μm (**b**) AFM scans of $(PDAC/SPS)_{10}$ multilayers assembled on substrates stamped with COOH thiol and back-filled by immersion in CF_3 thiol. Substrates **a** and **b** were prepared identically at different dates.

Multilayers of the strong polyelectrolytes (PDAC/SPS) adsorbed distinctly differently on acid and perfluoro-terminated regions in the absence of salt-induced electrostatic screening, but the patterning was only in terms of the film morphology. Within carboxylic acid regions, the adsorbed film was thin and smooth, whereas film adsorbed atop perfluoro regions was very irregular, with spidery clusters of film surrounded by empty regions (See Figure 2.2.3.1).

Notably, the film clusters within perfluoro regions were of greater height than the smooth film on carboxylic acid regions. It was at first thought that contamination of the gold source used for coating of silicon wafers was leading to poor SAM qualities, allowing polyelectrolytes to deposit on the defects within the perfluoro region and providing a foothold for subsequent multilayer accumulation. However, identical film morphologies were observed when gold substrates of verified quality were used, as well as when (PDAC/SPS) were assembled under identical conditions on continuous perfluoro SAMs (see Figure 2.2.2.2.2.a); quadrupling the perfluorothiol assembly time from 24 to 96 hours also had no significant effect. Clearly, perfluorinated SAMs do not prevent (PDAC/SPS) adsorption, but merely lead to lower film quality. The pattern is expected to disappear with continued addition of (PDAC/SPS) multilayers, with each deposited layer providing a slightly larger, smoother foothold for the next.

Identically-prepared $COOH/CF_3$ templates were then used for $(LPEI/SPS)_{10}$ and $(LPEI/Nafion^{®})_{10}$ film assembly.

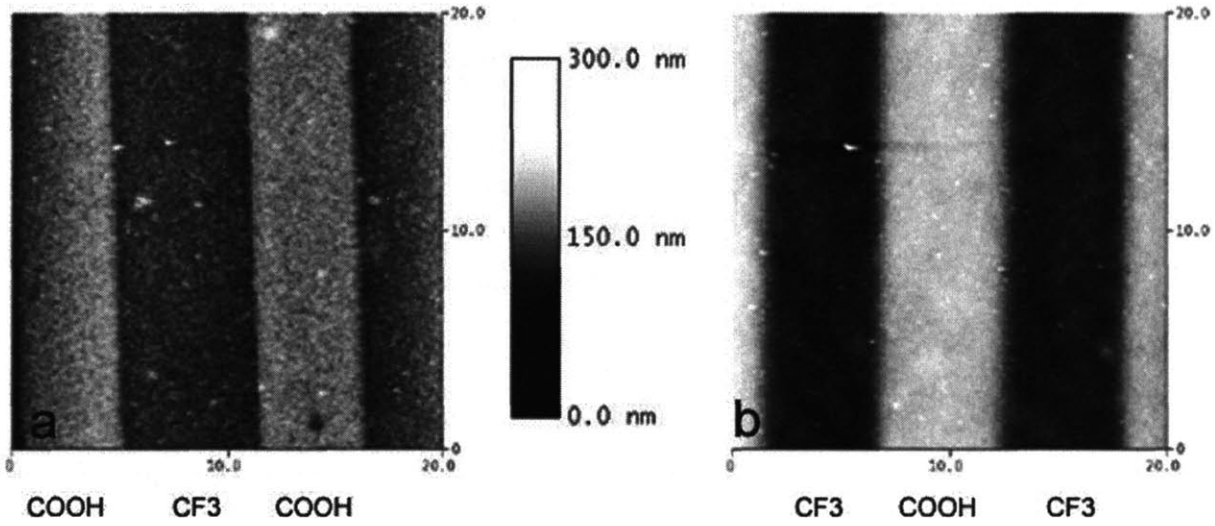

Figure 2.2.3.2. 20 μm x 20 μm AFM scans of $(LPEI/Nafion^{®})_{10}$ multilayers, assembled in the absence (**a**) and presence (**b**) of salt-induced electrostatic shielding, on substrates stamped with COOH thiol and back-filled by immersion in CF_3 thiol.

Clear patterning was again observed for $(LPEI/Nafion^{®})$ multilayers, with thick, smooth layers forming on the carboxylic acid regions and sharp definition of pattern features; when salt was added to increase electrostatic shielding, the height difference between COOH and CF_3

regions increased (see Figure 2.2.3.2). AFM examination of trenches cut into the above patterns with a sharp blade revealed that the perfluoro regions were not bare, but rather covered by a thinner but comparably smooth film. When electrostatic shielding was increased, the edges of the pattern lines became less vertical and the raised regions started to spread past the limits of the COOH regions into the CF_3 regions (see Figure 2.2.3.3). While (LPEI/Nafion®) did clearly adsorb differently on the two regions, pattern resolution can be expected to decrease with further multilayer construction as the raised regions broaden and as substrate effects weaken with increasing film thickness.

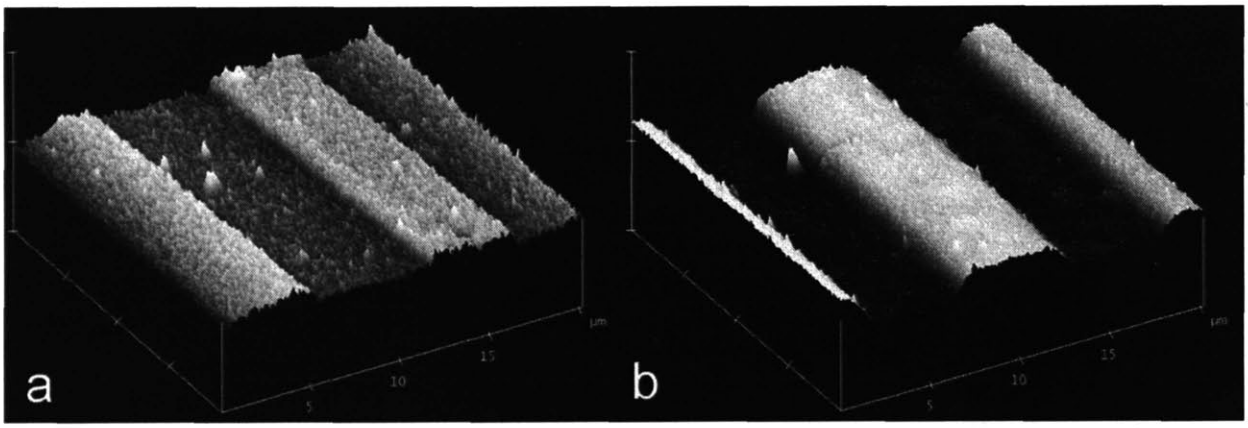

Figure 2.2.3.3. Section views of 20 μm x 20 μm AFM scans of (LPEI/Nafion®)$_{10}$ multilayers, assembled in the absence (**a**) and presence (**b**) of salt-induced electrostatic shielding, on substrates stamped with COOH thiol and back-filled by immersion in CF_3 thiol.

In Figure 2.2.3.4, different combinations of the above polyelectrolytes were studied on identical patterns to better characterize each component's influence. (PDAC/SPS) multilayers exhibited patterning, but only in terms of film morphology. When LPEI, a secondary amine with a heteroatomic backbone, was substituted for PDAC, a quaternary amine with a stiffer alkyl backbone, the morphology difference was greatly reduced and a pattern was only faintly apparent. When Nafion®, a perfluorinated polymer with sulfonic acid-terminated perfluorinated side chains, was substituted for SPS, clear patterning was observed, but the CF_3 regions were again not bare, but rather more thinly covered than the COOH regions.

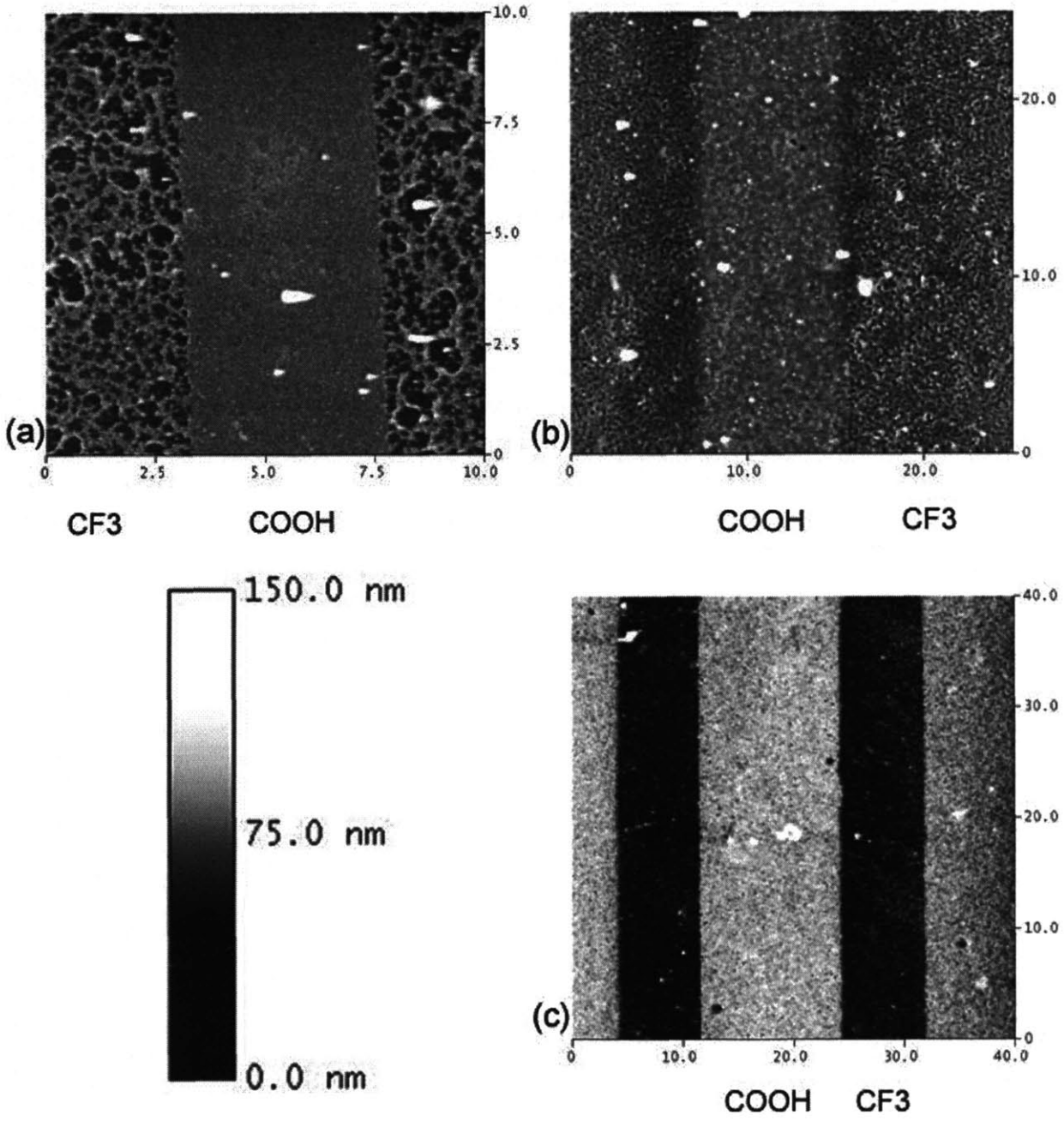

Figure 2.2.3.4. AFM scans of $(PDAC/SPS)_{10}$ (**a**), $(LPEI/SPS)_{20}$ (**b**), and (LPEI/Nafion®)$_{10}$ (**c**) multilayers, assembled in the absence of salt-induced electrostatic shielding on substrates stamped with COOH thiol and back-filled by immersion in CF_3 thiol.

Perfluorinated SAMs were explored as potential adsorption-resistant surfaces for patterned LbL film assembly, but were found to have limited effect on continuous film adsorption and to provoke patterning mostly in terms of film morphology and thickness differences, rather than preventing adsorption entirely. Clearly, the selectivity of certain LbL

systems to carboxylic versus perfluorinated surfaces is not absolute but *relative*, with films assembled on patterned substrates showing much stronger preferences than would be expected from their assembly on continuous surfaces of the same functionalities. For instance, ten bilayer (LPEI/Nafion®) films built on continuous perfluorinated surfaces with salt added for electrostatic shielding were only 50 nm thinner than those built on continuous carboxylic surfaces (see Figure 2.2.2.2.3), but when ten bilayers of (LPEI/Nafion®) were built on micron-scale patterns of carboxylic acid and perfluorinated surfaces under identical ionic-strength conditions (see Figure 2.2.3.2.b), the height difference was around 200 nm, a four-fold increase.

In the hopes of identifying a possible origin for relative selectivity phenomena, substrate effects on single polyelectrolyte and LbL adsorption were studied using a simple free energy model.

2.3 Theoretical Study of Selectivity

2.3.1 Methodology

In the 2001 publication "Anomalous Adsorption of Polyelectrolyte Layers," Mayes and coworkers sought to explain experimentally-observed supermonolayer adsorption behavior by constructing a free-energy model that captures the discrete nature of the charged surface groups by considering that "sticking" occurs between a single repeat unit and single surface charge group of equal size*[35, 36]*. This simple model will be used to examine possible theoretical origins for the relative selectivity experimentally observed in Section 2.2 by predicting the free energy of adsorption for a polyelectrolyte approaching surfaces of varying attractiveness. This free energy is calculated as the sum of contributions from conformational entropy, sticker group attraction, and intrachain repulsion. The essential equations constituting the model are reproduced in the following two pages; full details can be found in the original publications.

Free Energy of Adsorption

$$F_{ad} = F_{conf} + F_{stick} + F_{rep} \qquad \text{Eq 2.3.1}$$

Conformational entropy contribution:

$$F_{conf} = F_{elas} + F_{loop} \qquad \text{Eq 2.3.2}$$

$$\beta F_{elas} \approx \frac{3}{2}\left(\frac{R_0^2}{H^2} - 1\right) + \frac{3}{2}\left(\frac{H^2}{R_0^2} - 1\right) \qquad \text{Eq 2.3.3}$$

$$\beta F_{loop} \approx \frac{N}{n}\ln\left(\frac{H}{\sigma a}\right) - \frac{(1-\phi)}{\phi}\frac{N}{n}\ln(1-\phi) \qquad \text{Eq 2.3.4}$$

"Sticking" energy contribution:

$$\beta F_{stick} \approx -\delta \frac{N}{n} \qquad \text{Eq 2.3.5}$$

Segment-segment repulsion contribution:

Excluded volume:

$$\beta F_{vol} \approx \frac{1}{2} N\phi \qquad \text{Eq 2.3.6}$$

Electrostatic:

$$\beta F_{elec} \approx \frac{\pi N l_b \phi}{\kappa^3 H^3 a}\left(e^{-2\kappa H} - 1 + 2\kappa H\right) \qquad \text{Eq 2.3.7}$$

Variables and constants:

N	number of monomer units in chain
a	monomer segment length (in Å)
σ	number of surface sticking sites per a^2
n	loop length between sticking sites
R_0	ideal coil size
H	hydrated adsorbed layer height (in Å)
ϕ	segment volume fraction
δ	sticking energy, $\delta k_B T$ is the energy per sticker pair
l_b	Bjerrum length (in Å)
κ	Inverse Debye length (in $Å^{-1}$)
β	$1/(k_B T)$ (with k_B adjusted in terms of Å and T in K)

$$\frac{N}{n} \approx \frac{\sigma N a}{\phi H} \qquad \text{Eq 2.3.8}$$

$$R_0^2 \approx N a^2 \qquad \text{Eq 2.3.9}$$

$$l_b = \frac{e_c^{\ 2}}{4\pi\varepsilon_0\varepsilon_R k_B T} \qquad \text{Eq 2.3.10}$$

$$\kappa^2 = \frac{e_c^2}{\varepsilon_0\varepsilon_R k_B T}\sum_i z_i^2 n_{i\infty} \qquad \text{Eq 2.3.11}$$

e_c elementary charge (not to be confused with the exponential function *e* in F_{elec})

ε_0 permittivity of vacuum (adjusted in terms of Å)

ε_R dielectric constant of water at given salt conditions

z_i valence of ions of type *i*

$n_{i\infty}$ number of ions of type *i* per unit volume in bulk phase

For a given (N,a,σ,δ,l_b,κ), the corresponding equilibrium adsorbed amount Γ (Γ = ϕH/a) can be determined by minimizing the adsorption free energy F_{ad} and then comparing it to F_{mono}, the reference free energy for adsorption of a single monolayer. Minimizations were performed using the Matlab function *fminsearch*. If $F_{ad} > F_{ref}$, monolayer adsorption is predicted. If $F_{ad} < F_{ref}$, supermonolayer (loopy) adsorption is predicted.

To model layer-by-layer adsorption, the initial layer's thickness was determined as above and subsequent layer thicknesses were calculated by taking σ to be ϕ from the top-most layer. This is the "cumulative" approach from the Mayes model, which is better-suited to describing the earliest bilayers than the "iterative" model also presented. The sticking force δ can be adjusted to better describe a given polyelectrolyte pair.

The model can also be adapted to describe the behavior of weak (neutralizable) polyelectrolytes*[35]*. The only affected component of F_{ad} in such cases is F_{elec}, into which now enters *f*, the chain ionization fraction.

$$\beta F_{elec} \approx \frac{\pi N l_b f^2 \phi}{\kappa^3 H^3 a}\left(e^{-2\kappa H} - 1 + 2\kappa H\right) \qquad \text{Eq 2.3.1.12}$$

When dealing with partially-ionized polyelectrolytes, F_{mono} is calculated as previously (ϕ = 0.5*σ, H = a), but the $f^2\phi$ term in βF_{elec} is replaced with $(f\phi - 0.5*\sigma)^2 / \phi$.

$$F_{mono} = F_{ad}(\phi_{thin}, H_{thin}) \qquad \text{Eq 2.3.13}$$

$$\phi_{thin} = 0.5*\sigma \qquad \text{Eq 2.3.14}$$

$$H_{thin} = a \qquad \text{Eq 2.3.15}$$

2.3.2 Choice of Modeling Parameters

Poly(diallyldimethylammonium chloride) is a strong polycation with a quaternary amine charge group; the unit length (a for this model) is 6.2 Å. The PDAC used during the experimental observations of relative selectivity was of molecular weight 125,000 g/mol, so N ~ 1000 will be used for modeling.

Since salt-induced electrostatic shielding is known to affect selectivity, adsorption was modeled both with and without 0.1 M NaCl added. When no salt is added, the small ion concentration is equal to the polyelectrolyte concentration, which will be 0.02 M for all cases. With no added salt, $\varepsilon_R = 78.3$, so $l_b = 7.14$ Å and $\kappa = 0.0465$ Å^{-1} at 298 K; with 0.1 M NaCl added, $\varepsilon_R = 77.2$, so $l_b = 7.24$ Å and $\kappa = 0.115$ Å^{-1} at 298 K.*[37]*

Since the model is built on the assumption that all sticking sites are of equal size, exact simulation of LbL adsorption of (PDAC/SPS) is difficult, as the SPS repeat unit is much smaller than that of PDAC (2.5 Å vs. 6.2 Å). One possibility would be to consider PDAC a half-ionized polyelectrolyte of repeat unit length 3.1 Å, yielding a linear charge density approximately equal to the actual value for PDAC, and to model its adsorption using the weak-polyelectrolyte form of F_{ad}. The most obvious weakness in this representation is its inability to account for chain stiffness: true PDAC repeat units are bulky and inflexible and should be expected to behave differently than the combination of one charged and one uncharged repeat unit of equivalent total length. Chain stiffness could be taken into account by modifying the model to consider Kuhn equivalent segments rather than monomeric segments, but this would complicate the size-pairing of sticking sites. To get the most accurate qualitative insights, the adsorption of single layers of PDAC using $a = 6.2$ Å was modeled first, followed by layer-by-layer assembly of model strong polyelectrolytes with smaller $a = 2.5$ Å.

2.3.3 Adsorption of PDAC on Homogeneous Surfaces of Varying Attractiveness

2.3.3.1. Modeling intra-chain interactions

Two kinds of segment-segment repulsion are possible in PDAC: excluded-volume interactions and electrostatic self-repulsion. Using the excluded-volume form F_{vol} of F_{rep} will tend to overestimate segment-segment repulsion, while using F_{elec} will tend to underestimate it. The first task was to determine whether F_{vol}, F_{elec}, or both, should be included in F_{ad} calculations.

ϕ and H for minimal F_{ad} were calculated for N = 1000, a = 6.2 Å, $F_{rep} = F_{vol}$ *or* F_{elec}, δ = 5, and a range of σ values in the absence of added salt. The resulting layer thicknesses are reported in Figure 2.3.3.1.1. H is the hydrated layer height, but since most experimental measurements are done on dried films, so H_{dry} ($H_{dry} = \phi H$) was also calculated.

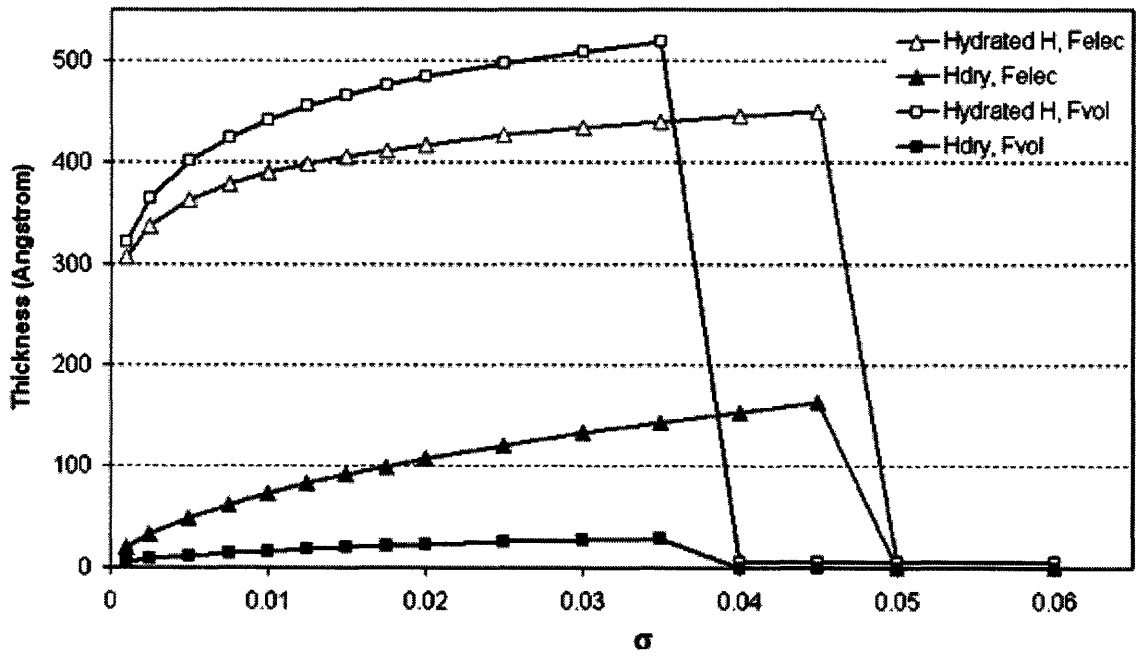

Figure 2.3.3.1.1. Comparison of excluded-volume and electrostatic forms of F_{rep}.

Clearly, F_{vol} and F_{elec} predict very different film morphologies. When F_{vol} is used, films are very thick when hydrated but sparsely-packed (ϕ on the order of 0.05), so their dried thickness does not exceed 30 Å. A transition to molecularly-thin films takes place once σ >

0.035. When F_{elec} is considered, the hydrated layer height is slightly reduced, but the segment volume fraction greatly increased, leading to dried thicknesses far greater than those calculated with F_{vol}. The transition to monolayer adsorption also takes place slightly later, for $\sigma > 0.045$. These differences are simply reflections of the fact that F_{vol} overestimates segment-segment repulsion, favoring lower segment density, while F_{elec} favors denser adsorption.

While the dried layer thicknesses for F_{vol} are closer to experimentally observed behavior for PDAC on an oppositely charged SAM in the absence of added salt, the fact that salt concentration enters only into F_{elec} requires that it be included, since experimental results clearly show an ionic concentration dependence. Thus, the question is whether to include both terms or only F_{elec} in calculating F_{rep}.

ϕ and H for minimal F_{ad} were calculated for N = 1000, a = 6.2 Å, $F_{rep} = F_{vol} + F_{elec}$, $\delta = 5$, and a range of σ values in the case of zero or 0.1 M added salt. The resulting layer thicknesses are reported in Figure 2.3.3.1.2.

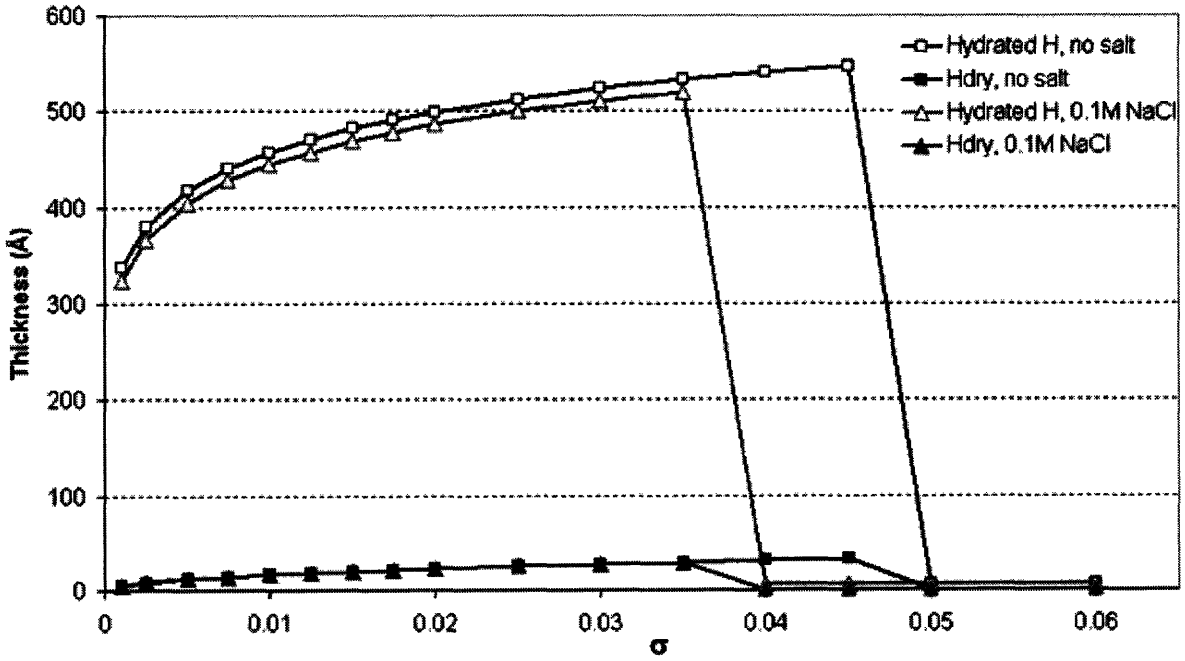

Figure 2.3.3.1.2. Adsorption behavior predicted when both electrostatic and excluded-volume contributions to F_{rep} are considered.

It is clear that under these conditions F_{vol} strongly dominates F_{rep} and virtually no increase in thickness is observed in response to increased salt concentration; F_{elec}'s sole significant influence is an increase in σ_{crit}. Thus, while F_{vol} leads to better quantitative descriptions of adsorbed PDAC thickness in the absence of shielding, F_{elec} alone must be considered in order to better qualitatively describe shielding effects. In Figure 2.3.3.1.3, PDAC adsorption on a surface with $\delta = 5$ is modeled in the absence and presence of added salt, using $F_{rep} = F_{elec}$. As one would expect and as is observed in experimental data, adding salt allows for denser layers by shielding segment-segment electrostatic repulsion and the total adsorbed amount is also increased by approximately 66%. Adding salt also reduces σ_{crit} very slightly from 0.045 to 0.04.

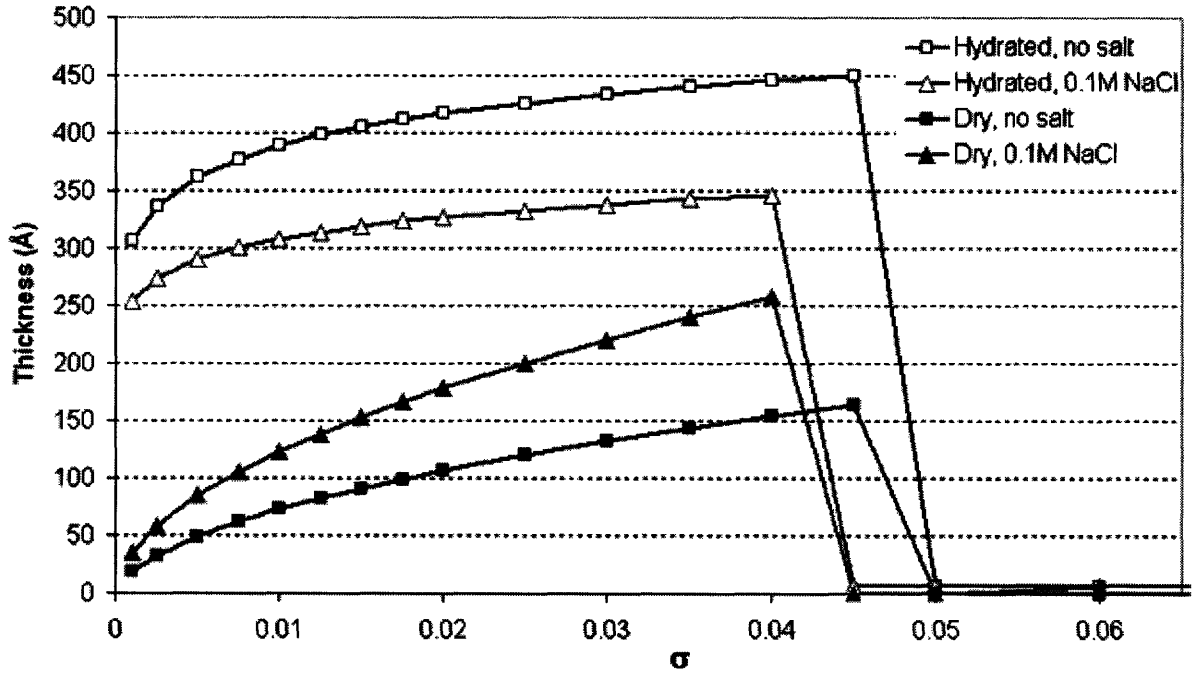

Figure 2.3.3.1.3. Predicted effect of electrostatic shielding on PDAC adsorption, neglecting excluded-volume contributions.

Having established that PDAC adsorption on an oppositely-charged surface and related shielding effects can be qualitatively described within this free energy model, the effects of surface interactions and polyelectrolyte size were studied next.

2.3.3.2. Effect of surface attractiveness

The Mayes model assumes that the interaction between the polymer and the surface is attractive; the greater δ, the greater the free energy reduction contribution from F_{stick}. While the exact nature of the interaction between PDAC and the CF_3 surface involved in the experimental observations of relative selectivity (vs. a COOH surface) is not well characterized, SAMs prepared from perfluorinated alkanethiols have been reported to have negative surface charge in water.*[28]* The charged nature of this seemingly neutral surface is thought to stem from the affinity for particular surfaces of ions naturally occurring in water. Thus, the perfluorinated surface was modeled as being electrostatically attractive to polycations, but less so than the carboxylic acid-functionalized surface. Surface S was assumed to contain groups with a strong affinity for PDAC segments (δ = 5) and surface W to contain groups with a weaker affinity (δ = 2). As previously, N = 1000 and a = 6.2 Å. The results of the free-energy minimizations for these adsorption conditions are presented in Figures 2.3.3.2.1 (in the absence of added salt) and 2.3.3.2.2 (with 0.1 M NaCl).

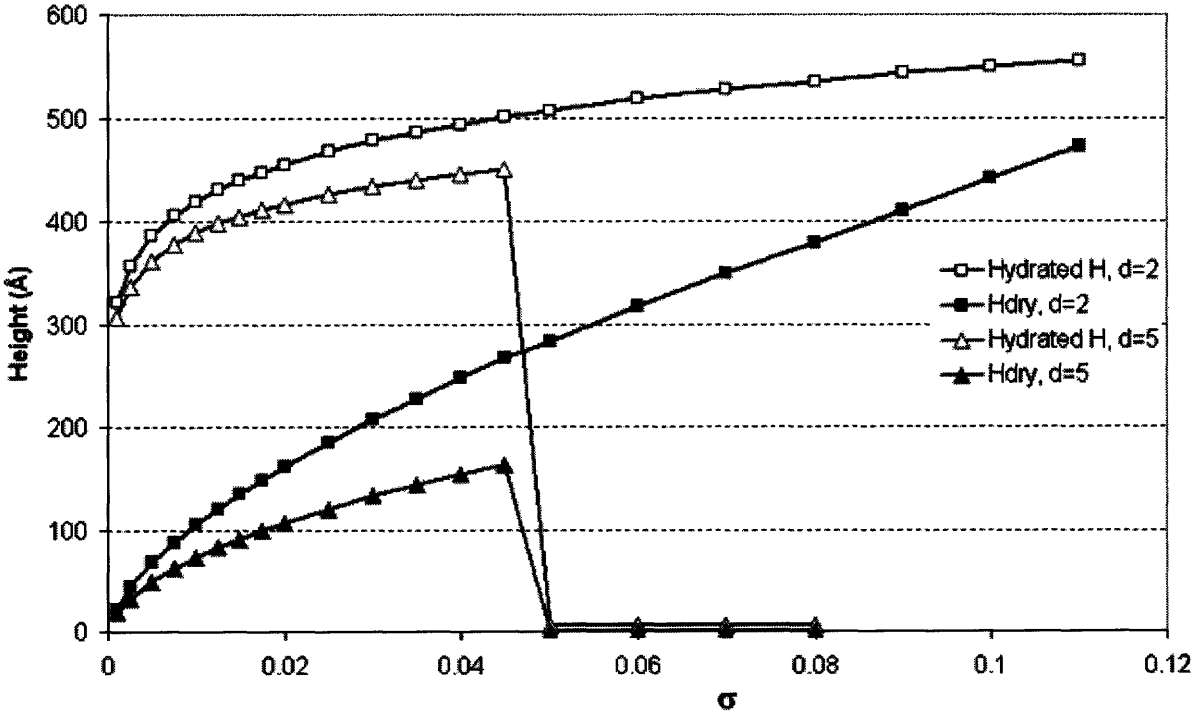

Figure 2.3.3.2.1. Predicted effect of the relative strength of sticking-site attractiveness on PDAC adsorption in the absence of electrostatic shielding.

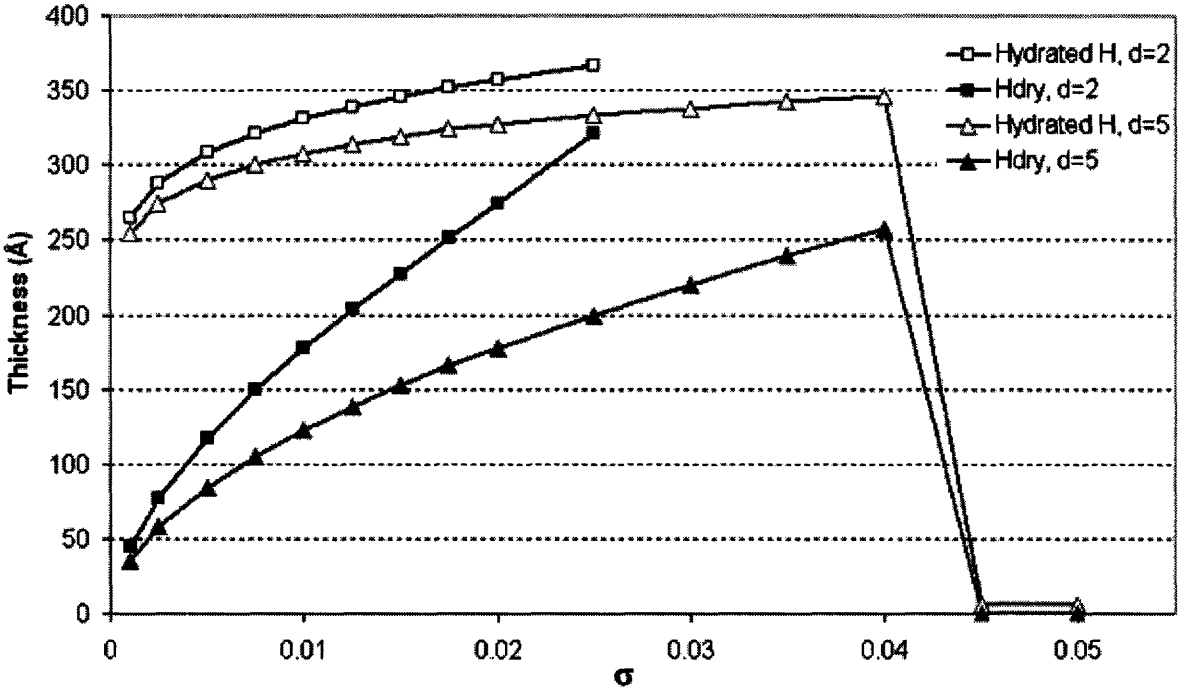

Figure 2.3.3.2.2. Predicted effect of the relative strength of sticking-site attractiveness on PDAC adsorption in the presence of salt-induced electrostatic shielding.

The most apparent observation from this simulation is that decreasing the attractive interaction between the polyelectrolyte and surface leads to denser, thicker adsorption. While this seems counter-intuitive at first, an argument can be made that when sticking is very energetically favored, chain mobility is greatly reduced – segment-site sticker pairs form quickly and chains are soon irreversibly tethered to the surface, their configurations frozen by a large energetic barrier, and their presence impedes access to the surface for other chains, so segment volume fraction is lowered. For smaller δ values, chains remain more mobile longer and denser packing is possible, especially when salt is added to shield segment-segment repulsion. Interestingly, no transition to molecularly thin layers is predicted for $\delta = 2 - F_{mono}$ never dips below F_{ad} and actually starts to increase again for large values of σ if only F_{elec} is considered. However, at this extreme the minimization starts to yield aphysical results ($\phi > 1$), indicating that the model is no longer an accurate description. Still, the model suggests that on weakly-attractive surfaces, adsorption can only take place in the supermonolayer regime. It should be further noted that F_{ad} is consistently higher for smaller δ values, as one would expect given the reduced energetic

advantage of sticking. This observation will be discussed in greater depth in the last part of this study.

2.3.4 LbL Assembly

Having confirmed that PDAC adsorption can be qualitatively described via this simple free-energy model and having studied the effect of chain length and surface attractiveness on the adsorption of a first layer of polyelectrolyte, the construction of polyelectrolyte multilayers on such surfaces was next studied. As discussed previously, this study considered model strong polyelectrolytes rather than PDAC and SPS, which are difficult to accurately describe within the constraints of this model.

The LbL assembly of two polyelectrolytes of equal segment size was modeled; PC (polycation) and PA (polyanion) are hypothetical strong polyelectrolytes of segment length 2.5 Å and mutual sticking energy δ_P. As previously, only F_{elec} will be included in F_{rep} so as not to obscure the effects of ionic charge screening. In Figure 2.3.4.1, the adsorbed thickness of PC on strongly or weakly-attractive surfaces is reported for N = 500 in the absence and presence of salt shielding; as expected, the trends are qualitatively if not quantitatively similar to those observed previously. One notable difference is that no transition to monolayer adsorption is predicted within the experimentally-relevant range of surface charge densities ($\sigma = 0.3$ corresponds to one charge group per 21 $Å^2$ when a = 2.5 Å, which is close to the maximum packing density generally reported for alkanethiol SAMs). It can also be noted that shielding has a much stronger effect when the surface sticking energy is lower.

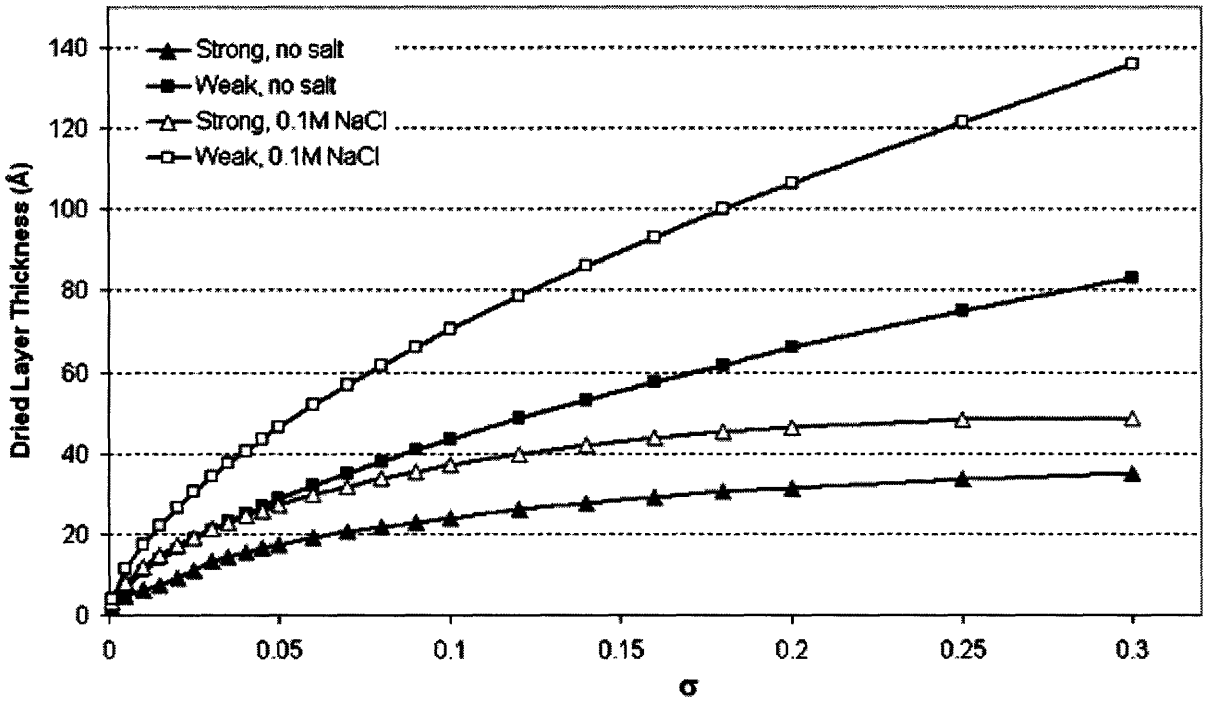

Figure 2.3.4.1. Predicted effect of surface sticking-site density on the adsorption of model polyelectrolytes PC and PA on strongly- and weakly-attractive surfaces with and without electrostatic shielding.

LbL adsorption of PC and PA was then modeled using the cumulative approach: the calculated segment density ϕ for the most recently adsorbed layer becomes the surface sticker density σ for the next adsorption step. In Figure 2.3.4.2, results are reported for $N_{PC} = N_{PA} = 500$, $\delta_P = 5$, and initial substrate $\delta = 5$ and $\sigma = 0.015$; low-salt conditions were used. While individual layer thickness increases quickly at first, after three bilayers an equilibrium is reached in which each adsorbed layer is of the same segment density and thickness as the preceding one. This is consistent with experimental observations of an initial super-linear growth regime followed by linear growth, although this transition often takes place more slowly in practice than predicted here.

In Figure 2.3.4.3, LbL assembly of PC/PA on strongly- (Surface S, $\delta = 5$) and weakly-attractive (Surface "W", $\delta = 2$) substrates was modeled with and without salt shielding. N_{PC}, N_{PA}, δ_P, and σ were not varied from Figure 2.3.4.2.

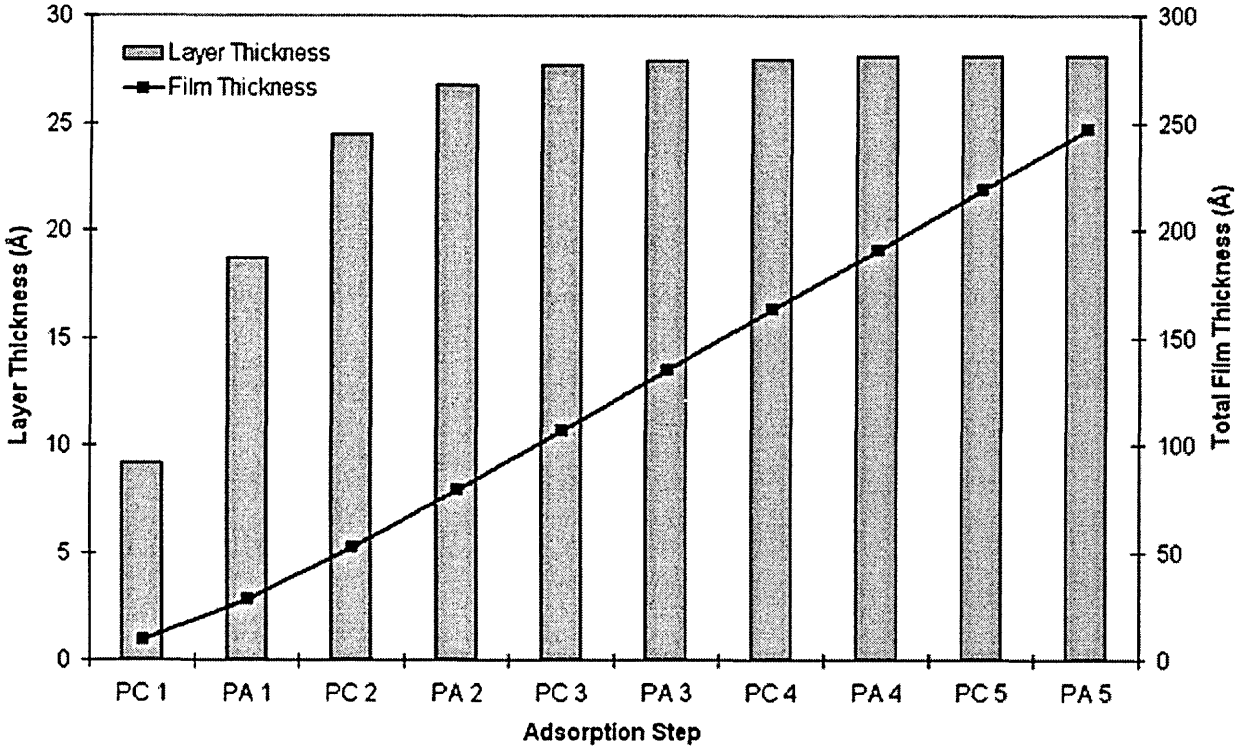

Figure 2.3.4.2. Predicted growth of a layer-by-layer film of PC and PA on a strongly-attractive surface in the absence of salt-induced electrostatic shielding, using the cumulative model for sequential adsorption.

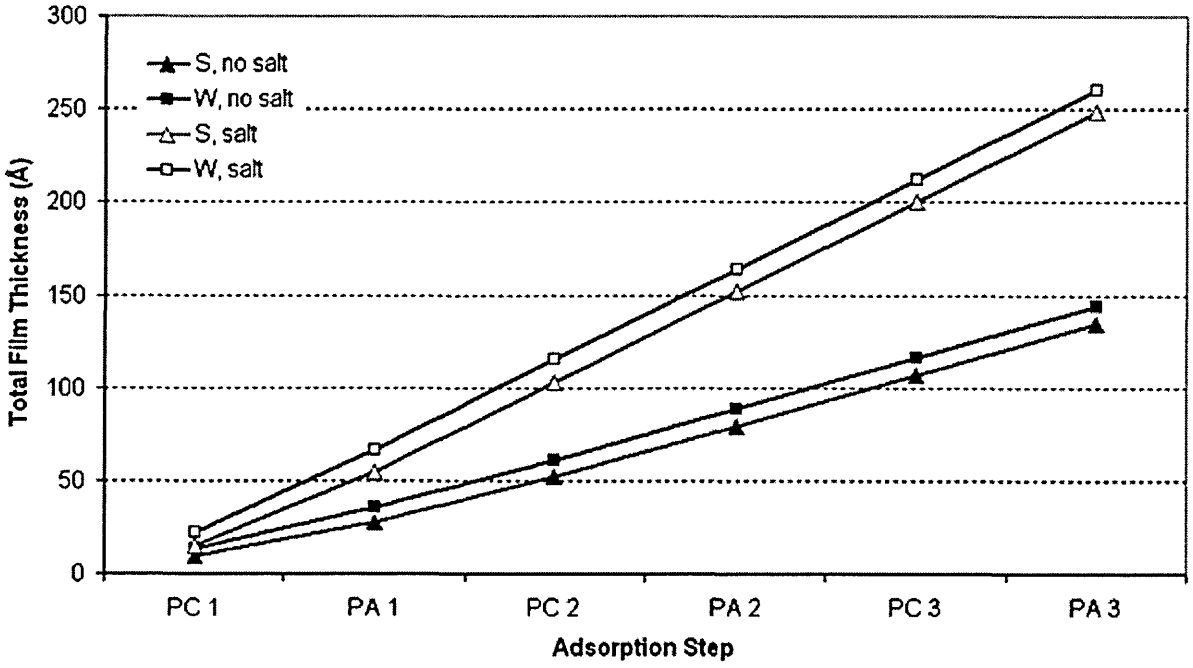

Figure 2.3.4.3. Predicted effect of surface attractiveness on layer-by-layer film growth in the absence and presence of ionic shielding, using the cumulative model.

It is clear that the assumptions of this model lead to a rapid extinction of substrate effects; within a few bilayers, the effect of initial surface attractiveness on total film thickness becomes insignificant. This is consistent with the experimental observation that 10-bilayer films of PDAC/SPS are of nearly equal thickness when built on COOH, CH_3, and CF_3 SAMs, despite the fact that these surface chemistries have very different interaction potentials with PDAC and SPS. So long as the initial substrate is not perfectly resistant to adsorption, the model predicts absolute selectivity will be weak. How, then, to explain the phenomenon of relative selectivity?

2.3.5 Competitive Adsorption on Micropatterned Surfaces

2.3.5.1 Theoretical modeling

In every situation modeled previously, polyelectrolytes adsorbed as thicker, denser layers on less attractive surfaces, all other parameters being equal, but with a higher F_{ad} than on the more attractive surfaces. However, substrate effects were quickly obscured by repeated adsorption steps, and the attractiveness of the underlying substrate was found to have little effect on LbL film thickness, consistent with experimental observations for PDAC/SPS films built on very different SAMs. Thus, it seemed natural to suspect that relative selectivity – the experimental observation that PDAC/SPS films on patterned SAMs exhibit distinctly patterned adsorption – might be related to the difference in free energy of adsorption.

The probability of a given chain adsorbing to a given surface was assumed to be directly related to the corresponding F_{ad}; that is, the smaller the energetic penalty, the more likely the adsorption. In this probabilistic approach, we consider a single polyelectrolyte chain in solution over a patterned surface, and assume that the chain can "see" each surface equally; i.e., solution mobility is such that all chains have equal exposure to both surfaces and where they adsorb is determined solely by energetic considerations. This does not mean that adsorption will only take place on the more advantageous surface, just that it is more likely to occur there. Having assumed that adsorption probability is directly related to adsorption free energy, this now implies that the relative probability of adsorption on two surfaces is inversely related to the relative free

energies of adsorption on those surfaces. Thus, film growth on the more attractive surface is expected to be faster. This model having been built on an assumption of thermodynamic equilibrium, only films having reached their equilibrium adsorbed amounts can be compared, and so we cannot draw a direct connection between the predicted free energy difference and the kinetics of adsorption on each surface. However, it seems reasonable to expect that if dipping time is limited to the time required for the more attractive surface to reach equilibrium, the film on the less attractive surface will not reach its own predicted (equilibrium) thickness; the greater the free energy difference, the greater the imbalance in polyelectrolyte accumulation on each surface.

Differences in free energy being a possible contributor to selective adsorption, the range of magnitudes possible for F_W/F_S under experimentally-accessible conditions was studied. In Table 2.3.5.1, the ratios on a substrate patterned with S ($\delta = 5$) and W ($\delta = 2$) regions of varying surface sticker site density are given for the model polycation PC with N set at 500 for consistence with earlier results.

σ(S) / σ(W)	.005	.010	.015	.020	.025	.030
.005	*0.88*	0.96	1.03	**1.13**	**1.21**	**1.32**
.010	*0.74*	*0.81*	*0.86*	0.95	1.02	**1.11**
.015	*0.67*	*0.73*	*0.78*	*0.85*	*0.92*	1.00
.020	*0.62*	*0.68*	*0.73*	*0.80*	*0.86*	*0.94*
.025	*0.59*	*0.64*	*0.69*	*0.75*	*0.81*	*0.88*
.030	*0.56*	*0.61*	*0.65*	*0.72*	*0.77*	*0.84*

Table 2.3.5.1. Ratio of predicted free energy of adsorption on the more attractive regions (F_S) vs. adsorption on the less attractive regions (F_W), depending on the sticker site density of each region. Calculated for N=500 and in the absence of added salt.

Electrostatic shielding was not found to have a significant effect on the adsorption ratios, but surface sticker density and attractiveness had strong effects. In most cases, italicized above, adsorption is predicted to be less favorable and thus thinner on W than on S, as one might expect, and the energetic advantage on S approaches 100% when σ_S is low and σ_W is high. However, when the strongly attractive surface has a high density of sticker sites and the weakly attractive

surface has a low density of groups, selectivity is predicted to reverse, with adsorption on W regions favored over S regions. These cases are highlighted in bold text above; ratios between 0.95 and 1.05 were assumed to be within error of unity. While perhaps counter-intuitive, these results are direct consequences of the increase in F_{ad} universally observed for increases in surface sticker density. Nearly-identical ratios were calculated for N = 2000 as for N = 500, so neither chain length nor shielding have significant effects on what we conclude is an entirely energetically-driven phenomenon.

These theoretical predictions not only support the possibility of relative selectivity – the fact that a given polymer may form a thicker layer on W than S when homogeneous surfaces are compared, but adsorb preferentially on the S regions of a microscale pattern – but also suggest that selectivity can be tuned via not only surface group chemistry, but also density.

For instance, when considering a surface stamped with a COOH-terminated thiol and then dipped in CF_3 thiol, it can be assumed that COOH group density will be lower than that for an alkyl-terminated thiol formed by immersion, both because of the bulkiness of the head group and because of the more limited SAM formation time. At typical LbL assembly conditions (pH ~5.5 for solutions prepared in MilliQ water without subsequent pH adjustment), the pKa of the COOH-terminated thiol indicates that only half of the groups will be charged, further reducing the density of sticker sites. Typically, well-packed alkylthiol SAMs are reported to have densities of 1 thiol per ~50 $Å^2$, which corresponds to $\sigma = 0.125$ for our a = 2.5 Å. Thus, given the partial ionization of COOH groups and the much sparser SAMs resulting from micro-contact printing, the range of σ values studied above is appropriate for modeling of COOH. Perfluorinated thiols are reported to pack very efficiently, so the CF_3 regions of our patterns are most appropriately modeled with the higher values of σ considered above, and in any case the CF_3 regions will have higher σ than the COOH regions, leading to relative selectivity towards the COOH regions. To test the prediction of reversed selectivity when $\sigma_W << \sigma_S$, we could either stamp the CF_3 and then immerse in COOH, or add a diluent to the CF_3 thiol solution – a shorter thiol which will reduce the surface CF_3 density without itself being "visible" to the approaching chains.

The fact that our proposed basis for relative selectivity is entirely energetically determined suggests that selectivity might also be tunable via temperature. Since temperature affects κ and l_b and since F_{elec} has a complicated dependence on κ, κ^3, and l_b, we studied whether F ratios would be affected by higher (324 K) or lower (274 K) temperatures, all previous

modeling having assumed typical T = 298 K ambient conditions. Figure 2.3.5.2 reports the free-energy ratios predicted for the three temperatures studied.

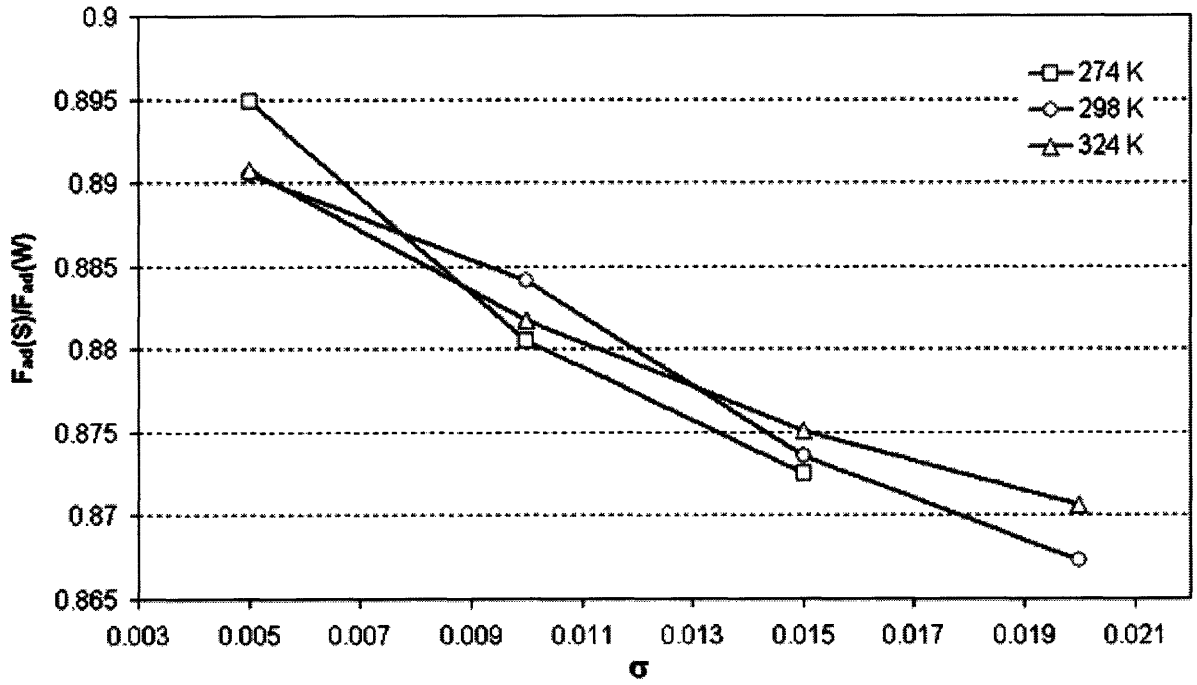

Figure 2.3.5.2. Effect of temperature on the predicted ratio of free energies of adsorption.

Despite the complex dependence of F_{elec} on temperature, T has no significant effect on F_{ad} ratios and thus is not expected to affect relative selectivity.

All of our modeling has assumed homogeneous layer formation on a given region, leading to rapid disappearance of substrate effects. However, we know that on certain less attractive surfaces, atomic force microscopy reveals that adsorption is not smooth but instead patchy, even after 10 bilayers are assembled. Patchy adsorption would extend substrate influence until the entire region has been covered by adsorbed layers, at which point layer thickness would converge on the equilibrium behavior for that polyelectrolyte pair. While accounting for this sort of intra-region heterogeneity is beyond the scope of this study, we can assume that the persistence of substrate influence will be greater in practice than as here modeled, consistent with the observation of distinct relative selectivity after $(PDAC/SPS)_{10}$ assembly.

2.3.5.2 Experimental results

Since our proposed basis for relative selectivity rests on the assumption of limited dipping time preventing the less-energetically favored regions from reaching equilibrium, varying dipping time should affect the degree of selectivity. To explore this, $(PDAC/SPS)_{10}$ multilayers were assembled on COOH and CF_3 surfaces using identical conditions (0.1 M NaCl added, sonication but no drying between cycles) but three different dipping times: 15 minutes, 30 seconds, and 1 second. The results are presented in Table 2.5.5. Absolute selectivity was defined as follows:

$$\frac{(H_{COOH} - H_{CF3})}{H_{COOH}}$$

Dipping time	**15 min**	**30 sec**	**1 sec**
COOH	325 Å	262 Å	102 Å
CF_3	311 Å	263 Å	85 Å
Selectivity	0.04	-0.01	0.17

Table 2.3.5.2. Ellipsometric thickness of $(PDAC/SPS)_{10}$ films built on continuous COOH and CF_3 SAMs in the presence of salt-induced electrostatic shielding. Films were built by hand using different polyelectrolyte bath immersion times.

Typically, PDAC/SPS multilayers are auto-dipped using 10-15 minute dipping times. However, a drastic reduction in dipping time to 30 seconds only reduced film thicknesses by roughly one-fifth and did not have a significant effect on the observed absolute selectivity. However, when dipping times were further reduced to the experimentally-feasible minimum, film thickness was sharply reduced (-70% compared to the 15 minute immersions) while absolute selectivity increased from nearly-zero to 0.17. It was not possible to derive accurate thickness data for films adsorbed on each region of $COOH/CF_3$ micropatterns, but the above results for continuous SAMs do suggest different adsorption kinetics for PDAC/SPS on surfaces of varying attractiveness. While further time studies will be required for definitive evaluation of the origins of relative selectivity, these limited data are consistent with the proposed role of competitive adsorption kinetics.

2.4 Comments and Conclusions

Self-assembled monolayers of perfluorinated alkylthiols did not prove absolute resists to polyelectrolyte adsorption; most LbL systems studied displayed only relative selectivity versus such surfaces, adsorbing near-equally on continuous surfaces of perfluorinated SAMs as on other SAMs. On micropatterned surfaces, however, distinct differences in adsorbed film morphology and thickness were often seen. Still, the near-absolute resistance to certain LbL systems exhibited by oligoethyleneglycol-terminated SAMs could not be achieved with the perfluorinated surfaces; for many applications, perfect resistance is desired so as to strictly segregate different components. Polyelectrolyte multilayers incorporating perfluorinated polyanions did not behave differently than others with respect to perfluorinated surfaces; rather, it was the choice of polycation that determined the total film thickness as well as the degree of patterning.

Thermodynamic modeling of polyelectrolyte adsorption confirmed the experimental observation that less favorable polyelectrolyte-surface interactions do not necessarily lead to reduced adsorption. However, the predicted free energy penalty for adsorption on such surfaces suggests that relative selectivity behavior may stem from the energetic favoring of certain regions of a pattern when adsorption time is limited.

In the next chapter, a novel approach to selective adsorption will be explored, in which selective polyelectrolytes will be used to functionalize arbitrary micro-objects and direct their surface interactions.

WORKS CITED

[1] P. W. Atkins, *Physical Chemistry*, W. H. Freeman, New York **1997**.
[2] C. Mayer, R. Moritz, C. Kirschner, W. Borchard, R. Maibaum, J. Wingender, H.-C. Flemming, *International Journal of Biological Macromolecules* **1999**, *23*, 3.
[3] P. C. Hiemenz, R. Rajagopalan, *Principles of Colloid and Surface Chemistry*, Marcel Dekker, New York **1997**.
[4] Y. N. Xia, J. Tien, D. Qin, G. M. Whitesides, *Langmuir* **1996**, *12*, 4033.
[5] S. Palacin, P. Hidber, J.-P. Bourgoin, C. Miramond, C. Fermon, G. M. Whitesides, *Chem. Mater.* **1996**, *8*, 1316.
[6] N. L. Jeon, R. G. Nuzzo, *Langmuir* **1995**, *11*, 3024.
[7] P. T. Hammond, G. M. Whitesides, *Macromolecules* **1995**, *28*, 7569.
[8] T. G. Vargo, J. M. Calvert, K. J. Wynne, J. K. Avlyanov, A. G. MacDiarmid, M. F. Rubner, *Supramolecular Science* **1995**, *2*, 169.
[9] S. L. Clark, M. F. Montague, P. T. Hammond, *Macromolecules* **1997**, *30*, 7237.
[10] S. L. Clark, M. F. Montague, P. T. Hammond, *Organic Thin Films* **1998**, *695*, 206.
[11] H. G. M. Van de Steeg, M. A. Cohen Stuart, A. De Keizer, B. H. Bijsterbosch, *Langmuir* **1992**, *8*, 2538.
[12] S. L. Clark, M. Montague, P. T. Hammond, *Supramolecular Science* **1997**, *4*, 141.
[13] S. L. Clark, P. T. Hammond, *Langmuir* **2000**, *16*, 10206.
[14] X. P. Jiang, C. Ortiz, P. T. Hammond, *Langmuir* **2002**, *18*, 1131.
[15] C. G. Gölander, J. N. Herron, K. Lim, P. M. Claesson, P. Stenius, J. D. Andrade, (Ed: J. M. Harris), Plenum Press, New York **1992**, 221.
[16] S. I. Jeon, J. D. Andrade, *Journal of Colloid and Interface Science* **1991**, *142*, 159.
[17] S. I. Jeon, J. H. Lee, J. D. Andrade, P.-G. De Gennes, *Journal of Colloid and Interface Science* **1991**, *142*, 149.
[18] P. Harder, M. Grunze, R. Dahint, G. M. Whitesides, P. E. Laibinis, *J. Phys. Chem. B* **1998**, *102*, 426.
[19] R. L. C. Wang, H. J. Kreuzer, M. Grunze, *J. Phys. Chem. B* **1997**, *101*, 9767.
[20] X. P. Jiang, S. L. Clark, P. T. Hammond, *Advanced Materials* **2001**, *13*, 1669.
[21] S. L. Clark, E. S. Handy, M. F. Rubner, P. T. Hammond, *Advanced Materials* **1999**, *11*, 1031.
[22] X. P. Jiang, H. P. Zheng, S. Gourdin, P. T. Hammond, *Langmuir* **2002**, *18*, 2607.
[23] X. P. Jiang, P. T. Hammond, *Langmuir* **2000**, *16*, 8501.
[24] Y. F. Miura, M. Takenaga, T. Koini, M. Graupe, N. Garg, R. L. Graham, T. R. Lee, *Langmuir* **1998**, *14*, 5821.
[25] M. W. Tsao, C. L. Hoffmann, J. F. Rabolt, H. E. Johnson, D. G. Castner, C. Erdelen, H. Ringsdorf, *Langmuir* **1997**, *13*, 4317.
[26] C. Naud, P. Calas, A. Commeyras, *Langmuir* **2001**, *17*, 4851.
[27] J. Tien, A. Terfort, G. M. Whitesides, *Langmuir* **1997**, *13*, 5349.
[28] T. Ederth, K. Tamada, P. M. Claesson, R. Valiokas, R. Colorado, M. Graupe, O. E. Shmakova, T. R. Lee, *Journal of Colloid and Interface Science* **2001**, *235*, 391.
[29] S. D. Evans, A. Ulman, *Chem. Phys. Lett.* **1990**, *170*, 462.
[30] R. Bertani, P. Metrangolo, A. Moiana, E. Perez, T. Pilati, G. Resnati, I. Rico-Lattes, A. Sassi, *Advanced Materials* **2002**, *14*, 1197.

[31] C. Pale-Grosdemange, E. S. Simon, K. L. Prime, G. M. Whitesides, *Journal of the American Chemical Society* **1991**, *113*, 12.
[32] M. Graupe, T. Koini, H. I. Kim, N. Garg, Y. F. Miura, M. Takenaga, S. S. Perry, T. R. Lee, *Colloids and Surfaces a-Physicochemical and Engineering Aspects* **1999**, *154*, 239.
[33] M. Graupe, T. Koini, H. I. Kim, N. Garg, Y. F. Miura, M. Takenaga, S. S. Perry, T. R. Lee, *Materials Research Bulletin* **1999**, *34*, 447.
[34] D. M. DeLongchamp, P. T. Hammond, *Chemistry of Materials* **2003**, *15*, 1165.
[35] S. Y. Park, M. F. Rubner, A. M. Mayes, *Langmuir* **2002**, *18*, 9600.
[36] S. Y. Park, C. J. Barrett, M. F. Rubner, A. M. Mayes, *Macromolecules* **2001**, *34*, 3384.
[37] R. Robinson, R. Stokes, *Electrolyte Solutions*, Buttersworth Scientific Publications, London **1959**.

CHAPTER 3 – ELECTROSTATIC COLLOIDAL ASSEMBLY

3.1 Introduction

Thus far, we have considered only the adsorption of polyelectrolyte multilayers, and have found that while most multilayer systems studied exhibit at least a relative selectivity towards certain surfaces, absolute selectivity is rare. The total mass adsorbed on the intended "resist" region may be less than that on the more attractive surface, but for many applications a height difference is not enough and we would like the resist to remain entirely bare. Also, given the difficulty in achieving selectivity from uncomplicated polyelectrolytes, the prospects for strong selectivity among more complex species – often carrying several different functional groups and thus capable of many kinds of intermolecular interactions – seem slim, but these are the types of species it would be most interesting to be able to selectively direct to different regions of a surface, motivating the development of new approaches to selective adsorption.

Chemical surface patterns have been shown capable of directing the adsorption of larger objects such as latex microspheres, silica nanoparticles, and biological species like proteins or even intact cells. Large (tens to hundreds of microns) charged glass microspheres can be directed to a patterned electrode under an electrical field. While this process is directed by larger-scale electromagnetic interactions than the intermolecular forces discussed above, it is an example of the potential applications of surface-directed assembly, requiring little time and simple conditions to produce colloidal arrays with very low defect rates. The patterned electrodes are also reusable, allowing for capture-and-release applications or high-throughput production of arrays assembled on the pattern and then transferred intact into a new matrix*[1]*

Diblock copolymers of PS and PMMA, whose self-organization into a variety of distinct micro-phase separated array configurations is well known, can direct the deposition of nanoparticles due to the polarity difference between the two phases*[2, 3]*. Once assembled on such a template, functionalized nanoparticles can be crosslinked in situ and released to create permanent free-standing assemblies.*[4]* Simple plus/minus electrostatic interactions can also be

used to selectively adsorb charged particles on templates patterned by μCP; to create nanoscale features beyond the maximum resolution of PDMS, other stamp materials such as polyurethanes have been used to create single-particle linear arrays of tiny particles.*[5]* Adhesion-controlling patterns are also of interest to biologists wishing to position and grow cells in precise arrangements on surfaces. Ghosh and Crooks created "cell corrals" by using a combination of μCP and polymer surface grafting to produce surfaces with raised poly(ethylene glycol)-functionalized walls surrounding micron-scale methyl-terminated thiol SAM regions. When mouse macrophages were plated and incubated on these films, cell growth occurred exclusively within the methyl-terminated corrals with no cellular interactions or bridging between corrals.*[6, 7]* One weakness of PEG-based cell templates is that the PEG layer begins to break down within days, allowing cells to proliferate throughout.*[8, 9]* By careful tuning of charge density within POPS patterns of weak polyelectrolytes, the Hammond and Rubner groups were able to create patterns with precise densities of cell ligand atop cytophobic multilayered platforms.*[10, 11]* Further investigation revealed that cell adhesion is very sensitive to surface compliance; multilayered films assembled from the same polyelectrolytes at different assembly pHs can have vastly different cytophobic/cytophilic properties.*[12]*

By coordinating secondary interactions with electrostatics, the assembly of two-component colloidal arrays has been demonstrated, although the process generally requires an intermediate blocking-layer step, preventing simultaneous selective adsorption (true surface sorting). Such work illustrates the delicate balance that must be achieved between forces discouraging adsorption, such as electrostatic repulsion or steric hindrance, and forces that encourage it, such as electrostatic attraction, hydrogen bonding and the class of van der Waals forces generally referred to as "hydrophobic interactions."*[13]* Recently, a protocol allowing for simultaneous adsorption of two kinds of specially-functionalized particles on a patterned surface was reported, with one particle type being directed by an electrostatic attraction and the other by a multiple hydrogen-bonding host/guest interaction. (Multiple hydrogen bonding will be the subject of detailed discussion in Chapter 4.)*[14]* As this example demonstrates, surface sorting requires that non-interfering interactions be combined.

Functionalized microparticles are also of interest in non-planar self-assembly applications. For example, functionalizing the surface of nanoparticles with a mixture of silanes bearing copper-binding and fluorescent groups can create particles whose fluorescence is

quenched upon binding of copper, allowing them to serve as sensors in solution. While copper sensing itself via this route is not of interest, since many simpler methods exist, the concept could be applied to detection of more interesting substances, such as antibodies.*[15]* Solution self-assembly of particles is also being investigated as a route to nanoelectronic or microphotonic device fabrication.*[16]*

While the selective adsorption of colloids has been studied, it has generally been limited to pairing a charged colloidal population with an oppositely-charged surface, and a neutral one with a hydrophobic surface, and intermediate steps may be required between the two colloidal adsorption steps to protect the first layer from overlayering. Knowing that like-charged polyelectrolytes can display very different selectivity behavior, and theorizing that relative resist surfaces might be more likely to stay bare through a single adsorption step rather than dozens of bilayer cycles, we decided to apply polyelectrolyte selectivity behavior to colloidal assembly.

One of the reasons colloids are of particular interest to us, in addition to the above hopes for improved selectivity, is their potential to act as vehicles for other species. That is, more functional but less selective materials could be packaged inside a microsphere with an outer layer selective to certain surfaces. In this section, these two aspects of colloidal adsorption will be explored. First, we will demonstrate the patterning via non-specific interactions of magnetic colloids to be used subsequently as tethers for magnetically-assembled chains; then, we will see whether selective polyelectrolytes can indeed direct colloidal assembly.

3.2 Tethering and Chaining of Magnetic Spheres

This section is reproduced in part from a prior publication, "Directed patterned adsorption of magnetic beads on polyelectrolyte multilayers on glass."[17]

Magnetorheological (MR) fluids consist of micrometer-sized superparamagnetic particles dispersed in a nonmagnetic medium. In the presence of an external magnetic field, these magnetic beads acquire a dipole moment that is proportional to the magnetic field strength. The dipole-dipole interactions induce aggregation of the particles, which form chains and crosslinked structures. The rapid structural response of these particles makes them of scientific interest*[18-22]*. The structural changes in MR fluids are accompanied by significant changes in their rheological properties, making MR suspensions of interest for incorporation into such devices as audio speakers and inertial dampers in motors.*[23]* Magnetically controlled suspensions also have potential biomedical applications including ophthalmic surgical aids in the repair of detached retina and ventricular assist devices in blood pumps*[24, 25]*.

We have studied a superparamagnetic suspension comprising polymer-encapsulated beads with a magnetite (Fe_2O_3) domain dispersed in an aqueous medium. In the presence of a magnetic field, these iron oxide domains acquire a dipole moment $\mu = 4/3\pi r^3 \mu_0 \chi H$, where r is the particle radius, μ_0 is the magnetic permeability in a vacuum, χ is the magnetic susceptibility and H is the external field. The interaction energy between two magnetic beads is $U(r,\theta) = (\mu^2/4\pi\mu_0)[1 - 3\cos^2(\theta)]/r^3$, where θ is the angle between the applied field and the axis between the bead centers. When the interaction energy of the induced dipoles overcomes thermal energy, kT, the particles aggregate via dipole-dipole interactions to form magnetic chains. It is of interest to control the arrangements of such chains through their manipulation at surfaces; one means of achieving this goal is through the use of chemically patterned surfaces designed to guide the formation of magnetic particle arrays.

Microcontact printing (μCP) is a powerful technique forming the basis for a revolution in self-assembly driven soft lithography*[26, 27]*. One application of μCP gaining recent attention is the directed deposition of colloids on printed templates carrying specific interaction chemistries*[28, 29]*. We have used a combination of directed polyelectrolyte adsorption and chemical templating to guide colloid assembly on polymer templates*[13, 30-32]*. This approach

has been used to pattern magnetic materials on gold or SiO_2 substrates; in particular, magnetite was deposited on gold-coated SiO_2 using selective wetting*[33]*. Also, various magnetic particles including Co, Ni, Fe and some ferrite complexes were adsorbed into patterns on oxidized Si wafers*[34]*. Our approach differs in that we deposit charged composite superparamagnetic particles on polyelectrolyte multilayer templates on glass with micrometer precision; we believe that polymer-on-polymer stamping yields more selective and stable adhesion sites than conventional microcontact printing of self-assembled monolayers. Superparamagnetic particles will only acquire a dipole moment upon the application of an external field, thus they behave as inert surface layers until needed as anchors to aggregates magnetic particles or control magnetic suspension flow. Polyelectrolyte multilayers on glass patterned by polymer-on-polymer stamping (POPS) or through selective deposition of multilayers has been demonstrated*[35, 36]*, and this approach provides a functional template for the deposition of magnetic particles, as a number of electroactive or optically functional systems can be incorporated within the layers. Features as small as 300 nm and as large as 50 μm within regular patterns covering 1-5 cm^2 of a polymeric surface have been created via POPS. Compared to traditional μCP approaches, POPS allows greater flexibility in the choice of substrate. The controlled adhesion of charged magnetic microparticles on a polymeric substrate provides a reproducible means for preparing ordered arrays of paramagnetic colloids on an optically transparent foundation. Finally, we show that individual magnetic colloids can be deposited in an ordered array with micrometer precision.

In the work reported here, a polyelectrolyte multilayer platform capped by a polyanionic surface was created through layer-by-layer assembly*[37]* and stamped with a polycationic pattern using POPS, to form docking sites for the negatively charged magnetic beads. The resulting polycationic patterns consisted of two-dimensional arrays of dots, with dot diameters ranging from 1.3 to 10.0 μm and or stripes of widths ranging from 1.3 to 16 μm. The magnetic colloids deposited in round clusters of average diameters from 1 to 12 μm on the dot patterns and in lines of average widths from 1 to 7 μm on the stripe patterns. Such a magnetizable layer can then be used as the foundation to grow magnetic chains in a microfluidic flow.

3.2.1 Materials and Methods

Aqueous solutions of 20 mM poly(diallydimethylammonium chloride) (PDAC, Sigma-Aldrich, MW = 100,000-200,000 g/mol) and 10 mM sulfonated poly(styrene) (SPS, Sigma-Aldrich, MW = 70,000 g/mol) in MilliQ water (18 MΩ*cm resistivity) with 0.1 M NaCl (Sigma-Aldrich) were prepared and passed through a 0.22 μm filter (Nalgene from Naige-Nunc International). All polyelectrolyte molarities are given on a repeat-unit basis.

A platform layer was created by layer-by-layer (LbL) adsorption on a glass slide after air plasma treatment for two minutes using a Harrick Scientific PDG-32 plasma cleaner. A modified slide stainer (Carl Zeiss) equipped with an ultrasonic bath (Advanced Sonic Processing) was used to build 5 bilayers of PDAC and SPS, terminating with a polyanionic SPS layer. For each bilayer cycle, the glass substrate was dipped into both polyelectrolyte solution for 20 min with two 1 min water immersions to rinse between polycation and polyanion addition; between bilayer cycles the substrate was sonicated for 3 min.

Polymer-on-polymer stamping (POPS) was used to create a pattern of polycationic PDAC on the top-most polyanionic SPS surface. Chromium photo masks (Advanced Reproductions) and corresponding silicon masters (Microsystems Technology Laboratory, MIT) were prepared as templates for poly(dimethylsiloxane) (PDMS, Sylgard 184, Dow-Corning) stamps. Two stamp designs were used: an array of dots of varying sizes (radius = 0.6 – 4.5 μm) and an array of stripes of various sizes (width = 1.2 – 9 μm). Prior to use, PDMS stamps were washed with soap and water, rinsed with MilliQ water, dried under nitrogen flow, and treated by air plasma for 20 s to create a hydrophilic surface. The stamp was then inked with a 0.25 M PDAC solution at 0.1 M NaCl in a 75:25 ethanol:water solvent using a cotton-tipped applicator. The stamp was dried under N_2 stream to evaporate the solvent and then held on the multilayer surface with slight pressure for 45 s to 1 min. After stamp removal, the surface was rinsed with MilliQ water and dried under N_2.

Charged magnetic beads were adsorbed on the POPS-patterned surface as shown in Figure 1 of section 3.2.2. Carboxylate-modified super-paramagnetic microspheres (Seradyn, d = 0.8 μm) were prepared as a 0.5 wt% aqueous suspension. The bead suspension was dropped over

the polyelectrolyte surface and left for a minimum of 1 hr before rinsing with MilliQ water and drying under N_2.

To distinguish the beads involved in chain growth from those used as anchors on the patterned surface, fluorescent beads were used for chaining. Carboxylate-modified superparamagnetic microspheres (Bangs Labs, d = 0.96 μm) loaded with the Dragon Green fluorophore (480 nm excitation, 520 nm emission wavelengths) were prepared as a 0.01 wt% aqueous suspension that was pipetted over the patterned magnetic array; the drop of suspension was then capped with a glass cover slip. A mercury arc lamp was used as the excitation source. A magnetic field was then applied using a block neodymium iron boron magnet (Indigo Instruments, 33 mT).

Optical micrographs were taken using an analog charge-coupled camera mounted to an optical microscope capable of fluorescence imaging. Colloidal assemblies were observed in both reflectance and transmittance mode. Images were digitized and processed using Scion Image (Scion Corp, Version Beta 4.0.2).

3.2.2 Tether Patterning

POPS was used to create 1 cm^2 arrays of cationic PDAC dots or stripes on an anionic SPS background. An aqueous suspension of anionic magnetic colloids was then exposed to these patterned surfaces and their adsorption was characterized by optical microscopy. Figure 3.2.2.1 summarizes the experimental protocol. Figures 3.2.2.2 and 3.2.2.3 show optical micrographs of the magnetic beads deposited on dot (Figure 3.2.2.2) and stripe (Figure 3.2.2.3) patterns; corresponding adsorption densities are reported in Tables 3.2.2.1 and 3.2.2.2.

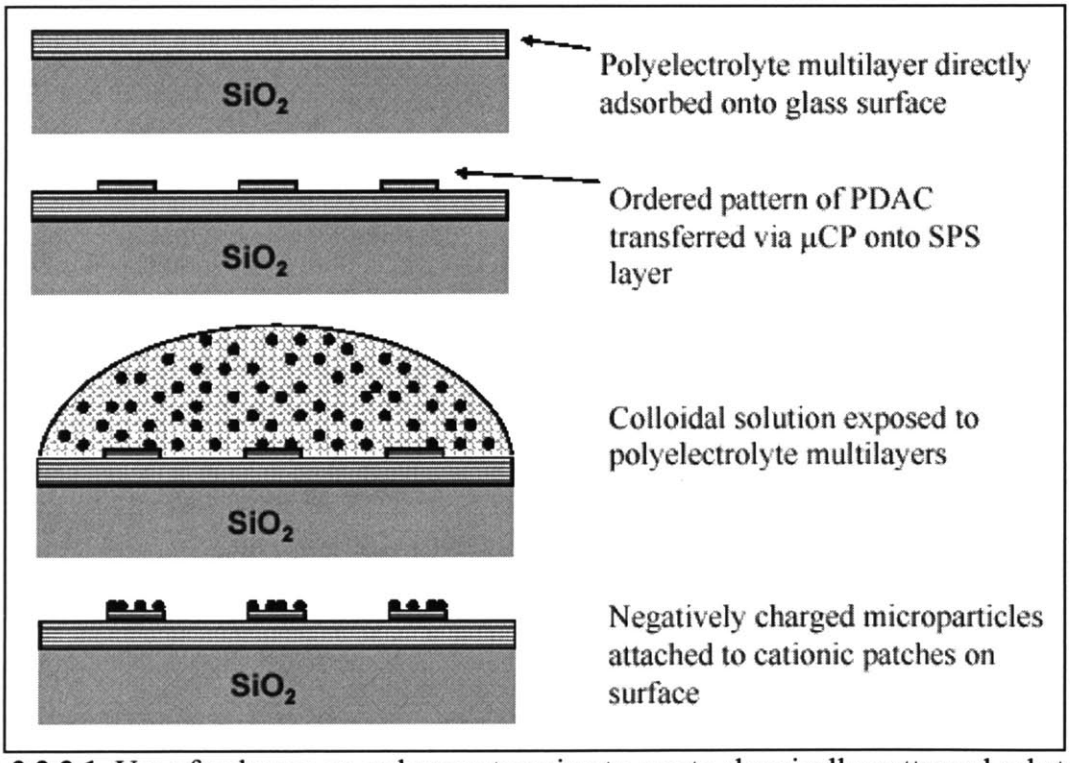

Figure 3.2.2.1. Use of polymer-on-polymer stamping to create chemically-patterned substrates capable of directing adsorption of magnetic colloids for subsequent use as tethers.

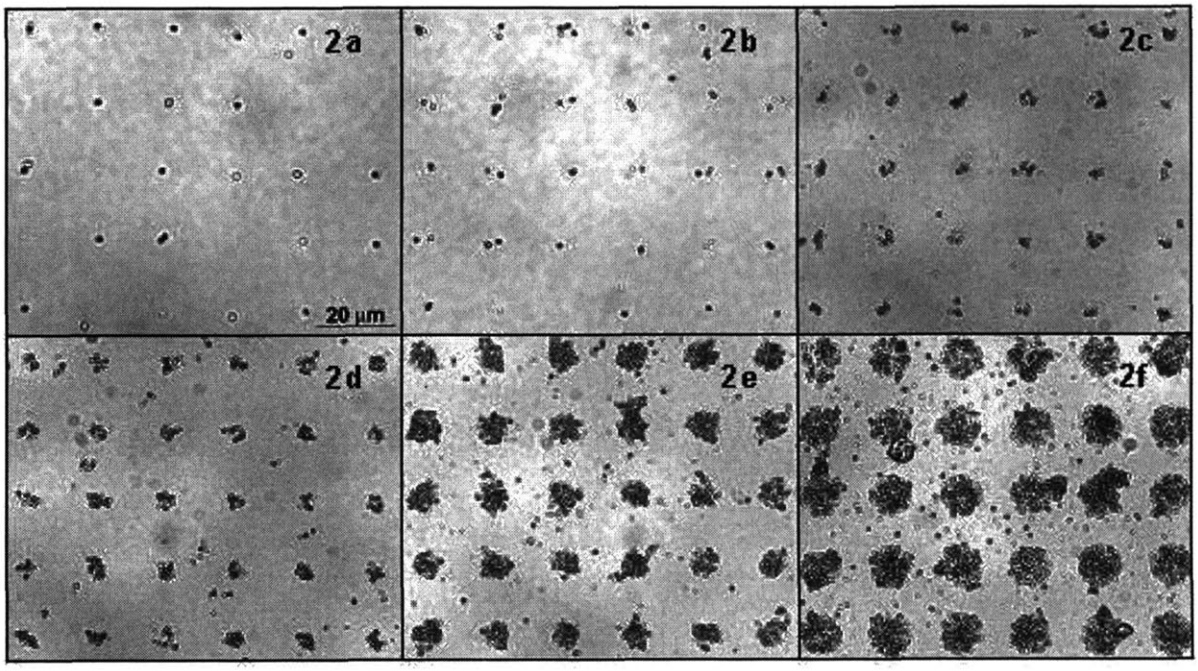

Figure 3.2.2.2. Optical micrographs of 0.8 µm carboxylate-modified magnetic beads selectively adsorbed on various sizes of printed PDAC dots on SPS.

Figure	Dot diameter (µm)	Avg. number of beads per dot
2a	1	0.8
2b	2	2.1
2c	3	6.9
2d	5	12.5
2e	8	35
2f	12	60

Table 3.2.2.1. Average number of carboxylate-modified magnetic beads adsorbed per printed PDAC dot of varying diameter.

The surface selectivity was found to be very high with few particles adsorbed outside of the printed pattern. The iron-loading of the magnetic colloids gives them a large Hamaker constant, so they tend to adhere even to like-charged glass surfaces; surfactants must often be added to prevent adsorption. Thus, the observation that the multilayer polyelectrolyte surface on our substrates is effective at preventing non-specific adsorption suggests that such surface coatings could be useful to other applications in which particle adsorption must be prevented.

The horizontal and vertical distances between dots reported in Table 1 were measured from the center-to-center spacing of the patterned dots. Figure 2a represents an image with nominally one bead per patterned site. Thus, if a sufficiently small cationic docking site is used, single magnetic colloids can be directed to different points in a two-dimensional array. As the patterned site diameter increases, the average number of beads per cluster increases. When the cluster diameter exceeds 8 μm, as in Figure 2e-f, beads no longer adsorb in a monolayer but rather in a stacked pseudo-double layer, making evaluation of the average number of beads per site difficult. With smaller dot diameters ($D < 3$ μm), the ratio of the dot diameter (D) to the magnetic bead diameter (d), D/d, is approximately equal to the average number of beads per dot. The packing density on docking sites could be tuned by adjustment of the pH or ionic strength of the colloidal suspensions, as well as variation of the ionic strength of the polyelectrolyte solutions during assembly to tune the availability of free charged groups at the surface.

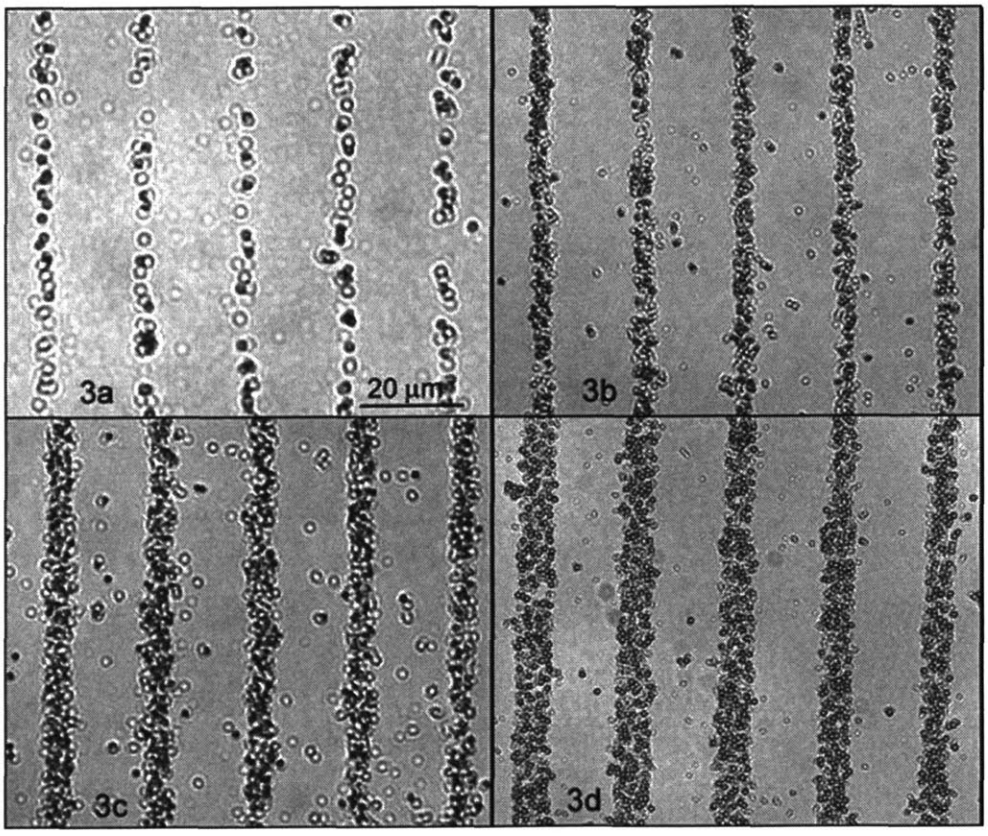

Figure 3.2.2.3. Optical micrographs of 0.8 μm carboxylate-modified magnetic beads selectively adsorbed on various sizes of PDAC stripes printed on SPS.

Figure	Stripe width (μm)	Avg. number of beads per stripe
3a	0.9	1
3b	2.8	3.5
3c	4.7	5
3d	6.9	6

Table 3.2.2.2. Average number of carboxylate-modified magnetic beads adsorbed per printed PDAC stripe of varying width.

The directed adsorption of anionic magnetic beads in stripes is described in Figure 3 and Table 2. The average stripe width was taken as the full width at half-maximum value from an intensity profile of the stripe. The average spacing between stripes was measured as the stripe midpoint-to-midpoint distance. Stripes range in width from 1 to 7 μm. Single-bead stripes are shown in Figure 3a, again confirming that linear arrays of magnetic colloids can be created with micron-scale precision. In areas patterned with broader PDAC stripes (Figure 3b-d), high packing densities and few interruptions of the stripes are observed.

3.2.3 Assembly Under Magnetic Field

Patterning of magnetic beads is of interest for microfluidic applications. Under an applied magnetic field, paramagnetic microparticles will self-assemble into chains in solution.*[18-22]* Recently, the Gast group (formerly of Stanford University and MIT, now at Lehigh University) have shown how rotating chains of magnetic beads can serve as micromixers in a microfluidic flow.*[38]* To use chains of magnetic particles in a microfluidic device, it is often necessary to be able to anchor them at specific points on the surface. In this work, the patterned magnetic colloidal arrays were used as nucleation sites for magnetic chain assembly, as illustrated in Figures 3.2.3.1 and 3.2.3.2.

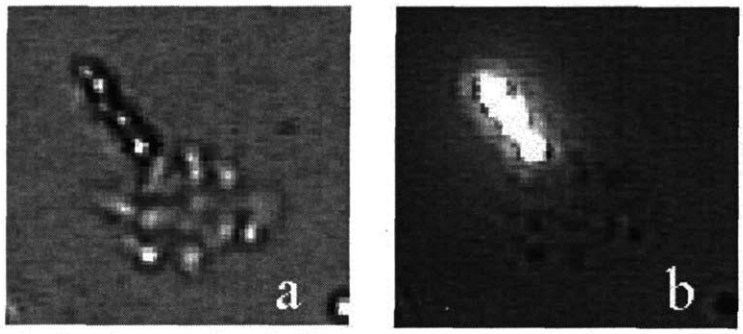

Figure 3.2.3.1. Optical micrograph of fluorescent magnetic beads chaining under applied magnetic field and tethered to magnetic anchor beads adsorbed on a 5.6 μm patterned dot, viewed under (a) white light and (b) Hg arc lamp.

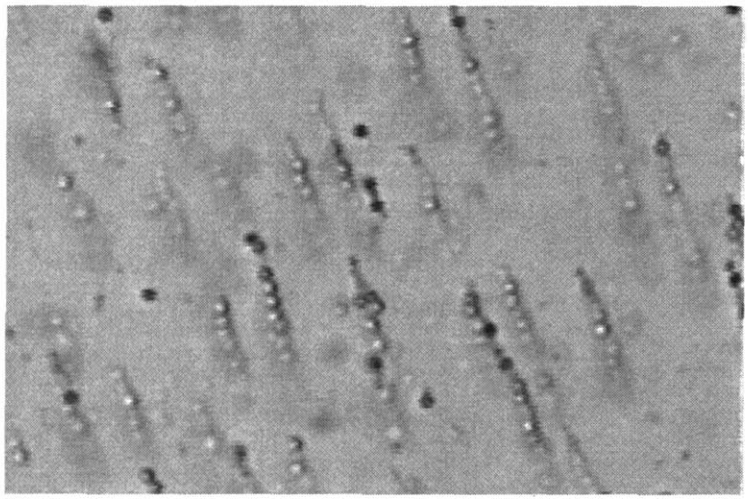

Figure 3.2.3.2. Optical micrograph of chains of superparamagnetic particles permanently-linked by addition of PEG-g-PAH and anchored to patterned surface of anchor particles.

Figure 3.2.3.1a shows a chain of fluorescently-labeled magnetic colloids tethered to a 6 μm patterned magnetic dot. Figure 3.2.3.1b shows the same chain illuminated by a mercury arc lamp, making it clear that the chained particles are distinct from the tethering array. Such magnetic chains may act as molecular speed bumps in flow cells, allowing for cross-flow separation of magnetic beads on the basis of size and magnetic susceptibility.

While some applications require that the chains be disruptable by removal of the magnetic field, permanent assembly of the chains is desirable for other applications. In Figure 3.2.3.2, a permanently-linked chain is shown, created by addition of 10 mM PAH-*g*-PEG to a

suspension of carboxylate-modified superparamagnetic beads previously chained under a magnetic field and tethered to patterned anchor beads. These chains remain tethered to the patterned spots and respond to fluid flow and applied magnetic fields as shown in Figure 5. The ability to permanently anchor chains of magnetic beads on surfaces opens the way for further interesting microfluidic devices in which the chains are used for magnetic field-driven mixing, flow actuation, or sieving.

3.3 Polyamine-Directed Selective Adsorption of Colloids

The polycations poly(allyl amine) and linear poly(ethylene imine) have bee found to display opposite selectivity towards carboxylic acid and ethylene glycol surfaces.*[39]* However, since they are like-charged, it was proposed that colloids functionalized with PAH and LPEI could form patterned monolayer arrays by depositing side-by-side on different regions of a COOH/EG template, with electrostatic repulsion preventing overlayering of the first adsorbed species by the second.

3.3.1 Materials and Methods

3.3.1.1. Template Preparation

Patterned self-assembled monolayers (SAMs) of alkyl thiols were built on gold-coated silicon substrates as described in 2.2.1. For these experiments, the patterns were generally composed of 16-mercaptohexadecanoic acid (hereafter, COOH) stamped from saturated hexadecane ink solutions and 11-mercaptoundecyltriethylene glycol (hereafter, EG) adsorbed from 2 mM solutions in ethanol. (See Figure 2.2.1.1 for structures of thiols used.)

3.3.1.2. Bead Preparation and Characterization

Polystyrene microspheres were functionalized by covalent or electrostatic attachment of a polyelectrolytic outer layer. Surfactant-free suspensions of sulfate-functionalized polystyrene latex of mean diameter 0.53 and 1.0 μm internally labeled with either Yellow-Green or Nile Red fluorescent dyes were obtained from Interfacial Dynamics Corporation (now Molecular Probes division of Invitrogen). The average surface charge density was one SO_4^- group per 400 $Å^2$. The Yellow-Green dye used has an excitation wavelength of 490 nm and an emission wavelength of 515 nm; the Nile Red dye has an excitation wavelength of 520 nm and an emission wavelength of 580 nm.

Equal volumes of 20 mg/ml aqueous colloidal suspension (as delivered) and either 20 mM aqueous linear poly(ethylene imine) (hereafter, LPEI) at pH 6.0 or 20 mM aqueous poly(allylamine hydrochloride) (hereafter, PAH) at pH 4.5 were combined and allowed to stir overnight. (See structures below.) The LPEI and PAH were of the same origin as those described in 2.2.1. To provoke covalent crosslinking of the polymer backbones to the polystyrene surface, the suspensions were irradiated using a van de Graff generator (MIT High Voltage Research Laboratory) for a total dose of 6 MRad. After irradiation, unbound polyelectrolytes were rinsed away by repeated centrifugation of the colloidal suspensions and redispersal in pure MilliQ water (18 MΩ*cm resistivity) using a Galaxy 7D microcentrifuge (VWR). In some cases, no irradiation was performed and the suspensions were simply mixed with polyelectrolyte solutions, allowed to sit for an hour, and then washed as above.

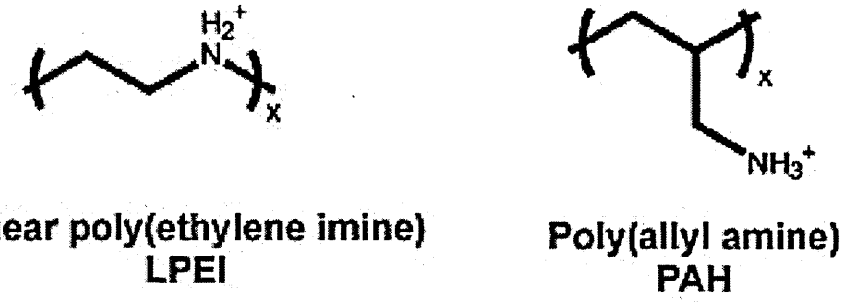

Figure 3.2.2.1.2.1. Repeat-unit molecular structure of the polyelectrolytes used to functionalize microspheres.

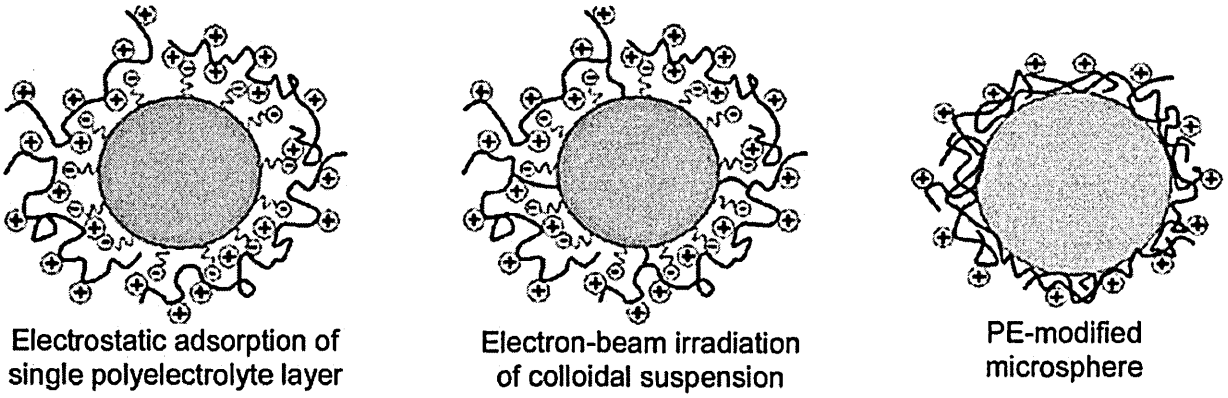

Figure 3.2.2.1.2.2. Colloidal surface functionalization via polyelectrolyte adsorption.

The surface charge of the colloids before and after functionalization was evaluated by measuring zeta potential using a ZetaPALS zeta potential analyzer (Brookhaven Instruments). Fluorescence microscopy (Zeiss Axioplan2) was also used to verify that the fluorescent tagging had not been degraded during functionalization.

3.3.1.3. Array Assembly and Characterization

LPEI- and PAH-functionalized microspheres (hereafter, LPEI-PS and PAH-PS) were exposed to patterned COOH/EG surfaces and their adsorption behavior was observed. Typically, a few drops of 10 mg/ml suspensions of either LPEI-PS or PAH-PS were dropped onto patterned substrates and left for 15-180 min. Substrates were then rinsed by 2 immersions in pure MilliQ with gentle agitation and dried in a vacuum oven. Colloidal adsorption was characterized by optical (OM) and fluorescence (FM) microscopy using the previously mentioned instruments. Some patterned substrates were reused after complete removal of any adsorbed colloids by 1 min sonication in ethanol using a Bransonic 1210 sonication bath (Branson Ultrasonics).

3.3.2 Polyelectrolyte-Functionalization of Colloids

To examine the hypothesis that polyelectrolyte coatings would confer greater selective behavior on colloids than that seen with existing functionalized latexes, we used a combination of electrostatic and covalent interactions to adsorb various single polyelectrolyte layers on microspheres. The effects of adsorption conditions on the extent and stability of the polyelectrolyte layer were characterized by zeta potential analysis to determine how best to prepare beads to be used in selective adsorption studies. First, we sought to examine whether covalent crosslinking via irradiation is necessary or if simple electrostatic attraction could suffice, which would greatly reduce preparation time and expense. Second, we studied the effect of polyelectrolyte charge density and/or ionic shielding during adsorption on the extent of functionalization. Finally, we exposed functionalized colloids to extreme pH or pI conditions to study the stability of the adsorbed layer, especially in the absence of covalent crosslinking.

50 mM solutions of PAH, LPEI, and PDAC (polycations having, respectively, primary, secondary, and quaternary amine groups) were prepared. PAH and LPEI were then each adjusted to three different pHs corresponding to 20%, 50%, and 80% ionization (for PAH, 4.8, 8.5, and 10.0; for LPEI, 2.0, 4.8, and 9.0).*[40-44]* PDAC solutions were not pH adjusted, but 0.1 M NaCl was added to one batch to increase electrostatic shielding. Eight samples were prepared, each containing 0.2 ml of an 8 wt% suspension of 1.0 μm sulfate-modified polystyrene latex plus 3.0 ml of one of the LPEI, PAH, or PDAC solutions. After stirring overnight, the eight batches were split and half were exposed to 6 x 1 MRad e-beam irradiation. All sixteen batches were then washed by precipitation and resuspension into pure MilliQ water, repeated three times. Samples from each batch were kept for zeta potential evaluation of the "as prepared" state. Two more samples from each batch were then precipitated and resuspended in either water of pH high enough such that both LPEI and PAH would be entirely neutralized, or undiluted 10X PBS concentrate (1.4 M NaCl, 30 mM KCl, 100 mM phosphate buffer). All of these were then sonicated for two hours, then washed by precipitation and resuspension in pure MilliQ, repeated three times. The 48 resulting batches of beads were analyzed via zeta potential, as was the original sulfate-latex suspension.

Although every effort was made to keep suspension concentrations identical and to prepare all ZP solutions identically, the sensitivity of ZP analysis to suspension concentration makes direct comparison of the data collected for each sample inappropriate. However, measured zeta potentials could be characterized as either "very positive" (> 45 mV), "positive" (15-45 mV), "neutral/amphiphilic" (-15 mV to 15 mV), or "negative" (< -10 mV) for comparisons. For reference, the unmodified sulfate latex had a zeta potential of –40 mV. Suspensions with clearly positive or clearly negative ZPs gave consistent results over repeated measurement cycles. However, the suspensions characterized as "neutral/amphiphilic" typically gave very inconsistent results, with ZP often oscillating between slightly positive and slightly negative values. The zeta potentials of the functionalized beads after various treatments are reported in Tables 3.3.2.1 (PAH), 3.3.2.2 (LPEI), and 3.3.2.3 (PDAC).

Irradiated / **Not Irr.**	**As prepared**	**After extreme salt**	**After extreme pH**
80% ionized during adsorption	45 / 43	0-10 / -22	-30 / -27
50% ionized during adsorption	60 / 45	25 / ~0	-30 / -23
20% ionized during adsorption	60 / 45	23 / ~0	-30 / -24

Table 3.3.2.1. Effect of polyelectrolyte adsorption pH on the charge (in mV) of polystyrene latex suspensions modified by PAH and on the stability of this charge to washes at extreme pI and pH.

Irradiated / Not Irr.	As prepared	After extreme salt
80% ionized during adsorption	-35 / ~0	-36 / -33
50% ionized during adsorption	~0 / -10	-25 / -20
20% ionized during adsorption	33 / 55	17 / 12

Table 3.3.2.2. Effect of polyelectrolyte adsorption pH on the charge (in mV) of polystyrene latex suspensions modified by LPEI and on the stability of this charge to washes at extreme pI and pH.

Irradiated / Not Irr.	As prepared	After extreme salt
No salt added during adsorption	40 / 45	20 / ~0
0.1 M NaCl added	40 / 55	22 / ~0

Table 3.3.2.3. Effect of polyelectrolyte adsorption pI on the charge (in mV) of polystyrene latex suspensions modified by PDAC and on the stability of charge to washes at extreme pI and pH.

The two major conclusions to be drawn from the above data are that LPEI adsorbed best when nearly-neutral and that irradiation had limited success.

PAH successfully adsorbed at all conditions studied and slightly better when not highly ionized. Irradiated batches were slightly more positive, suggesting that in this case covalent crosslinking did occur and did improve the stability of the polyelectrolyte layer to normal washing. Irradiated batches also had better resistance to extreme salt conditions, but not to extreme pH, which rendered all batches fully negative again.

LPEI proved much more difficult to functionalize, with only the batches prepared from mostly-neutral LPEI displaying full charge reversal, suggesting that LPEI adsorption on these surfaces is promoted via hydrophobic effects. In addition, irradiation seems to have been

detrimental, reducing the extent of charge reversal. Since all of the colloids studied here were prepared and irradiated together, the different effect of irradiation in PAH and LPEI may stem from their different backbones, heteroatomic LPEI being more vulnerable to chain breakdown. The irradiated batch did prove more resistant to extreme salt conditions.

As with LPEI, PDAC functionalization was somewhat reduced by irradiation, but irradiated batches were much more resistant to extreme salt conditions. Ionic strength during assembly did not have a significant effect.

3.3.3 Directed assembly of PE-functionalized colloids

Having prepared and characterized micron-scale colloids functionalized with a single polycationic layer, the adsorption from solution of these microspheres onto chemically-patterned substrates was studied and compared to results obtained for polyelectrolyte multilayers. Since these colloids are all positively-charged, electrostatic repulsion was expected to prevent adsorption beyond a single monolayer.

3.3.3.1. Selective adsorption of a single component

This approach to selectivity having been inspired by the observation that like-charged but differently-structured polymers could exhibit opposite selectivity towards certain types of surfaces, we first sought to replicate this behavior in this new system. COOH and EG thiol SAMs were patterned on gold substrates, onto which either LPEI-PS or PAH-PS was then adsorbed from solution. Larger patterns (feature size at least 10x colloid diameter) allowed for better visual evaluation of adsorption, as the mutual electrostatic repulsion of the colloids prevented dense packing.

Precise control of colloidal suspension pH proved critical, as expected from published chemical force microscopy results,*[39]* but difficult to achieve. In early experiments, LPEI-PS suspensions in plain MilliQ showed some preference for COOH regions, but even there adsorption was limited. Although the pH of the MilliQ water used was 5.5, only slightly higher than the 4.8 pH reported to yield optimal COOH/EG selectivity of LPEI, it would seem that the secondary amine groups were largely deprotonated (neutral) under experimental conditions, while the carboxylic acid groups of the SAM were mostly deprotonated (negatively-charged), leading to limited attractive interactions. It is likely that the pKa of surface-grafted LPEI chains is lower than that observed for free LPEI in solution. LPEI-PS suspensions were then acidified to pH 3 and again exposed to COOH/EG substrates. At this pH, LPEI should be only partially charged while the carboxylic acid groups should be mostly neutral. Thus, uncharged LPEI segments should display some attractive hydrogen bonding interactions with the COOH regions,

but should also be expected to have some affinity for EG regions. Fluorescent LPEI-PS adsorbed at pH 3 on COOH/EG are shown in Figure 3.3.3.1.1.

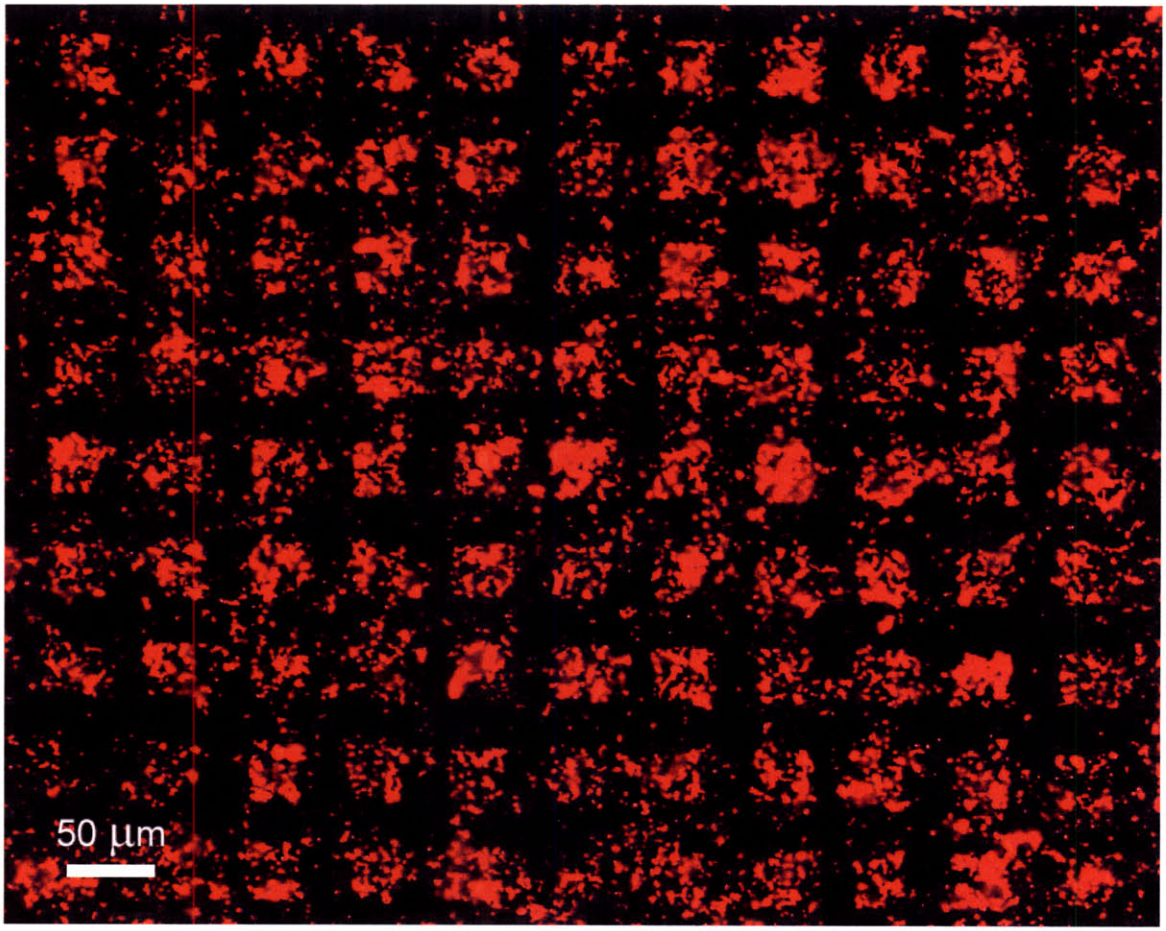

Figure 3.3.3.1.1. LPEI-functionalized 1 µm Nile Red-loaded latex spheres adsorbed from acidified suspension (pH < 3) on a gold surface patterned with 25 µm COOH squares in an EG background, seen under a Rhodamine fluorescence filter.

As expected, at this pH LPEI showed a distinct preference for COOH regions, but did not entirely resist EG regions. LPEI-PS was then resuspended in MilliQ adjusted to pH 4.8 with the minimum amount of salt added, so as not to promote ionic shielding of the $LPEI^{+}/COO^{-}$ interaction. PAH-PS was also suspended at this pH, and both types of colloids were adsorbed on separate COOH/EG substrates. Images of these samples after immersion rinsing and drying under vacuum are given in Figure 3.3.3.1.2.

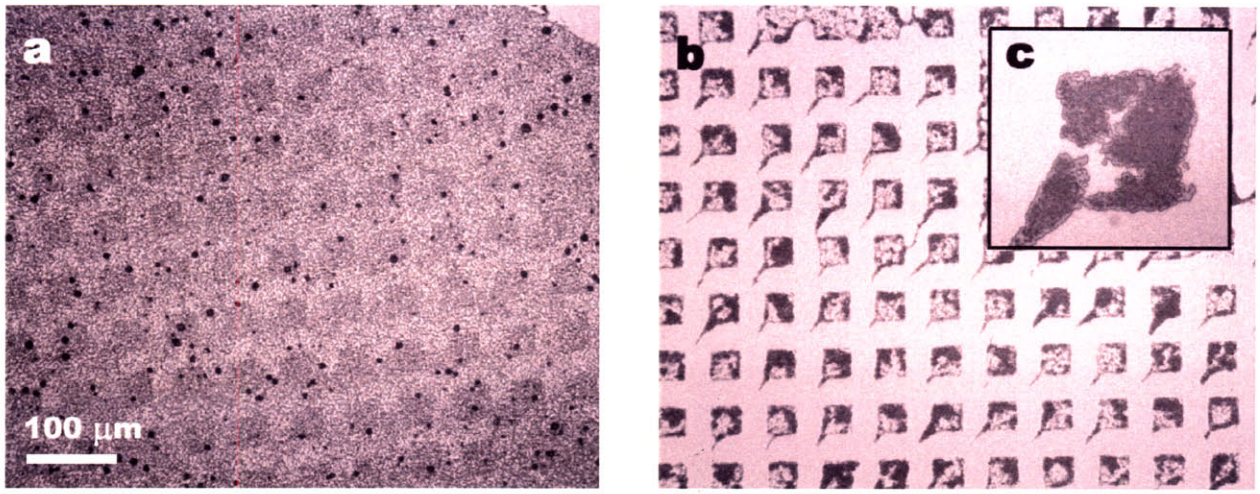

Figure 3.3.3.1.2. PAH-functionalized (**a**) and LPEI-functionalized (**b**) 1 μm latex spheres adsorbed from pH 4.8 suspension on separate gold surfaces both patterned with 25 μm COOH squares in an EG background. Detail from **b** is enlarged in **c**. "Tails" on squares are drying artifacts.

At pH 4.8, LPEI beads showed strong resistance to the EG surface (Figure 3.3.3.1.2. **b**) and adsorbed more densely on COOH regions than at pH 3. In some areas, bilayers of LPEI-PS were observed (inset **c**). In raising the pH from 3 to 4.8, it is expected that more of the LPEI became neutralized, but there should also have been an increase in the deprotonation of the carboxylic acid surface groups. Thus, inter-bead repulsion was reduced, allowing for denser packing, while there still existed a strong electrostatic attraction between the surface and remaining charged LPEI segments, directing adsorption. The high observed resistance of LPEI-PS to EG is consistent with earlier LbL and chemical force microscopy studies.

PAH-PS beads, however, were able to adsorb throughout the COOH/EG surface, with slightly denser packing observed on the COOH regions. A few larger clusters of beads are visible over the adsorbed monolayer in Figure 3.3.3.1.2. **a**, most likely resulting from incomplete rinsing away of unbound particles and subsequent drying in place under vacuum. These aside, the adsorbed PAH-PS beads form a clean monolayer of consistent density on a given surface functionality. While PAH was found to have a stronger attraction to EG than COOH at this pH, it is likely that a shift in the pKa of the bound PAH changed the balance of forces existing at pH 4.8. Still, it is notable that PAH-functionalized colloids were able to form a regular monolayer over EG while LPEI-functionalized beads resisted EG strongly, suggesting the possibility of two-component colloidal assembly by combining the two systems.

Given the interesting LbL relative selectivity behavior observed for several polycations towards perfluorinated SAMs, the adsorption of both LPEI-PS and PAH-PS on COOH/CF_3 patterns was studied and is reported in Figure 2.4.3.1.3. Other than the substitution of CF_3 for EG, substrate preparation and adsorption conditions were identical to the samples shown in Figure 3.3.3.1.2.

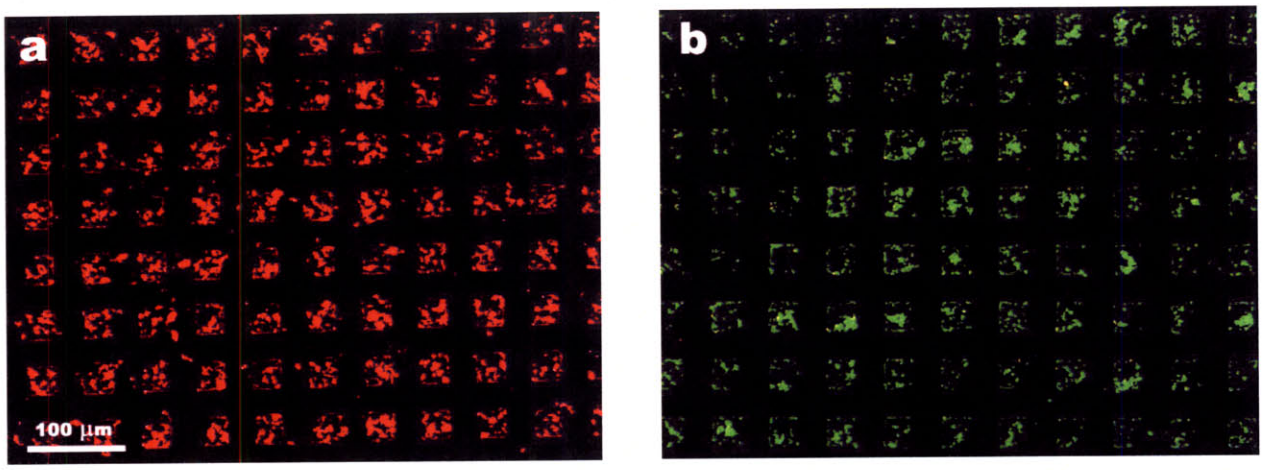

Figure 3.3.3.1.3. Nile Red-loaded LPEI-functionalized (**a**) and Yellow-Green-loaded PAH-functionalized (**b**) 1 µm latex spheres adsorbed from pH 4.8 suspension on separate gold surfaces both patterned with 25 µm COOH squares in a perfluorinated (CF_3) background, observed under a Rhodamine (**a**) or FITC (**b**) fluorescence filter.

Both LPEI-PS and PAH-PS showed strong selectivity towards the carboxylic acid regions vs. the perfluorinated surface, the latter remaining nearly perfectly bare. In LbL studies, both PAH/Nafion® and LPEI/Nafion® films adsorbed on homogeneous perfluorinated surfaces in thicknesses close to that observed for homogeneous COOH surfaces, yet both also showed some selectivity to the acid regions of a COOH/CF_3 pattern. In the case of the LbL films, this relative selectivity means that all regions of the template are covered, just with varying thicknesses; however, in this new colloidal adsorption approach, the difference in affinity for COOH vs. CF_3 was sufficient to keep the perfluorinated regions nearly free of adsorption. This suggests that resistance to polyelectrolyte-functionalized colloids is easier to achieve than resistance to LbL systems, making patterned colloidal adsorption a more efficient approach to surface-directed assembly in addition to its advantages for functional material incorporability previously discussed.

3.3.3.2. Two-component patterning

Having established that polyelectrolyte-functionalized colloids not only follow, but in some aspects improve upon, the selectivity properties of free polyelectrolytes, we next explored the creation of two-component colloidal assemblies. A gold substrate patterned with COOH squares on an EG background was exposed to a suspension of LPEI-PS for three hours, rinsed by immersion, and then exposed to a suspension of PAH-PS for three hours before immersion rinsing and vacuum drying. All colloidal suspensions were prepared at pH 4.8.

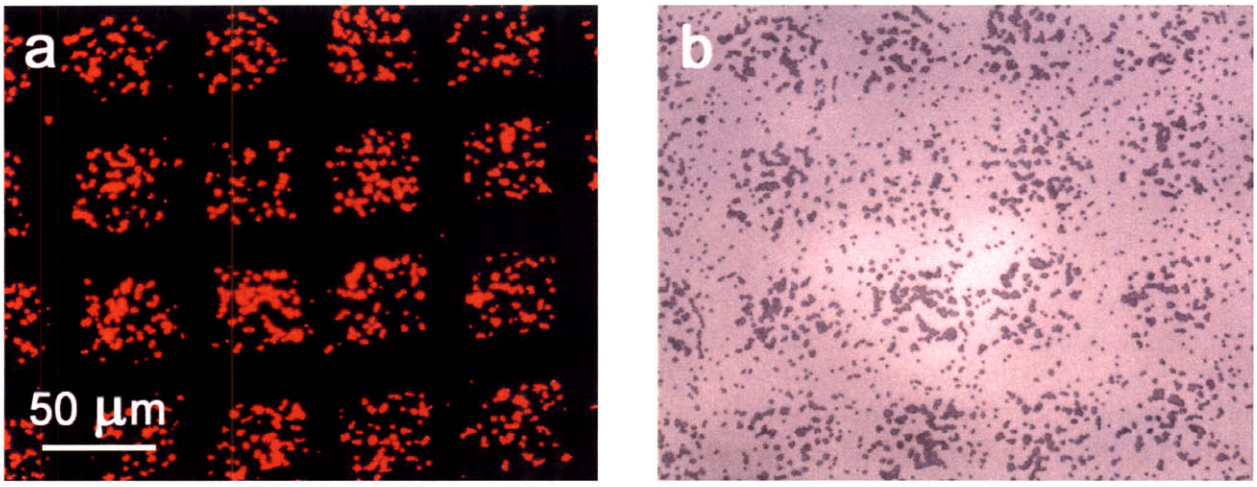

Figure 3.3.3.2.1. Nile Red-loaded LPEI-functionalized 1 µm and Yellow-Green-loaded PAH-functionalized 0.5 µm latex spheres serially adsorbed from pH 4.8 suspension on a gold surface patterned with 25 µm COOH squares in an EG background, observed under a Rhodamine fluorescence filter (**a**) or visible light (**b**). Both particle populations can be seen under visible light, but only LPEI beads are visible under the Rhodamine filter.

Side-by-side assembly of LPEI-PS and PAH-PS was clearly observed. LPEI-PS, labeled with Nile Red fluorescent dye, displayed good resistance to the EG regions, while PAH-PS, labeled with Yellow-Green (YG) fluorescent dye, was able to adsorb on the EG regions. The broad spectrum of the Nile Red dye allows for simultaneous detection of both colloid types. Under a Rhodamine filter, Nile Red appears bright red, while the narrower-spectrum YG is invisible (Figure 3.3.3.2.1); however, under a DAPI filter, Nile Red remains visible, now looking bright yellow, while YG appears turquoise. (Both Nile Red and YG are visible under a FITC filter as well, but are then too close in color to be easily distinguishable.) A DAPI image of the above serially-assembled two-component colloidal array is given in Figure 3.3.3.2.2 below.

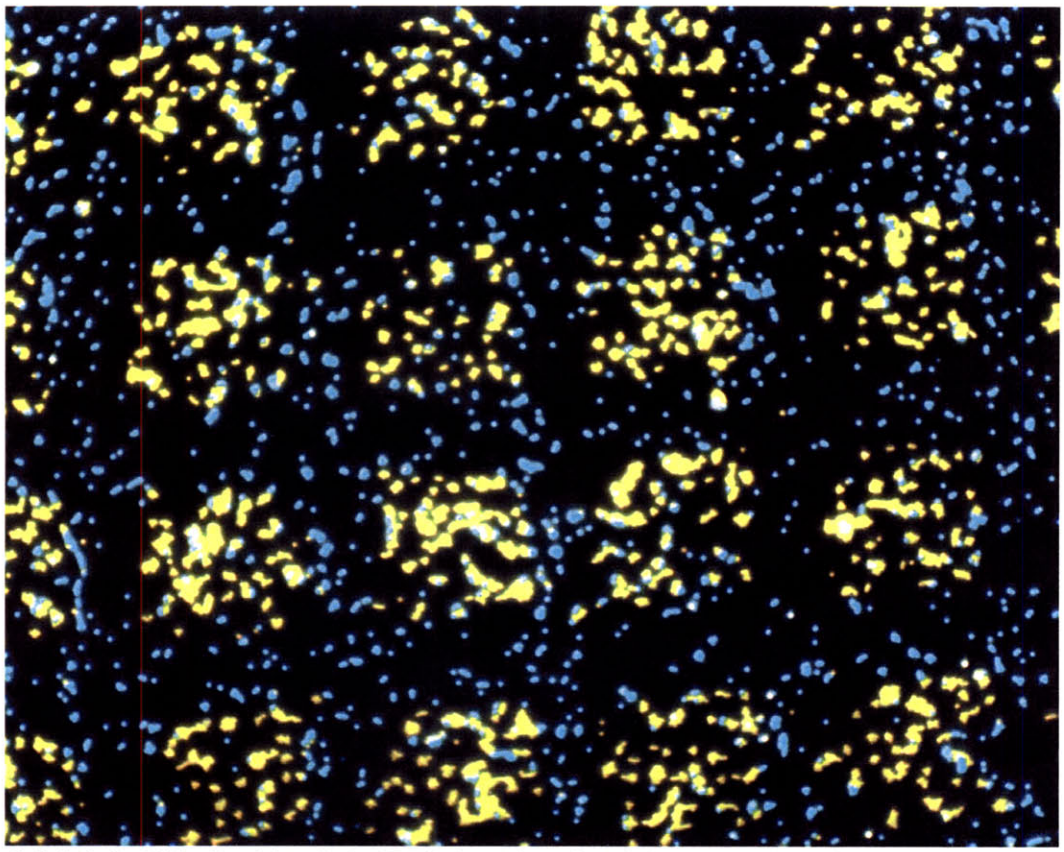

Figure 3.3.3.2.2. Nile Red-loaded LPEI-functionalized 1 μm and Yellow-Green-loaded PAH-functionalized 0.5 μm latex spheres serially adsorbed from pH 4.8 suspension on a gold surface patterned with 25 μm COOH squares in an EG background, observed under a DAPI fluorescence filter. The Nile Red dye, which has a broad emission spectrum, appears yellow under DAPI filters, while the Yellow-Green dye appears blue.

While packing was sparser than in previous experiments, careful control of pH and ionic strength should lead to optimized colloidal packing density as well as adsorption selectivity. Identification of bead functionalizations able to direct adsorption on perfluorinated SAMs should enable three-component assembly via serial exposure of a COOH/EG/CF_3 pattern to beads resistant to both EG and CF_3, such as LPEI-PS, followed by beads resistant to CF_3, such as PAH-PS, and finally beads able to adsorb on CF_3. The results reported in Figure 2.2.2.2.3 suggest that both LPEI and PAH are good candidates for this, especially if colloidal suspensions are prepared at increased ionic strength. Since the surface polyelectrolyte's role is merely to direct the adsorption of small containers of functional materials, not to be functional itself, using the same polyelectrolyte to guide two kinds of particles is not a problem. So long as good packing is achieved with each step, the filling of first the COOH and then the EG regions will leave only

the perfluorinated region available to the third colloid type added; this is yet another area in which relative selectivity can be better exploited by directed monolayer adsorption of functionalized colloids than traditional LbL film assembly.

Thus far, we have focused on improving the complexity of applications of selective adsorption, but we have not yet addressed its adaptability to different substrates. Thiolate SAMs allow for efficient creation of stable, high-resolution patterns of chemical functionality, but the gold surfaces required are hardly ideal for potential practical applications of these techniques. (Thiols can also self-assemble on silver and copper, but not only are these materials hardly more practical than gold, they also affect the orientation and packing of the monolayer; the same EG-terminated thiols found to promote resistance when assembled on gold had no such effect assembled on silver.*[45]*) One response to this challenge has been the use of polymer stamping and multilayer transfer techniques to directly assemble patterned features on polymeric substrates, topics explored by other members of this group; in the next section, we examine an alternative approach in which lateral heterostructures of colloids are assembled on a gold substrate before being transferred into another matrix.

3.3.3.3. Array stabilization and transfer

In early colloidal assembly experiments, rinsing methods proved critical to success. When a flow of water was used to rinse away unbound beads, it tended to also dislodge many of the adsorbed beads. However, immersion of the substrate into a small beaker of water and gentle movement within the water (minimizing shear forces), repeated once or twice with fresh volumes of water, preserved the adsorbed array while effectively eliminating unbound material. Drying was an equally delicate process – to dry LbL films, a nitrogen flow is typically used, but even the gentlest flow tended to cause too forceful a movement of the remaining water droplets, disrupting adsorbed particles in their path.

The best drying approach proved to be placing the samples horizontally in a vacuum oven and gently applying vacuum and heat to accelerate evaporation. Since any colloid suspension will stick to nearly any surface if dried in place, the samples were observed by optical

microscopy after immersion rinsing as well as after evaporative drying to verify that no beads were left in suspension above the adsorbed layer before drying and that the patterning and packing of adsorbed beads did not change during drying. In some cases, small drying artifacts were visible in the form of "tails" (see Figure 3.3.3.1.2.**b**) at the edges of features, created by too-rapid vacuum application. With these techniques, colloidal assemblies were stable to rinsing as well as subsequent adsorption steps, as in the creation of the two-component array shown in Figure 3.3.3.2.1. However, in order to make such assemblies more useful, methods of stabilization were evaluated.

The first approach considered was the construction of a LbL film on top of the assembled array. While such films could be built without damaging the array, a $(PDAC/SPS)_2$ coating did not prevent bead removal by sonication. Given the relative thickness of so few multilayers compared to the size of the colloids, this is not surprising. Rather than subjecting the array to repeated rinsing steps to create a multilayer film thick enough to trap the beads at the surface, cast polymeric coatings were considered next.

A 20% aqueous solution of poly(acrylic acid) (MW ~90,000) was cast over an array and allowed to dry fully by overnight vacuum heating; the resulting PAA layer was approximately 0.3 mm thick. Thus encased, the array survived sonication without loss while remaining visible under optical and fluorescence microscopy. However, while PAA casting protected the array, it also firmly attached it to the gold substrate(reflective, opaque), limiting its usefulness and preventing reuse of the template. Cast PAA layers could be removed from the gold surface if sufficient pressure was applied to wedge a sharp blade under them; although the array was successfully transferred from the gold surface, the PAA film was too brittle to be removed in one piece. Transfer into PDMS was explored next and found to be a far superior approach.

A 10:1 mixture of PDMS prepolymer and crosslinking agent (the same blend used to make μCP stamps) was cast over a two-component array of LPEI-PS and PAH-PS and cured overnight at 40 °C. (Rapid curing of PDMS at high temperatures increases the degree of shrinking, which would prevent faithful conservation of the array.) The 3 mm slab of PDMS was then removed from the surface by simple peeling using tweezers. In Figure 3.3.4.1, a colloidal array and gold template are seen before and after PDMS casting and peeling. After removal of the PDMS slab, virtually no colloids remained on the gold surface, while the entire array could be seen transferred into the slab with no distortion of the pattern. The resulting PDMS-encased

array was flexible, optically clear, and impervious to sonication in any solvent not able to swell or degrade PDMS itself; in such form, many more applications are possible than on the original gold-coated silicon substrate.

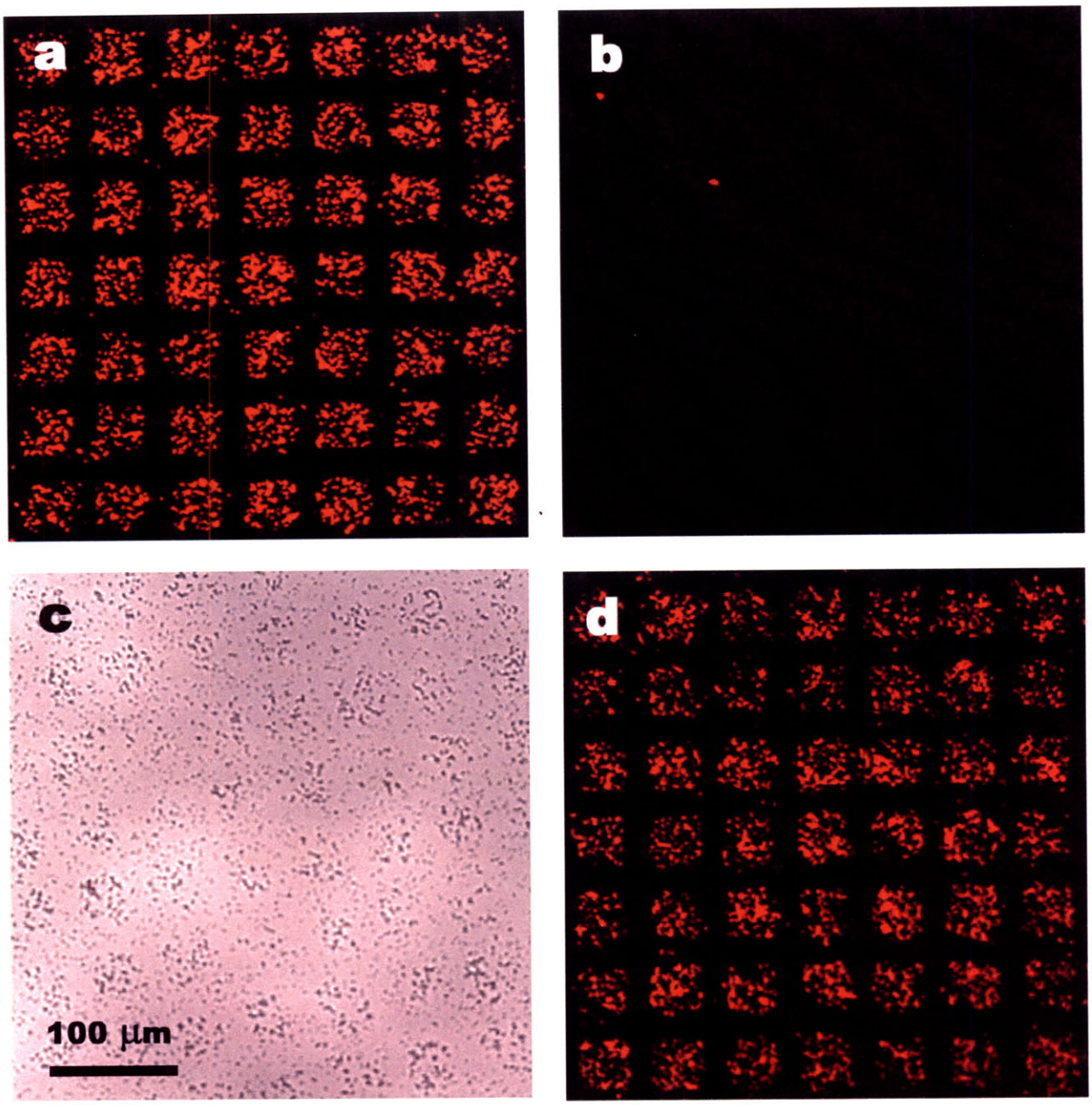

Figure 3.3.4.1. Transfer of a two-component colloidal array from an adsorption-directing gold surface into a 2 mm PDMS slab. **a**) The original array, viewed under a Rhodamine filter. This is the same array shown in Figure 3.3.3.2.2. **b**) The gold surface, observed under a Rhodamine filter after lift-off of the PDMS and before any washing. **c**) The PDMS slab after lift-off, observed under visible light. **d**) The PDMS slab after lift-off, observed under a Rhodamine filter.

This complete transfer of the array into a new matrix raised the possibility of template recycling, which would further expand the usefulness of this technique. Templates were sonicated for a minute in ethanol after PDMS removal and rinsed with water before being reused. In some cases, templates behaved exactly as before; however, in other cases no or even reversed patterning was observed. In Figure 3.3.4.2, two regions from a single re-used template are shown under a Rhodamine filter after LPEI-PS adsorption. In 3.3.4.2.**a**, the expected selectivity towards COOH regions is observed, although resistance is not as high as before. However, in **b**, elsewhere on the same sample, fully reversed selectivity is seen, with little to no adsorption within COOH regions and fairly dense packing on EG regions.

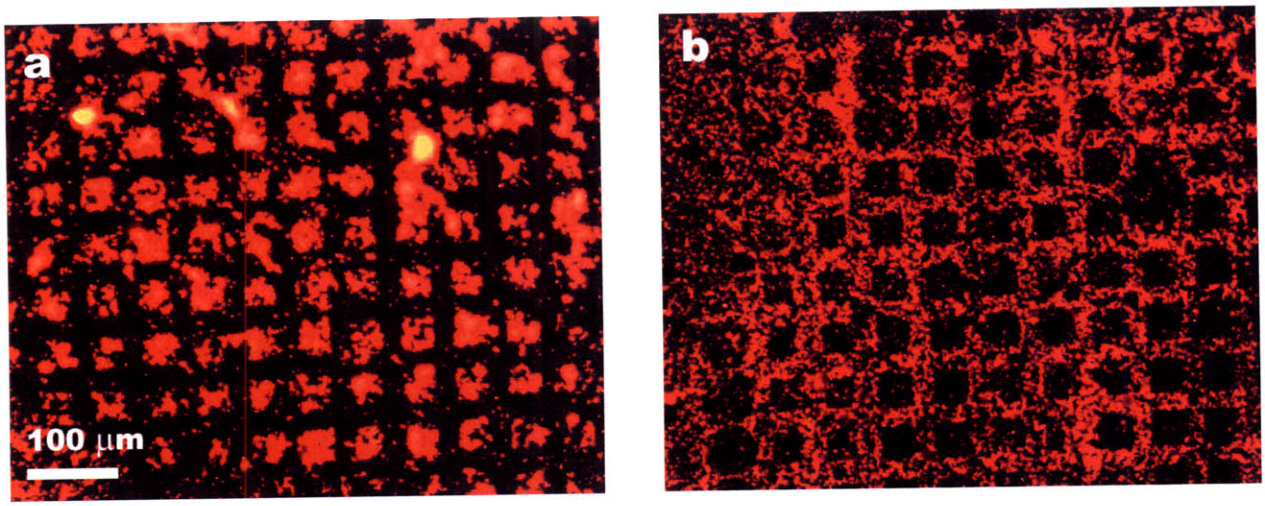

Figure 3.3.4.2. Nile Red-loaded LPEI-functionalized latex spheres adsorbed from suspension at pH 4.8 on the same template shown in Figure 3.3.4.1.b after it was rinsed and dried. Images **a** and **b** were taken at different spots on the same sample.

Clearly, the template has not been fully reconditioned after PDMS removal. Given the importance of hydration to the adhesion resistance of EG SAMs, it is possible that the substrate was not given enough time to rehydrate after ethanol sonication; the region of positive patterning may well have been the at the impact point of the water stream used in post-sonication rinsing and thus more thoroughly rid of ethanol. Another likely explanation is that the PDMS left behind it a thin film of small-molecule contaminants, possibly unreacted prepolymer having migrated out of the cast slab during curing. If this is the case, more thorough cleaning of the substrate with

additional solvents could be the solution. While thiol SAMs are known to be mobile within a surface and rearrange under heating, the fact that exactly opposite behaviors are seen, with bare regions in both, rather than the sparse adsorption throughout expected if the COOH/EG SAMs had become mixed, seems to absolve thiol mobility from blame. Clearly, further investigation of the effect of PDMS lift-off on patterned SAMs is required to see template recycling is feasible.

3.4 Comments and Conclusions

In this chapter, polyelectrolytes previously shown to exhibit strong surface preference in LbL adsorption proved successful in controlling the adsorption of colloids functionalized with them. This approach would allow for functional materials to be packaged inside selective coatings, making surface-directed deposition more widely applicable. In addition, absolute resistance proved more readily achievable when adsorbing colloidal monolayers than multilayers, and the electrostatic prevention of overlayering further facilitated the assembly of complex systems via serial adsorption steps. Colloidal arrays assembled on thiol-patterned gold substrates could be transferred into a new matrix afterwards, including thin, flexible, transparent, free-standing films. It is possible that thiol templates can be reused after array transfer, which would be of obvious value to the efficiency of assembly, but questions remain and further work will be needed on the cleaning and reconditioning of SAMs.

While polyelectrolyte-directed colloidal assembly is a promising technique, more specific interactions than electrostatics and hydrophobicity are desired for the patterning of complex, multicomponent patterns and for the exploration of simultaneous selective assembly (true surface sorting). In the next chapter, specific recognition of multiple-hydrogen bonding motifs will be used to guide assembly.

WORKS CITED

[1] A. Winkleman, B. D. Gates, L. S. McCarty, G. M. Whitesides, *Advanced Materials* **2005**, *17*, 1507.
[2] R. W. Zehner, W. A. Lopes, T. L. Morkved, H. Jaeger, L. R. Sita, *Langmuir* **1998**, *14*, 241.
[3] R. W. Zehner, L. R. Sita, *Langmuir* **1999**, *15*, 6139.
[4] R. Shenhar, E. Jeoung, S. Srivastava, T. B. Norsten, V. M. Rotello, *Advanced Materials* **2005**, *17*, 2206.
[5] J. Park, Y. S. Kim, P. T. Hammond, *Nano Letters* **2005**, *5*, 1347.
[6] P. Ghosh, M. L. Amirpour, W. M. Lackowski, M. V. Pishko, R. M. Crooks, *Angewandte Chemie-International Edition* **1999**, *38*, 1592.
[7] P. Ghosh, R. M. Crooks, *Journal of the American Chemical Society* **1999**, *121*, 8395.
[8] Y.-Y. Luk, M. Kato, M. Mrksich, *Langmuir* **2000**, *16*, 9604.
[9] E. Ostuni, R. G. Chapman, N. N. Liang, G. Meluleni, G. Pier, D. E. Ingber, G. M. Whitesides, *Langmuir* **2001**, *17*, 6336.
[10] M. C. Berg, S. Y. Yang, P. T. Hammond, M. F. Rubner, *Langmuir* **2004**, *20*, 1362.
[11] M. C. Berg, J. Choi, P. T. Hammond, M. F. Rubner, *Langmuir* **2003**, *19*, 2231.
[12] M. T. Thompson, M. C. Berg, I. S. Tobias, M. F. Rubner, K. J. Van Vliet, *Biomaterials* **2005**, *26*, 6836.
[13] H. P. Zheng, I. Lee, M. F. Rubner, P. T. Hammond, *Advanced Materials* **2002**, *14*, 569.
[14] H. Xu, R. Hong, T. Lu, O. Uzun, V. M. Rotello, *Journal of the American Chemical Society* **2006**, *128*, 3162.
[15] E. Rampazzo, E. Brasola, S. Marcuz, F. Mancin, P. Tecilla, U. Tonellato, *Journal of Materials Chemistry* **2005**, *15*, 2687.
[16] R. Shenhar, V. M. Rotello, *Accounts of Chemical Research* **2003**, *36*, 549.
[17] B. F. Lyles, M. S. Terrot, P. T. Hammond, A. P. Gast, *Langmuir* **2004**, *20*, 3028.
[18] J. H. E. Promislow, A. P. Gast, *Langmuir* **1996**, *12*, 4095.
[19] J. H. E. Promislow, A. P. Gast, *Physical Reviews E* **1997**, *56*, 642.
[20] M. Hagenbuchle, J. Liu, *Journal of Applied Optics* **1997**, *36*, 7664.
[21] E. M. Furst, A. P. Gast, *Physical Reviews E* **2000**, *61*, 6732.
[22] E. M. Furst, A. P. Gast, *Physical Reviews E* **2000**, *62*, 6916.
[23] K. Raj, G. Moskowitz, R. Casciari, *J. Magn. Magn. Mater.* **1995**, *149*, 174.
[24] J. P. Dailey, J. P. Phillips, C. Li, J. S. Riffle, *J. Magn. Magn. Mater.* **1999**, *194*, 140.
[25] A. Nethe, T. Schoppe, H.-D. Stahlmann, *J. Magn. Magn. Mater.* **1999**, *201*, 423.
[26] A. Kumar, G. M. Whitesides, *Applied Physics Letters* **1993**, *63*, 2002.
[27] Y. N. Xia, M. Mrksich, E. Kim, G. M. Whitesides, *Journal of the American Chemical Society* **1995**, *117*, 9576.
[28] J. Tien, A. Terfort, G. M. Whitesides, *Langmuir* **1997**, *13*, 5349.
[29] J. Aizenberg, P. V. Braun, P. Wiltzius, *Physical Review Letters* **2000**, *84*, 2997.
[30] H. P. Zheng, M. F. Rubner, P. T. Hammond, *Langmuir* **2002**, *18*, 4505.
[31] I. Lee, H. P. Zheng, M. F. Rubner, P. T. Hammond, *Advanced Materials* **2002**, *14*, 572.
[32] K. M. Chen, X. P. Jiang, L. C. Kimerling, P. T. Hammond, *Langmuir* **2000**, *16*, 7825.
[33] S. Palacin, P. Hidber, J.-P. Bourgoin, C. Miramond, C. Fermon, G. M. Whitesides, *Chem. Mater.* **1996**, *8*, 1316.

[34] Z. Zhong, B. Gates, Y. N. Xia, D. Quin, *Langmuir* **2000**, *16*, 10369.
[35] X. P. Jiang, H. P. Zheng, S. Gourdin, P. T. Hammond, *Langmuir* **2002**, *18*, 2607.
[36] X. P. Jiang, P. T. Hammond, *Langmuir* **2000**, *16*, 8501.
[37] G. Decher, *Science* **1997**, *277*, 1232.
[38] S. L. Biswal, A. P. Gast, *Phys. Rev. E* **2003**, *68*, 021402.
[39] X. P. Jiang, C. Ortiz, P. T. Hammond, *Langmuir* **2002**, *18*, 1131.
[40] M. F. Rubner, D. Yoo, S. S. Shiratori, *Macromolecules* **1998**, *31*, 4309.
[41] K. F. Weyts, E. J. Goethals, *Makromolekulare Chemie, Rap. Comm.* **1989**, *10*, 299.
[42] R. G. Smits, G. J. M. Koper, M. Mandel, *J. Phys. Chem.* **1993**, *97*, 5745.
[43] C. J. Bloys van Treslong, *Recueil, J. Royal. Neth. Chem. Soc.* **1978**, *97*.
[44] M. Mandel, *Euro. Polym. J.* **1970**, *6*, 807.
[45] P. Harder, M. Grunze, R. Dahint, G. M. Whitesides, P. E. Laibinis, *J. Phys. Chem. B* **1998**, *102*, 426.

CHAPTER 4 – MULTIPLE HYDROGEN BONDING-DIRECTED COLLOIDAL ASSEMBLY

4.1 Introduction

4.1.1 Non-Covalent Assembly via Multiple Hydrogen Bonding

Hydrogen bonding, whose nature and relative strength were discussed in Chapter 2, is of particular interest for selective adsorption applications due to its directionality and tuneability. Multiple hydrogen bonding (MHB) – the formation of two or more hydrogen bonds between neighboring groups on each interacting species, is of even greater interest, since the coordination of multiple bonds not only increases the overall strength of the interaction, but also its selectivity, requiring precise geometric alignment of the different bonding sites. MHB interactions are essential to host-guest chemistry as well as being at the heart of molecular genetics, directing the hybridization of nucleic acids.

MHB motifs can be separated into two principal classes: self-complementary and non. Self-complementary motifs are those able to MHB with an identical motif, such as DA (donor-acceptor), DDAA, and DADA; non self-complementary motifs must be matched up with an opposite sequence of donors and acceptors, such as AA/DD, ADA/DAD, ADDA/DAAD, etc. Self-complementarity is of most use for self-assembly of ordered two- and three-dimensional crystal-like lattices of a single molecule. Non self-complementary motifs, conversely, are better choices when distinct populations of host and guest species are desired, as in recognition and selectivity applications. Schematic illustrations of common types of MHB architectures are given in Figure 4.1.1.*[1]*

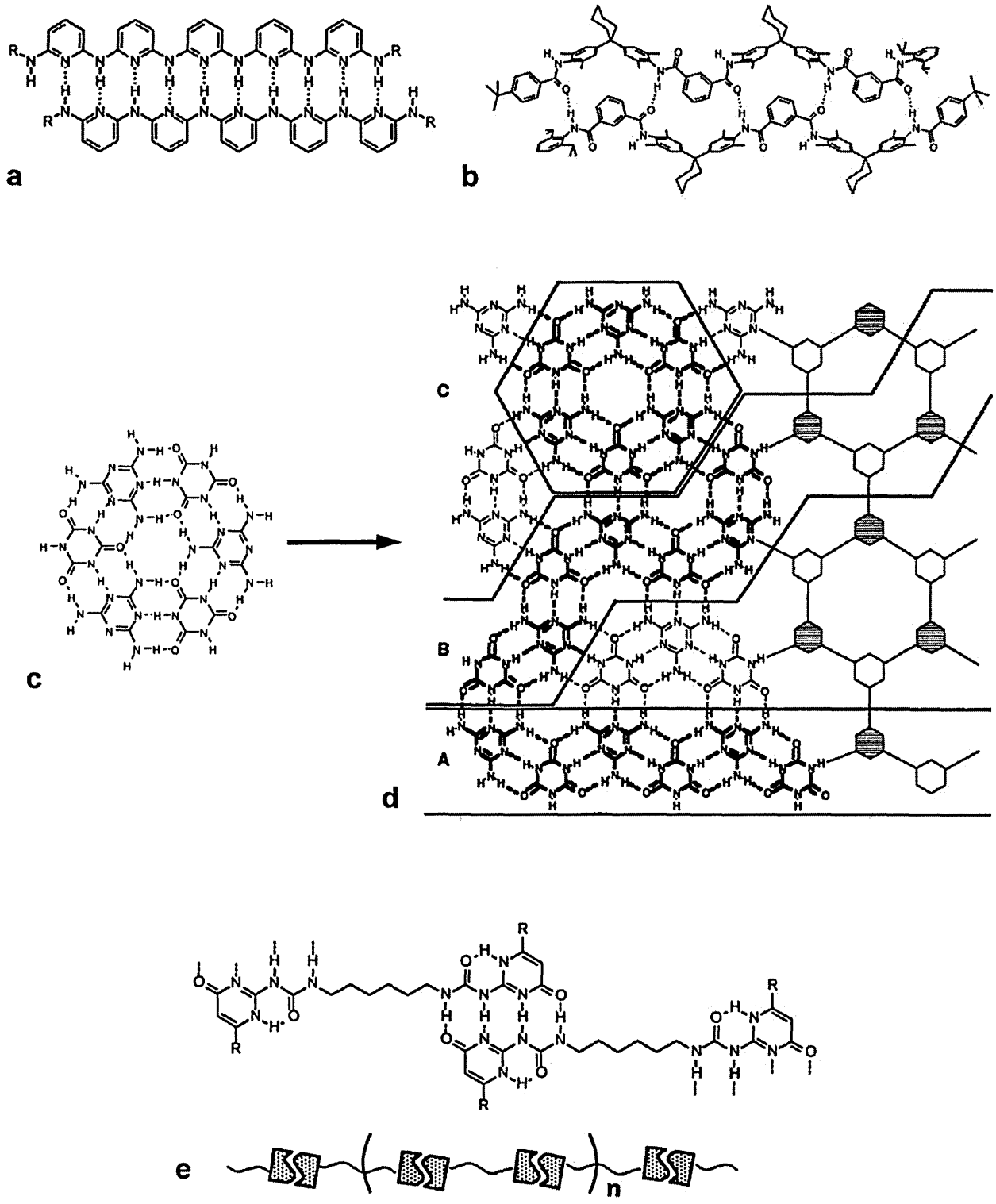

Figure 4.1.1. Some well-known MHB architectures: Planar ladder (**a**), twisted zipper (**b**), lattices based on cyanuric acid and melamine: cyclic hexamer (rosette) (**c**), 3D hexagonal-cell lattice of rosettes (**d-A**), crinkled-tape (**d-B**), linear tape (**d-C**), and supramolecular assembly of bifunctional linear ureidopyrimidones (**e**).*[2-4]*

By strategic positioning of MHB motifs, super-molecules can be built from non-covalently linked building blocks. Since hydrogen bonding can be modulated via temperature and pH, supramolecules of this sort can reversibly disintegrate and reassemble in response to environmental conditions; a large array of building blocks have been designed for use in such "plug and play" chemistry.*[5]* Bifunctional derivatives of 2-ureido-4[1H]-pyrimidone (UPy), which carry two self-complementary quadruple hydrogen bonding motifs, can form cyclic, linear, or micellar supramolecular assemblies; the shape and size of these supramolecules can be varied by using different linker structures. For example, if two UPy motifs are linked by an alkylic segment, its parity determines the orientation of one motif relative to the other and thus the tendency of the molecules to form cyclic vs. linear chains.*[6]* Stable, well-organized dendrimers can be grown divergently from a single monomer tri-functionalized with self-complementary MHB motifs.*[7]*

Polystyrenes with MHB side chains (diaminotriazine or diacyldiaminopyridine groups, both having DAD motifs) have also been synthesized, providing linear building blocks with an affinity for binding ADA motifs; similarly, a mixed solution of thymine- and pyridine-functionalized polystyrenes (thymine and pyridine are complementary) can reversibly self-assemble into microspheres via non-covalent crosslinking.*[8]* These modified polystyrenes can also be incorporated into bulk materials, whose surfaces (planar or more complex) will thus contain recognition groups which can be used as tethers.*[9]* Intramolecular MHB in diaminotriazine-functionalized polystyrenes can provoke folding into micellar structures which can then be reversibly dispersed and reformed by adding small species with competitive MHB potential or by altering solvent polarity.*[10]* Non-covalent supramolecular assembly of this sort requires very strong hydrogen bonding and the resulting structures present a unique combination of polymer-like viscoelastic qualities that transition to liquid-like qualities as the temperature is raised and the hydrogen bonding weakens.*[11]*

In order to optimize use of MHB recognition for non-covalent self-assembly, much work has also been done on quantifying the strength of MHB interactions as well as their modulation via structural modification or environmental control.*[12]* When designing MHB structures *de novo*, the strength of a given hydrogen-bonding motif can be varied by careful selection of nearby atoms, exploiting the strong influence of electron density distribution on hydrogen bonding (see Chapter 2.1 for discussion of the nature and origin of hydrogen bonding), or by

tailoring the molecular architecture such that the MHB groups are in the right relative orientations for multidentate binding. A consideration specific to multiple hydrogen bonding is the positioning of donors and acceptors within the same motif to minimize the unfavorable electrostatic interactions between two donors or two acceptors; for quadruple hydrogen binding, DDAA motifs have been found to bind more strongly than DADA (see Figure 4.1.2).*[1]*

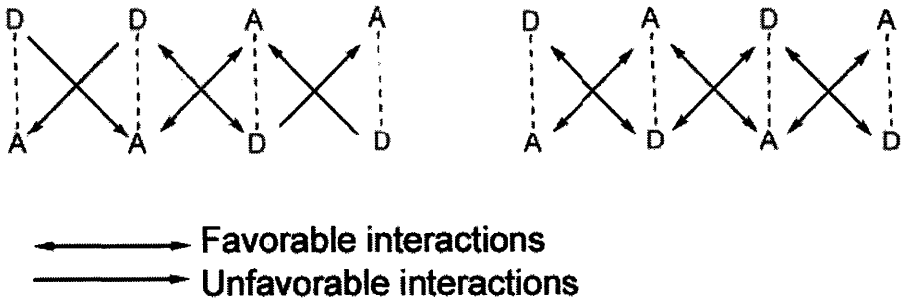

Figure 4.1.2. Comparison of the force balances (not including the hydrogen bonds themselves) resulting from different configurations possible for quadruple MHB. Overall, the DDAA arrangement has four favorable interactions and two unfavorable, while the DADA arrangement has exclusively repulsive interactions. Adapted from *[12]*.

In a very sophisticated form of tuning interaction strength via molecular design, light-responsive species have been synthesized in which reversible UV-induced *cis/trans* isomerisms activate and deactivate MHB by altering stereochemistry.*[13, 14]* Hydrogen bonding can also be supplemented by pairing it with coordinating interactions. Aromatic stacking, in which π-orbital interactions promote parallel stacking of aromatic rings, has been used frequently to this end since it does not interfere with MHB; diamidopyridine (DAP) groups are frequently used for this sort of multitopic self-organization. When gold colloids functionalized with mixed monolayers of thymine- and pyrene-terminated thiols were exposed to DAP-grafted polymers, the mobility of thiols on gold allowed the monolayer to rearrange so as to maximize multitopic interaction sites.*[15]* The Rotello group have also studied the adsorption of block copolymers with DAP-grafted segments, finding that their deposition rate and adsorbed layer morphology depends on the density of recognition sites both on the surface and within the polymer, consistent with the predictions of free-energy modeling examined in Chapter 2.3.*[16, 17]* When the DAP graft density of polystyrene exceeds 10%, spontaneous solution assembly of giant (1-5 μm) vesicles can be observed.*[18]* DAP-thymine MHB has also been used for selective colloidal adsorption in

parallel with electrostatically-driven selective adsorption; the non-interference of the interactions allowed such colloidal assemblies to be simultaneously adsorbed from mixed solution.*[19]*

4.1.2. Nucleic base pairing

Possibly the most famous of the MHB systems is the nucleic base-pairing at the heart of molecular genetics. It is the double hydrogen bonding between adenine and thymine and triple hydrogen bonding between cytosine and guanine that determine DNA structure and function, providing a self-correcting syntax for the transmission of genetic information. Multiple hydrogen bonding within the double-helical structure of DNA and between free nucleic bases are shown in Figure 4.1.2.1.

The strong specificity of complementary DNA sequences (e.g., ACATTAG/TGTAATC) has been applied by many to direct specific recognition of other species. For instance, gold wires 200 nm in diameter and up to 6 μm long have been end-functionalized with thiolated oligonucleotides to create self-assembling conductive bridges and junctions.*[20]* By using sequences of different length and GC:AT ratios, temperature can be used to control the order in which different element pairs bind or unbind, an approach sometimes called temperature-programmed assembly (TPA).*[21]* Similar tiny, self-assembling junctions were made by Fitzmaurice and coworkers entirely from oligonucleotides designed to self assemble into either linear or Y-shaped scaffolds; the structures' 50 nm arms were capped with avidin moieties to allow binding of biotinylated metal nanoparticles.*[22, 23]* Oligonucleotide recognition can also mediate micron-scale colloidal assembly, yielding well-ordered crystal packing.*[24]* Sequence-recognition driven assembly can be rather slow; using optical tweezers to directly measure interactions between colloids with 14-base DNA tags, Crocker and Biancaniello found that binding dynamics were on the order of several days, although assembly can be accelerated by increasing the density of linker sequences grafted on the surface.*[25]* While extremely selective, sequence-directed assembly requires costly custom synthesis of oligonucleotides, making it impractical for large-scale functionalization. Protein-substrate binding (such as streptavidin-biotin, antibody-antigen) is considered by many an even more promising approach to the biologically-directed self-assembly of nano-objects than

oligonucleotide recognition, as the methods of protein design and production via genetic engineering are well-established and more apt to provide simple, robust materials.*[26]*

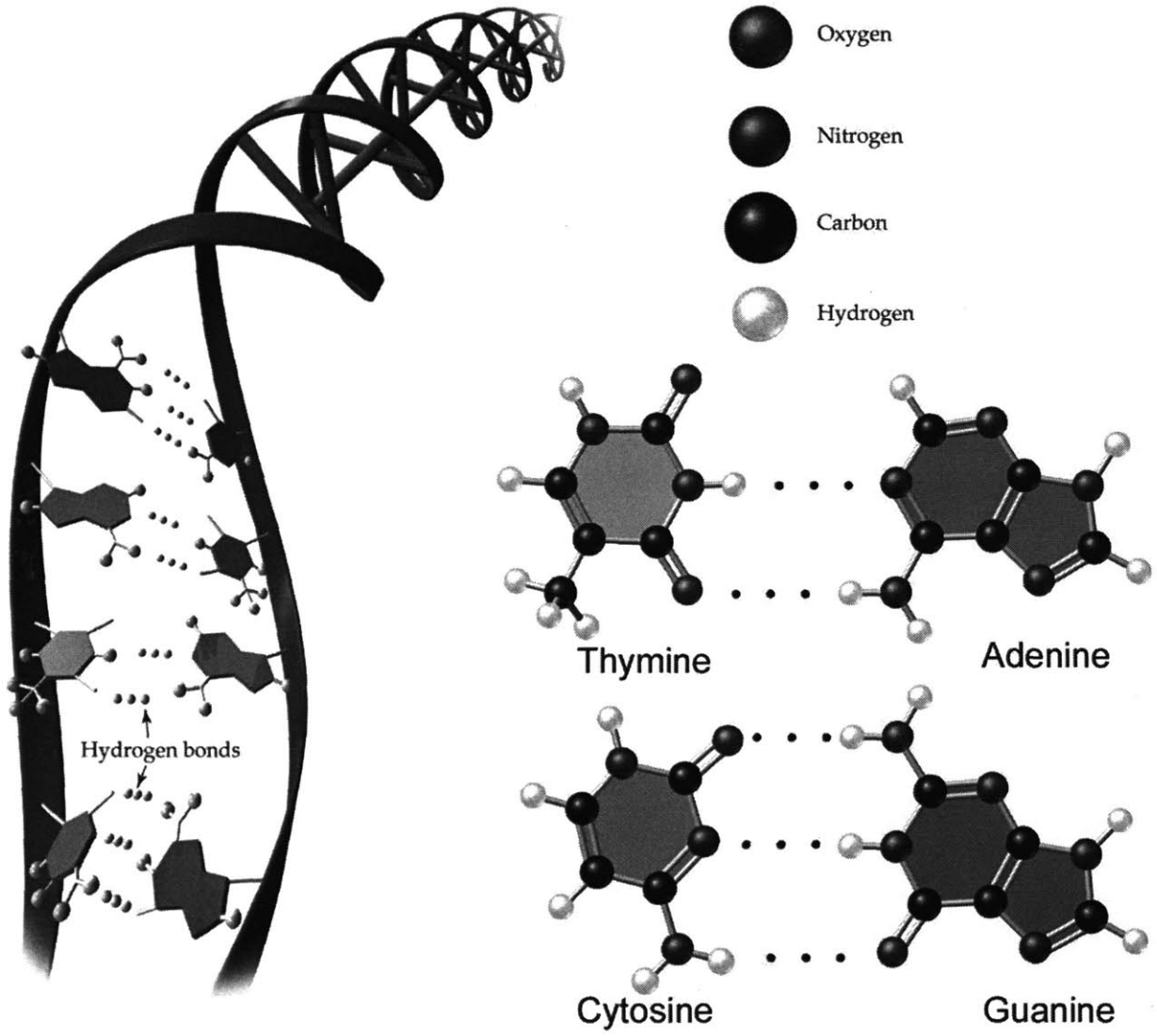

Figure 4.1.2.1. Nucleic base-pairing and its role in DNA structure. Reproduced from *[27]*

Another alternative to custom-synthesis of oligonucleotides when cost and efficiency are more important than the ability to distinguish dozens of different adsorbate-surface pairings is the use of homopolymeric nucleotides or nucleotide analogues, that is, to use species functionalized with a single type of nucleic base each. For instance, Hest et al have synthesized block copolymers of poly(ethylene oxide) and either thymine- or adenine-grafted poly(methacrylic acid) and have found that the addition of the nucleobases shifts the

hydrophobic-to-hydrophilic balance towards hydrophilicity when mixed solutions of the block copolymers are studied, providing further degrees of control over the range of morphologies displayed by polyamphiphiles in solution (micelles, rods, vesicles, etc).*[28]* Such PEG-nucleic base block copolymers could be interesting materials for polymer-on-polymer stamping to create adsorption-resisting PEG brush surfaces.

Polystyrene end-capped with adenine or thymine groups is found to associate in solution in ways clearly impossible for plain PS; in particular, heat can be used to reversibly promote and disrupt intermolecular organization. *[29]* In the bulk, end-capping of PS, poly(isoprene) and PS-PI block copolymers raised their T_g and increased their melt viscosity by two orders of magnitude. *[30]* Similar rheological changes were observed when UPy side chains were grafted throughout poly(butyl acrylate), with the modified polymers having much greater cohesive strength. *[31]* When styrenes and thymine-grafted styrenes were copolymerized, the resulting randomly-grafted chains reversibly adsorbed on adenine-functionalized surfaces depending on solvent environment; adsorbed chains were impervious to apolar solvents but dissociated from the surface in DMSO.*[32]*

While these results highlight the ability of a single MHB pairing to dramatically modify polymer behavior and properties, the synthesis of the above compounds is complex and leads to neutral nucleobase-grafted species. Given the methods of particle and surface modification previously found advantageous for selective adsorption systems, polyelectrolytes compatible with aqueous experimental conditions would be better-suited to our purposes. Currently, the most readily available such compounds are natural RNA homopolymers, which will be the starting point for our exploration in this chapter of the application of nucleic base pairing to directed assembly. MHB-directed assembly is particularly intriguing for asymmetric functionalization, which will be briefly introduced next.

4.1.3. Approaches to Asymmetry

Asymmetric functionalization of symmetric objects is an essential but challenging aspect of micro and nanoscale assembly. Bifunctional colloids and nanowires can serve as interaction mediators, enabling coupling of two different species or introducing anisotropy in composite

materials by enforcing a certain organization and orientation of components. While numerous methods exist for the creation of complex functionality on a single object at a time, approaches allowing simultaneous modification of large populations are of greater potential usefulness as well as difficulty. Colloids having distinctly segregated surface chemistries would be of particular interest for selective adsorption applications.

One route to asymmetry is to guide the bulk formation of the object itself. For example, Velev and coworkers have been able to create what they call "eyeball" particles (microspheres with a large and distinctly different spot on one side) by using an electric field to trap nanodroplets containing a mix of different polymer solutions at an oil/air interface. Simple evaporative drying can then induce self-segregation of the different components; blends of three or more species, including inorganic nanoparticles as well as polymer precursors, can similarly be used to create even more complex stratified architectures.*[33]* While this technique has great potential for the creation of objects with full-depth anisotropy (density, magnetic susceptibility, porousness, etc) rather than just contrasting surface functionalities, its material constraints are a poor match for our desired application.

Another technique, also reported by the Velev group among others, is to partially mask a monolayer array of colloids by embedding it in a protective matrix from which it can be easily freed after modification of the unmasked regions. By evaporating a sulfate latex monolayer onto a planar substrate from a glucose solution, for example, cationic surfactants can be deposited on the exposed surface – from an organic solvent to which glucose is insoluble, or by μCP – creating a microsphere with oppositely-charged regions.*[34]* This method does require that both the object to be modified and the modifier be stable to subsequent rinsing away of the mask, but it is still a far more flexible approach than the previous.

In a simpler twist on the masking approach, Velegol and Snyder have found that simply stably adsorbing large colloids on a planar surface is enough to mask the contact region while adsorbing a modifier on the rest of the sphere. After resuspension of the particles, the bare region can be functionalized as well. This technique has fewer material constraints than use of an actual masking layer but results in highly-asymmetric particles, with masking typically protecting only 1-3% of the surface area unless very globular species – polymers with high R_g or nanoparticles – are adsorbed onto a very dense colloidal monolayer.*[35]* Spot-functionalization of this sort is best suited for creating heterodoublets while preventing larger aggregation.

Depending on the conditions required for transfer of the modifier to the particle surface, no masking may be necessary. Cohen and Rubner have shown that a polycation can be stamped from a flat PDMS slab onto a monolayer of colloids previously functionalized with a polyanion-terminated polyelectrolyte multilayer film.*[36]* As with glucose masking, the area modified by POPS can cover close to half of the particles, which would be ideal for creating particles with MHB-complementary hemispheres promoting linear and reversible self-assembly in solution.

In this chapter, the ability of nucleic base pairing to direct assembly was investigated by functionalizing colloids and surfaces with either natural RNA or a synthetic analogue. Natural RNA was used first for proof of concept, then replaced by a biomimetic polyelectrolyte to reduce costs and improve reproducibility.

4.2 Materials and Methods

4.2.1. Materials Discussion

Non-degradable polyelectrolytes having nucleic base side-chains as well as nucleic base-terminated silanes were synthesized to replace natural RNA when more robust materials were desired. The structure and properties of these novel materials will be briefly given here; their design, preparation, and characterization will be more fully discussed in Chapter 6.

Poly(allyl amine) was grafted with thymine by amidation; the resulting polymer, shown in Figure 4.2.1.**a**, was found to be 35% grafted (one thymine-grafted repeat unit per 1.7 per unmodified acrylic acid repeat unit) and was readily soluble in pure water and 0.1X PBS. Poly(acrylic acid) was grafted with uracil or with adenine, also by amidation; the resulting polymers, shown in Figure 4.2.1.**b** and 4.2.1.**c**, were found to be 12% and 7% grafted, respectively, and were also readily soluble in pure water and dilute buffer. These grafted polyelectrolytes were used to introduce nucleic base groups on charged colloids and functionalize surfaces via POPS as well as to build multilayered thin films. PAAs grafted with cytosine and guanine were also synthesized, although less frequently used due to their lower grafting rates.

Adenine and cytosine were attached to alkyl triethoxysilanes, shown in Figure 4.2.1.**d** and 4.2.1.**e**. These silanes were used to introduce nucleic base groups on silica surfaces (planar or colloidal) via SAM formation. Pure nucleic base-grafted silane surfaces proved too crowded for effective interaction with potential adsorbates; instead, mixed SAMs with a 3:1 ratio of mercapto (non-specific hydrogen bonding ability) or vinyl (inert to hydrogen bonding) and nucleic base surface groups were used.

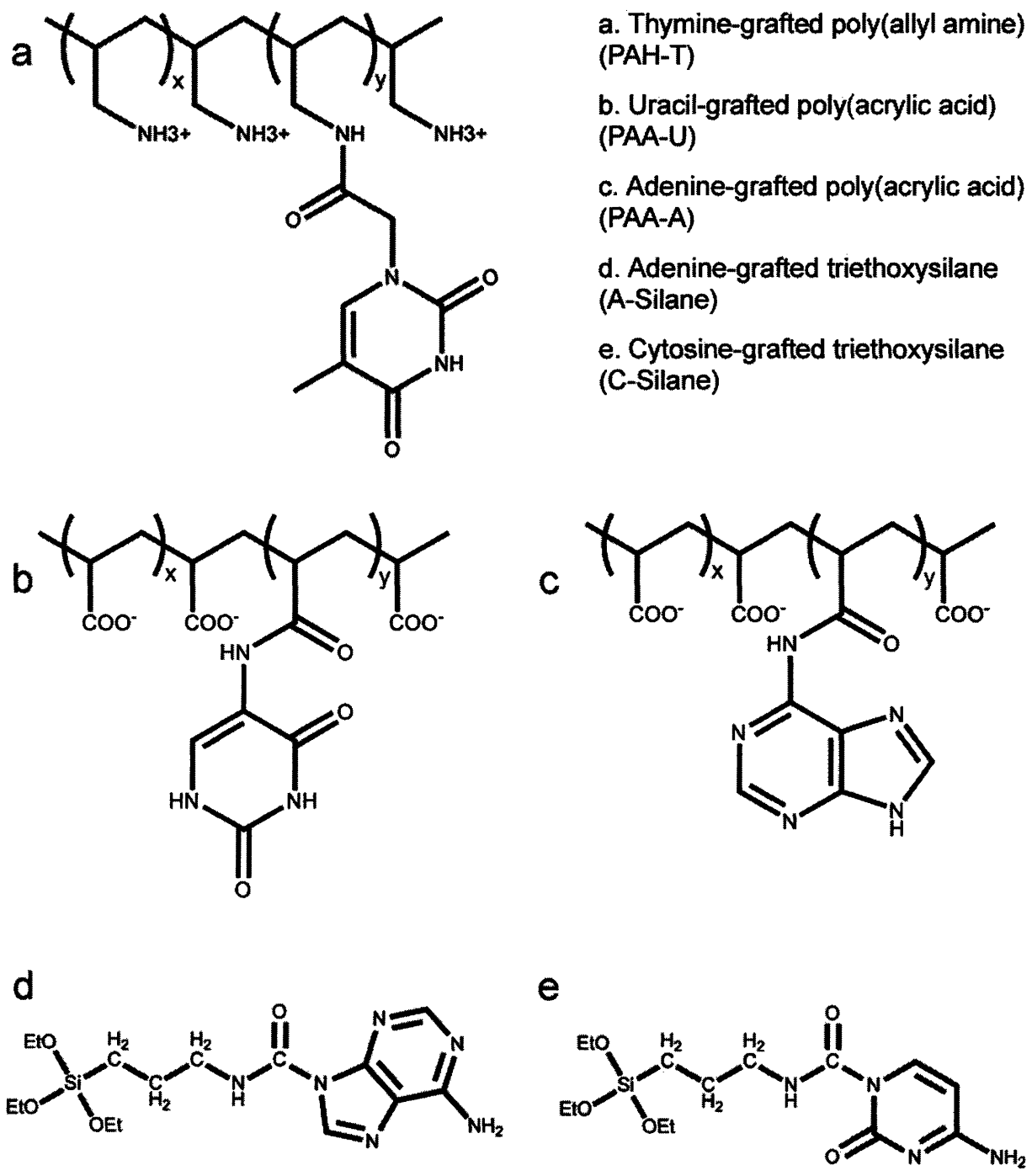

Figure 4.2.1. Chemical structure of the nucleic base-grafted polyelectrolytes and triethoxysilanes custom-synthesized for use in MHB-directed selective adsorption studies. See Chapter 6 for synthesis and characterization details.

4.2.2 Template preparation

Adenine-, cytosine-, and uracil-terminated triethoxysilanes (A-silane, C-silane, U-silane) were synthesized as described in Chapter 4.2. 3-(Aminopropyl)triethoxysilane was purchased from Aldrich. Allyltriethoxysilane was purchased from Gelest (Morrisville, PA).

Chromium photo masks (Advanced Reproductions) and corresponding silicon masters (Microsystems Technology Laboratory, MIT) were prepared as templates for poly(dimethylsiloxane) (PDMS, Sylgard 184, Dow-Corning) stamps. Prior to use, PDMS stamps were washed with soap and water, rinsed with MilliQ water, and dried under nitrogen flow.

Silicon substrates to be functionalized with ethoxysilanes were stamped or immersed immediately after cleaning by Piranha treatment, an immersion into a 70:30 mixture of concentrated sulfuric acid and 30% aqueous hydrogen peroxide followed by copious rinsing with MilliQ water. CAUTION – PIRANHA SOLUTION IS AN EXTREMELY STRONG OXIDIZER AND WILL REACT EXPLOSIVELY WITH ORGANIC COMPOUNDS. EXTREME CARE MUST BE USED IN PROPER PREPARATION, HANDLING, AND DISPOSAL OF PIRANHA SOLUTIONS. Stamps were inked with 2-8 mM solutions of ethoxysilanes in ethanol using a cotton-tipped applicator and then thoroughly dried under nitrogen flow before being brought into contact with the substrate. After 30-60 s, the stamp was removed and the surface was rinsed with ethanol and dried under nitrogen flow before being immersed into the second ethoxysilane solution, also 2-8 mM in ethanol. Silane inks were often mixed solutions of one of the nucleic base-terminated triethoxysilanes and either mercapto- or allyl-terminated triethoxysilanes.

For POPS, stamps were immersed in aqueous solutions of the "ink" polyelectrolyte for 1-12 hours and dried, without rinsing, immediately before being brought into contact with the substrate. After 5-30 minutes, the stamp was removed and the surface was rinsed with MilliQ and dried under nitrogen flow before being immersed in the second polyelectrolyte solution for 5-30 minutes. The resulting patterned surfaces were again rinsed with MilliQ, dried under nitrogen flow, and stored under vacuum until use. Optical microscopy and scanning force microscopy were used to characterize the POPS-transferred polymeric layer. To prepare homogeneous (non-patterned) surfaces, only the latter immersion step was used.

Three-dimensional "hole" templates were prepared by casting and curing a 1 mm layer of polyurethane (NOA, Norland Optical Materials) over a PDMS column stamp, according to published procedure,*[37]* and then building a $(PDAC/SPS)_{5.5}$ multilayered film over the whole NOA substrate. A final layer of RNA or a PAA derivative was added by immersion. A flat PDMS stamp was then used to stamp a second RNA or PAH derivative on only the upper surfaces of the template. See Figure 4.3.2.3. for schematic explanation of three-dimensional templates. Templates incorporating natural RNA were prepared immediately before use.

4.2.3 Colloid Preparation and Characterization

Sulfate-modified polystyrene latex microspheres of diameters 1.0 and 8.7 μm were obtained from Interfacial Dynamics Corporation as surfactant-free suspensions in distilled, deionized water. Aliphatic amine polystyrene latex microspheres of diameters 1.9 and 7.5 μm were obtained from Interfacial Dynamics Corporation as surfactant-free suspensions in distilled, deionized water. Aliphatic amine polystyrene latex microspheres of diameters 870 nm and hydroxylated (Si-OH surface functional groups) silica microspheres of diameters 450 nm, 1.0 μm, and 5.1 μm were obtained from Bangs Laboratories as 10 wt% suspensions in distilled, deionized water. Anthracene-labeled poly(methacrylic acid) (PMAA-fluo, MW = 8,000 g/mol excluding anthracene, PDI = 1.10) was obtained from Polymer Source (Montréal, PQ).

Polystyrene microspheres were functionalized by electrostatic attachment of an oppositely-charged polyelectrolytic outer layer; sulfate-functionalized latex was functionalized with poly(allyl amine) derivatives, while aliphatic amine-functionalized latex was coated with natural RNA or poly(acrylic acid) derivatives. 0.2 ml of aqueous colloidal suspension (used as delivered, generally 2-5 % solids by weight) was added to 1.5 ml aqueous polyelectrolyte solutions prepared as follows. For RNA functionalization, 2-5 mg RNA was dissolved in 1.5 ml RNAase-free 0.1X PBS (1:100 dilution of 10X PBS stock in RNAase-free water). For PAA or PAH-derivative functionalization, reaction mixtures were used after repeated dialysis against first MilliQ water, and then 0.1X PBS; typical polymer concentrations were on the order of 0.5-1 wt%. After 1 hour of occasional mixing, unbound polyelectrolytes were rinsed away from the colloidal suspensions by repeated centrifugation and redispersal in 0.1X PBS using a Galaxy 7D

microcentrifuge (VWR). Colloidal surface charge was evaluated before and after polyelectrolyte modification using a ZetaPALS zeta potential analyzer (Brookhaven Instruments). Functionalized colloids were refrigerated until needed, except for RNA colloids, which were prepared on an as-needed basis immediately before use to avoid degradation.

Hydroxylated silica microspheres were functionalized with a SAM of one of the nucleic base-grafted triethoxysilanes described above. 0.2 ml of microsphere suspension (typically, 5-10 wt% solids) was washed with ethanol and then combined with 1.5 ml of 2 mM silane solutions in ethanol. After 1-3 hrs, unbound silane was washed away from the colloidal suspensions by repeated centrifugation and redispersal first into ethanol and then into 0.1X PBS.

4.2.4 Array Preparation and Characterization

Substrates patterned with silane SAMs were incubated in 0.1X PBS for 30 minutes prior to use to rehydrate and reequilibrate the terminal groups to the intended pH and pI conditions. Two- or three-dimensional substrates patterned with natural RNA were used immediately after assembly to avoid RNA degradation.

One or two drops of functionalized microsphere suspension were dropped over the patterned surface and left for 15-180 min. Substrates were then rinsed by two immersions in 0.1X PBS with gentle agitation and dried either under vacuum or under very gentle nitrogen flow. The resulting arrays were characterized by optical and fluorescence microscopy when colloids and pattern features were >500 nm; for smaller features, scanning electron microscopy (JEOL 5910 SEM) was performed after gold sputter-coating. Some patterned silane substrates were reused after complete removal of any adsorbed colloids by 1 min sonication in ethanol using a Branson 1210 ultrasonication bath (Branson Ultrasonics).

The methods of preparation of asymmetric colloids are of particular complexity and will be presented separately in Section 4.4.

4.3 Two- and Three-Dimensional Selective Surfaces

4.3.2 Assembly Directed by Natural RNA

To explore the potential of nucleic base pairing to direct adsorption selectivity, RNA was used to functionalize colloids by addition of a single layer of a single homopolymer, analogously to the polyamine functionalization discussed in Chapter 2.4.2. Surfaces were then patterned with nucleic bases by POPS of RNA homopolymers onto positively-charged substrates, and the adsorption behavior of RNA-beads on RNA-patterns was studied. All work was done in dilute PBS at pH 7.4 unless otherwise noted.

RNA stamping proved difficult due to the incompatibility of hydrophobic PDMS and hydrophilic RNA. RNA could not be dissolved in any non-aqueous solvent, so stamps were either plasma-treated before inking or allowed to soak overnight in the ink solution, a method used by others in this group to stamp aqueous inks.*[38]* Pattern transfer was often incomplete, especially when stamps were plasma-treated. In Figure 4.3.2.1, the pU transferred by stamping onto an LPEI adhesion platform is actually visible under optical microscopy and large defects are seen in the pattern (40 μm x 150 μm rectangles).

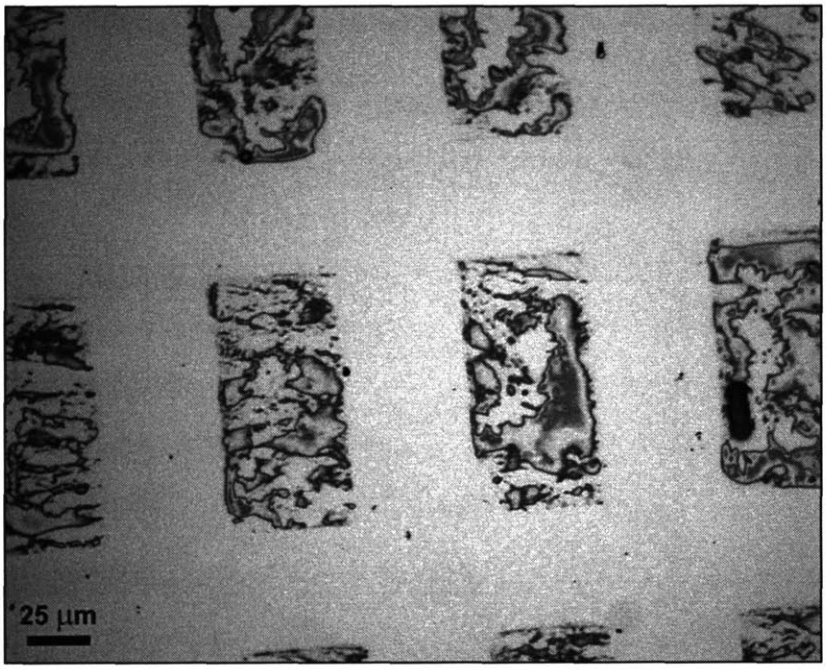

Figure 4.3.2.1. Optical micrograph of an LPEI-coated silicon substrate stamped with pU. The stamp was plasma-treated for 20 s under O_2 before being immersed in 0.1 wt% pU in PBS for one hour before use. Stamp-substrate contact time was 30 min.

Comparably poor quality was observed with other large-featured stamps (> 20 μm), while transfer of features on the order of 1 μm could not be seen at all. Such surfaces rarely led to patterned adsorption of beads with complementary functionality even on the visible ink regions, so it is possible the transferred material was degraded in some way, or that we are actually observing damage to the LPEI platform rather than ink transfer, although the optical evidence supports transfer.

The best results were achieved when large-featured stamps were immersed overnight in 0.1 wt% RNA in PBS without plasma treatment. After stamping, the background of the pattern was filled by immersion in another RNA solution in PBS. In Figure 4.3.2.2, two surfaces prepared in this way are shown after adsorption of colloids functionalized with the complement to one of the pattern regions.

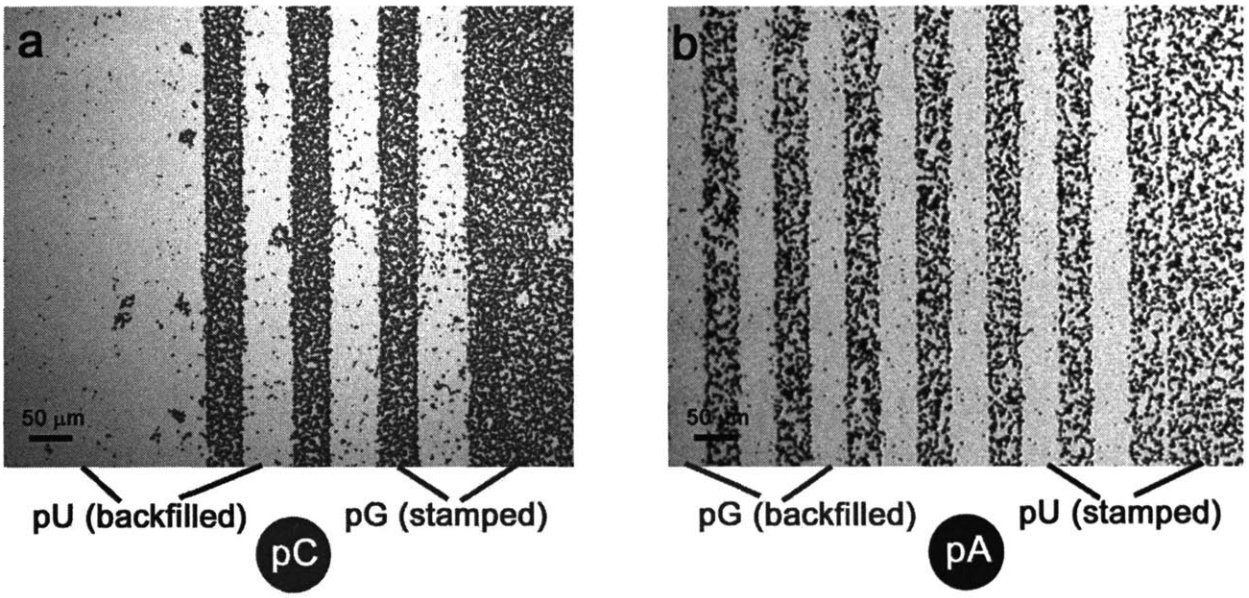

Figure 4.3.2.2. Selective adsorption of RNA-functionalized beads on RNA POPS patterns. Surface **a** was stamped with pG and backfilled with pU, while surface **b** was stamped with pU and backfilled with pG, using the same stamp design. Suspensions of microspheres coated in either pC (sample **a**) or pA (sample **b**) were dropped over the patterns and then rinsed away by immersion.

The patterned surfaces presented in Figure 4.3.2.2 provoked strong adsorption selectivity. Colloids adsorbed in dense monolayers on their complementary regions (pC on pG, pA on pU) while exhibiting high resistance to the non-complementary surface. Compared to the polyamine-directed colloidal arrays shown in Chapter 2.4.2, bead packing is much denser and resistance is comparable or improved, leading to more sharply-defined features. While zeta potential confirmed that the RNA-functionalized beads were negatively-charged, it would appear that electrostatic repulsion between beads is negligible. Also notable is the fact that in this approach, the same surfaces serve as both "adsorption resisters" and "adsorption promoters" – each nucleic base is selective to its complement and indifferent to the non-complementary regions. With two highly-selective but non-interfering surface/bead pairs, two-component assembly from mixed solutions (simultaneous rather than serial adsorption steps) should be possible, achieving the goal of true surface selectivity.

Unfortunately, RNA proved an extremely unreliable experimental subject and subsequent attempts at preparing adsorption-directing POPS RNA patterns failed despite exact replication of previously-successful conditions. The fragility of natural RNA coupled with the requirement of

extremely long inking times make this system extremely vulnerable; given the high cost of RNA homopolymers, the use of stable synthetic analogues of RNA was explored instead and is reported in Chapter 3.4.

RNA also proved successful in functionalizing three-dimensional patterns. Such relief patterns were originally explored as a way of partially masking colloids so as to further functionalize only the portion exposed above the well's edge. Polyurethane substrates with 100 μm circular wells 2 μm deep were functionalized by adsorbing pA on top of a LbL adhesion platform, and a flat PDMS stamp inked with pU was then used to functionalize only the top surface of the relief pattern (see Figure 4.3.2.3 for schematic illustration). Large (8 μm) microspheres coated in pU adsorbed exclusively within the pA wells, as shown in Figure 4.3.2.3. Inter-particle electrostatic repulsion again appears to be negligible, but many beads were lost in rinsing, so wells were only partially filled. However, resistance was high, again showing the promise of nucleic base-pairing for selective adsorption applications.

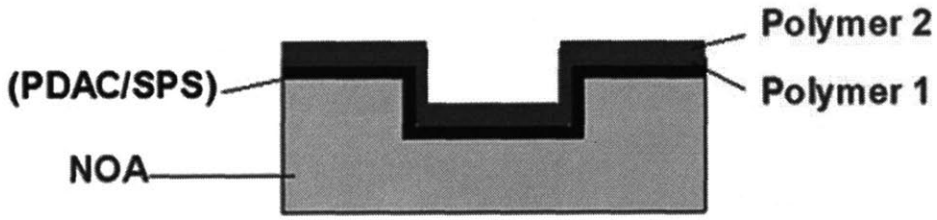

Figure 4.3.2.3. Section profile of a three-dimensional template created by LbL assembly and POPS onto a molded polyurethane substrate. For the template shown in Figure 4.3.2.4, "Polymer 1" was pA and "Polymer 2" was pU.

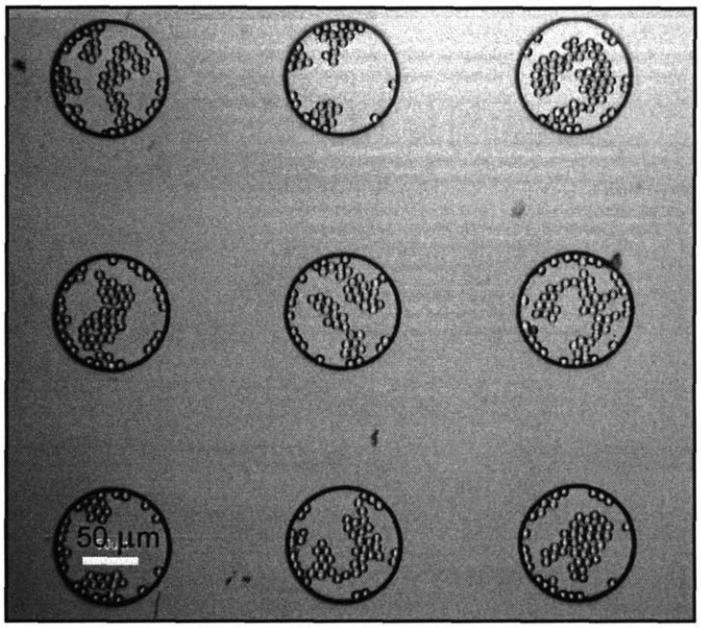

Figure 4.3.2.4. Optical micrograph of large pU-functionalized colloids (8 µm) selectively adsorbed inside 100 µm wide pA-functionalized wells while avoiding adsorption on the pU upper surface of the 3D patterned substrate.

Having been designed to replace natural RNA, nucleic base-grafted polyelectrolytes and silanes were next used to functionalize surfaces and microspheres with specific recognition groups. As previously, all adsorption work was done in dilute PBS buffer, but there was no longer a need to guarantee RNAase absence nor to prepare materials immediately before use.

4.3.3 Assembly Directed by Synthetic RNA Analogues

Surfaces patterned with nucleic bases groups were prepared both by microcontact printing (µCP) of triethoxysilanes and by polymer-on-polymer stamping (POPS) of grafted polyelectrolytes.

For POPS of nucleic base-grafted PAA derivatives, substrates were first made positively-charged by adsorption of either a single LPEI layer or a polycation-terminated multilayer film. LPEI adhesion layers were made by immersing freshly plasma-treated silicon wafer substrates in

LPEI at pH 2 (fully charged). Immediately before use, LPEI substrates were rinsed with MilliQ and dried; if dried and left exposed to air too long, the substrates were found to become hydrophobic, a change attributed to rearrangement of the LPEI chains in response to the environmental shift. LbL adhesion platforms were less sensitive to storage. PDMS stamps were inked by overnight immersion in 0.5 wt% solutions of PAA derivatives in dilute PBS after light plasma treatment (20 s under O_2). In Figure 4.3.3.1, atomic force microscopy was used to characterize LPEI substrates after stamping of a grafted PAA (no subsequent backfilling). In **a**, an LPEI substrate is seen before stamping; its surface is quite smooth and regular. In **b**, an LPEI substrate stamped with PAA-A is seen immediately after stamping, while the LPEI substrate shown in **c** was rinsed with MilliQ and dried under N_2 after stamping with PAA-C.

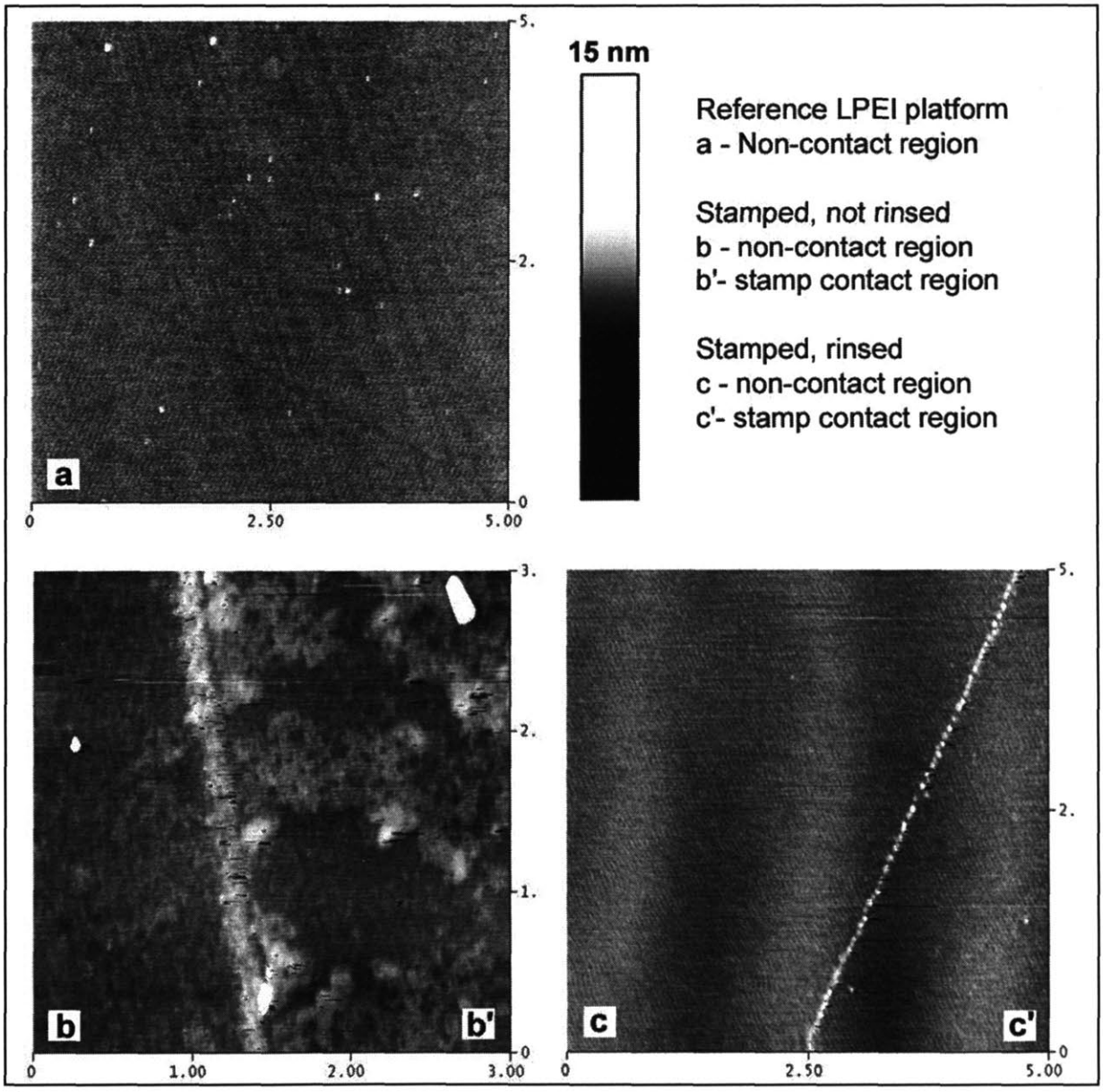

Figure 4.3.3.1. AFM study of LPEI substrates before (**a**) and after (**b**, **c**) stamping of grafted PAAs. Sample **c** was rinsed after stamping while **b** was not. The two all-white zones of **b** are salt crystals formed by drying of the PBS-carried ink.

The substrate imaged immediately after stamping has clearly-defined pattern edges and transferred material can be seen within the stamped area, although coverage is patchy. The thickness of the transferred layer looks to be a few nanometers inside the feature and about twice that at the edges. This heavier edge adsorption and incomplete interior coverage suggests that stamp plasma treatment was too short; similar behavior has been observed in the past.*[39]* It is also possible that different adsorption conformation of chains on flat vs. featured PDMS regions

contributed to different transfer fidelity. On the substrate rinsed after stamping, the edges of the patterns are still sharply defined but little to no transferred material is seen within the stamped areas. This further supports the hypothesis of incomplete plasma modification of the stamps; the absence of ink within the stamped region could indicate that only loosely-bound material was transferred, or that the stamp used in **c** was even less hydrophilized that that in **b** and only picked up ink at its edges. Given the presence of salt crystals in unrinsed patterns and given the risk that the transferred material is not actually physisorbed, increased plasma treatment coupled with rinsing seems the best approach to POPS of the PAA derivatives. Inking without plasma treatment could also be improved by pH modification of the PAA solutions and/or lengthier stamp immersions according to previously-published protocols.*[38, 40]*

To avoid electrostatic repulsion between colloids and surfaces both functionalized with PAA derivatives, silica surfaces patterned with nucleic base-terminated triethoxysilane SAMs were used more frequently than templates prepared by POPS. In Figure 4.3.3.1, silica microparticles functionalized with uracil-terminated silane were adsorbed on a pattern of A and C silanes.

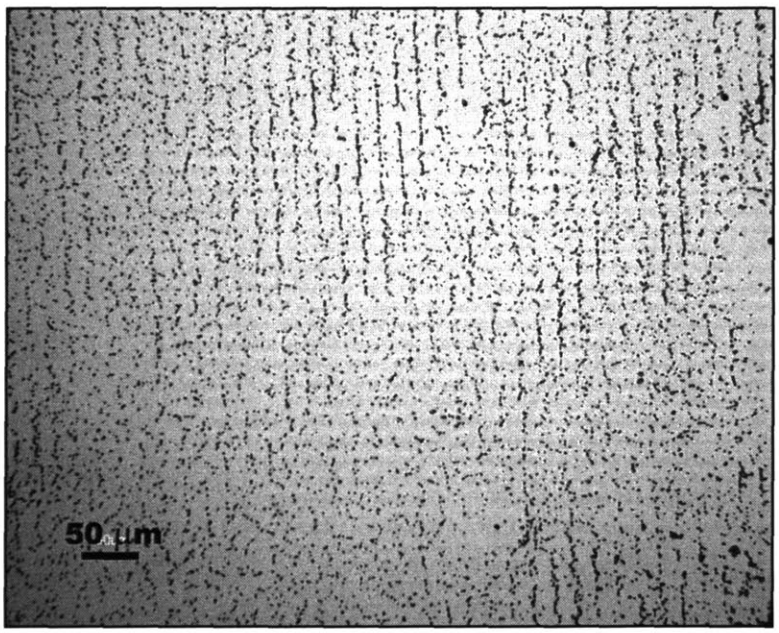

Figure 4.3.3.2. 1.0 µm Si-OH beads functionalized with U-silane adsorbed from suspension in dilute PBS on silicon surface stamped with 2 µm stripes of A-silane on a C-silane background.

The lines of the A-silane pattern are in clear evidence in the distribution of adsorbed particles, although resistance to the C-silane surface is not perfect. Rinsing again proved critical, with delicate handling required to avoid disrupting adsorbed beads. Adsorption throughout was more frequently observed than complete absence of beads. In Figure 4.3.3.3, polystyrene beads functionalized with pU (natural RNA homopolymer poly(uridylic acid)) and suspended in dilute PBS were adsorbed on a substrate patterned with A and C-silanes.

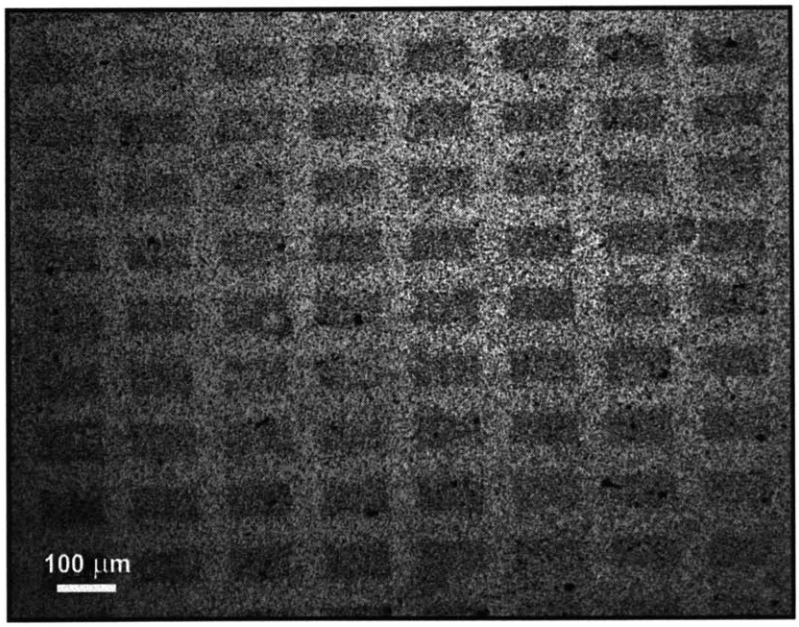

Figure 4.3.3.4. 0.9 μm PS beads functionalized with pU adsorbed from suspension in dilute PBS on a pattern of 40 x 100 μm A-silane rectangles in a C-silane background on silicon.

Again, the non-complementary surface is far from bare but the pattern's influence is clearly seen in the density of adsorption. This suggests that non-specific hydrogen bonding is occurring between C and U. While the carbonyl-secondary amine (acceptor-donor) motif in U does resemble part of the G motif, allowing it to form two hydrogen bonds to C, the presence in U of another carbonyl where G has a secondary amine should discourage formation of those bonds by electrostatic repulsion with the carbonyl completing the C motif. (See Figure 4.3.3.4 for illustration of the attractive and repulsive interactions between U and C.)

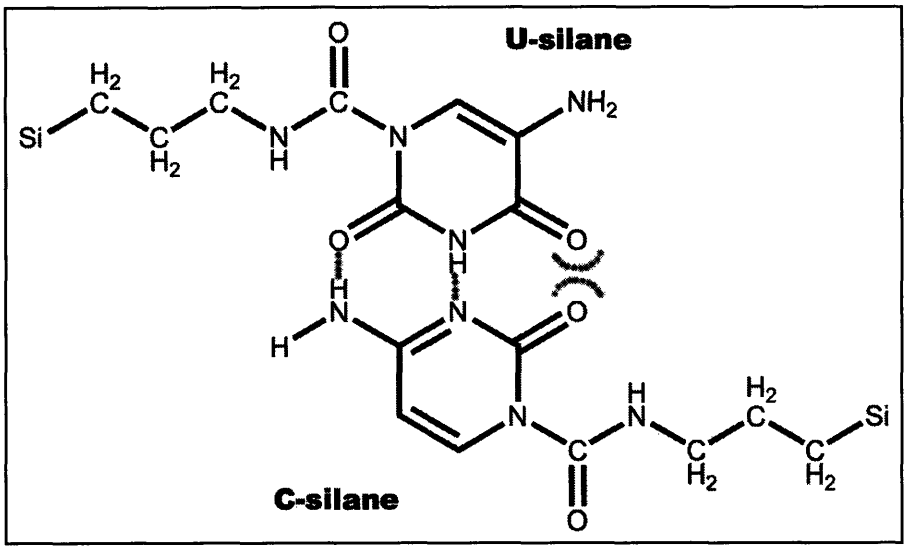

Figure 4.3.3.4. Favorable and unfavorable intermolecular interactions between the MHB motifs of uracil and cytosine (mismatched nucleic base pair).

The non-specific adsorption of U beads on C surfaces suggests that normal MHB behavior is being disrupted. The patterned substrates shown in Figures 4.3.3.2-3 were not further treated after rinsing with ethanol upon removal from the C-silane immersion bath; it is possible that this left the MHB groups in a disordered conformation or that residual ethanol interfered with particle-surface interactions. Residual DMSO, present at 1-5 % in the silane inks (see Chapter 4.2 for silane preparation and purification details), could also be interfering. Subsequent templates were copiously rinsed with water and then immersed in PBS for at least 30 min to rehydrate and recondition the surfaces. Comparison of Figures 4.3.3.2-3 also indicates that optimal pattern visibility is achieved when beads are much smaller than feature sizes, especially given the excellent packing density displayed by the pU-modified beads. Recalling the incomplete ink transfer observed in Figure 4.3.3.1, it would seem that colloids are best modified by polymeric coatings, while patterns are best prepared by silane μCP.

In Figure 3.4.1.5, beads functionalized with PAA-U adsorbed selectively on the A-silane background of a substrate rehydrated in PBS one hour after A/C silane patterning. Resistance was much improved compared to the substrate in 3.4.1.4, which was not rehydrated, although all beads were more vulnerable to disruption during rinsing. This figure additionally shows that selectivity is indeed towards the complementary nucleic base group, regardless of which silane was stamped and which was back-filled from solution.

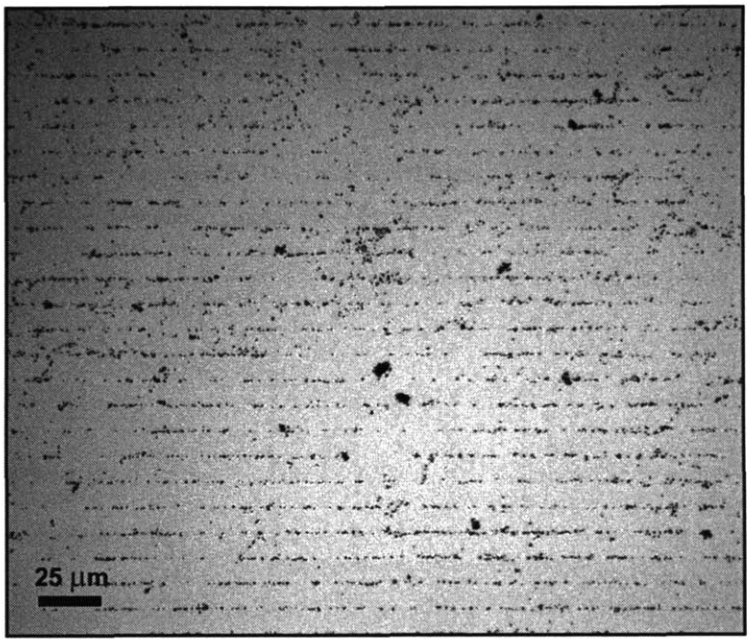

Figure 4.3.3.5. 0.9 μm PS beads functionalized with pU adsorbed from suspension in dilute PBS on a pattern of 12 μm C-silane stripes spaced 3 μm apart in an A-silane background. After patterning, the substrate was rehydrated in PBS for one hour before use.

Another possible contributor to both non-selective adsorption and weakened bead-surface interactions, leading to higher rinsing loss, is that crowding in pure SAMs impedes access to the nucleic base groups and that many particles bind non-specifically via single hydrogen bonds in the absence of available MHB motifs. The Long group, which first prepared A-silanes for surface modification, report that they performed best when mixed with another silane in a 1:3 ratio; the silane they used had a terminal mercapto (-SH) group.*[32]* In Figure 4.3.3.6, PAA-U beads were adsorbed on a surface patterned with A and C silanes, diluted with mercaptosilane.

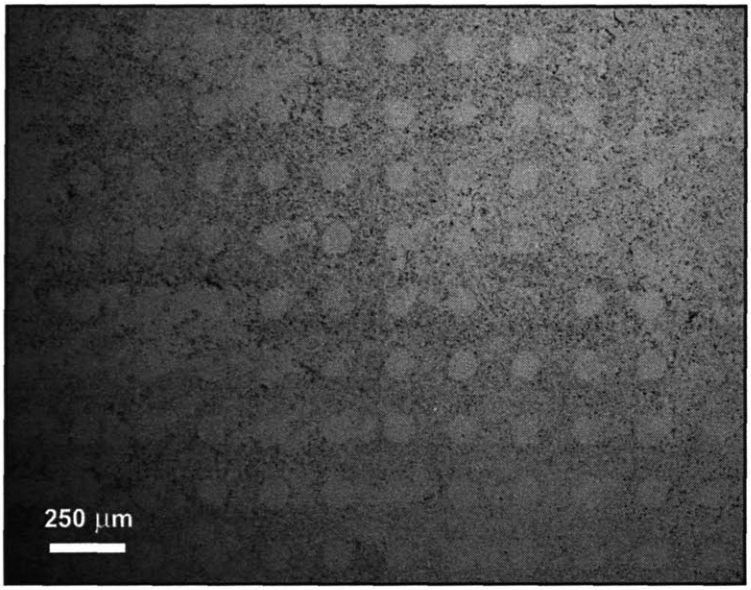

Figure 4.3.3.6. 1.0 μm PS beads functionalized with PAA-U adsorbed from suspension in dilute PBS on a pattern of 100 μm (25% C-silane/75% mercapto silane) dots in a stamped (25% A-silane/75% mercapto silane) background. After patterning, the substrate was rehydrated in PBS for one hour before use.

Resistance was much improved in 4.3.3.6 compared to 4.3.3.4, but beads were still vulnerable to rinsing; this could indicate that many U beads are forming single hydrogen bonds between one of their two carbonyl oxygens and the mercapto proton rather than double hydrogen bonds with the A-silane. For our purposes, the optimal diluent would be indifferent to hydrogen bonding, ensuring steric accessibility of nucleic base groups without interfering with the MHB interactions. The sample shown in Figure 4.3.3.7 was prepared identically to that in 4.3.3.6 in every way except for the use of a vinyl-terminated silane in the place of the mercaptosilane.

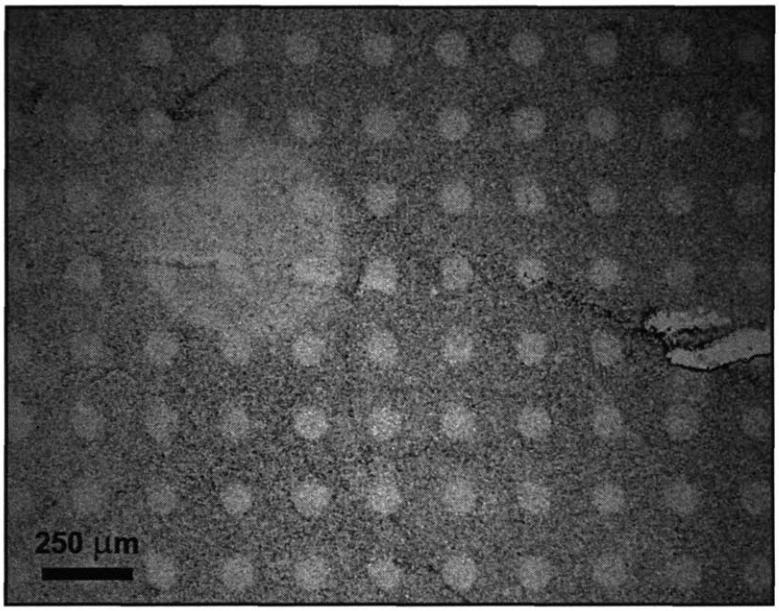

Figure 4.3.3.7. 1.0 μm PS beads functionalized with PAA-U adsorbed from suspension in dilute PBS on a pattern of 100 μm (25% C-silane/75% vinyl silane) dots in a stamped (25% A-silane/75% vinyl silane) background. After patterning, the substrate was rehydrated in PBS for one hour before use.

Replacing mercaptosilane with vinyl silane reduced rinsing instability, allowing for better removal of loosely-bound PAA-U particles on C regions and thus improving selectivity while still allowing for dense packing on the complementary A regions. Another surface was then prepared by stamping C rather than A, reversing the pattern; the adsorption of PAA-G-functionalized beads on this substrate is shown in Figure 4.3.3.8.

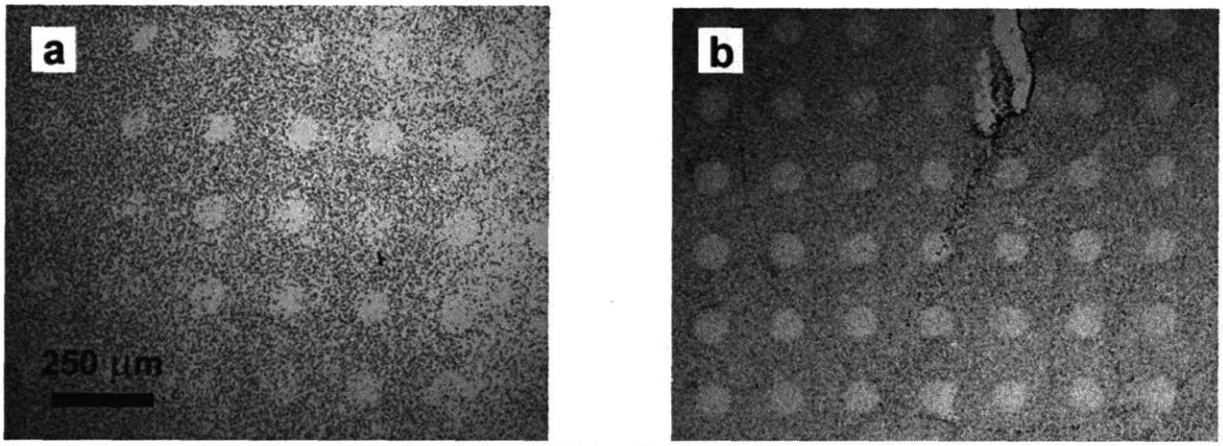

Figure 4.3.3.8. Comparison of (**a**) 1.9 µm PS beads functionalized with PAA-G on a pattern of 100 µm (25% A-silane/75% vinyl silane) dots in a stamped (25% C-silane/75% vinyl silane) and (**b**) 1.0 µm PS beads functionalized with PAA-U on a pattern of 100 µm (25% C-silane/75% vinyl silane) dots in a stamped (25% A-silane/75% vinyl silane) background. Both substrates were rehydrated in PBS before use.

The results in Figure 4.3.3.8 confirmed that nucleic base-grafted PAA and nucleic base-terminated silanes could be used to create highly-selective adsorption templates without the instability and unpredictability incurred by using natural RNA. Similar results can be expected from grafted PAH, since the neutrality of the SAM surfaces (at pH 7.4 always) means that the residual surface charge of the beads should not affect adsorption. From a practical point of view, PAH-vectored functionalization is appealing because a greater variety of negatively-charged colloids is commercially available.

A hybrid system combining natural RNA for template modification and grafted silanes for colloidal functionalization allowed for the selective placement of nanoparticles inside nanoscale wells, as shown in Figure 4.3.3.9. With the increased stability of synthetic RNA analogues to POPS, such three-dimensional templating should become even more efficient, which will be of interest as a method of partially-masking colloids for asymmetric functionalization, which will be explored in the next section.

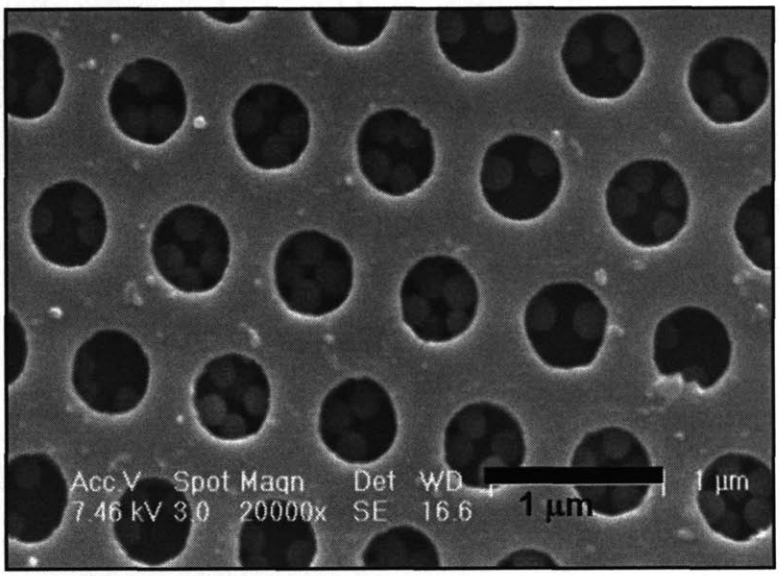

Figure 4.3.3.9. Selective adsorption of 150 nm silica nanoparticles functionalized with U-silane in a 3D template contrasting pA (inside the 450 nm-wide, 300 nm-deep wells) and pC (upper surface), observed by scanning electron microscopy.

4.4 Asymmetric Functionalization of Microspheres

Asymmetric functionalization of microspheres with complementary nucleic base groups was of particular interest as such particles should display programmable solution self-assembly, forming linear arrays under conditions favorable to hydrogen bonding and redispersing upon shifts in solvent pH, ionic strength, or polarity. As discussed in Section 4.1.3, the challenge of asymmetric colloidal functionalization lies in finding a way to temporarily mask part of the sphere while leaving the rest available for modification. Three different experimental approaches were investigated with the goal of creating half-adenine/half-uracil or half-guanine/half-cytosine beads.

4.4.1. Protocols for Asymmetric Functionalization

The first method, referred to here as double-stamping (DS), is the most conceptually simple and yet the most difficult to implement. In this approach, two flat PDMS slabs are inked with complementary surface modifiers (either polymeric or thiol/silane) and a colloidal monolayer is then trapped between these two slabs, stamping opposite surfaces of the colloidal array (see Figure 4.4.1.1). In theory, this method is ideal because it is symmetrically-asymmetrical – that is, the resulting beads should have functionalized regions at each pole of identical size and morphology. In practice, the obtention of such a sandwiched colloidal monolayer is quite challenging. Simultaneous stamping, the squeezing of a drop of colloidal suspension between two inked stamps, would require extremely flat, rigid, and perfectly-aligned stamps in order to create a monolayer; in addition, the two inks would need to be stably-enough adsorbed on PDMS to survive the squeezing out of solvent without mixing. A more realistic implementation of DS is to create the monolayer on one stamp surface and then apply the second stamp after removal of any super-monolayer beads. For example, this can be done by pressing a silane-inked stamp against dry silica spheres, removing loosely-bound spheres under N_2 flow, and then pressing a second silane-inked PDMS slab against the beads. After leaving the stamp

sandwich in a warm, slightly-humid atmosphere to promote formation of siloxane bonds, the beads can be recovered by sonication. DS of this sort could also be applied to POPS.

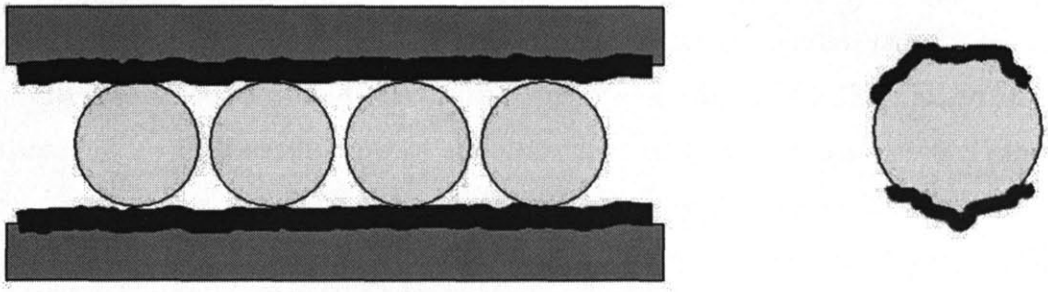

Figure 4.4.1.1. Double-stamping (DS) approach, in which a colloidal monolayer is sandwiched between two flat inked stamps. The resulting beads are symmetrically-asymmetrical.

A variation on DS is immersion-stamping (IS). In this approach, beads are first homogeneously functionalized in solution with one nucleic base and then stamped with the other (see Figure 4.4.1.2). This method can obviate the need to create a regular colloidal monolayer by use of a slightly-flexible stamp material; after pressing the stamp against an irregular agglomeration of colloids, it is lifted and only the beads stuck to its surface are kept. If particle-particle interactions allow some multilayer colloidal transfer to the PDMS, loosely-bound particles can be removed under N_2 flow. Since the two inks feature complementary nucleic bases, the second ink used should be polymeric, while the first can be either polymeric or silane. Given the lack of electrostatic repulsion observed between particles functionalized with grafted PAAs, stamping a grafted PAA onto its complement should be possible. While this method is more easily implemented than DS, the resulting beads are asymmetrically-asymmetrical, with a much larger area covered by the first ink than the second.

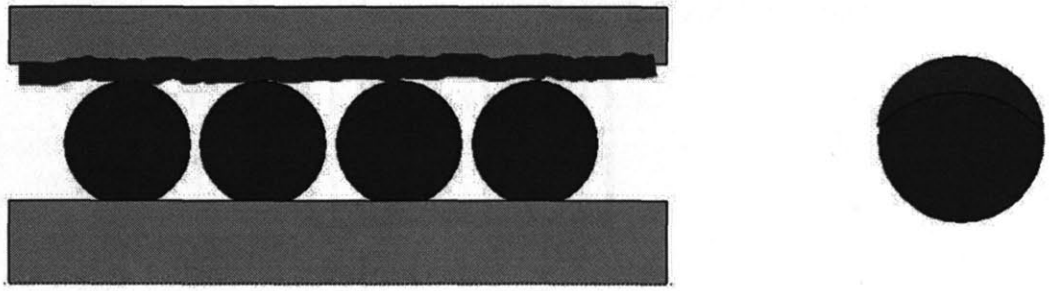

Figure 4.4.1.2. Immersion-stamping (IS) approach, in which a flat inked stamp is pressed over a monolayer of beads fully coated by one ink. The resulting colloids are asymmetrically-asymmetric.

The final approach explored was a method developed in the Velegol group*[35]*, referred to here as contact-masking (CM), in which large, positively-charged, colloids are allowed to settle from suspension in a negatively-charged glass dish. The resulting monolayer is stable to rinsing of the original solution, which is then replaced by a solution of the first ink, which cannot access those regions of the beads in contact with the dish (see Figure 4.4.1.3). After rinsing away the first ink, particles are recovered by sonication; the bare patch can then be functionalized in solution. This method requires that the second ink not adsorb on the first, which can be prevented when using grafted PAAs by performing the second functionalization at a pH incompatible with hydrogen bonding. The disadvantage of this method is that the masked region is quite small – on the order of 1-3% of the total sphere surface area, depending on the R_g of the ink and size of the spheres.

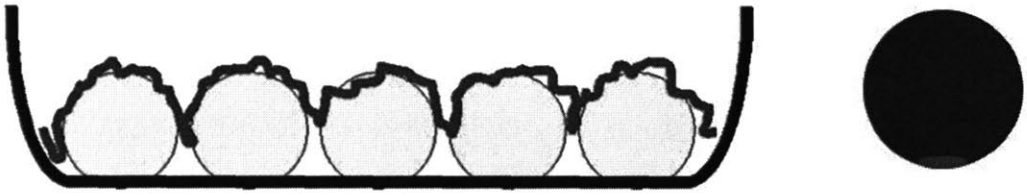

Figure 4.4.1.3. Velegol protocol for contact-masking (CM) asymmetric functionalization, in which only the upper surface of a colloidal monolayer is exposed to an ink solution.*[35]* The resulting beads can then be further functionalized by another ink. The resulting beads are highly asymmetrically asymmetric.

All three methods were explored for the asymmetric functionalization of large (5-7 μm) colloids with natural RNA or nucleic base-grafted PAA.

4.4.2. Evaluation of Asymmetric Functionalization Approaches

Large (5.5 μm) hydroxylated silica spheres were asymmetrically functionalized with A and U-silanes by DS. Recovery of beads from the stamp sandwich was difficult, reducing yield. However, those few beads that were recovered formed linear arrays in buffer. Given how dilute the bead suspension was, the fact that beads were able to find each other and remain chained is very encouraging.

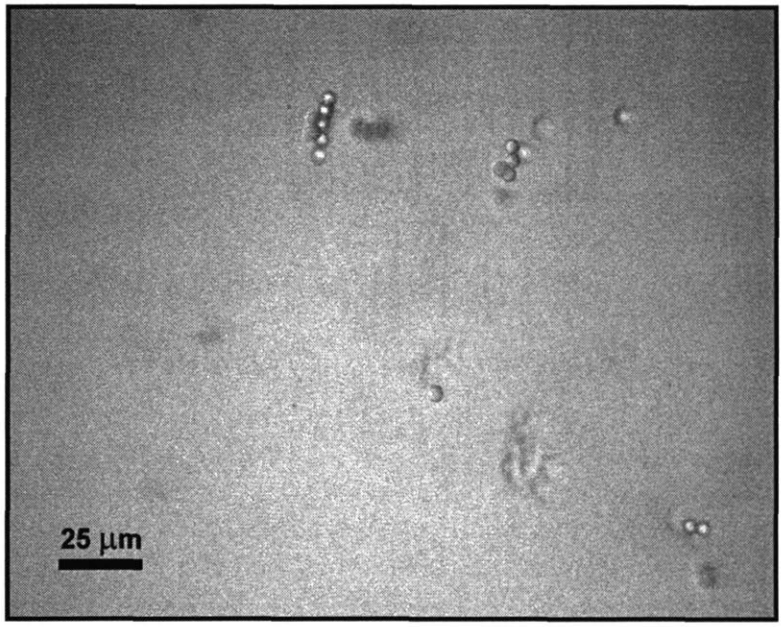

Figure 4.4.2.1. 5.5 μm silica spheres asymmetrically functionalized with A and U-silanes via DS, viewed in a fluid cell after washing and resuspension in 0.1X PBS.

Since natural RNA does not lend itself well to the DS approach, large (8 μm) amine-functionalized polystyrene beads were asymmetrically functionalized by immersion in poly(adenylic acid) (natural RNA, pA) followed by stamping with poly(uridylic acid) (pU). Beads recovered from the stamp surface and resuspended in 0.1X PBS were observed in a fluid cell and are shown in Figure 4.4.2.2, with colorization of the image file for visual clarity.

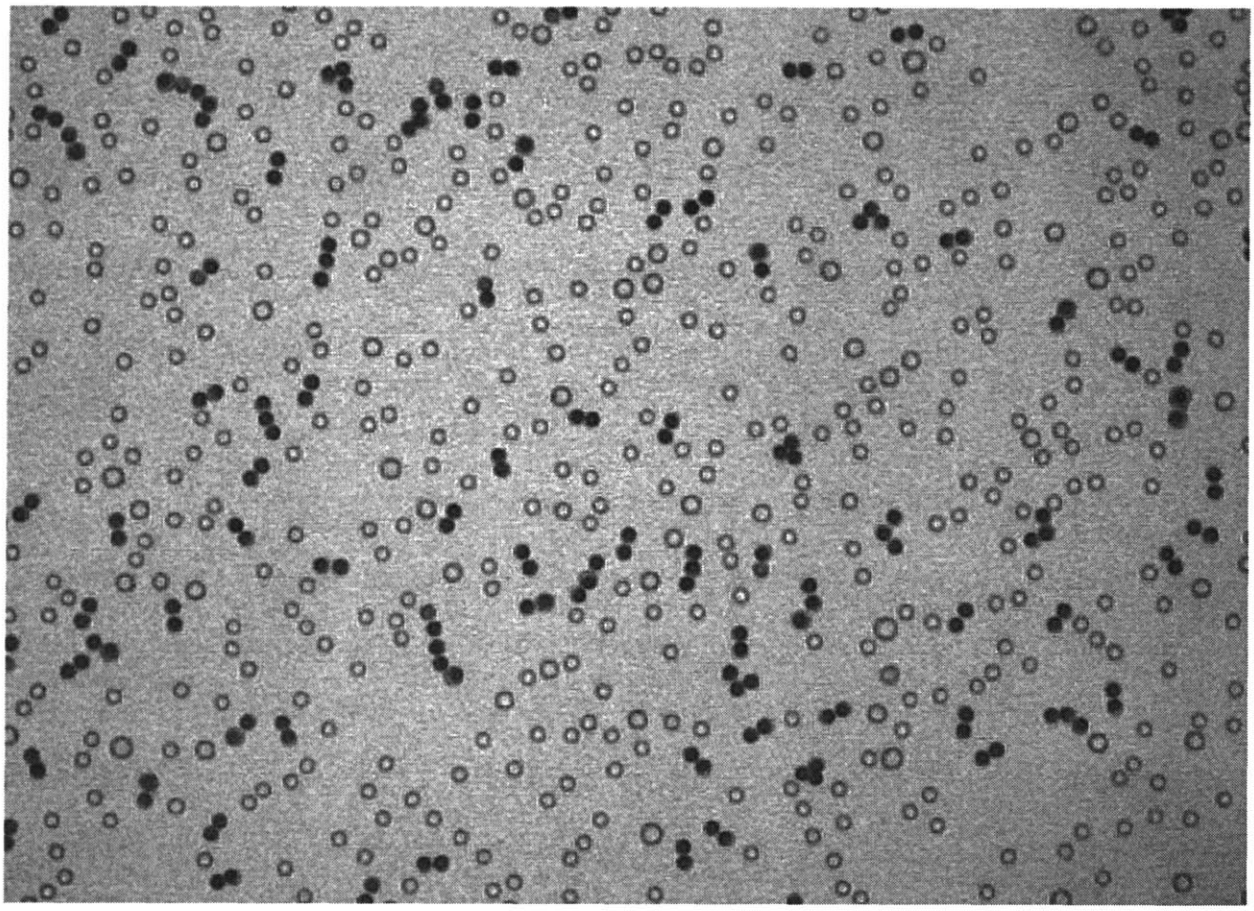

Figure 4.4.2.2. 8 μm amine latex asymmetrically modified by immersion in pA followed by stamping with pU. Beads recovered from the stamp surface were washed and resuspended in 0.1X PBS and are here observed 2 hours after being placed in an OM fluid cell. After inspection of the image at high magnification, beads clearly in contact with other beads were colorized for visual clarity.

While physical contact between beads could be mere chance rather than evidence of attractive MHB interactions, the number of beads observed in linear arrays, including two quintets, is encouraging, especially given that the beads do not seem otherwise inclined to aggregate. Still, proof of asymmetry is desired. Given the fragility of natural RNA, subsequent asymmetric functionalization was pursued using nucleic base-grafted PAA.

To evaluate the feasibility of CM for our purposes, large polystyrene beads were allowed to settle on a glass dish and then functionalized with plain PAA. After recovery and rinsing, the beads were immersed in a solution of anthracene-labeled poly(methacrylic acid), which will

fluorescently tag regions successfully masked during PAA addition. Such beads are seen under fluorescence microscopy in Figure 4.4.2.3.

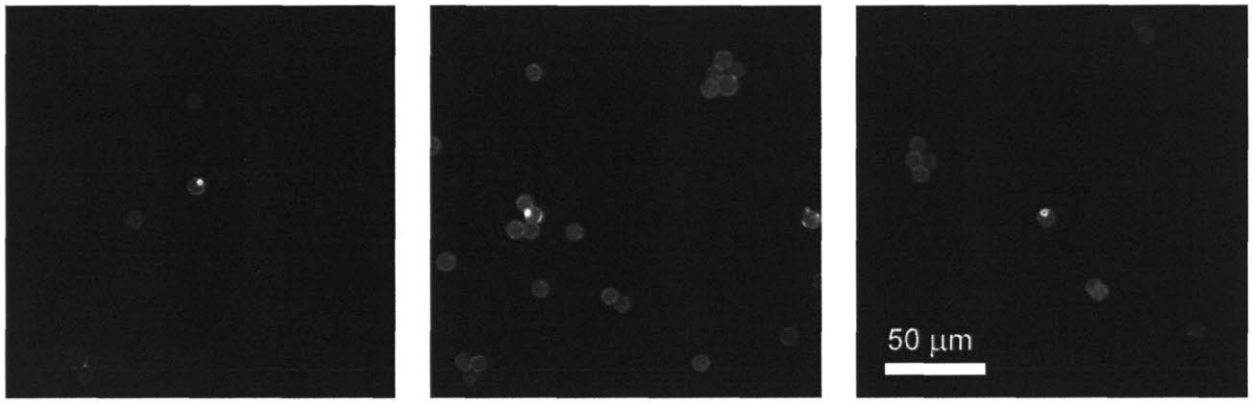

Figure 4.4.2.3. Large (8 μm) PS microspheres asymmetrically functionalized with plain PAA (first adsorption step) and fluorescently-labeled PMAA via the Velegol approach. A dilute suspension of the resulting beads was dried onto a silicon substrate for observation.

Asymmetric PMAA-Anth adsorption is in clear evidence, although the overall prevalence of asymmetric beads is low. A close-up of one of the tagged beads is given in Figure 4.4.2.4.

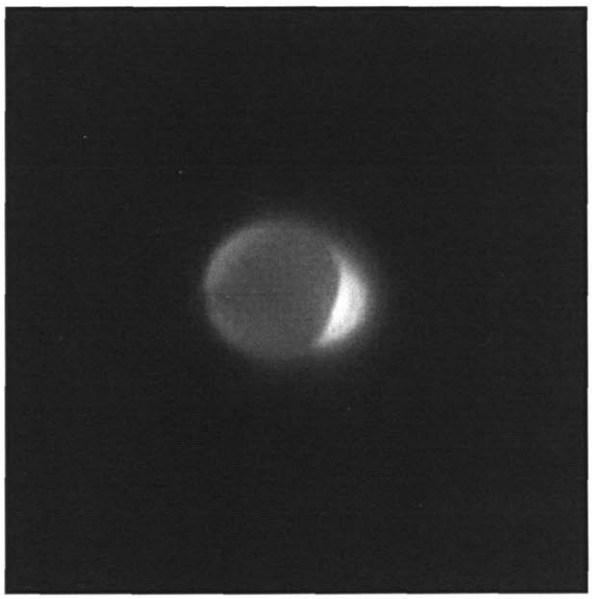

Figure 4.4.2.4. 8 μm PS bead asymmetrically fluorescently tagged via CM as described for Figure 4.4.2.3.

The area covered by PMAA-Anth is small, as expected; a few beads with two fluorescent spots were observed, suggesting that blocking is taking place via bead-bead contact as well as bead-dish contact. Having demonstrated the ability to asymmetrically label beads via CM, the method was then used to functionalize beads with beads with complementary nucleic bases via contact-masked PAA-A addition followed by PAA-U+PMAA-Anth co-adsorption at pH 12. At this pH, adenine/uracil MHB is prevented by deprotonation of uracil's secondary amine. (The secondary amine in adenine is also deprotonated at this pH, further disrupting MHB by altering electron density distribution within the ring.) To ensure that the underlying colloid surface would remain positively charged, sulfate-latex beads were first coated with the strong polycation PDAC; commercially-available positively-charged PS beads are functionalized with groups neutral at this pH. Beads prepared in this way are shown in Figure 4.4.2.5 after rinsing and resuspension in 0.1X PBS.

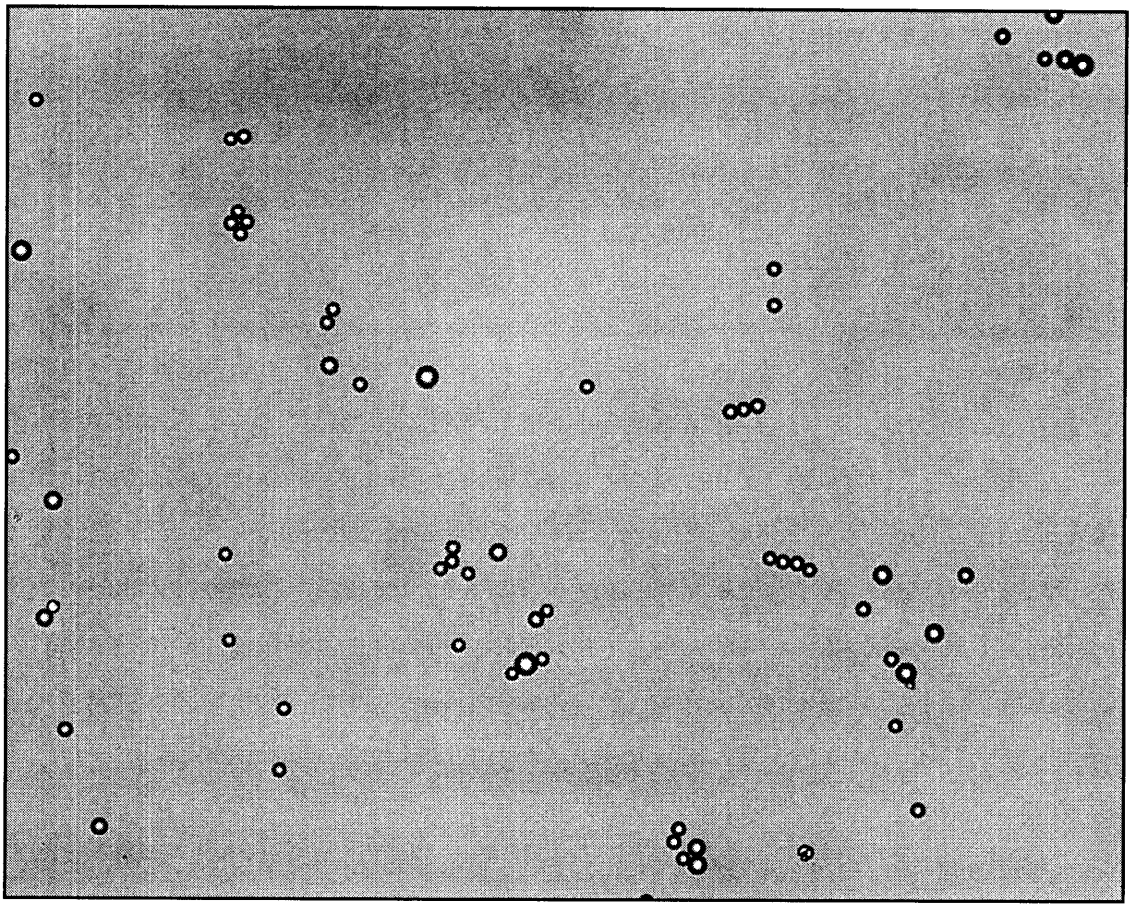

Figure 4.4.2.5. 8 μm PS microspheres asymmetrically functionalized with PAA-A (first adsorption step) and (PAA-U + PMAA-Anth) via AM, viewed under visible light while suspended in dilute PBS.

No fluorescence was observed in these beads. Subsequent homogeneous functionalization of comparable beads with a mixed solution of PAA-U and PMAA-Anth also showed no fluorescence, indicating that PAA and PMAA might be competitively adsorbing to the detriment of PMAA. While this needs to be addressed in order to verify that particle-particle contacts occur in the fluorescently-tagged spots, the presence of chained beads is encouraging. Pyramid and diamond bead formations are observed, which we would expect to see when the two functionalized areas have a large size imbalance.

4.5 Comments and Conclusions

In this chapter, the adsorption-directing potential of nucleic base multiple hydrogen bonding interactions was investigated.

Homopolymeric RNA was used first to functionalize colloids and surfaces with nucleic base groups, continuing the focus on using polyelectrolytes to direct colloidal interactions first explored in Chapter 3. Results of this work were both extremely encouraging and extremely frustrating; strong evidence of highly-selective RNA-directed adsorption was seen, but reproducibility was poor due to the instability of RNA under typical experimental conditions. The fragility of RNA made its stamping particularly difficult, leading us to search for an alternate method of patterning nucleic base functionality on surfaces. Non-degradable polymeric analogues of RNA were also desired so as to reduce costs and improve reliability.

In response to these challenges, nucleic base-functionalized triethoxysilanes and polyelectrolytes were designed and prepared, the full details of whose synthesis and characterization will be discussed in the sixth chapter.

With these custom-made materials, we were able to evaluate the selectivity of nucleic base pairing and found it well-suited to directing assembly of patterned colloidal arrays. While the modified PAAs could be stamped, microcontact printing of triethoxysilanes proved a more efficient route to two-dimensional pattern creation; for this, controlling the density of nucleic base groups at the surface, proved essential. Both uracil- and guanine-functionalized beads could be directed to their complementary surfaces with high selectivity, and the non-interference of the two systems makes them good candidates for simultaneous directed assembly from mixed solutions, a higher level of surface sorting than possible in the polyamine-directed approach described in Chapter 3.

Asymmetric functionalization of microspheres with complementary nucleic bases was also explored, with several methods for achieving this asymmetry being compared. Silica spheres could be doubly-stamped with silanes, producing desirable symmetry of asymmetry, but

polyelectrolyte functionalization would seem a preferable approach if possible, creating a looser, more mobile network of nucleic bases available for interparticle interactions than thin siloxane monolayers. Immersion-stamping and adsorption-masking both showed promise, with the former being better-suited to the creation of particles with a preference for linear assembly.

While the nucleic base-grafted polyelectrolytes were prepared expressly for use in directing colloidal adsorption, their novel combination of electrostatic and MHB interaction potential also makes them of interest as multilayer film components, a topic that will be explored in the next chapter.

WORKS CITED

[1] R. P. Sijbesma, E. W. Meijer, *Chemical Communications* **2003**, 5.
[2] J. A. Zerkowski, J. C. MacDonald, C. T. Seto, D. A. Wierda, G. M. Whitesides, *Journal of the American Chemical Society* **1994**, *116*, 9025.
[3] R. P. Sijbesma, E. W. Meijer, *Current Opinion in Colloid & Interface Science* **1999**, *4*, 24.
[4] J. A. Zerkowski, C. T. Seto, D. A. Wierda, G. M. Whitesides, *Journal of the American Chemical Society* **1990**, *112*, 9025.
[5] R. Shenhar, T. B. Norsten, V. M. Rotello, *Advanced Materials* **2005**, *17*, 657.
[6] A. T. ten Cate, H. Kooijman, A. L. Spek, R. P. Sijbesma, E. W. Meijer, *Journal of the American Chemical Society* **2004**, *126*, 3801.
[7] Y. Ma, S. V. Kolotuchin, S. C. Zimmerman, *Journal of the American Chemical Society* **2002**, *124*, 13757.
[8] R. J. Thibault, P. J. Hotchkiss, M. Gray, V. M. Rotello, *Journal of the American Chemical Society* **2003**, *125*, 11249.
[9] F. Ilhan, M. Gray, V. M. Rotello, *Macromolecules* **2001**, *34*, 2597.
[10] R. Deans, F. Ilhan, V. M. Rotello, *Macromolecules* **1999**, *32*, 4956.
[11] F. Beijer, R. P. Sijbesma, H. Kooijman, A. L. Spek, E. W. Meijer, *Journal of the American Chemical Society* **1998**, *120*, 6761.
[12] G. Cooke, V. M. Rotello, *Chem. Soc. Rev.* **2002**, *31*, 275.
[13] S. Goswami, K. Ghosh, M. Halder, *Tetrahedron Letters* **1999**, *40*, 1735.
[14] A. Goodman, E. Breinlinger, M. Ober, V. M. Rotello, *Journal of the American Chemical Society* **2001**, *123*, 6213.
[15] R. Shenhar, V. M. Rotello, *Accounts of Chemical Research* **2003**, *36*, 549.
[16] A. Sanyal, T. B. Norsten, O. Uzun, V. M. Rotello, *Langmuir* **2004**, *20*, 5958.
[17] T. B. Norsten, E. Jeoung, R. J. Thibault, V. M. Rotello, *Langmuir* **2003**, *19*, 7089.
[18] F. Ilhan, T. H. Galow, M. Gray, G. Clavier, V. M. Rotello, *Journal of the American Chemical Society* **2000**, *122*, 5895.
[19] H. Xu, R. Hong, T. Lu, O. Uzun, V. M. Rotello, *Journal of the American Chemical Society* **2006**, *128*, 3162.
[20] J. K. N. Mbindyo, B. D. Reiss, B. R. Martin, C. D. Keating, M. J. Natan, T. E. Mallouk, *Advanced Materials* **2001**, *13*, 249.
[21] L. M. Dillenback, G. P. Goodrich, C. D. Keating, *Nano Letters* **2006**, *6*, 16.
[22] S. E. Stanca, A. Ongaro, R. Eritja, D. Fitzmaurice, *Nanotechnology* **2005**, *16*, 1905.
[23] D. Iacopino, A. Ongaro, L. Nagle, R. Eritja, D. Fitzmaurice, *Nanotechnology* **2003**, *14*, 447.
[24] P. L. Biancaniello, A. J. Kim, J. C. Crocker, *Physical Review Letters* **2005**, *94*, 058302.
[25] A. J. Kim, P. L. Biancaniello, J. C. Crocker, **2006**, *1991-2001*.
[26] S. Mann, W. Shenton, M. Li, S. Connoly, D. Fitzmaurice, *Advanced Materials* **2000**, *12*, 147.
[27] N. J. Tro, *Introductory Chemistry Essentials*, Prentice Hall, **2006**.
[28] H. J. Spijker, A. J. Dirks, J. C. M. Van Hest, *J. Polym Sci. Part A: Polym. Chem.* **2006**, *44*, 4242.
[29] K. Yamauchi, J. R. Lizotte, T. E. Long, *Macromolecules* **2002**, *35*, 8745.

[30] K. Yamauchi, J. R. Lizotte, D. M. Hercules, M. J. Vergne, T. E. Long, *Journal of the American Chemical Society* **2002**, *124*, 8599.
[31] K. Yamauchi, J. R. Lizotte, T. E. Long, *Macromolecules* **2003**, *36*, 1083.
[32] K. Viswanathan, H. Ozhalici, C. L. Elkins, C. Heisey, T. C. Ward, T. E. Long, *Langmuir* **2006**, *22*, 1099.
[33] J. R. Millman, K. H. Bhatt, B. G. Prevo, O. D. Velev, *Nature Materials* **2005**, *4*, 98.
[34] O. Cayre, V. N. Paunov, O. D. Velev, *Journal of Materials Chemistry* **2003**, *13*, 2445.
[35] C. E. Snyder, A. M. Yake, J. D. Feick, D. Velegol, *Langmuir* **2005**, *21*, 4813.
[36] Z. Li, D. Lee, M. F. Rubner, R. E. Cohen, *Macromolecules* **2005**.
[37] J. Park, Y. S. Kim, P. T. Hammond, *Nano Letters* **2005**, *5*, 1347.
[38] M. C. Berg, J. Choi, P. T. Hammond, M. F. Rubner, *Langmuir* **2003**, *19*, 2231.
[39] H. P. Zheng, M. F. Rubner, P. T. Hammond, *Langmuir* **2002**, *18*, 4505.
[40] M. C. Berg, S. Y. Yang, P. T. Hammond, M. F. Rubner, *Langmuir* **2004**, *20*, 1362.

CHAPTER 5 – MULTIPLE HYDROGEN BONDING-DIRECTED LBL ASSEMBLY

5.1 Introduction

The incorporation of biological materials into multilayered films has been of interest from the earliest explorations of layer-by-layer assembly, often for delivery applications in which controlled disassembly or degradation of the film allows release of the biological component in response to a specific environmental stimulus. Both linear and plasmid DNA have been layered into and then released from LbL structures; these films rely on electrostatic attraction between the anionic polyphosphate backbone of DNA and a polycation.*[1-4]* Lately, LbL assembly involving the multiple hydrogen bonding motifs as well as the polyanionic backbone of nucleic acids has been explored. Using homopolymeric RNA, Schlenoff and coworkers found that, though complementary, poly(adenylic acid) and poly(uridylic acid) could not be layered alone due to the strong electrostatic repulsion between them. However, trilayers of branched poly(ethylene imine), pA, and pU could be built under certain pH and pI conditions.*[5]* When salt concentration was increased, shielding charged groups, films assembled more thinly, indicating that the MHB interactions promoted more linear adsorbed chain conformations. Synthetic RNA analogues such as those used in Chapter 4, having stabler structures and better-characterized molecular weight, would provide a more efficient approach to such studies. In addition, it would be interesting to see whether like-charged PAA derivatives carrying complementary MHB motifs can assemble without need for a third component, something not yet achieved with natural RNA.

Films built with significant contributions from hydrogen bonding as well as electrostatic attraction also have potential as responsive materials, with variations in temperature, pH, and solvent polarity inducing changes in the film structure as the balance of interactions shifts. Each

electrostatic or hydrogen bonding site within a multilayered film can be compared to a junction within a crosslinked network, and so the effective crosslink density, and thus porosity and elasticity, of the film can be tuned by promoting or disrupting each of these interactions.

In this chapter, polyelectrolytes partially grafted with nucleic base groups were assembled into LbL films. A number of polyelectrolyte pairs were studied so as to compare the relative contributions of electrostatic attraction or repulsion, multiple hydrogen bonding, non-specific hydrogen bonding, and the steric effect of adding a bulky side group. Both natural RNA homopolymers and synthetic analogues were used, and the sensitivity of such films to changes in solvent condition was also probed.

5.2 Materials and Methods

Poly(allyl amine hydrochloride) (PAH, MW 65,000 g/mol), sulfonated poly(styrene) (SPS, 70,000 g/mol), and poly(diallydimethylammonium chloride) (PDAC, 100,000-200,000 g/mol) were obtained from Sigma-Aldrich. Linear poly(ethyleneimine) (LPEI, 35,000 g/mol) and poly(acrylic acid) (PAA, 90,000 g/mol) were purchased from Polysciences. Poly(adenylic acid), poly(uridylic acid), poly(cytidylic acid), and poly(guanylic acid) sodium salts (pA, pU, pC, and pG) were purchased from Sigma. All polyelectrolyte concentrations are calculated on a repeat-unit basis.

Poly(allyl amine-*g*-thymine), poly(acrylic acid-*g*-adenine), poly(acrylic acid-*g*-uracil), poly(acrylic acid-*g*-cytosine), and poly(acrylic acid-*g*-guanine) (PAH-T, PAA-A, PAA-U, PAA-C, and PAA-G) were synthesized as described in Chapter 6.3. The PAH and PAA used for grafting were of the same molecular weight as those above.

Phosphate-buffered saline (PBS) was obtained as 10X standard concentration from EMD. All water was filtered through a MilliQ filter to a final resistivity of 18 MΩ*cm, except for experiments involving pA, pU, pC, or pG, in which case sterile, RNAase-free water was obtained from EMD. Methanol, ethanol, dimethylsulfoxide (DMSO), and hexadecane were purchased from Aldrich. All chemicals were used as delivered.

Polyelectrolyte multilayers were assembled on silicon wafer substrates (SiliconQuest) via the LbL technique described in Chapter 2.2. A modified Carl Zeiss DS50 programmable slide stainer was used to automate polyelectrolyte adsorption, except for films containing homopolymeric RNA, which were dipped by hand. Rinse baths were adjusted to the same pH and pI as the polyelectrolyte solutions being used. After assembly, films were rinsed with MilliQ water, dried under nitrogen flow, and stored under vacuum until characterization.

Ellipsometry (LSE Stokes Ellipsometer from Gaertner Scientific) was used to determine the film thickness in the dry state; very thick films were also studied by profilometry (P10 Surface Profiler from KLA-Tencor). Atomic force microscopy (AFM, Dimension 3000 SPM from Veeco Instruments in tapping mode) was used to characterize film morphology.

5.3 Natural RNA Multilayer Assembly

Homopolymeric RNA presents a unique combination of polyelectrolyte and MHB interaction potentials, making it an intriguing candidate for LbL assembly. If composite films could be built knit together by both electrostatics and MHB, it might be possible to induce reversible switching between a tight, dense conformation when MHB bonds are present to a looser, more porous, structure when those bonds are disrupted; such films would be of use in delivery or filtering applications. It would also be interesting to study the balance of forces at work – can MHB be enough to assemble films from electrostatically-repulsive materials?

To explore some of these topics, films were built pairing either homopolymeric RNA and a polycation, or two complementary RNA homopolymers and a polycation. If like-charged but MHB-complementary RNAs can layer with each other at all, it would likely be in a very extended (linear) conformation so as to maximize MHB contacts while minimizing both inter- and intra-molecular backbone interactions; this kind of assembly is not well-suited to the overcompensation required for cyclic multilayer assembly.

Indeed, when four identical substrates previously functionalized with a positively-charged SAM were cycled between pA and pU ten times under conditions designed to prevent RNA degradation (4 °C, RNA dissolved in RNAase-free PBS immediately before use, short adsorption cycles), ellipsometry revealed a total thickness of only 10 Å on all four samples, corresponding to the underlying SAM plus a single adsorbed RNA layer.

Films were then built by bilayer addition of pA/LPEI and by trilayer addition of pA/pU/LPEI. Assembly was performed in PBS adjusted to pH 5, at which LPEI should be half-protonated and both adenine and uracil's MHB motifs should be active; growth curves for both systems are given in Figure 5.3.1.

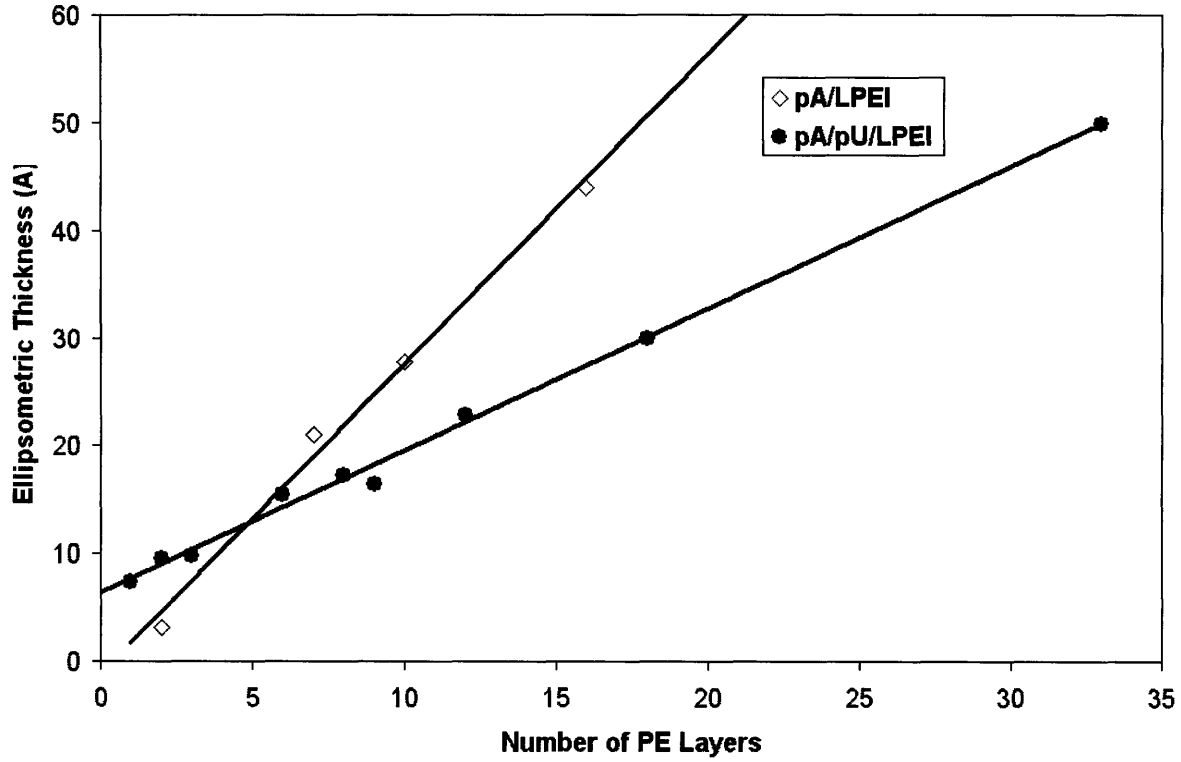

Figure 5.3.1. Ellipsometric thickness of films assembled by layering of natural homopolymeric RNA with the polycation LPEI in bilayer (RNA/LPEI) and trilayer (pA/pU/LPEI) adsorption cycles.

Bilayers of (pA/LPEI) grew faster than trilayers of (pA/pU/LPEI) when analyzed in terms of total number of polyelectrolyte layers added – an average of 3 Å/layer vs. 1.5 Å/layer. If plotted instead with reference to the total number of *cycles*, the difference is smaller but still in favor of the bilayer system – 6 Å/cycle vs. 4 Å/cycle. Thus, not only does including pU not increase thickness added per cycle, but it actually slows down assembly. That is, if pU were merely unable to adsorb on pA and thus irrelevant to assembly, the growth rate per cycle should be identical, with each "trilayer" actually composed only of pA and LPEI. However, what we observe instead is a slowing of growth per cycle. This could indicate that pA, after having adsorbed in a loopy layer atop LPEI by electrostatic attraction, with the PBS shielding intrachain repulsion, changes conformation when immersed in the pU solution, rearranging so as to expose mostly MHB groups rather than the negatively-charged backbone. The net effect would be a slowing of pA/LPEI bilayer growth due to the reduced surface charge of the pA layers.

5.4 Grafted PAA/Grafted PAA Multilayer Assembly

Having found that alternating assembly of complementary RNA homopolymers was strongly disfavored, even when a polycation was included to temper electrostatic self-repulsion, and that, in fact, the presence of the second RNA homopolymer impeded the growth of RNA/LPEI multilayers, the behavior of nucleic base-grafted PAA analogues of RNA under comparable conditions was next explored.

Layer-by-layer assembly was attempted by alternating immersion of silicon substrates in two PAAs grafted with different nucleic bases, either complementary to each other or not. All solutions (polyelectrolytes and rinsing baths) were made from phosphate-buffered saline at pH 7.4, either dilute (0.1X) or full-strength (1X). Substrates were given an initial polycationic platform by adsorption of a single LPEI layer at pH 2.0 or construction of a 5.5 bilayer (PDAC/SPS) film.

Despite strong electrostatic repulsion, all-PAA films were successfully built. Assembly was thicker and more reproducible in 1X PBS, which offered the most ionic shielding, but these films were covered with tiny salt crystals even if rinsed with pure water after assembly. Since these crystals obscured optical and atomic force microscopy, most films were built in dilute PBS. Thicknesses for films built from various grafted PAA pairs under a range of ionic strengths are reported in Figure 5.4.1; repeats of identical conditions are listed separately rather than averaged to accurately reflect the unpredictability of these films.

Both PAA-A/PAA-U and PAA-C/PAA-G films were assembled, although C/G assembly was generally thinner and less reliable. Some substrates showed no growth at all despite identically-prepared ones having previously assembled, evidence of the instability and consequent vulnerability to minor changes in conditions. Films assembled at the highest ionic strength were thickest, pointing to the importance of shielding PAA/PAA electrostatic repulsion. Often, thickness increased over the first 5-10 bilayer addition cycles but reached a plateau and began to decrease if assembly was pursued further. Comparison of 5 bilayer and 20 bilayer A/U

film thicknesses also suggests that growth did not continue linearly, and it is possible that the 20 bilayer films had already begun to thin when examined. Non-complementary A/A and A/C pairings showed negligible growth corresponding to addition of a single PAA layer on the positive substrate and no further assembly, but several C/U pairings grew 7-9 nm thick within the first five addition cycles, then reached a plateau and thinned over the next 15 cycles. The potential for cytosine/uracil mismatch-pairing, unlikely but possible, will be discussed in greater detail in Chapter 3.5.1.

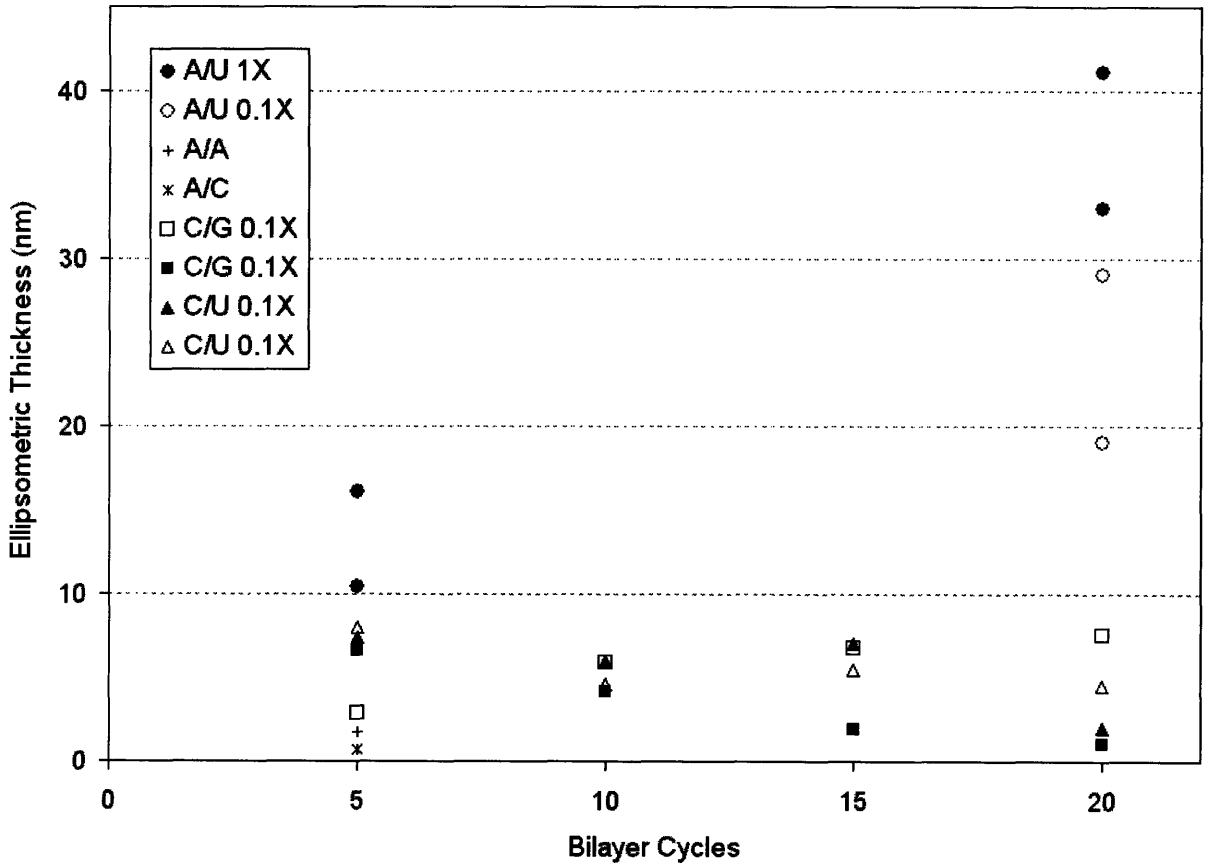

Figure 5.4.1. Ellipsometric thickness of LbL films assembled exclusively from grafted PAAs. The reported thickness is the difference between the total film height and the height of the adhesion platform (LPEI or $(PDAC/SPS)_{5.5}$), measured before PAA-*x*/PAA-*y* additions. Starred films are featured in Figures 5.4.2-3.

To further characterize these unlikely all-PAA films, atomic force microscopy was used to study surface morphology. Films were found to be smooth early in assembly but increasingly pitted as assembly continued. To verify that this morphology was not just a reflection of the

underlying adhesion layers, bare silicon and $(PDAC/SPS)_{5.5}$ substrates were also examined. In Figure 5.4.1, a 20-bilayer film of C and G PAA is seen immediately after assembly and then after an hour's incubation in dilute 4 ° C PBS buffer.

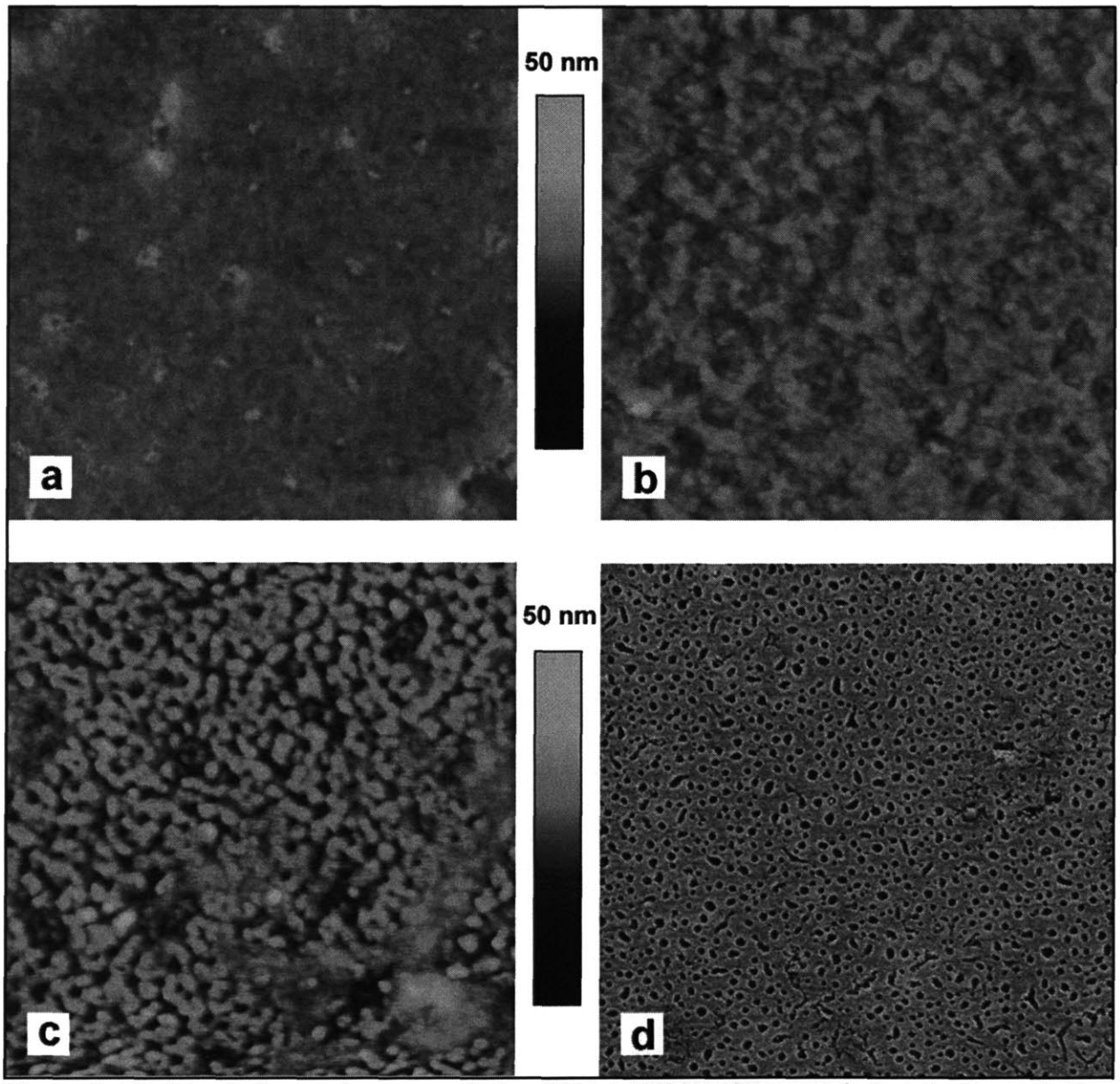

Figure 5.4.2. Atomic force microscopy study of $(PAA\text{-}C/PAA\text{-}G)_{20}$ morphology before and after incubation in dilute PBS. In **a**, the $(PDAC/SPS)_{5.5}$ adhesion platform is shown. In **b**, the same substrate is seen after adding $(PAA\text{-}C/PAA\text{-}G)_{20}$. In **c** and **d**, the substrate is shown after 1 hr incubation in 4 °C 0.1X PBS. Images **a, b,** and **c** are 2 x 2 μm scans, while **d** encompasses 10 x 10 μm.

The 20 bl (PAA-C/PAA-G) film had an ellipsometric thickness of 76 Å after assembly and the AFM image in 5.4.2.**b** reveals that the film is patchy. After an hour's incubation, the surface has become much rougher, with pits of depths corresponding to the full thickness of the original C/G film. Since ellipsometry reflects data averaged over a 1 mm^2 area, the original patchy film was probably closer to 100-150 Å in its thickest areas, judging from the pitting depth. In Figure 5.4.3, another (PAA-C/PAA-G) film was imaged immediately after assembly.

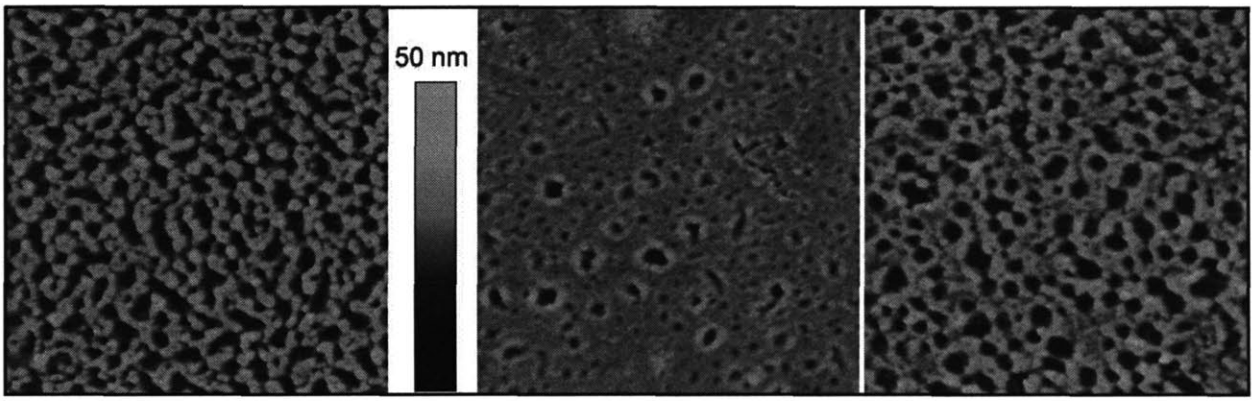

Figure 5.4.3. 2 x 2 μm AFM imaging of various areas of a second $(PAA\text{-}C/PAA\text{-}G)_{20}$ substrate immediately after assembly. For this LbL film, 15 min immersions in each polyelectrolyte were used, allowing the adsorbed layers to start rearranging and pitting during assembly.

In this film, assembled separately from the one shown in Figure 5.4.2, pitting was already well-advanced by the end of the multilayer buildup, explaining the declining ellipsometric thickness data reported in Figure 5.4.1 (square data markers). This degradation phenomenon, also observed in (PAA-A/PAA-U) multilayers is indicative of the inherent instability of electrostatically-repulsive all-PAA bilayers. Given the relatively low grafting rates determined from NMR and elemental analysis (see Chapter 6.3), all of the multilayer materials have significant polyanionic character at this pH. Thus, unless remaining backbone charge is screened by high ionic strength, the polyelectrolytes will self-repel, resisting multilayer formation. The pKa of PAA is too low to allow assembly at conditions in which PAA is fully neutral, since the MHB groups would be inactivated at that pH.

The fact that layers did build indicates that screening was sufficient, but the resulting structure remains highly unstable. In buffer, given the presence of both water (which readily

forms hydrogen bonds) and salt (to screen backbone charge), the polymers should be highly mobile and thus free to rearrange into a more energetically optimal configuration. In this case, it appears that the polymers prefer to form globular complexes rather than stratified linear structures; the longer the polymers are exposed to water, including during dipping, the rougher the film becomes. When incubated in low-salt water, the increased electrostatic self-repulsion further destabilizes the layers, which rapidly roughen and eventually fall away from the surface entirely. Films immersed in low-salt water overnight were found to have reverted to thicknesses corresponding to the platform layers alone, indicating complete loss of the grafted PAA multilayers.

Despite their instability, the fact that PAA-*x*/PAA-*y* multilayers could be built at all, but only if *x* and *y* were complementary, is evidence of the adsorption-directing force of MHB interactions. Thus, nucleic base-grafted PAA was next paired with nucleic base-grafted PAH to examine the assembly of films incorporating MHB groups and facilitated by electrostatic attraction.

5.5 Grafted PAH/Grafted PAA Multilayer Assembly

Having found that PAA derivatives grafted with complementary nucleic bases were able to assemble despite strong electrostatic repulsion, PAA derivatives were then paired with PAH derivatives to study multilayer assembly in the presence of both electrostatic and MHB attractions. In order to evaluate the relative importance of the different driving forces for adsorption, films were assembled from the following permutations of grafted or unmodified PAH and grafted or unmodified PAA, with all assembly and rinsing taking place at pH 7.4 in 0.1X PBS.

- **PAH/PAA**, the reference multilayer. At pH 7.4, PAH is expected to be ~90% charged, while PAA should be ~50% charged; *[6-10]* Thus, electrostatic interactions will dominate assembly.
- **PAH-T/PAA**. The PAH-T used in these films has a roughly 2:1 ratio of unmodified allyl amine repeat units and repeat units grafted with thymine. Assuming that any pKa shift as a result of grafting is negligible, the dominant interaction is still predicted to be electrostatic interaction, but some non-specific hydrogen bonding between thymine and protonated carboxylic acid groups is possible. The thymine groups should also affect LbL assembly by making the PAH chains bulkier.
- **PAH-T/PAA-A**. Again, assuming pKa shifts are negligible, electrostatic interactions should dominate, but adenine/thymine MHB bonding should also be significant, given their role in allowing (PAA-A/PAA-U) assembly, especially since the PAH-T and PAA-A used for these films was more highly grafted.
- **PAH-T/PAA-U**. Comparison of these films with (PAH-T/PAA) and films should provide information about the steric effect of including more bulky groups when these groups do not also allow for MHB with the second polyelectrolyte.

The growth of the above multilayer systems, tracked over the course of 50 bilayer addition cycles using strictly identical conditions and averaged from quadruplicate samples of each type of film, is reported in Figure 5.5.1.

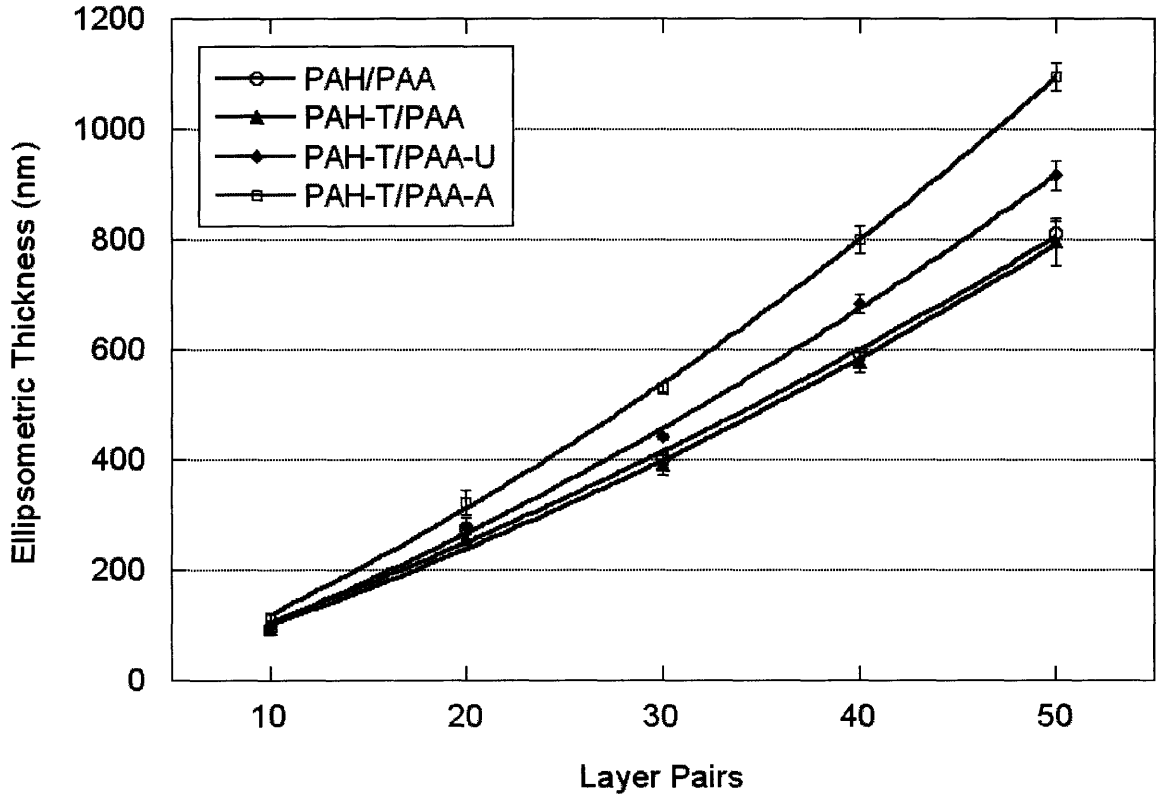

Figure 5.5.1 LbL film growth of nucleic base-grafted poly(allyl amine) and poly(acrylic acid) assembled in dilute PBS at pH 7.4. Thickness of dried films was measured by ellipsometry every ten layer cycles. Each data point and associated error bar reflect average values from quadruplicate samples prepared in parallel and evaluated in ten spots each.

All of the multilayer systems studied assembled successfully and reproducibly. No significant difference was observed between (PAH-T/PAA) films and the reference (PAH/PAA) films. Thus, both the steric effect of replacing 37% of allyl amine side chains with thymine and associated reduction in linear charge density would appear to be negligible. However, films pairing PAH-T with PAA-A or PAA-U both grew significantly thicker than films built from unmodified PAA. Having established that the presence of the thymine groups alone does not affect film growth, the observed difference must originate in thymine-adenine and thymine-uracil interactions.

Thymine and adenine obviously have the potential to interact via their classic double hydrogen bond motif; in this, the 6% grafting rate of PAA-A is most likely fortuitous, with the wide spacing of grafted groups giving the chain the flexibility required for adenine groups to

orient as required for formation of the A-T motif, which involves a proton from the nitrogen in the amide link. While coupling via groups para to the MHB motif, as in PAH-T and PAA-U, would have been ideal, successful MHB interactions have been reported for methacrylate polymers grafted to adenine through its primary amine group, as done here.*[11]* The nature of the thymine-uracil interaction is less clear and requires closer analysis of the LbL assembly behavior as well as the structures of the two polyelectrolytes.

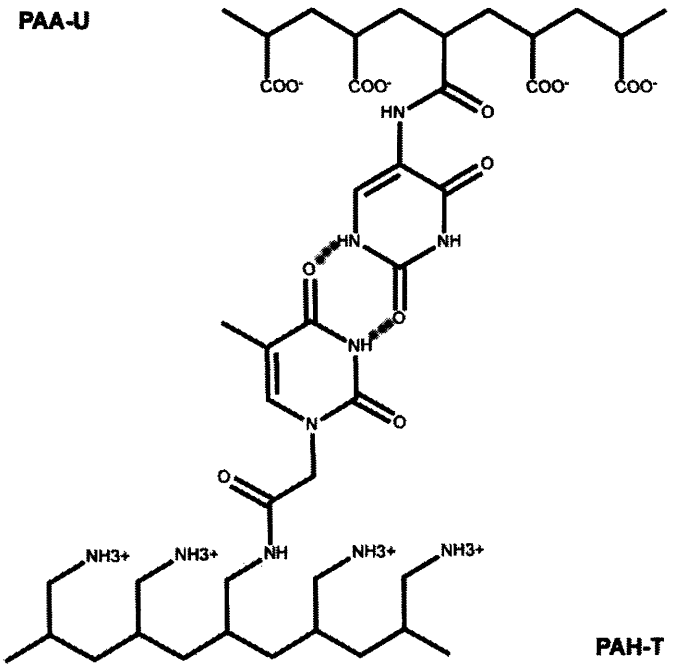

Figure 5.5.2. One potential thymine-uracil multiple-hydrogen bonding alignment.

In Figure 5.5.2, a potential MHB interaction between PAH-T and PAA-U is illustrated. Given the LbL assembly data, it would appear that whatever provokes the different behavior of (PAH-T/PAA-A) compared to (PAH-T/PAA) also takes place between when PAH-T and PAA-U are paired, but with a reduced effect. One possible explanation is that the A-T MHB motif leads to a stronger bond energy than the U-T motif. Visualizing these polyelectrolytes in solution, formation of A-T or U-T bonds is energetically favored but, upon adsorption, speeds the kinetic freezing of the multilayer by discouraging reorientation of the chains; electrostatic points of contact are similarly near-irreversible when polymeric chains are considered, but have less strict orientation requirements. Mobility effects could also contribute to the thickness difference between (PAH-T/PAA-A) and (PAH-T/PAA-U) films. Thymine has an ADA motif

and uracil a DADA motif; in both of these, all donors are secondary amines and all acceptors are carbonyl oxygens. Identical ring geometries mean that there are actually several different double hydrogen bond arrangements possible, and so it would seem that uracil/thymine interactions would be less restrictive of chain rearrangement, delaying kinetic freezing and allowing for tighter entanglements. The size of the nucleic base groups and their MHB pairing also requires greater separation of the polymeric backbones near a MHB dyad, further restricting the formation of dense, close-knit chain entanglements.

Having observed an increase in multilayer thickness as a result of introducing MHB groups, the effect on surface morphology was investigated next. In Figure 5.5.3, 10-bilayer films of each of the four polyelectrolyte pairings were observed by atomic force microscopy after drying under N_2 stream; in Figure 5.5.4, 50-bilayer films are similarly shown. All of the 10-bilayer films display the wrinkled "brain matter" texture characteristic of PAH/PAA films assembled in this pH range. This wrinkling is thought related to the collapse upon drying of highly-swollen PAH/PAA multilayers. The PAH-T/PAA surface image in 5.5.3.**b** is in part obscured by the presence of some taller surface contaminants, but identical wrinkling is in evidence. Close comparison of 5.5.3.**a, c,** and **d**, all shown with identical height scales over identical 5 x 5 μm areas, suggests that **c** and **d** are slightly smoother, with less-deep wrinkles despite their greater overall thickness. Additionally, the wrinkle feature size in **d** is noticeably larger than in **a** and **c**, further suggesting that the films built from polyelectrolytes having MHB interactions in addition to electrostatic had a looser-knit morphology.

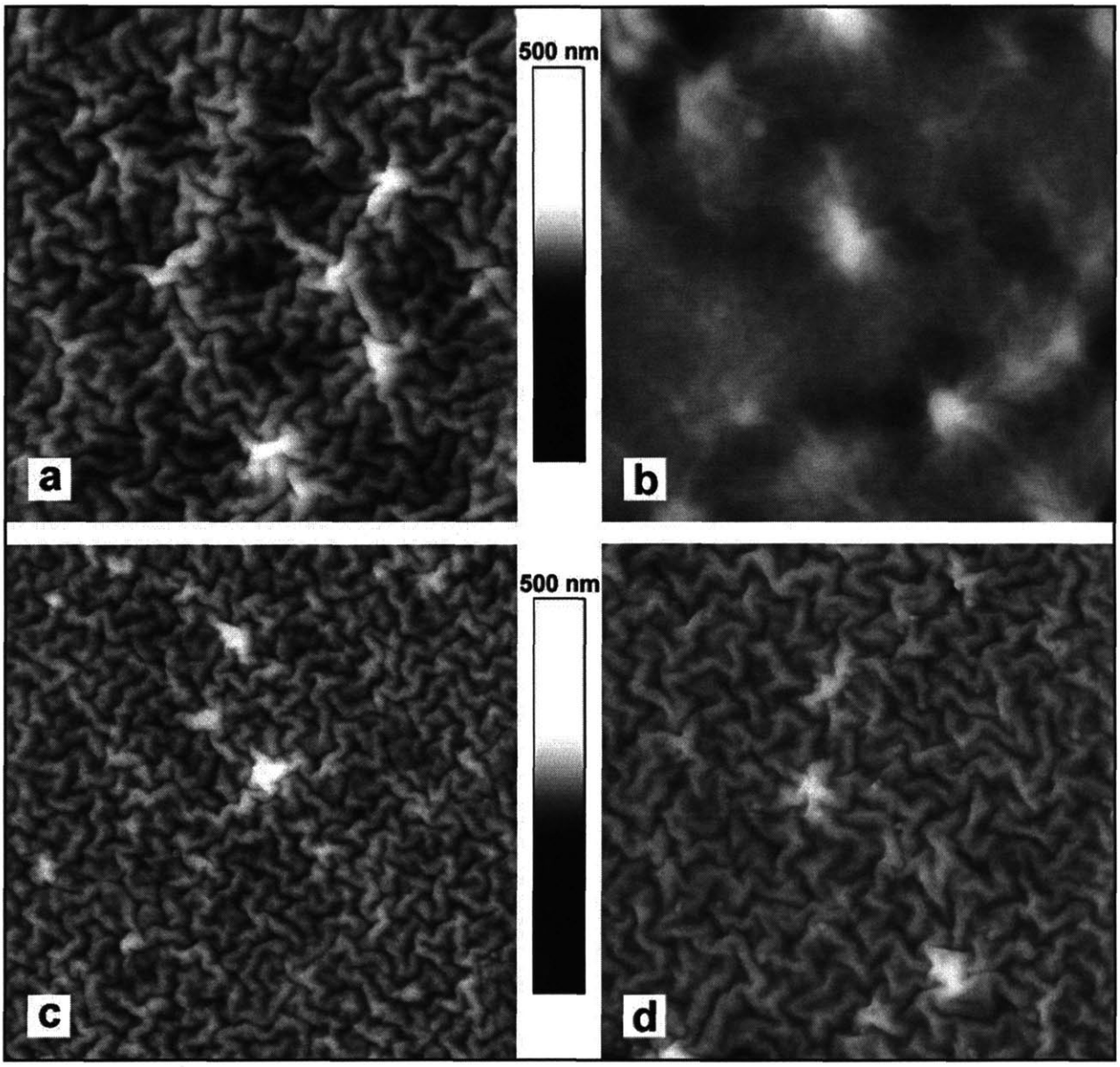

Figure 5.5.3. 5 x 5 μm tapping mode atomic force microscopy scans of $(PAH/PAA)_{10}$ (**a**), $(PAH\text{-}T/PAA)_{10}$ (**b**), $(PAH\text{-}T/PAA\text{-}U)_{10}$ (**c**), and $(PAH\text{-}T/PAA\text{-}A)_{10}$ (**d**) assembled on bare silicon in dilute PBS at pH 7.4. All films were imaged after drying under nitrogen stream.

After forty additional bilayers were built, the surface, shown in Figure 5.5.3, still shows wrinkling, but it is less deep and larger-featured than in the thinner films. Interestingly, despite the near-identical thickness of (PAH/PAA) and (PAH-T/PAA) films, their surfaces are not identical, with the latter having distinctly smaller wrinkling features. Examination of several areas on both films confirmed that this difference was consistently seen. The origin of this behavior is unclear, especially since the loosened chain entanglement theorized for (PAH-

T/PAA-A) and (PAH-T/PAA-U) appears to have provoked smoother and less-tightly convoluted wrinkling, as also observed in the 10-bilayer films. This phenomenon should be examined further with PAH-T of different grafting densities.

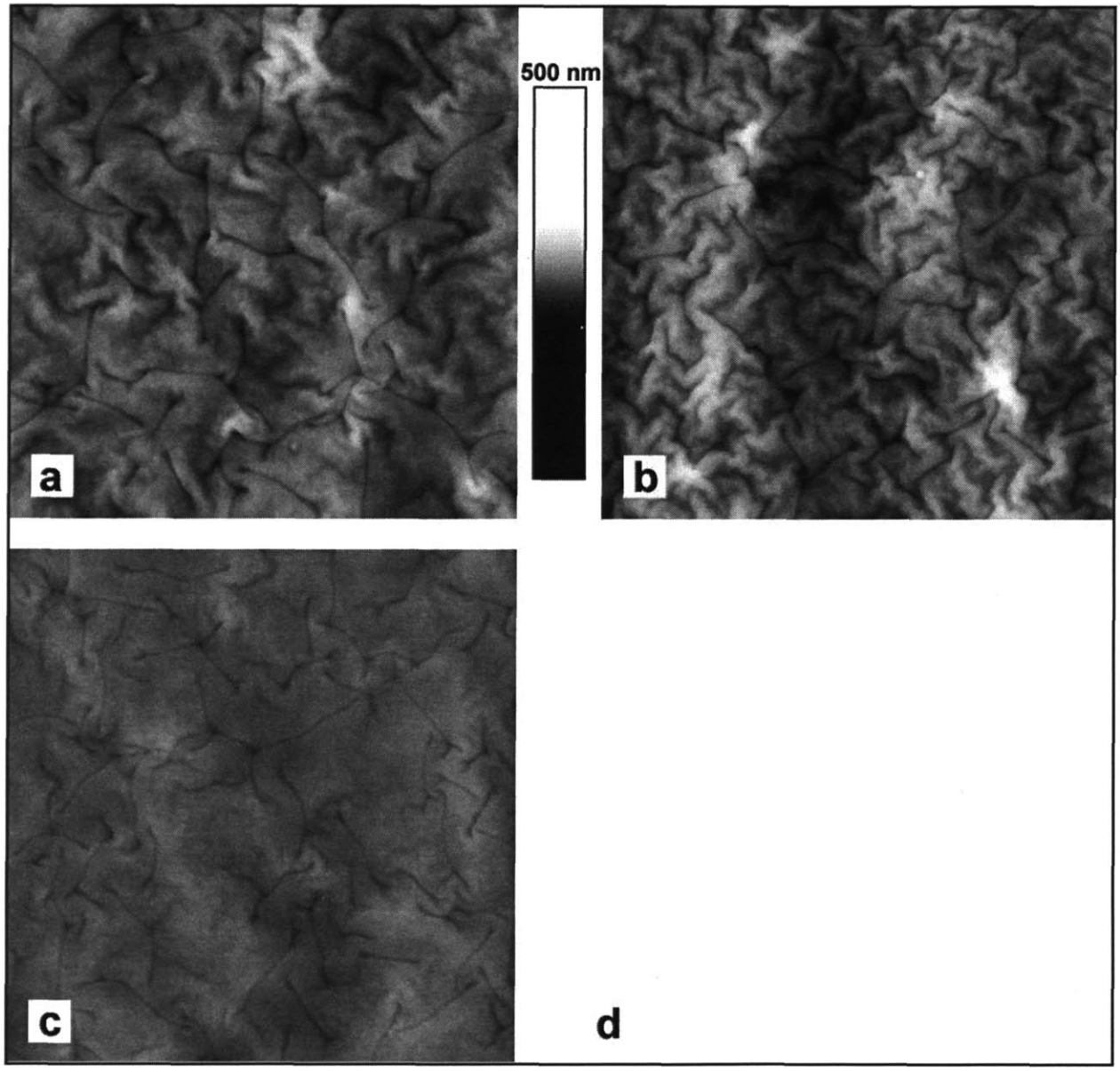

Figure 5.5.4. 5 x 5 μm tapping mode atomic force microscopy scans of $(PAH/PAA)_{50}$ (**a**), $(PAH\text{-}T/PAA)_{50}$ (**b**), $(PAH\text{-}T/PAA\text{-}U)_{50}$ (**c**), and $(PAH\text{-}T/PAA\text{-}A)_{50}$ (**d**) assembled on bare silicon in dilute PBS at pH 7.4. All films were imaged after drying under nitrogen stream.

Given the apparent influence of MHB interactions on the morphology of PAH/PAA multilayers during assembly, the effect on films of disrupting those interactions after assembly was of obvious interest. In Figure 5.5.5, 50-bilayer films were imaged after a 3-hour immersion

in methanol, a known hydrogen bonding disrupter. Films were dried rapidly and without rinsing immediately after removal from methanol to prevent any rearrangement.

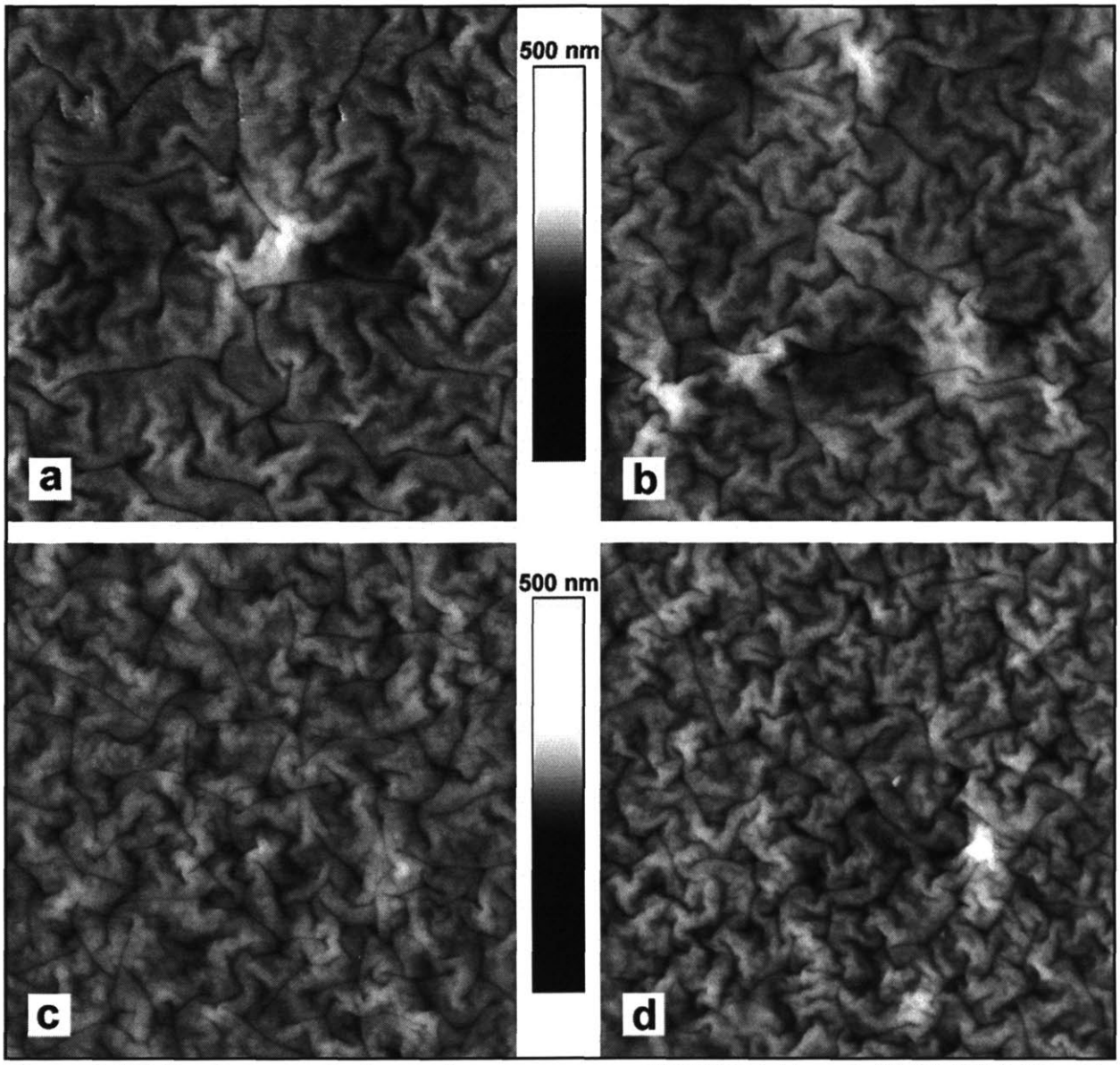

Figure 5.5.5. 5 x 5 μm atomic force microscopy scans of $(PAH/PAA)_{50}$ (**a**), $(PAH\text{-}T/PAA)_{50}$ (**b**), $(PAH\text{-}T/PAA\text{-}U)_{50}$ (**c**), and $(PAH\text{-}T/PAA\text{-}A)_{50}$ (**d**) originally assembled in dilute PBS after 3-hour immersion in pure methanol followed by immediate drying under N_2 flow.

A striking change to the surface morphology of the (PAH-T/PAA-A) and (PAH-T/PAA-U) films was observed, with both films now displaying deeper, more tightly-convoluted wrinkles. By comparison, (PAH/PAA) and (PAH-T/PAA) film topography was not significantly altered by methanol exposure, consistent with the very limited extent of neutral PAH-neutral

PAA hydrogen bonding present under these assembly conditions and the imperviousness of the dominating electrostatic interaction to methanol. The fact that (PAH-T/PAA) films did not exhibit rearrangement when immersed in methanol indicates that non-specific thymine-neutral COOH hydrogen was also negligible despite the 33% grafting rate and 50% ionization of PAA. This is consistent with the lack of thickness effect previously noted, and suggests that the reduced smoothing of (PAH-T/PAA) films with continued bilayer addition, observed in Figure 5.5.4.**b,** might stem from steric effects on chain mobility.

The strong effect of MHB groups on the morphology and solvent stability of polyelectrolyte multilayers suggests that these materials could be used to build thin films whose swelling behavior can be reversibly tuned without need to change pH or temperature. MHB disruption could also be provoked in aqueous environments by high concentrations of small molecules able to infiltrate films and competitively hydrogen bond. Such films would offer an additional degree of control for multilayer film morphology in solution, of great usefulness to release/encapsulation-type applications.

5.6 Comments and Conclusions

In this chapter, the multilayer assembly of biomimetic polyelectrolytes carrying nucleic base moieties was explored, with the relative roles of electrostatic and MHB interactions being of particular interest; even light grafting (~5% of repeat units) with MHB groups proved to have a significant effect on film morphology.

When oppositely-charged polyelectrolytes grafted with complementary MHB groups were layered in buffer, films were much thicker and looser than those built from comparable polyelectrolytes without MHB groups. However, when the nucleic base-incorporating films were exposed to hydrogen bond-disrupting solvents, their morphology changed dramatically and left them nearly indistinguishable from the films without MHB groups, which were not affected by such solvents. Assembly of films pairing uracil and thymine groups suggest that this non-standard pair is also capable of favorable hydrogen bonding.

Notably, films could be built exclusively from grafted-PAAs, but only when the grafted groups were complementary. These films were thin and prone to rapid degradation by rearrangement in hydrogen-bonding solvents, but that they assembled at all is striking evidence of the influence of even a limited number of MHB motifs on the interactions between two species.

WORKS CITED

[1] E. Vazquez, D. M. Dewitt, P. T. Hammond, D. M. Lynn, *Journal of the American Chemical Society* **2003**, *125*, 11452.

[2] J. Zhang, L. S. Chua, D. M. Lynn, *Langmuir* **2004**, *20*, 8015.

[3] X. Liu, J. W. Wang, A. D. Miller, E. A. Nack, D. M. Lynn, *Macromolecules* **2005**, *38*, 7907.

[4] R. Dootz, J. Nie, B. Du, S. Herminghaus, T. Pfohl, *Langmuir* **2006**, *22*, 1735.

[5] M. Z. Markarian, M. D. Moussallem, H. W. Jomaa, J. B. Schlenoff, *Biomacromolecules* **2007**, *8*, 59.

[6] M. F. Rubner, D. Yoo, S. S. Shiratori, *Macromolecules* **1998**, *31*, 4309.

[7] K. F. Weyts, E. J. Goethals, *Makromolekulare Chemie, Rap. Comm.* **1989**, *10*, 299.

[8] R. G. Smits, G. J. M. Koper, M. Mandel, *J. Phys. Chem.* **1993**, *97*, 5745.

[9] C. J. Bloys van Treslong, *Recueil, J. Royal. Neth. Chem. Soc.* **1978**, *97*.

[10] M. Mandel, *Euro. Polym. J.* **1970**, *6*, 807.

[11] K. Viswanathan, T. C. Ward, T. E. Long, *Polymer Preprints* **2005**, *46*, 1133.

CHAPTER 6 – SYNTHESIS OF ROBUST RNA ANALOGUES

6.1 Introduction

As discussed in Chapter 4, nucleic base pairing can not only be used to direct colloidal adsorption, but the nature of the multiple-hydrogen bonding (MHB) interactions involved makes simultaneous side-by-side assembly of lateral heterostructures – true surface sorting - a real prospect. Via previously-designed protocols for polyelectrolyte functionalization of colloids and polymer-on-polymer stamping (POPS), homopolymeric RNA was used to functionalize microspheres as well as substrates, yielding promising adenine-uracil and cytosine-guanine selectivity behavior was observed. However, the high cost and low stability of natural RNA make it poorly-suited to such applications beyond proof-of-concept, leading us to search for more robust alternatives.

The object of the work presented in this chapter was the design and synthesis of chemical species incorporating the MHB motifs of the nucleic bases while also readily applicable to microparticle and micropatterned substrate functionalization. While such compounds are of inherent interest as novel biomimetic materials, our approach was strongly guided by the original impetus for this undertaking, which dictated that the synthesis be as time- and cost-efficient as possible.

The two approaches to surface modification best suited to our work are the formation of self-assembled monolayers and the adsorption from solution of a polymeric coating. Thiolate or alkoxysilane SAMs could be used to stably modify surfaces as well as colloids, but the nature of their assembly imposes constraints on substrate selection, especially as concerns colloids. Polyelectrolytes could be used to homogeneously coat nearly any type of surface, but are more difficult to stamp than thiols or silanes. Thus, materials designed for both functionalization approaches were considered. The synthesis of materials for nucleic base-terminated SAM formation will be discussed first, followed by the synthesis of biomimetic polyelectrolytes carrying nucleic base groups.

6.2 Nucleic Base-Terminated Triethoxysilanes

6.2.1 Background and Strategies

The objective of this section will be the design and synthesis of materials allowing the formation of nucleic base-terminated self-assembled monolayers. To this end, either thiols or silanes could be used. While thiol SAMs are generally of better quality than silane SAMs*[1]*, they also require access to gold evaporation. In addition, the crosslinked structure of SAMs prepared from chloro or alkoxysilanes, which covalently bond not only to surface hydroxyl groups but also to neighboring silanes via Si-O bonds, makes for more stable patterning than thiols, whose thermal mobility can blur high-resolution patterns. Silane SAM assembly is more vulnerable to environmental conditions, with precise control of moisture levels required. Under anhydrous conditions, monolayers are generally incomplete, but an excess of water tips the balance in favor of siloxane crosslinking rather than reaction with surface hydroxyls. With thiol and silane approaches each having advantages and disadvantages, both options should be explored. For patterning of selective surfaces we require surface modification capabilities with at least two different, non-complementary terminal nucleic bases, and since we cannot combine silane and thiol SAMs practically, we would prefer a method easily adaptable to all of the nucleic bases.

Biomolecular recognition being the subject of much interest, several synthetic routes to MHB-terminated thiols have been reported. Mittler, et al, have prepared 11-[2-(9-adeninyl)-propionyloxy]-undecyl disulfide, while Hayes, et al, have prepared *n*-1-mercapto-10-thymyldecane.*[2, 3]* While no published syntheses of cytosine- and guanine-terminated thiols could be found, examination of the chemical structures of the nucleic bases (see Figure 6.3.3.1.1) shows that the secondary amine through which adenine is reacted above has a close analogue in guanine, suggesting that the same route could be used; the same can be said for the secondary amine targeted in thymine and cytosine. However, both syntheses require multiple steps, including intermediate purifications, and final yield is low - 20% for the adenine thiol and 37% for the thymine – so this seems an inefficient approach to take.

Considering instead the silane option, the preparation of an adenine-terminated triethoxysilane has been reported by Long and coworkers. In this approach, the selective coupling of a terminal isocyanate, carried by a triethoxy silane, and the secondary amine of adenine allows for the one-step synthesis of 3-(triethoxysilyl)-propyl-adenine (see Figure 6.2.2.1).*[4]* As above, examination of the other nucleic bases suggests that the same reaction will be possible via their own secondary amines. The simplicity and high reported yield of this synthesic route make it an ideal starting point for our own work.

6.2.2 Preparation

Materials

Adenine, cytosine, and 5-aminouracil were purchased from Sigma. 3-(Triethoxysilyl)-propyl isocyanate (liquid, 95% purity) was purchased from Aldrich. Anhydrous ethanol and anhydrous dimethylsulfoxide (DMSO) were purchased from Aldrich. Celite filtering agent was obtained from VWR. All chemicals were used as delivered, without further purification. The triethoxysilane and anhydrous solvents were used and stored exclusively within an argon-flushed glove box with moisture levels kept below 8 ppm H_2O. Self-assembled monolayers of the synthesized silanes were created on <1 0 0> n-type silicon wafers from Silicon Quest International (Santa Clara, CA) thoroughly rinsed with MilliQ water after Piranha treatment, an immersion into a 70:30 mixture of concentrated sulfuric acid and 30% aqueous hydrogen peroxide. CAUTION – PIRANHA SOLUTION IS AN EXTREMELY STRONG OXIDIZER AND WILL REACT EXPLOSIVELY WITH ORGANIC COMPOUNDS. EXTREME CARE MUST BE USED IN PROPER PREPARATION, HANDLING, AND DISPOSAL OF PIRANHA SOLUTIONS.

Synthetic protocol

Adenine-terminated silane (A-silane). To prepare A-silane for use in surface modification, 0.5 g of adenine (3.6 mmol) was dried in a 110 °C oven for three days before being transferred to an argon-flushed glove box. After dissolving the adenine in 50 ml of anhydrous DMSO, 0.90 ml of 3-(triethoxysilyl)-propyl isocyanate was added dropwise by syringe. The reaction mixture was stirred at room temperature under argon for 18 hours. No purification was carried out and the solution was stored under argon until needed.

To prepare A-silane for chemical characterization, 0.25 g of adenine (1.8 mmol) was dissolved in 300 ml of anhydrous ethanol after lengthy reflux under nitrogen. After cooling the mixture (no adenine precipitation observed after 24 hours) 0.48 ml of 3-(triethoxysilyl)-propyl

isocyanate (1.8 mmol) was added dropwise by syringe and the mixture was allowed to stir overnight under continued nitrogen flush. Ethanol was then removed under vacuum in a rotary evaporator.

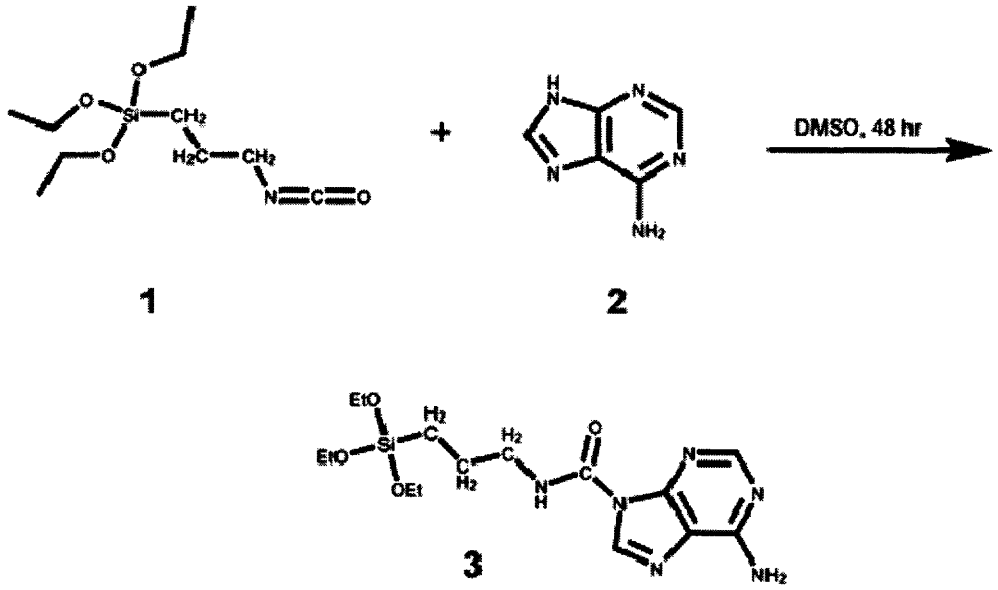

Figure 6.2.2.1. Synthesis of adenine-terminated triethoxysilane (**3**) from 3-(triethoxysilyl)-propyl isocyanate (**1**) and adenine (**2**). Performed under anhydrous argon atmosphere.

Cytosine-terminated silane (C-silane). C-silane was prepared in DMSO (for surface modification) and in ethanol (for characterization) in the same manner as A-silane. The reaction scales were 4.3 mmol of cytosine and 3.8 mmol 3-(triethoxysilyl)-propyl isocyanate in 50 ml DMSO and 2 mmol each of cytosine and 3-(triethoxysilyl)-propyl isocyanate in 300 ml ethanol.

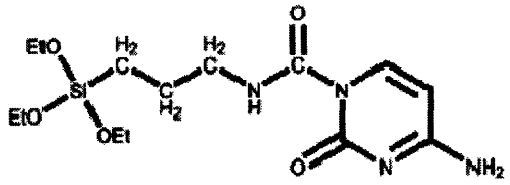

Figure 6.2.2.2. Cytosine-terminated triethoxysilane, synthesized from 3-(triethoxysilyl)-propyl isocyanate and cytosine via the same scheme as in Figure 6.2.2.1.

Uracil-terminated silane (U-silane). U-silane was prepared in DMSO in the same manner as A-silane. The reaction scale was 4 mmol of 5-aminouracil and 4 mmol 3-(triethoxysilyl)-propyl isocyanate in 50 ml DMSO.

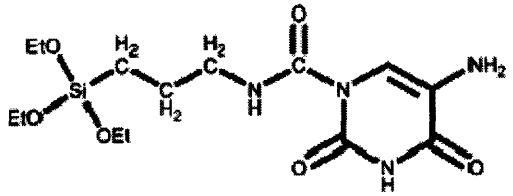

Figure 6.2.2.3. Uracil-terminated triethoxysilane, synthesized from 3-(triethoxysilyl)-propyl isocyanate and 5-aminouracil via the same scheme as in Figure 6.2.2.1.

6.2.3 Characterization

Instrumentation

Infrared spectroscopy was performed using a Nicolet Magna-IR 500 Spectrometer Series II on KBr windows prepared in a Mini-Arbor desktop press from International Crystal Laboratories. Proton (^{1}H) and carbon (^{13}C) nuclear magnetic resonance spectroscopy was performed using a Varian Inova 500 MHz NMR spectrometer equipped with an Oxford Instruments superconducting magnet. Carbon-hydrogen-nitrogen-oxygen elemental analysis was done by Midwest Microlab (Indianapolis, IN). Self-assembled monolayers of the synthesized silanes were analyzed on a Stokes LSE ellipsometer from Gaertner Scientific (Skokie, IL) and by attenuated total reflection (ATR) on a Nicolet Magna 860 Fourier Transform Infrared Spectrometer.

Structure confirmation

Nucleic-base terminated silane synthesis was complicated by the limited solubility of adenine, cytosine, and 5-aminouracil which in their neutral form have a saturation point around 100 mM in DMSO and 10 mM in ethanol at reflux. While the DMSO solubility is adequate for the very small amounts of silane needed for surface modification, the extremely low vapor pressure and high boiling point of DMSO make solvent removal virtually impossible. Luckily, the silanes do not need to be isolated in order to serve their intended purpose and inking/immersion solutions could be prepared by diluting the reaction mixture itself into ethanol (see Chapter 3.5). Small amounts were also prepared in ethanol, which is easily removed, for structural characterization.

After being filtered through Celite, A-silane was cast from ethanol onto NaCl spectroscopy crystals. The FTIR spectra of A-silane and adenine are given in Figure 6.2.3.1. As expected, the two spectra are quite similar, with all of the characteristic peaks in adenine being

found also in A-silane. The A-silane, however, has a strong absorbance peak at 1100 cm^{-1} not found in adenine and characteristic of C-H bending in the n-propyl group of the silane. The propyl group should also contribute some sharp C-H stretching peaks; although interpretation of the region around 3000 cm^{-1} is complicated by the numerous and broad peaks present in adenine, two new peaks are visible around 2950 cm^{-1}. Carbonyl stretching vibrations in the newly-formed amide linkage are also reflected in the broadening of the peak at 1700 cm^{-1}, which also contains contributions from the primary amine N-H bending vibrations in adenine, not affected by reaction.

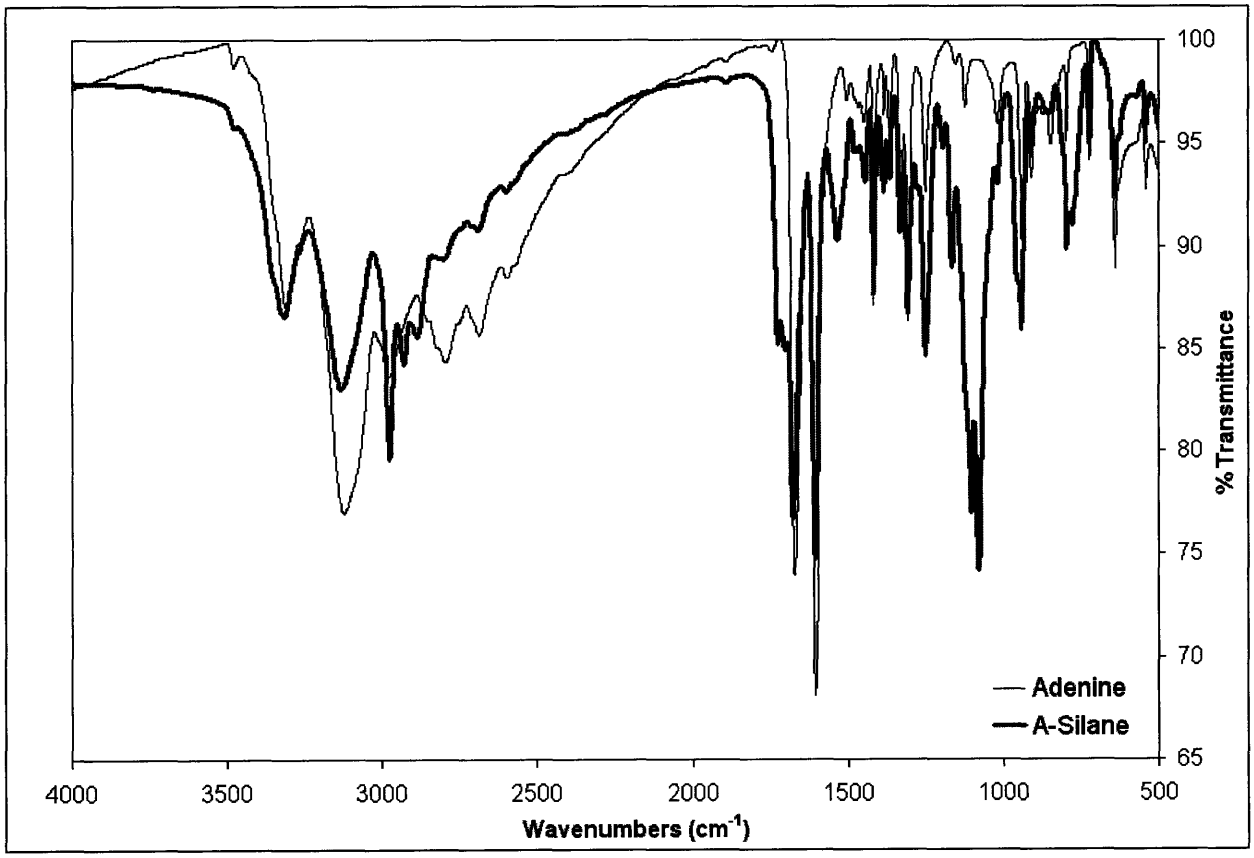

Figure 6.2.3.1. Superimposed FTIR spectra of adenine and A-silane. Adenine was prepared as a KBr window while A-silane was evaporated from ethanol onto a polished NaCl substrate.

In the absence of NMR data, elemental analysis was also performed for confirmation of structure. Combustion analysis of the solid precipitate formed when the A-silane in ethanol crosslinked in the presence of water (the reaction in ethanol was not performed under anhydrous

conditions) revealed a 9.7:1 mass ratio of C:O and a 1.13:1 mass ration of C:N. Oxygen in Si-O bonds cannot be detected by the method used, so all oxygen must come from amide carbonyls. The mass ratios predicted for the proposed product are 6.7:1 C:O and 1.3:1 C:N; if the silane had not reacted with adenine, its crosslinked form would be expected to have a 3.0:1 ratio of C:O and a 4.4:1 C:N ratio. While EA suggests that purity and yield are not yet perfect, the persistence of some unmodified silanes in the solution is not expected to affect the intended application for these materials. To the contrary, the MHB-functionalized silanes will most often be used in mixed solutions, with a non-interacting silane added as a diluent to prevent surface crowding of the MHB motifs.

SAM Characterization

Self-assembled monolayers of A-silane, C-silane, and U-silane were formed on freshly-hydroxylated silicon substrates by overnight immersion in 1:15 ethanol dilutions of untreated reaction products in DMSO. After rinsing away any unbound material, thicknesses were measured by ellipsometry and are reported in Table 6.2.3.

A-silane	**C-silane**	**U-silane**
5.9 Å +/- 2.0	1.5 Å +/- 1.1	4.3 Å +/- 1.1

Table 6.2.3. Ellipsometric thicknesses of nucleic base-grafted SAMs on hydroxylated silicon surfaces. Only data points with extremely high matches between Psi and PsiC were retained.

Ellipsometry confirmed the formation of a film on each of the substrates. The A SAM was slightly thicker but also less homogeneous than the U and C, which is consistent with the presence of a larger terminal group provoking more disordered and less dense packing.

6.3 Nucleic Base-Grafted Polyelectrolytes

6.3.1 Background and Strategies

The objective of this section will be the design and synthesis of robust polymers with nucleic base side chains; a charged backbone is also desired to make these polymers maximally useful for colloidal modification and POPS. There are two principal synthetic approaches to such structures available to us: attachment of the desired side-chain to monomeric units and subsequent polymerization, or attachment of the side-chains to an existing polymeric backbone.

Hest and coworkers have reported the synthesis via ATRP of PEG-poly(adenine) and PEG-poly(thymine) block copolymers in which adenine and thymine are carried by a non-degradable backbone.*[5]* While their method could be used to make an all-polyA or polyT species, whose layer-by-layer assembly would be of great interest, the synthesis requires carefully controlled reaction conditions as well as previous synthesis of the monomers, which are not commercially available. While this approach does not meet our efficiency criteria, it could be of great use if more sophisticated species are desired later.

The Long and Rotello groups have both synthesized polystyrene derivatives partially grafted with nucleic bases, generally via reaction with chloromethylstyrene repeat units, but neutral polystyrene is not suitable for our purposes, nor are random copolymers of sulfonated polystyrene and chloromethylstyrene readily available or synthesizable.*[4, 6, 7]* However, the approach of grafting onto a polymer having reactive chemical functions within its repeat unit seems a promising route to our desired structure.

Amidation coupling by reaction of a carboxylic acid with a primary amine, a well-known and well-understood synthetic method, is ideally suited to our purposes. Polymers with carboxylic acid or primary amine side groups are readily and inexpensively available, making them practical starting materials, and partial grafting would yield a charged polymer with nucleic base side chains, as desired for colloid and substrate functionalization. Several prior reports of such grafting were reviewed to identify reaction conditions likely to enable our own synthetic plans.

Poly(allyl amine) has been grafted with lactobionic acid side chains by carbodiimide-promoted coupling under mild aqueous conditions; while the reaction and subsequent

purification by dialysis are slow, they are also extremely simple. Kim and coworkers do not report a grafting rate for their lactobionic-modified PAH, but they do confirm the formation of amide linkages and the presence of the added groups. Notably, the Kim synthesis uses a water-soluble carbodiimide coupling agent alone, without addition of NHS.*[8]* The Kawaguchi group reports extremely high grafting efficiency in their own modification of PAH via reaction of the primary amines with N-carboxyanhydrides, but their approach requires a carefully-controlled environment and prior modification of the groups to be grafted.*[9]*

Reactions of polyacids with primary amines have also been explored by a number of groups, often in order to add functionality to the degradable biopolymer poly(γ-glutamic acid): Bugg, et al, have tagged PGA with UV-absorbing units, while Akashi and coworkers found that grafting PGA with the heparinoid taurine (H_2N-CH_2-CH_2-SO_3H) improved its anticoagulant activity. Both of these polymers could be prepared under slow but simple aqueous conditions.*[10, 11]* Similarly, the Michielsen group has explored grafting of PAA with a wide variety of alkylic and perfluorinated amines, aiming to improve the stain resistance of PAA fibers. In that work, they concluded that DMTMM was a superior alternative to carbodiimides for large-scale aqueous condensation reactions due to its lower cost.*[12]*

First synthesized and characterized by Kunishima and coworkers in the 90s, 4-(4.6-dimethoxy-1,3,5-triazin-2-yl)-4-methylmorpholinium chloride (DMTMM) is a triazine derivative allowing for the one-step activation of carboxylic acids towards reaction with amines. Highly-efficient condensation of carboxylic acids and amines can be achieved under remarkably simple and safe conditions by use of DMTMM, whose solubility and stability in water, methanol, and ethanol make it particularly suited to the modification of water-soluble polyelectrolytes like PAA and PAH. DMTMM is commercially available, relatively inexpensive, and presents no particular hazards. The mechanism of DMTMM-promoted condensation of carboxylic acids and amines is given in Figure 6.3.1.2.*[13, 14]*

Several groups have reported high grafting efficiencies (number of converted acid groups per primary amine groups in starting materials), even for high grafting rates (percentage of converted repeat units in the resulting polymer). Michielsen, et al, report grafting efficiencies near 50% for most of the studied DMTMM reactions and in some cases were able to approach 100% conversion, while similarly high grafting rates and ~50% grafting efficiencies are reported for several of the carbodiimide reactions of PGA and PAA.*[11]* However, quantification of

conversion is a complicated endeavor and closer examination of the cited reports reveals that grafting rates calculated from integration of NMR peak intensities for backbone and graft protons, the primary method of quantification, often differ greatly (in one case, by a factor of 10) from those calculated by spectrophotometric analysis of polyacids grafted with UV-absorbing groups.*[10]* This could be explained by a lowering of the UV-active group's extinction coefficient when polymer-bound rather than free, but NMR analysis of polymers has its own challenges given the broadening and overlap of peaks provoked by the range of solution conformations adopted by seemingly-identical monomeric units.

In the two following sections, the nucleic base-grafting of poly(allyl amine) and poly(acrylic acid) via carbodiimide- or triazine-promoted coupling will be reported. Mechanistic description of the latter, a novel synthetic route, is given in Figure 6.3.1.

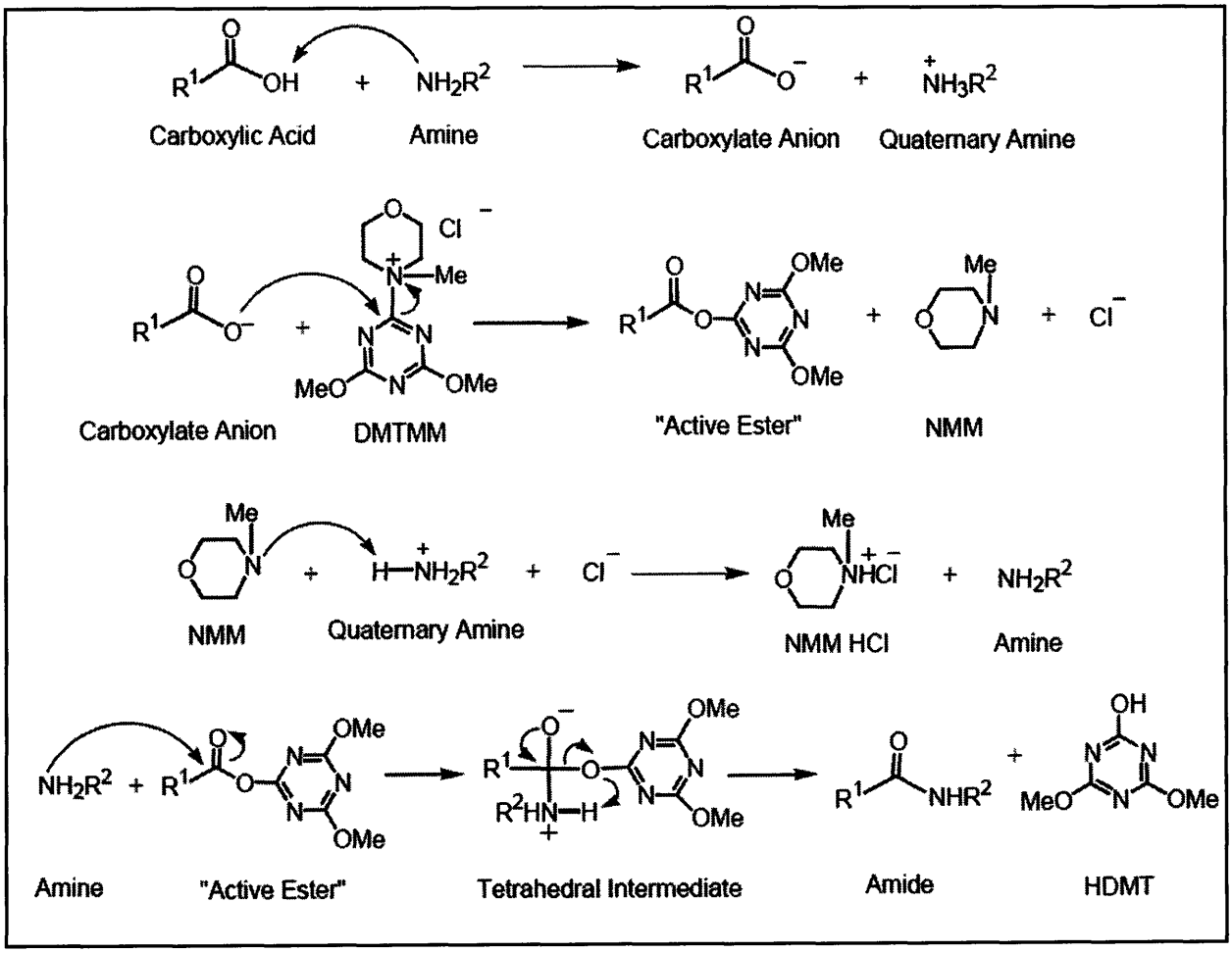

Figure 6.3.1. Mechanistic reaction scheme for the DMTMM-activated coupling of carboxylic acids and primary amines under aqueous conditions. Reproduced from *[15]*.

6.3.2 Derivatives of Poly(Allyl Amine)

6.3.2.1 Preparation

Materials

Poly(allyl amine) (PAH, non-salt form, nominal molecular weight 70,000 g/mol, 20% solution in water), thymine-1-acetic acid (ThAc), and 1-[3-(Dimethylamino)propyl]-3-ethylcarbodiimide methiodide (EDCI) were purchased from Aldrich. Sodium hydroxide (NaOH, solid pellets) was purchased from Mallinckrodt. Water was filtered through a MilliQ filter to a final resistivity of 18 MΩ*cm. Deuterium oxide (D_2O, 99% D) and dimethylsulfoxide-d_6 (DMSO-d_6, 99.9% D, 0.1% TMS) were purchased from Cambridge Isotope Laboratories for use as NMR solvents. Potassium bromide (KBr) for IR sample preparation was purchased from EMD. All chemicals were used as delivered without further purification. SnakeSkin dialysis tubing (regenerated cellulose, MWCO 3,500) was purchased from Pierce.

Synthetic protocol

Poly(allyl amine-graft-thymine) (PAH-T). ThAc (1.53 g, 8.3 mmol) and EDCI (2.475 g, 8.3 mmol) were dissolved in 100 ml MilliQ adjusted to pH 12 with NaOH. This high pH was required in order to solubilize ThAc by protonation of its secondary amine group. PAH (1 g, 16.7 mmol) was diluted to 100 ml in MilliQ adjusted in pH 12. The two solutions were combined and stirred at room temperature for 96 hours under air, after which the reaction mixture was brought to neutral pH by HCl addition and then dialyzed against a twenty-fold volume of MilliQ for three days with twice-daily water changes. Lyophilization of the dialyzate yielded very small, slightly yellow, glassy pellets.

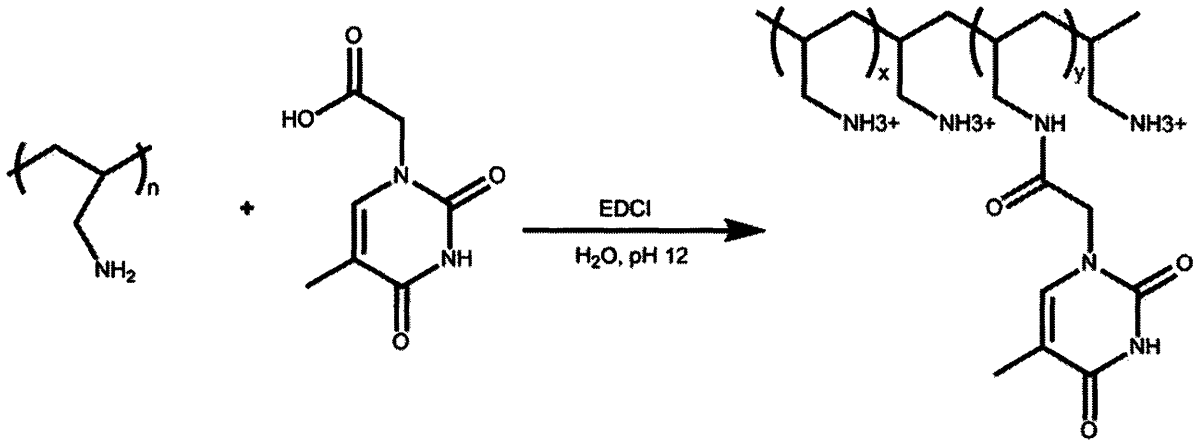

Figure 6.3.2.1. Synthesis of PAH-T by carbodiimide coupling grafting of 1-thymine acetic acid to poly(allyl amine) under basic aqueous conditions.

6.3.2.2 Characterization

Instrumentation

Dialyzed reaction products were lyophilized using a Labconco freeze dryer. Infrared spectroscopy was performed using a Nicolet Magna-IR 500 Spectrometer Series II on KBr windows prepared in a Mini-Arbor desktop press from International Crystal Laboratories. Proton (^{1}H) nuclear magnetic resonance spectroscopy was performed using a Varian Inova 500 MHz NMR spectrometer equipped with an Oxford Instruments superconducting magnet. Carbon-hydrogen-nitrogen-oxygen elemental analysis was done by Midwest Microlab (Indianapolis, IN).

Structure confirmation

After dialysis and lyophilization, solid polymer samples were dissolved in D_2O or DMSO-d_6 for NMR analysis. Solubility in pure DMSO was very low, so the polymer was first dissolved in a minimal amount of water before addition of the deuterated DMSO. H_2O rather than D_2O was used to avoid introduction of exchangeable deuterons, which would render amine

and carboxylic acid protons invisible to NMR and thus complicate quantitative analysis. 0.1% TMS was included to allow referencing of proton shifts, since hydrogen bonding between DMSO and water affects the position of the solvent peaks. The broadening and overlap of peaks typical of polymers in solution make substitution rates difficult to calculate accurately by comparison of the relative abundance of protons within grafted groups and protons within the polymeric backbone. While substitution rates calculated in this way are routinely reported in the literature, the inconsistency of NMR integration data collected from duplicate samples of the same batch of PAH-T, compared to the consistency of elemental analysis results, lead us to conclude that while NMR is essential for structural confirmation, grafting rates must be determined by elemental analysis. Reference ^{1}H spectra of all reagents were also collected under identical conditions.

Lyophilized PAH-T samples were studied by IR spectroscopy through KBr windows prepared by grinding 1% by mass of the analyte with pure KBr; the transmission spectrum is given in Figure 6.3.2.2.1. A reference spectrum for PAH was also obtained by casting pure aqueous PAH (from the same supply as the starting material) on a ZnSe crystal and is given in Figure 6.3.2.2.2. The strong peak at 1680 cm^{-1} is characteristic of carbonyl stretching and cannot be attributed to any vibrations of the alkyl and primary amine making up PAH, as seen in Figure 6.3.2.2.2. Deconvolution of this peak (see Figure 6.3.2.2.3) reveals that it is the sum of three peaks at 1661, 1676, and 1695 cm^{-1}, confirming the presence of three distinct carbonyl groups. Also notable is the strong decrease in intensity of the two-banded peak at 3285 and 3363 cm^{-1} characteristic of the primary amine side-chains of PAH, suggesting a high grafting rate.

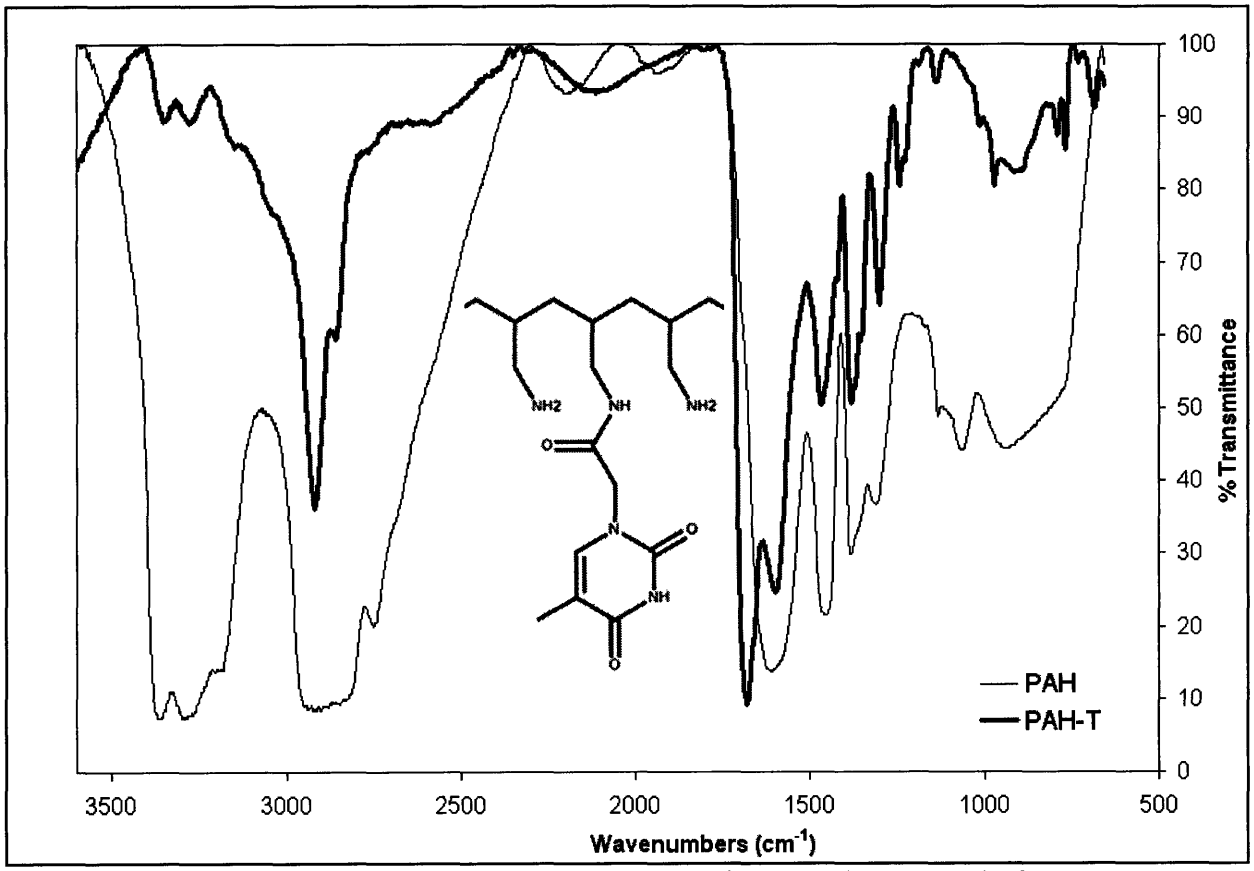

Figure 6.3.2.2.1. FTIR spectra of unmodified PAH (blue) and PAH-T (red, top-most curve except at 1680 cm^{-1}). PAH-T was prepared as a KBr window after dialysis and lyophilization, while PAH was cast on ZnSe from 20 wt% aqueous solution (starting material). Deconvolution of the PAH-T peak at 1680 cm^{-1} is shown in Figure 6.3.2.2.2.

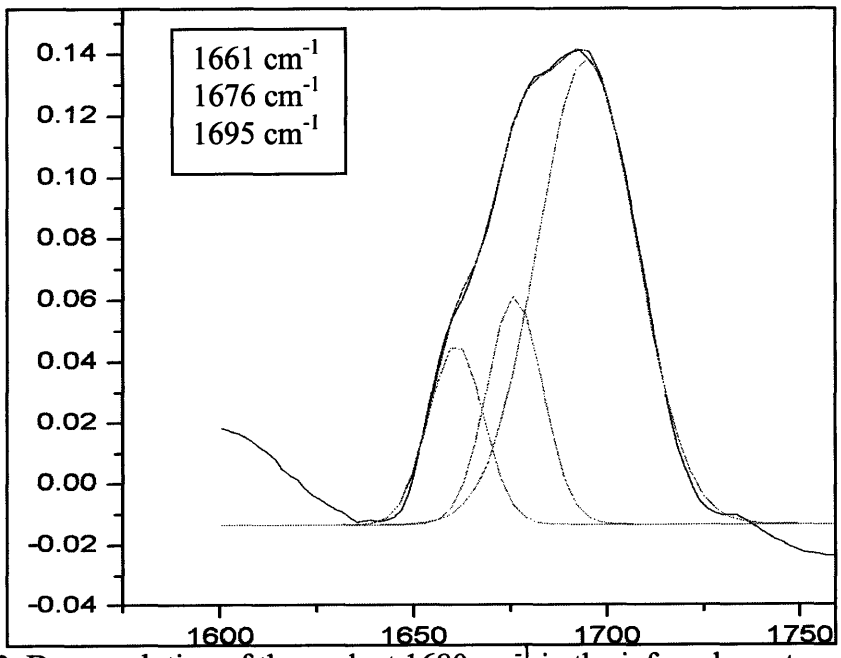

Figure 6.3.2.2.2. Deconvolution of the peak at 1680 cm^{-1} in the infrared spectrum of PAH-T.

The proton NMR spectrum of purified PAH-T in DMSO/H_2O is given in Figure 6.3.2.2.3. While amine protons remained difficult to detect despite the use of non-deuterated water (they are generally visible in the first scan collected, but disappear into noise with longer measurements), the other characteristic ThAc groups show up as sharp peaks at δ = 1.8 (-CH_3) and δ = 7.5 (C=CH within ring), easily distinguishable from the broad peaks of the backbone protons. The alkyl protons of grafted side-chains are also in evidence as a sharp peak at δ = 3.1, shifted slightly downfield from those in unmodified allyl amine repeat units. When the proton spectrum is integrated and contributions from ThAc are excluded, a 2:1 abundance ratio is found for (Protons **g** and **j**):(Protons **h** and **f**). The actual ratio of main-chain protons and side-chain protons in PAH is 3:2, demonstrating the quantitative unreliability of proton integration of polymer NMR. Integration of peak **a** vs. main-chain peaks yields a grafting rate of 3-5%, depending on which main-chain abundance is used, a rate much lower than suggested by the strong extinction of the primary amine IR peak. Given the inconsistency of the main-chain abundances and the conflict with IR data, the NMR spectrum of PAH-T provides strong qualitative structural confirmation of reaction, but not a quantitative measure of grafting.

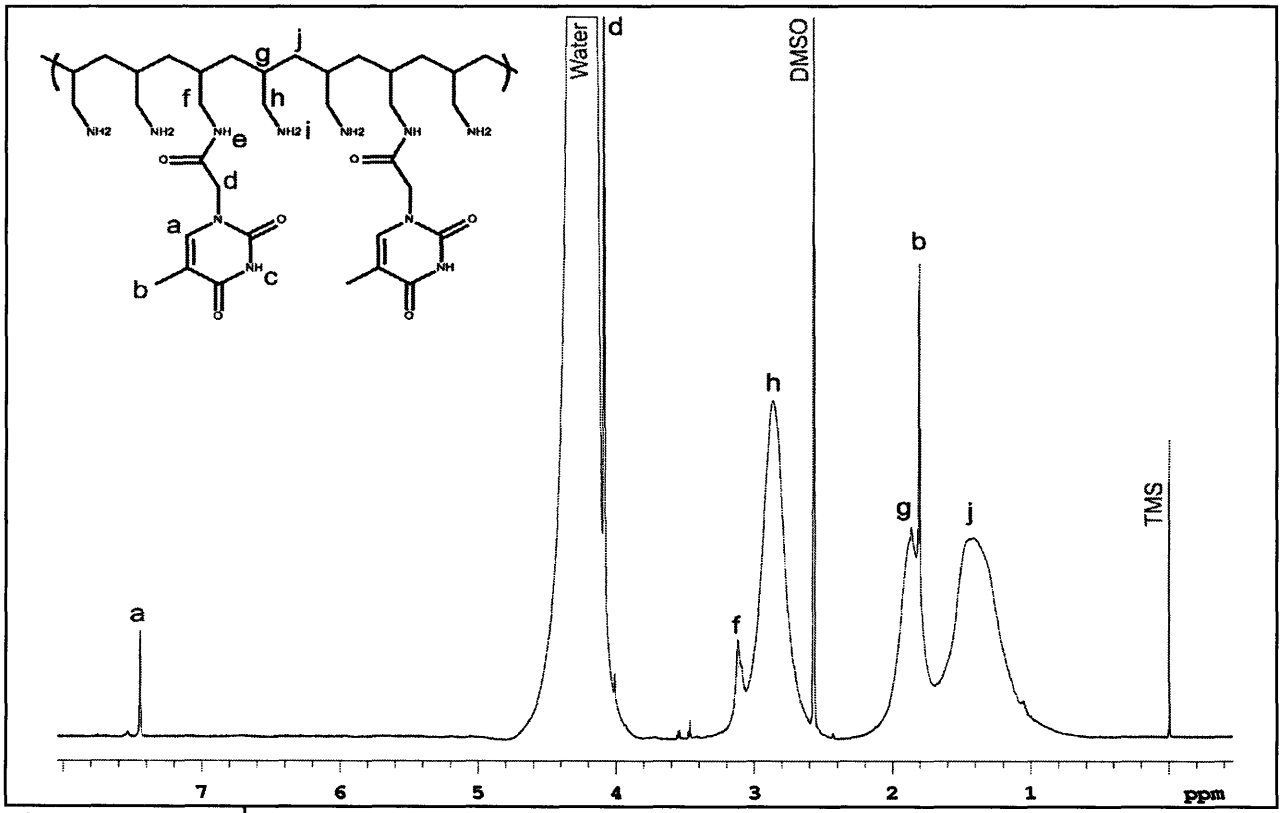

Figure 6.3.2.2.3. ^{1}H NMR spectrum and peak assignments of dialyzed, lyophilized PAH-T in H_2O/DMSO. Amine protons c, e, and i are not visible.

Grafting rates

Since integration of ^1H spectra could not provide quantitative data on the relative abundance of grafted repeat units versus unreacted repeat units, elemental analysis was used instead. Since poly(allyl amine) contains only C, H, and N, any oxygen detected in the purified reaction product must come from grafted thymine groups. Poly(allyl amine-g-thymine) is expected to be constituted of a random sequence of repeat units with molecular formula C_3H_7N (unreacted) and repeat units with molecular formula $C_{10}H_{13}N_3O_3$ (grafted) so grafting rates can be calculated as follows, in which x is the number of unreacted units present per grafted unit.

$$Grafting\ Rate = \frac{\#\ grafted\ repeat\ units}{\#\ unreacted\ repeat\ units + \#\ grafted\ repeat\ units} = \frac{100}{x+1}$$

$$Molar\frac{C}{O} = Mass\frac{\%C}{\%O} \times \frac{16}{12} = \frac{3x+10}{3}$$

$$Molar\frac{N}{O} = Mass\frac{\%N}{\%O} \times \frac{16}{14} = \frac{x+3}{3}$$

CHNO elemental analysis was performed by Midwest Microlab on duplicate samples of dialyzed and lyophilized PAH-T. The reported mass abundances and corresponding grafting rate (for the average x calculated from the two ratios) are given in Table 6.3.2.2.

	% C	% N	% O	x	Grafting Rate
Sample 1	35.68	13.26	9.60	1.68	37 %
Sample 2	35.64	13.44	9.46	1.78	36 %

Table 6.3.2.2. Mass abundance of carbon, nitrogen, and oxygen in duplicate PAH-T samples determined by combustion analysis and corresponding grafting rates.

The EA data are consistent with the high side-chain amine-to-amide conversion suggested by the IR data rather than the very low 3-5% grafting calculated from ^1H NMR integration; the fact that elemental analyses of duplicate samples yielded nearly-identical grafting rates is further indication that NMR should be used for structural confirmation only.

6.3.3 Derivatives of Poly(Acrylic Acid)

6.3.3.1 Preparation

Materials

Poly(acrylic acid) (PAA, nominal molecular weight 90,000 g/mol, 25% solution in water) was purchased from Polysciences. 4-(4,6-dimethoxy-1,3,5-triazin-2-yl)-4-methylmorpholinium chloride (DMTMM) was purchased from Acros Organics. 1-[3-(Dimethylamino)propyl]-3-ethylcarbodiimide methiodide (EDCI) was purchased from Aldrich. Adenine, 5-aminouracil, cytosine, and guanine were purchased from Sigma. Sodium hydroxide (NaOH, solid pellets) was purchased from Mallinckrodt. Water was filtered through a MilliQ filter to a final resistivity of 18 MΩ*cm. Deuterium oxide (D_2O, 99% D) and dimethylsulfoxide-d_6 (DMSO-d_6, 99.9% D, 0.1% TMS) were purchased from Cambridge Isotope Laboratories for use as NMR solvents. Potassium bromide (KBr) for IR sample preparation was purchased from EMD. All chemicals were used as delivered without further purification. SnakeSkin dialysis tubing (regenerated cellulose, MWCO 3,500) was purchased from Pierce.

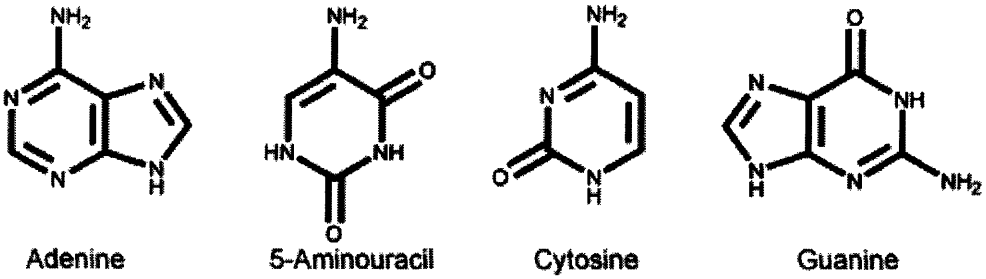

Figure 6.3.3.1.1. Chemical structures of the nucleic base building blocks used to modify poly(acrylic acid).

Synthetic protocol

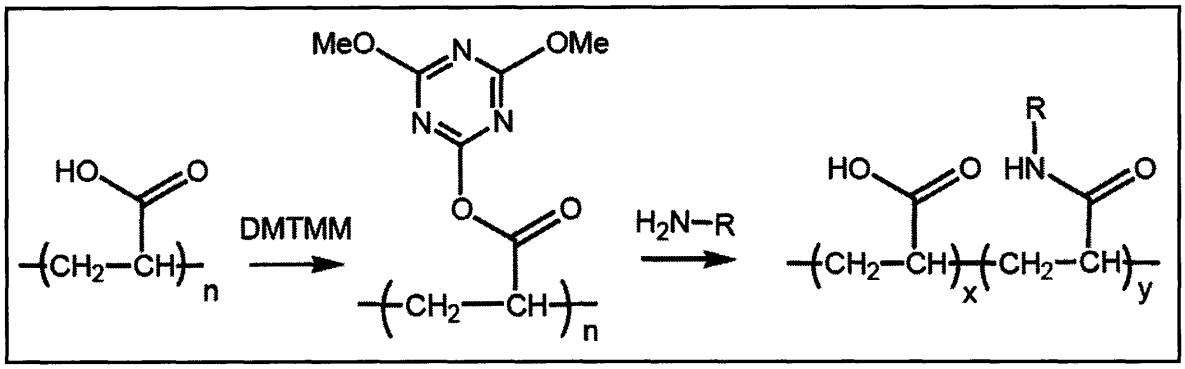

Figure 6.3.3.1.2 Mechanistic reaction scheme for the DMTMM-activated grafting of primary amines to poly(acrylic acid) under aqueous conditions. Reproduced from *[15]*.

Poly(acrylic acid-graft-adenine) (PAA-A). PAA and DMTMM were dissolved in MilliQ water (20 ml). For all reactions, the amount of PAA used was 0.432 g (1.5 mmol on a repeat unit basis). The amount of DMTMM and adenine used varied according to the desired COOH:NH_2 ratio. Adenine was dissolved in MilliQ water (80 ml) adjusted to pH 12 by addition of NaOH. This high pH was required for adenine solubility. After dissolution of all reagents, the two solutions were combined, re-adjusted to pH 12 if necessary, and then stirred 48 hours at room temperature under air. After 48 hours, the reaction mixture was brought to neutral pH by HCl addition and then dialyzed against a twenty-fold volume of MilliQ for three days with twice-daily water changes. Lyophilization of the dialyzate yielded a fluffy white solid.

Alternate synthesis of PAA-A. Adenine (0.676 g, 5 mmol) was dissolved in 100 ml of MilliQ water adjusted to pH 12 by addition of NaOH. After adenine dissolution, 1.485 g (5 mmol) of EDCI was added, followed by 0.1438 g (2.5 mmol on a repeat-unit basis) of PAA. The mixture was stirred 48 hours at room temperature under air before being neutralized and lyophilized as described above.

Poly(acrylic acid-graft-5-aminouracil) (PAA-U). PAA-U was prepared from the reaction of PAA with 5-aminouracil with DMTMM as the coupling agent exactly as described for PAA-A. The dialyzed and lyophilized product was fluffy and slightly yellow.

Alternate synthesis of PAA-U. PAA-U was prepared from the reaction of 3 mmol PAA with 6 mmol 5-aminouracil in the presence of 6 mmol EDCI exactly as described in the alternate PAA-A synthesis above.

Poly(acrylic acid-graft-cytosine) (PAA-C). PAA-C was prepared from the reaction of PAA with cytosine with DMTMM as the coupling agent exactly as described for PAA-A. The dialyzed and lyophilized product was a fluffy white solid.

Poly(acrylic acid-graft-guanine) (PAA-G). PAA-G was prepared from the reaction of PAA with guanine with DMTMM as the coupling agent as described for PAA-A with slight modification of the dialysis protocol. Due to the extreme aqueous insolubility of guanine at neutral pH, reactions using guanine in stoichiometric excess were first dialyzed against water at pH 12, and then against neutral water. The dialyzed and lyophilized product was a fluffy white solid.

6.3.3.2 Characterization

Instrumentation

Dialyzed reaction products were lyophilized using a Labconco freeze dryer. Infrared spectroscopy was performed using a Nicolet Magna-IR 500 Spectrometer Series II on KBr windows prepared in a Mini-Arbor desktop press from International Crystal Laboratories. Proton (^{1}H) and carbon (^{13}C) nuclear magnetic resonance spectroscopy was performed using a Varian Inova 500 MHz NMR spectrometer equipped with an Oxford Instruments superconducting magnet. Carbon-hydrogen-nitrogen-oxygen elemental analysis was done by Midwest Microlabs (Indianapolis, IN).

Structure confirmation

After dialysis and lyophilization, solid polymer samples were dissolved in D_2O or DMSO-d_6 for NMR analysis. Solubility in pure DMSO was very low, so the polymer was first dissolved in a minimal amount of water before addition of the deuterated DMSO. H_2O rather than D_2O was used to avoid introduction of exchangeable deuterons, which would render amine and carboxylic acid protons invisible to NMR and thus complicate quantitative analysis. 0.1% TMS was included to allow referencing of proton shifts, since hydrogen bonding between DMSO and water affects the position of the solvent peaks. As discussed in Section 6.3.2, the relative ^{1}H abundance of protons in grafted repeat units vs. main-chain protons was not expected to yield accurate substitution rates, for which elemental analysis was used instead. However, the presence of ^{1}H peaks characteristic of the nucleic bases and of amidation did allow structural confirmation of grafting. Reference ^{1}H spectra of all reagents were also collected under identical conditions.

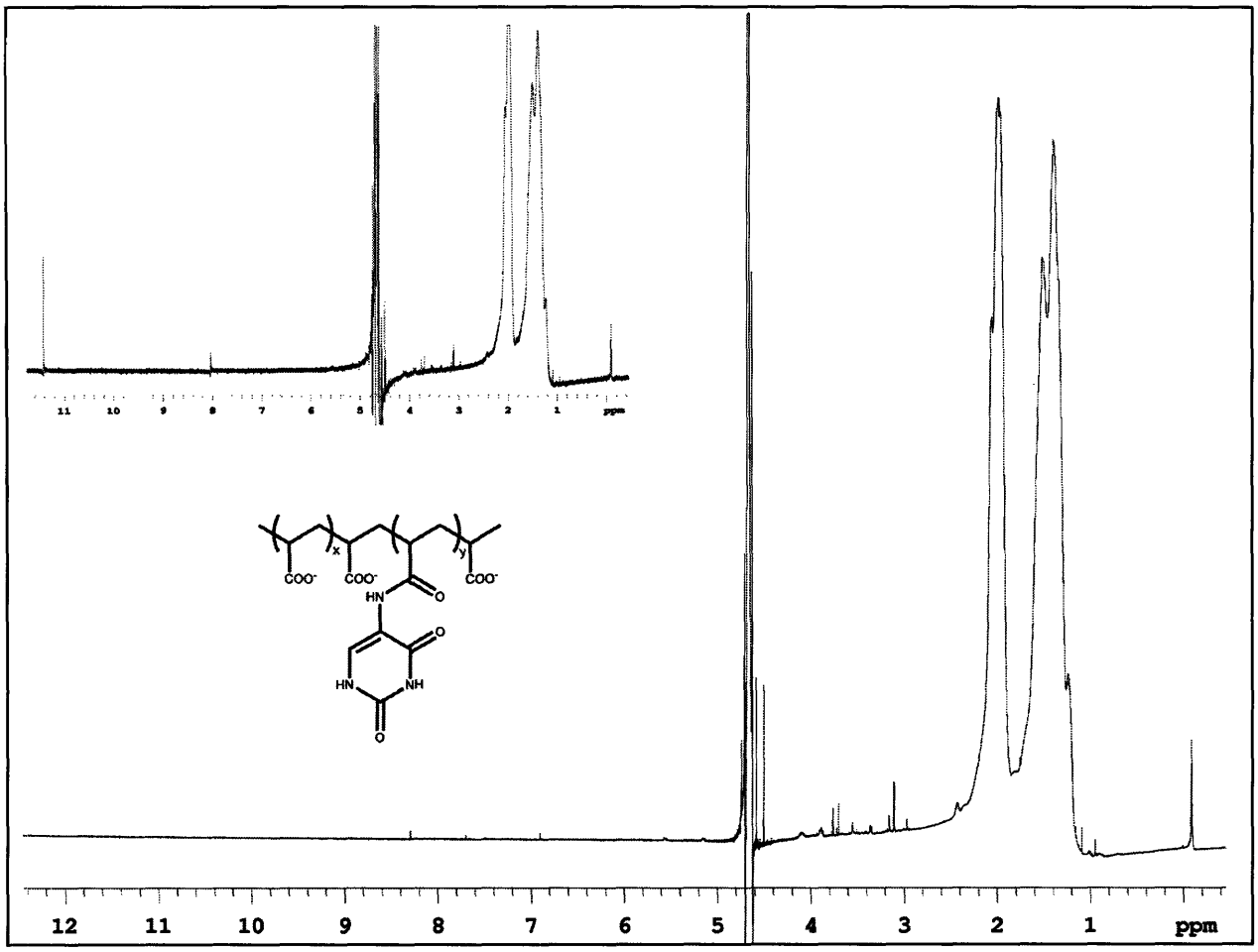

Figure 6.3.3.2.1. 128-scan ^{1}H NMR spectrum of PAA-U in D_2O. In the inset on the left, a single-scan spectrum of the same sample is shown. In the insert on the right, the region of the spectrum corresponding to the main-chain protons is enlarged.

In Figure 6.3.3.2.1, ^{1}H NMR spectra of a PAA-U sample are shown collected using single and 128 scans. In the single-scan spectrum, peaks at δ = 11.3 and δ = 8.0 are visible, corresponding to the two secondary amines in the uracil ring (at 11.3) and the secondary amine of the amide linkage (at 8). However, after 128 scans, the peaks have disappeared into noise due to rapid exchange and relaxation. The C=CH proton is also hard to detect. However, comparison of the main-chain proton region of PAA-U with that of unmodified PAA and a PAA-C sample examined under identical solvent conditions and the same spectrometer, given in Figure 6.3.3.2.2 reveals a distinct change in the shape and position of the peak corresponding to the single proton on the tertiary carbon linking the side chain and main-chain. In unmodified PAA, these protons

show up as a broad but clean singlet at $\delta = 2.2$. In PAA-U, the peak has become jagged and has shifted to $\delta = 2.0$. In PAA-C, the peak is now clearly split into three. While these changes do not conclusively identify the grafted group, they do confirm that amidation has occurred.

Clearer NMR spectra could not be collected, and so elemental analysis was used to confirm composition.

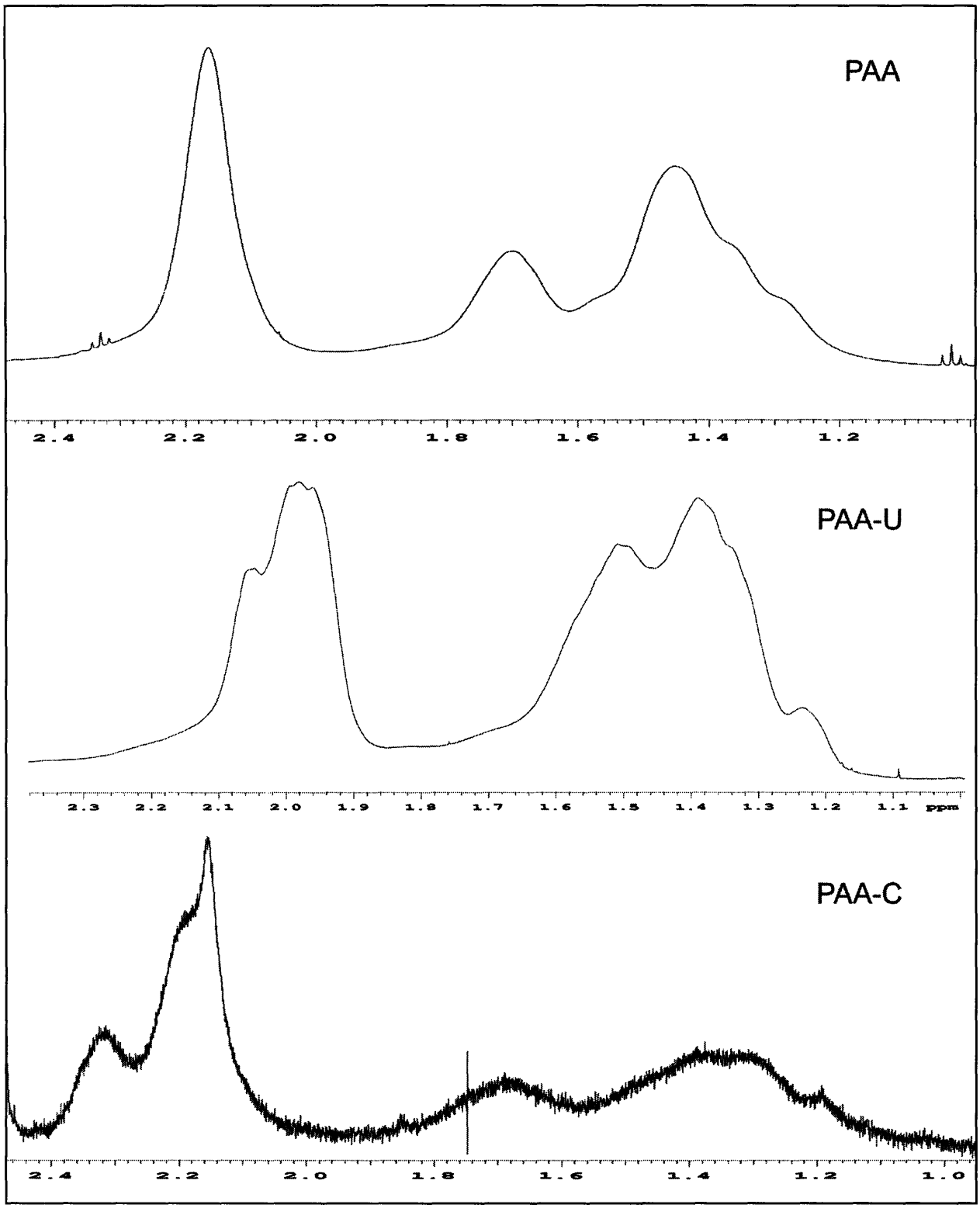

Figure 6.3.3.2.2. Main-chain proton region of ^{1}H NMR spectrum of unmodified PAA, PAA-U, and PAA-C, all in H_2O/DMSO.

Grafting rates

Since integration of ^1H spectra could not provide quantitative data on the relative abundance of grafted repeat units versus unreacted repeat units, elemental analysis was used instead. Since poly(acrylic acid) contains only C, H, and O, any nitrogen detected in the purified reaction product must come from grafted nucleic base groups.

Poly(acrylic acid-*g*-adenine) is expected to be constituted of a random sequence of repeat units with molecular formula $C_3H_4O_2$ (unreacted) and repeat units with molecular formula $C_8H_7N_5O$ (grafted) so grafting rates can be calculated as follows, in which x is the number of unreacted units present per grafted unit.

$$Grafting\ Rate = \frac{\#\ grafted\ repeat\ units}{\#\ unreacted\ repeat\ units + \#\ grafted\ repeat\ units} = \frac{100}{x+1}$$

$$Molar\frac{C}{N} = Mass\frac{\%C}{\%N} \times \frac{14}{12} = \frac{3x+8}{5}$$

$$Molar\frac{O}{N} = Mass\frac{\%O}{\%N} \times \frac{14}{16} = \frac{2x+1}{5}$$

CHNO elemental analysis was performed by Midwest Microlab on duplicate samples of dialyzed and lyophilized PAA-A, PAA-U, PAA-C, and PAA-G prepared via the DMTMM route and PAA-A and PAA-U prepared via the EDCI route. The reported mass abundances and corresponding grafting rates (for the average x calculated from the two ratios) are given in Tables 6.3.3.2.1 (DMTMM route) and 6.3.3.2.2 (EDCI route).

Batch	Amine	Acid:Amine:Coupler	%C	%N	%O	x	% Grafted
U1	5-AU	10 : 1 : 1	35.85	1.31	25.76	27	3.6
U2	5-AU	4 : 1 : 1	32.04	1.22	34.33	32	3.0
U5	5-AU	2 : 1 : 1	34.53	0.12	35.93	308	0.3
UX	*5-AU*	*2 : 3 : 3*	*34.61*	*2.45*	*34.2*	*15*	*6.1*
A5	Adenine	2 : 1 : 1	38.17	0.15	31.18	473	0.2
A10	Adenine	1 : 1 : 1	35.86	0.18	33.7	397	0.25
AX	*Adenine*	*2 : 3 : 3*	*39.68*	*1.47*	*35.86*	*51*	*1.9*
C5	Cytosine	2 : 1 : 1	38.13	0.27	n/a	162	0.6
CX	*Cytosine*	*2 : 3 : 3*	*39.31*	*0.47*	*n/a*	*95*	*1.0*
GX	*Guanine*	*2 : 3 : 3*	*35.03*	*0.09*	*n/a*	*754*	*0.13*

Table 6.3.3.2.1. Mass abundance of carbon, nitrogen, and oxygen in various nucleic base-functionalized PAA samples prepared using DMTMM as the coupling agent and corresponding grafting rates calculated from C/N and O/N ratios. In the case of C5, CX, and GX, oxygen analysis was not performed and only C/N was used to determine grafting rate. Syntheses performed with an excess of the nucleic base, targeting maximal substitutions, are italicized.

Batch	Amine	Acid:Amine:Coupler	%C	%N	%O	x	% Grafted
93U	5-AU	1:2:2	42.43	4.76	30.85	7.5	11.7
93A	Adenine	1:2:2	40.37	4.26	24.32	13.9	6.7

Table 6.3.3.2.2. Mass abundance of carbon, nitrogen, and oxygen in various nucleic base-functionalized PAA samples prepared using EDCI as the coupling agent and corresponding grafting rates calculated from C/N and O/N ratios.

The elemental analysis data reveal very low grafting rates despite stoichiometric excess of amine groups, explaining the difficulty in detecting these changes via NMR other than by monitoring the shape of the main-chain proton peaks. These low grafting rates and grafting efficiencies are in sharp contrast to the results reported by Michielsen for DMTMM-activated amidation of PAA, including at pH 12. Repeating the synthesis using EDCI instead, which allowed for greater than one-third grafting of PAH with thymine with only slight stoichiometric excess, improved grafting somewhat but still nowhere near the targeted rates.

6.4 Comments and Conclusions

In this chapter, polyelectrolytes and triethoxysilanes grafted with nucleic bases were successfully synthesized for use as colloidal and surface functionalization agents. These novel bio-inspired materials are intended to replace natural RNA in studies of nucleobase-directed selectivity as described in Chapter 3, their lower cost and improved stability making them better suited to experimental use.

In addition to a previously-reported adenine-terminated silane, novel cytosine and uracil-functionalized triethoxysilanes were also synthesized, expanding the range of patterning applications possible. While alkylthiols can also be prepared with nucleic base terminal groups, the silane synthetic route is far simpler and thus a better choice for large-scale production of experimental supplies. Spectrometry and elemental analysis confirmed that the desired structures were obtained in high yield. Incorporation of guanine moieties remains challenging due to the extreme insolubility of guanine in anything other than strongly basic aqueous conditions not suitable to ethoxysilane work. If a guanine-terminated silane is desired, it could likely be achieved via an intermediate coupling under basic conditions of guanine to a linker group allowing later reactivity with the terminal group of an ethoxysilane. Alternately, if more readily soluble molecules having the same MHB motif as guanine can be found, a guanine-analogue silane could be prepared instead.

Both poly(acrylic acid) and poly(allyl amine) were successfully grafted with nucleic bases, although high conversion rates for PAA proved elusive regardless of reaction stoichiometry. This was a disappointing surprise, as others have reported extensive coupling of PAA to primary amines under similar conditions. Michielsen and Thompson, in particular, report success using DMTMM at the same high pH employed in this work. Given that EDCI gave high grafting rates for PAH but not for PAA under equivalent reaction conditions, the problem seems specific to PAA. One possible explanation is that the pH adjustment required for nucleic base solubilitization increased the ionic strength of the reaction medium enough to allow PAA to adopt a coiled conformation despite being fully ionized. Two options present themselves for future improvement of PAA grafting efficiency: performing the reaction in DMSO, in which

several of the nucleic bases are more soluble without requiring pH adjustment, or performing the reaction in neutral water kept saturated with a nucleic base by periodic replenishment. The two strategies could of course be combined for maximal impact. An additional objective of future work should be the improvement of yield so as to produce as much material for selectivity studies as efficiently as possible.

While our synthesis of nucleic base-grafted polyelectrolytes was inspired by a need for a robust synthetic analogue of RNA, such biomimetic materials could be of interest for many other applications. In layer-by-layer assembly, highly-grafted PAA and PAH could build films with programmable swelling or even decomposition. Random mixed grafting (such as PAA-*g*-A/C and PAH-*g*-T/G) would offer further complexity by allowing the relative strength of hydrogen bonding and electrostatic interactions to be tuned via the comparative abundance of the two base pairs. Since PAH grafting proved efficient, other reaction stoichiometries and ionic strengths should be studied to explore the relative influence of chain conformation, grafted-group steric hindrance, and molar equilibrium on substitution rates.

WORKS CITED

[1] A. Ulman, *Chemical Reviews* **1996**, *96*, 1533.
[2] M. Weisser, J. Käshammer, B. Menges, J. Matsumoto, F. Nakamura, K. Ijiro, M. Shimomura, S. Mittler, *Journal of the American Chemical Society* **2000**, *122*, 87.
[3] S. Abbott, J. Ralston, G. Reynolds, R. Hayes, *Langmuir* **1999**, *15*, 8923.
[4] K. Viswanathan, H. Ozhalici, C. L. Elkins, C. Heisey, T. C. Ward, T. E. Long, *Langmuir* **2006**, *22*, 1099.
[5] H. J. Spijker, A. J. Dirks, J. C. M. Van Hest, *J. Polym Sci. Part A: Polym. Chem.* **2006**, *44*, 4242.
[6] R. Shenhar, T. B. Norsten, V. M. Rotello, *Advanced Materials* **2005**, *17*, 657.
[7] A. Sanyal, T. B. Norsten, O. Uzun, V. M. Rotello, *Langmuir* **2004**, *20*, 5958.
[8] I.-K. Kang, J.-S. Moon, H. M. Jeon, W. Meng, Y. I. Kim, Y. J. Hwang, S. Kim, *Journal of Materials Science: Materials in Medicine* **2005**, *16*, 533.
[9] M. Higuchi, T. Inoue, H. Miyoshi, M. Kawaguchi, *Langmuir* **2005**, *21*, 11462.
[10] E. C. King, W. J. Watkins, A. J. Blacker, T. D. H. Bugg, *Journal of Polymer Science: Part A: Polymer Chemistry* **1998**, *36*, 1995.
[11] M. Matsusaki, T. Serizawa, A. Kishida, T. Endo, M. Akashi, *Bioconjugate Chemistry* **2002**, *13*, 23.
[12] K. Thompson, S. Michielsen, *Journal of Polymer Science: Part A: Polymer Chemistry* **2006**, *44*, 126.
[13] M. Kunishima, C. Kawachi, K. Hioki, K. Terao, S. Tani, *Tetrahedron* **2001**, *57*, 1551.
[14] M. Kunishima, C. Kawachi, J. Morita, K. Terao, F. Iwasaki, S. Tani, *Tetrahedron* **1999**, *55*, 13159.
[15] K. Thompson, *Modification of Polymeric Substrates Using Surface-Grafted Nanoscaffolds*, School of Polymer, Textile & Fiber Engineering, Georgia Tech **2005**.

CHAPTER 7 – SUMMARY, CONCLUSIONS, AND FUTURE DIRECTIONS

In this work, the expansion of directed adsorption capabilities was pursued by the identification of highly-selective interactions as well as the design of experimental methods allowing such selectivity to be practically and effectively applied to the construction of microscale features.

In Chapter 2, selectivity based on electrostatic and other non-specific interactions such as hydrophobicity was studied. Self-assembled monolayers of perfluorinated alkylthiols allowed vastly different layer-by-layer film formation when micropatterned alongside a SAM of contrasting chemical functionality than when considered alone, a phenomenon termed "relative selectivity." Despite reports of perfluorinated SAMs resisting the adsorption of both cationic and anionic species, all of the polyelectrolyte multilayer systems studied were able to assemble on such surfaces, with the choice of polycation appearing to have the largest influence on film thickness and morphology. When assembled on micron-scale patterns of perfluorinated and carboxylic acid SAMs, most multilayer films were distinctly patterned, but only in the amount of material deposited; the less-attractive regions were conformably coated, just less so than the more attractive regions. In a few cases involving multilayer systems known to assemble very thinly on both continuous and patterned carboxylic and perfluorinated SAMs, adsorption was actually thicker on perfluorinated regions, albeit rougher.

To explore possible origins of relative selectivity, a simple free-energy model was used to study the influence of surface interactions on the adsorption of single polyelectrolyte layers and

LbL films. Theoretical predictions paralleled experimental observations, with polyelectrolytes predicted to adsorb in thicker layers on less attractive surfaces (either in the sense of weaker polymer-surface group interactions, or of paucity of surface groups). However, the free energy of adsorption was found to be consistently higher for less attractive surfaces. Thus, it was suggested that relative selectivity might stem from energetic favoring of adsorption on the more strongly-interacting of two equally-available surfaces.

In collaborating with another group on the patterned positioning of magnetic microspheres to be used as tethers for subsequent assembly under magnetic fields, colloidal adsorption became of interest. Colloids functionalized with single polyamine layers, originally intended for use as chemical force microscopy probes, were found to exhibit the same selectivity as multilayers based on those polyamines, selectivities far more specific than the simple electrostatic interactions previously used for directed assembly of colloids. Additionally, chemical functionalities which had previously shown only relative selectivity to multilayer adsorption were absolute resists to colloidal adsorption. Electrostatic repulsion existing between these universally cationic species restricted adsorption to monolayers, preventing the second component of a side-by-side pattern from overlayering and obscuring the first adsorbed component, as is frequently the case when attempting side-by-side assembly of two different polyelectrolyte multilayer systems. Beyond these improvements in efficiency, the true strength of polyelectrolyte-directed colloidal adsorption is in allowing highly-selective, but not otherwise functional, species to control the deposition of more interesting materials by packaging them inside tiny, functionalized containers. For example, LPEI and PAH were used to create a two-color pattern of fluorescent dyes without needing to find dyes that could be stably incorporated

into a multilayer film. Unlike highly-interpenetrated multilayer films, colloidal arrays could be lifted off of assembly templates by encasement in a new matrix, such as PDMS cast and cured over the array before being easily peeled away from the surface. Faithfully and completely transferred, arrays were now stable to sonication and friction as well as contained in a transparent, flexible material greatly increasing potential uses. If selective templates could be reused after array transfer, this would further promote applications by allowing a single gold template to repeatedly direct the assembly of component arrays later transferred into matrices more amenable to practical use. The regenerability of alkanethiols on gold substrates is as of yet unclear, however, and requires further study.

In the next section, selectivity via nucleic base pairing was examined. While two-component arrays could be assembled via polyamine selectivity, and while some prospects for three-component arrays were identified, all of these require sequential adsorption steps. Multiple hydrogen bonding interactions are far more specific and several MHB pairs can be coordinated simultaneously without interferences, making true surface sorting – patterned assembly from mixed solutions – a possibility. Commercially-available homopolymeric RNA was used to demonstrate the ability of single nucleic base-pairing (as opposed to oligonucleotide sequence matching) to direct colloidal adsorption with high selectivity. However, natural RNA is not an appropriate material for a technique intended to be as efficient and robust as possible. In the absence of commercially-available replacements suitable to surface patterning as well as particle functionalization, RNA analogues specifically tailored to these applications were designed and synthesized.

To allow microcontact printing of nucleic base patterns, triethoxysilanes were modified by coupling of a terminal isocyanate with the secondary amines present in all of the nucleic bases. Triethoxysilanes were chosen over alkyl thiols due to the simpler synthetic routes available; adenine, cytosine, and uracil-terminated silanes were each prepared via one-pot reactions requiring limited purification.

For colloidal functionalization as well as surface modification by polymer-on-polymer stamping, stable polyelectrolytes randomly grafted with nucleic base groups were synthesized by amidation of poly(acrylic acid) with primary amines in nucleic bases or of poly(allyl amine) with carboxylic acid derivatives of thymine. While PAH-T could be extensively modified (conversion of one-third of side chains was readily achieved), PAA grafting was more limited despite published reports to the contrary. Substitution rates should be improvable via adjustment of reaction conditions, but even 5-10% substitution had a significant effect on the solution and surface interactions of PAA.

Most notably, multilayered films could be assembled exclusively from complementarily-grafted PAAs. As expected given the electrostatic impediment to assembly, such films were quite thin and rapidly degraded under solvent conditions allowing rearrangement of chains into more energetically-favorable conformations. However, the mere fact that films could be assembled, but only if the nucleic bases involved were complementary, is evidence of the major impact of even limited grafting with MHB groups.

That grafted PAH could be assembled with grafted PAA was not particularly surprising; rather, it was the morphology of such films that was of interest. Multilayers combining electrostatic and MHB attraction were consistently thicker than comparable multilayers featuring

only electrostatics, and evidence suggests that this change was indeed due to MHB interactions rather than mere steric effects of introducing a bulky side chain. When electrostatic/MHB multilayers were exposed to hydrogen bonding-disrupting conditions, they transitioned to the same morphologies observed for electrostatic-only films. These films thus have the potential to be cycled between loose, porous structures and flatter, more entangled states, allowing for the creation of environmentally-responsive conformal coatings on arbitrary objects.

While the incorporation of MHB into multilayered films proved an interesting topic in its own right, the nucleic base-grafted polyelectrolytes also fulfilled their central *raison d'être*, successfully replacing RNA as directors of colloidal assembly. Colloids functionalized with grafted PAAs selectively adsorbed to complementary regions of chemically-patterned surfaces, provided access to the MHB groups was not hindered by monolayer crowding or the presence of chaotropic agents. When mixed monolayers of the nucleic base-grafted silanes and a non-interacting diluent silane were prepared and rehydrated in PBS prior to use, they effectively controlled adsorption of species functionalized with complementary versus non-complementary nucleic bases. Surfaces could also be patterned by stamping of grafted PAAs, but this approach was reserved for applications incompatible with silane SAMs, such as the creation of three-dimensional polymeric templates.

The custom-synthesized RNA analogues proved particularly superior to natural RNA for asymmetric functionalization of colloids. Complementary MHB groups could be put on opposite sides of microspheres by stamping or masked adsorption, with some approaches favoring symmetric asymmetric functionalization – optimal for linear self-assembly - while others led to large imbalances in the area covered by each functionality. Asymmetric asymmetry is generally

less desirable, but can be useful for the creation of surface tethers. The monolayer addressing requirement inherent to asymmetric functionalization restricts yields, but the more stable the functionalization agent, the more efficient the recovery of modified particles. The choice of silanes over thiols proved fortuitous in this application, since the crosslinked nature of siloxane monolayers makes them stable to lengthy sonication, which can allow mixing of more mobile alkylthiolate SAMs.

The next steps in this work will be the serial and parallel assembly of multicomponent arrays of both nucleic base pairs as well as characterization of the environmental changes by which MHB interactions can be reversibly activated and silenced.